Spatial and temporal dynamics of the terrestrial carbon cycle

Assimilation of two decades of optical satellite data into a process-based global vegetation model

Birgit Schröder

Institut für Geoökologie,
Universität Potsdam
und
Potsdam Institut für
Klimafolgenforschung e.V.

Elektronisch veröffentlicht auf dem
Publikationsserver der Universität Potsdam:
http://opus.kobv.de/ubp/volltexte/2008/1759/
urn:nbn:de:kobv:517-opus-17596
[http://nbn-resolving.de/urn:nbn:de:kobv:517-opus-17596]

Spatial and temporal dynamics of the terrestrial carbon cycle

Assimilation of two decades of optical satellite data into a process-based global vegetation model

Birgit Schröder

Dissertation
zur Erlangung des akademischen Grades
“doctor rerum naturalium” (Dr. rer. nat.)
in der Wissenschaftsdisziplin “Geoökologie”

eingereicht an der
Mathematisch-Naturwissenschaftlichen Fakultät
der Universität Potsdam

Potsdam, den 8. Mai 2007

Institut für Geoökologie
und
Potsdam Institut für Klimafolgenforschung e.V.

ACKNOWLEDGEMENTS

My principal advisor, Prof. Dr. Wolfgang Lucht, is gratefully acknowledged for his advice and support. I highly benefited from many fruitful discussions and support in all kinds of scientific questions. Moreover, I greatly appreciate his confidence in me and his patience and encouragement during my doubtful phases and during the childbearing period.

I am very grateful to Prof. Dr. Wolfgang Cramer who gave me the opportunity to work at PIK and to participate at a summer school in the Netherlands as well as at LPJ meetings, and who always had an open ear to scientific and personal problems.

I also gratefully acknowledge Ranga Myneni and Dong Huang from the University of Maryland, who provided me with the latest updates of the global fPAR datasets immediately after release, as well as Compton C. Tucker from NASA Goddard Space Flight Center who helped me to understand and define the differences of various fPAR datasets.

Many thanks go to Sibyll Schaphoff who supported me in all kind of programming issues with great patience, which was often necessary.

I'd also like to thank Dieter Gerten who introduced me to statistical issues and for his valuable comments.

Kirsten Thonicke is gratefully acknowledged for helpful hints concerning the fire module in LPJ, programming issues, and childbearing affairs.

Thanks go also to Tim Erbrecht who became my "contact person" for remote sensing and biomass issues and for providing me with interesting music and hints for concerts going on in Berlin.

This manuscript benefited from critical readings and by Wolfgang Lucht, Dieter Gerten, Claudia Kubatzki, Elfrun Lehmann, and Tim Erbrecht.

I really appreciated the discussions, support and the fun I had with the members of the LPJ consortium, (if they not have already been mentioned before): Stephen Sitch, Alberte Bondeau, Tanja Rixecker, Christoph Müller, Sönke Zaehle, Pascalle Smith, Markus Reichstein, Herrmann Lotze-Campen, Thomas Hickler, Wolfgang Knorr.

The German Climate Research Programme DEKLIM under the Ministry for Education and Research (BMBF) funded this work as part of the project 'Climate, Vegetation and Carbon' (CVECA).

Last, but not least, I'd like to thank Gerhard Kaulard for his support and encouragement during the difficult phase of pregnancy.

Finally, I'd like to dedicate this dissertation to my parents. I am highly indebted to them as they spent a lot of time taking care for me and my little son during the last phase of this PhD thesis and without their emotional, financial and temporal support this thesis would have never been completed.

ABSTRACT

Current understanding of the factors that determine the magnitude and temporal variations of global terrestrial uptake and release and which regions contribute most to these patterns is still incomplete. Several modelling approaches have provided estimations of the spatio-temporal patterns of net ecosystem production, but there is still a need for an improved and more realistic global carbon cycle model with good resolution that does not only simulate potential vegetation but also allows quantification of regional carbon storage and fluxes.

This PhD thesis presents the spatio-temporal distribution of terrestrial carbon fluxes for the time period of 1982 to 2002 simulated by a combination of the process-based dynamic global vegetation model LPJ (Sitch et al. 2003) and a 21-year time series of global AVHRR-fPAR data (fPAR – fraction of photosynthetically active radiation), provided by Ranga Myneni of Boston University at 0.5° resolution. Assimilation of the satellite data into the model allows improved simulations of carbon fluxes on global as well as on regional scales.

Assimilation of the fPAR data was implemented as a two-step process: after a spin-up of the potential vegetation to determine a base-line vegetation composition satellite-observed fPAR values were ingested. The fPAR value of each grid-cell was decomposed into fractions corresponding to the vegetation present at each location, where winter values were used to determine the evergreen versus deciduous fractions. In agricultural areas the model-predicted vegetation was replaced by grass; the satellite-observed fPAR provided the seasonality of planting and harvesting as well as the temporal trajectory of agricultural vegetation growth.

As it is based on observed data and includes agricultural regions, the model combined with satellite data produces more realistic carbon fluxes of net primary production (NPP), soil respiration (Rh), carbon released by fire and the net land-atmosphere flux than the potential vegetation model. It also produces a good fit to the interannual variability of the CO_2 growth rate. The current study adds to results obtained by other approaches, even though the results are not always consistently and should be seen as supporting a better understanding of the different processes contributing to the terrestrial carbon budget.

On a global scale, NPP is the main contributor to the interannual variability of net ecosystem production (NEP), whereas its magnitude and timings are mainly determined by heterotrophic respiration. The interannual variability of global NPP is dominated by tropical regions where it is mainly a function of variations in precipitation. The temperate and boreal zone NEP variations are also controlled by changes in NPP, but these are determined by changes in temperature. Net fluxes are highly correlated to El Niño-Southern Oscillation (ENSO) events in the tropics and southern mid latitudes, whereas no tele-connection to the northern hemisphere can be found. An influence of the North Atlantic Oscillation (NAO) on carbon fluxes on a latitudinal scale could not be detected. During the post-Pinatubo period boreal NEP declined, whereas the northern temperate regions show an enhanced uptake due to increased NPP and decreased Rh. Although temperature rise was strongest in the northern latitudes during 2000 to 2002, this was not reflected in an enhanced net terrestrial uptake.

This study presents a way to assess terrestrial carbon fluxes and elucidates the processes contributing to interannual variability of the terrestrial carbon exchange. Process-based terrestrial modelling and satellite-observed vegetation data are successfully combined to improve estimates of vegetation carbon fluxes and stocks. As net ecosystem exchange is the most interesting and most sensitive factor in carbon cycle modelling and highly uncertain, the presented results complementary contribute to the current knowledge, supporting the understanding of the terrestrial carbon budget.

CONTENTS

LIST OF FIGURES

LIST OF TABLES

1. INTRODUCTION

Several international conventions such as the Kyoto protocol (1997) or the IPCC Third Assessment Report (2001) document that the terrestrial carbon cycle plays a prominent role in the uptake of atmospheric CO_2, contributing substantially to the so-called 'missing sink', which partly offsets the anthropogenic CO_2 emissions. Thus, it is essential to investigate and understand the spatio-temporal behaviour of terrestrial carbon fluxes, i.e. the sources and sinks. However, current understanding of the regional patterns of biospheric uptake and release of CO_2 as well as their quantification is still fragmentary.

Additionally, the terrestrial biosphere drives most of the interannual changes in atmospheric CO_2 (Conway et al. 1994, Kaduk & Heimann, 1996, Houghton et al. 1998, Lloyd 1999, Tans & Wallace 1999, Battle et al. 2000, Houghton 2000b, Prince et al. 2000, Rödenbeck et al. 2003a, Murayama et al. 2004), but the contribution of the controlling factors such as climate, land-use change, natural disturbances such as fire, as well as fertilization effects are still uncertain (Conway et al. 1994, Bousquet et al. 2000, Fung 2000, Houghton 2000a, Schaefer et al. 2002). Several studies with biogeochemistry models suggest that interannual variability is predominantly sensitive to temperature and precipitation changes, but they differ in their description of the underlying mechanisms (Kaduk & Heimann 1996, Lloyd 1999, Dickinson 2000, Houghton 2000b). Schaefer et al. (2002) showed the predominant influence of climate on the interannual variability of terrestrial CO_2 fluxes with precipitation dominating the tropical and temperature dominating the extra-tropical variability. With some modelling approaches respiration is considered to be the controlling factor in some regions (Houghton 2000b), others consider photosynthesis (Kaduk & Heimann 1996).

Several approaches provide estimations of the spatio-temporal patterns of terrestrial uptake and release of atmospheric CO_2: Atmospheric inverse modelling achieves estimates of global NEP with high temporal resolution, but with only a very coarse spatial (continental) resolution and without elucidating the underlying causes of the variability (Bousquet et al. 1999, Law 1999, Peylin et al. 1999, Rayner et al. 1999, Bousquet et al. 2000, Enting 2002, Rödenbeck et al. 2003a, Peylin et al. 2005). Direct measurements by the eddy-covariance flux method, although providing all relevant carbon fluxes, are confined to local measurement sites (Valentini et al. 2000, Barford et al. 2001) and forest inventories only account for local estimations of biomass and NPP (Dong et al. 2003, Zheng et al. 2003). In order to quantify the terrestrial carbon storage and fluxes and to understand the underlying mechanisms of the eco-physiological processes modelling approaches based on remote sensing (Potter et al. 1993, Prince & Goward 1995, Knorr & Heimann 1995, Ruimy et al. 1996, Potter et al. 1999, Goetz et al. 2000, Cao et

al. 2002, Potter et al. 2003, Zeng et al. 2005) or on process-based biogeochemical relations have been developed (Foley et al. 1996, Kindermann et al. 1996, Friend et al. 1997, Cao & Woodward 1998b, Cramer et al. 2001, Sitch et al. 2003). The first group includes human influence based on earth observation, but only allows estimations since the beginning of digital satellite remote sensing in the early eighties. Biogeochemical modelling also provides high spatio-temporal resolution and permits to quantify future projections, but mostly lacks representations of human influence on the carbon cycle. Mechanistic carbon cycle modelling supports the need for realistic estimation of future CO_2 concentrations and global climate change.

This study contributes to the current knowledge about the terrestrial carbon cycle's variability and its regional patterns by coupling a process-based dynamic global vegetation model with 21 years of satellite-observed vegetation data providing a view at the world's carbon sources and sinks with good spatio-temporal resolution for the period of 1982 to 2002. As this model is forced with climatic parameters as well as with earth observation data, which reflects many aspects of human influence, it allows to give quantitative estimates of ecosystem carbon uptake and release, to identify the spatio-temporal patterns in the terrestrial carbon sink, and to reveal the underlying mechanisms and its main drivers. Only the CASA model approach (Potter et al. 1993, Field et al. 1995, Thompson et al. 1996, Potter et al. 1999, 2001) is able to produce similar estimations based on a different approach with remote sensing data, a light use efficiency (LUE) model and a soil model (Parton et al. 1993, Randerson et al. 1997).

Several modelling studies as well as measurements suggest that the terrestrial carbon sink increased from the 1980s to the 1990s (Battle et al. 2000, Bousquet et al. 2000, IPCC 2001, Bopp et al. 2002, Plattner et al. 2002, Houghton 2003a, House et al. 2003), but the causes and the spatial patterns are not well understood. Climate variability seems to be the most relevant factor for interannual changes in terrestrial carbon fluxes (Houghton 2000b, Schaefer et al. 2002, Zeng et al. 2005), influencing the most important of the contributing processes such as photosynthesis, autotrophic and heterotrophic respiration. Long-term investigations indicate that there are climatic and geological events which influence the global and regional carbon cycles particularly (Angert et al. 2004, Zeng et al. 2005, Peylin et al. 2005). The interannual variability of the CO_2 growth rate is highly correlated with the El Niño Southern Oscillation (ENSO) (Bacastow 1976, Keeling et al. 1995), but high uncertainties exist in the exact determination of the regional patterns and the underlying physical and biological mechanisms (Braswell et al. 1997, Kirschbaum 2000, Foley et al. 2002, Zeng et al. 2005). During El Niño events a tropics-wide release of carbon to the atmosphere due to reduced rainfall followed by lower GPP and NPP occurs. Often increased temperature additionally leads to a lower soil moisture and enhanced respiration carbon loss (Tian et al. 1998, Foley et al. 2002, Nemani et al. 2003, Zeng et al. 2005). During La Niña episodes the opposite occurs with wetter conditions

followed by a strengthened carbon uptake of the tropical biosphere. Volcanic eruptions such as those of Mt. Pinatubo (1991) or El Chichón (1982) influence the solar radiation budget due to enhanced aerosol input into the atmosphere leading to various effects in different latitudinal zones. It was proposed by Roderick et al. (2001) and Gu et al. (2003) that the tropics and the temperate zones became a stronger sink due to an enhanced photosynthesis induced by an increase in diffuse radiation. The boreal zone behaves different: NEP declines after the Pinatubo eruption due to cooler temperatures and a shortage of the growing season (Lucht et al. 2002). The strong El Niño/La Niña event of 1997 to 1999 as well as the post-Pinatubo period (1991 – 1993) will be analysed in more detail.

For the following analysis I used 0.5° resolution global monthly fPAR data from the AVHRR to constrain the Lund-Potsdam-Jena Dynamic Global Vegetation Model (LPJ-DGVM). The time series covers the period from January 1982 to December 2002 as derived from GIMMS version 3 NDVI at Boston University (Myneni et al. 1997). Post-processing was performed by interpolating data gaps and excluding pixels with snow cover to avoid masking of the vegetation signal. Corresponding wintertime values were reconstructed using a maximum-value criterion on periods defined by a +5°C phenological temperature threshold. The LPJ-DGVM combines the capabilities of biogeographical with those of biogeochemical models (Sitch et al 2003). The land surface water and carbon balances are computed on a daily basis, including feedbacks between photosynthesis and evapotranspiration. The model simulates dynamic processes on the ecosystem level such as primary production, carbon allocation, competition between plant functional types (PFTs), turnover of tissue, soil and litter carbon, and the occurrence of natural fires. The composition of vegetation is determined by the competitive dynamics of vegetation types. Model simulations in the standard mode are driven by monthly inputs of the climatic variables temperature, precipitation and cloudiness, yearly atmospheric CO_2 concentration, and soil type. After a thousand years spin-up, allowing the LPJ model to predict the potential vegetation composition of each pixel, the model was constrained by introducing the observed fPAR for 1982 to 2002, with the vegetation composition adjusts into the new constraint. By this method, carbon pools at the outset of the relevant simulations are in a realistic initial state. The fPAR value for each pixel was decomposed into fractions allocated to the PFTs present at each location. Winter values were used to determine the prevalent fraction of evergreen versus deciduous components. Evergreen and deciduous PFT composition and associated fPAR fractions were decomposed following the PFT composition estimated by the model. In agricultural areas, the model-predicted PFTs were replaced by a non-woody (C3 or C4 grass) PFT and constrained by satellite-observed fPAR, providing the human-caused patterns of planting and harvesting as well as the climate-controlled patterns of crop growth and senescence. Agricultural areas were defined to be 0.5° grid cells where the MODIS-derived 1x1 km global land cover dataset of 2001 produced by Boston University shows more than 42.5%

agricultural pixels giving a realistic global area of agricultural land use. Areas used for pasture and fodder production have also been considered by using the Special Report on Emission Scenarios (SRES, IPCC 2000) land cover data sets for the year 1970, which were produced with the IMAGE-2.2 model (IMAGE Team 2001).

This study aims at assessing terrestrial carbon stocks and fluxes at a global and regional scale, their variability over time and their interactions with the climate system. Terrestrial biosphere models are a necessary tool for such an assessment, and they promise more reliable results when data of vegetation status and its changes over time serve as input.

The brief review given above highlights a variety of approaches for assessing the terrestrial sources and sinks and the uncertainties of model results concerning the exact determination of the regional patterns and the underlying physical and biological mechanisms. This study presents an additional approach to carbon cycle simulation. It addresses the following questions:

- Is it feasible to couple a stand-alone dynamic vegetation model with 20 years of satellite-observed fPAR data without changing the model's inherent logical structure?
- Can carbon fluxes be simulated more accurately with this supporting spatio-temporal information on vegetation status?
- What is the effect of the satellite data input on the different carbon stocks and fluxes such as net land-atmosphere flux, net primary production, soil respiration, carbon released by fire, as well as soil and vegetation carbon stocks?
- Which processes contribute most to the changes in carbon fluxes? Several possible factors will be investigated: The additional accounting for human influence (agricultural areas, forest management and selective logging in natural vegetation areas), the reproduction of a more heterogeneous landscape with more open vegetation, changes of PFT distribution, and/or an improved seasonality?
- Which regions contribute in which way to the net terrestrial land-atmosphere flux?
- Which factors influence the variability of net ecosystem production?
- How does the terrestrial carbon cycle respond to anomalous climate events such as NAO or ENSO, on global and regional scales?

This study will demonstrate that the coupling between a process-based dynamic vegetation model and satellite-observed fPAR data is feasible and provides more reasonable results than the stand-alone model. The magnitude of carbon storage and fluxes is significantly reduced, now converging better with the results of several other studies (Andreae & Merlet 2001, IPCC 2001, Bopp et al. 2002, Cao et al. 2002, House et al. 2002, Plattner et al. 2002, Houghton 2003a, Nemani et al. 2003). The reduction occurrs predominantly for two reasons: the implementation of agricultural areas and a changed density of vegetation coverage inferred

from the satellite signal together with an improved seasonality capturing also very specialized or adapted ecosystems like savannas which are not included in the original model.

With this approach, new estimations of net ecosystem production (NEP), representing the terrestrial ability to uptake and release atmospheric CO_2, are determined and compared to several shortly published recalculations of the net land-atmosphere flux. Global carbon uptake of the terrestrial biosphere has increased by -0.54 PgC yr^{-1} between the 1980s and the 1990s, in agreement with the results of independent studies (IPCC 2001, Bopp et al. 2002, Plattner et al. 2002, Houghton 2003a, House et al. 2003). The Sahel and the Amazon regions contribute most to this change with uptake rates of -0.2 and -0.4 PgC yr^{-1}, respectively. These results underline the importance of protection of forests and of reforestation of semi-arid areas. In contrast to several studies that reported a positive trend in NPP (+0.4 PgC yr^{-1}) for the boreal zone, the current model results simulate a relative reduction of the net fluxes in somer regions during the 1990s. As soil respiration (Rh) has not decreased as much as NPP, the net fluxes have changed towards a weak source (+0.24 PgC yr^{-1}).

As the annual growth rate of atmospheric CO_2 is mainly determined by terrestrial carbon fluxes, its interannual variability will be analysed in comparison to the modelled carbon fluxes and the influence of climatic parameters will be investigated. On a global scale, NPP is the main contributor to the temporal trajectory of NEP and CO_2 growth rate variability which both show a range of variation between –2.5 and +2.7 PgC yr^{-1}. In contrast, its magnitude and timing are mainly determined by changes in Rh, whereas fire carbon variability follows NPP, balancing offsets produced by Rh. The interannual variability (IV) of NPP is predominantly determined by tropical regions and mainly responds to variations in precipitation. Also the positive trend in NPP is strongest in the tropics with 8.15 % increase for the period of 1982 to 2000, contributing 63.5 % of the global total. The temperate and boreal regions behave differently, showing a generally lower variability which is mainly determined by variations in NPP, which is controlled by changes in temperature. The carbon fluxes of the tropical and southern temperate regions are significantly sensitive to the ENSO cycle, resulting in a carbon release during the El Niño phase and carbon uptake in La Niña seasons. A significant tele-connection between the northern hemispheric regions and ENSO could not be found. The Northern Atlantic Oscillation (NAO) seems to have no influence on carbon cycles on a latitudinal scale. The years after the Pinatubo eruption show a decline of NPP within the more general trend of increasing NPP, which can be found in the boreal regions according to several studies (Myneni et al. 1997, Myneni et al. 2001, Zhou et al. 2001, Murayama et al. 2004). This reduction of NPP has been attributed to cooler temperatures and a resulting 2-year shortening of the growing season (Lucht et al. 2002). During this period, the temperate zone strongly uptakes CO_2 due to increased NPP additionally strengthened by a decrease of Rh. An analysis of the period with strongest warming during the investigated time series shows a globally

enhanced carbon sink composed by an increase in NPP and a less pronounced increase in Rh by 1.8 PgC yr^{-1} and 1.4 PgC yr^{-1}, respectively. The tropics and southern temperate region contribute most to this enhanced uptake although being offset by the land use change emissions. In the northern latitudes, although exhibiting a strengthened vegetation growth due to the accentuated warming in combination with the CO_2 fertilization effect, this is not reflected in a net terrestrial uptake, because the enhanced NPP is offset by soil decomposition increase.

Concluding, the current study will give a more detailed introduction into nature and scope of the carbon cycle problem and will demonstrate a suitable method to quantify it.

This thesis is organized as follows: Chapter 2 introduces into the current understanding of the terrestrial carbon cycle and into a variety of methods to infer terrestrial carbon balances including remote sensing techniques and modelling approaches. Chapter 3 presents the research questions and the method developed to investigate the problem. The results are given in chapters 4 to 6, addressing to spatial patterns of and temporal variations and trends in the terrestrial carbon cycle and to the influence of singular events on regional and global carbon storage and fluxes. The findings of this study will be summarized and discussed in chapter 7, leading to some general conclusions linking this approach to the current scientific research.

2. SCIENTIFIC BASIS

2.1 The terrestrial carbon cycle

2.1.1 Why is it important to look at the terrestrial carbon cycle?

One of the most intense human influences on the global environment is the increasing atmospheric CO_2 concentration since the beginning of the industrial revolution. In 1750, before the industrial era started, atmospheric CO_2 concentration was 280 ± 10 ppm. It has risen in the following 250 years to **367** ppm in 1999 (IPCC, 2001), **373,7** ppm in 2002 *(*Keeling & Whorf, 2004), **375.7** ppm in 2003, **377.4** ppm in 2004 and **379.9** ppm (Keeling & Whorf, 2005).

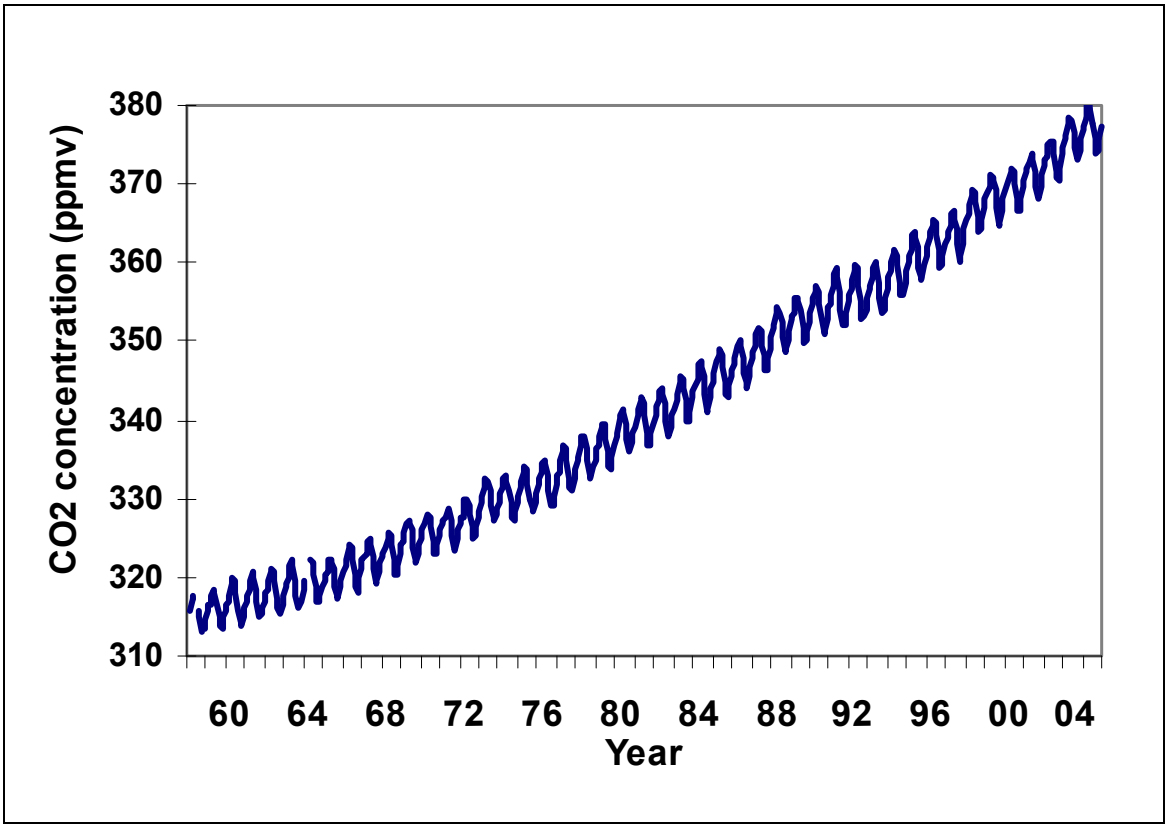

Fig. 2.1. The Mauna Loa record of monthly mean CO_2 concentration, 1958 to 2004 (Keeling & Whorf 2004).

Main consequence of the increase of atmospheric CO_2 is rising temperature and climate change in general. As the earth processes form a physically nearly closed system, which show cyclic behaviour, it is necessary to understand the cycles to be able to simulate the future behaviour of aspects of the Earth system, and design efficient strategies to cope with potential problems.

Fig. 2.1 shows the long-term increase and the seasonal cycle of atmospheric CO_2. The annual cycle is dominated by vegetation seasonality, and the intra-annual amplitude is most

pronounced in the records from the northern high latitudes. As most of the vegetated land surface is on the northern hemisphere, the CO_2 concentration lowers in late spring and summer when deciduous vegetation assimilates atmospheric carbon by photosynthesis. On the other hand terrestrial carbon is released from autumn to early spring, when atmospheric concentration reaches its maximum as decomposition exceeds carbon assimilation (Buchmann & Schulze 1995, Keeling et al. 1995 , Schimel et al. 1996).

As a consequence, the terrestrial biosphere plays a decisive role in the global carbon cycle and its interannual behaviour. Additionally, this role is strengthened due to the vegetation effects upon the planet's albedo and the water cycle, which both feed back to climate.

The increase of atmospheric CO_2 is mainly caused by anthropogenic emissions from fossil fuel burning, cement production and land use change, such as deforestation. Main contributor is the use of fossil fuels with 5.5 ± 0.5 PgC yr^{-1} (Schimel et al. 1995) in the 1980s, and 6.5 PgC yr^{-1} in the 1990s (IPCC 2001). Deforestation and land use change contributed 1.7 (0.6 to 2.5) PgC yr^{-1} (IPCC 2001): 1.99 ± 0.8 (Houghton 2003c) in the 1980s and 2.18 ± 0.8 PgC yr^{-1} in the 1990s (Houghton 2003a). This results in total anthropogenic CO_2 emissions of about 7.2 ± 1.6 PgC (1980s) and 8.68 PgC (1990s), though the net increase of atmospheric CO_2 is remarkably lower: 3.3 PgC yr^{-1} in the 80s and 90s (IPCC 2000). Several mechanisms and feedbacks provide an additional uptake obviously leading to a much lower CO_2 growth rate as expected. Measurements of carbon isotopes and atmospheric O_2/N_2 ratios suggest that 2.0 ± 0.8 PgC yr^{-1} are transferred to the oceans leaving 1.8 ± 1.6 PgC yr^{-1}, which are likely absorbed by the terrestrial system, referred to as the 'missing sink' (Broecker et al. 1979, IPCC 1994, Houghton 2003a). This missing sink is composed of land-use change processes such as forest re-growth on abandoned agricultural land in the mid-latitudes, and of ecological processes such as enhanced forest growth attributable to CO_2 fertilization, nitrogen deposition and response to climatic anomalies (Orr et al. 2001, Prentice et al. 2001, LeQuéré et al. 2003).

It is an important research challenge to investigate this missing sink because there is large uncertainty concerning its magnitude and its location (Fung 2000). The latter is particularly important concerning international emissions trading accompanying the Kyoto Protocol (1997). However, although carbon sinks are included in the Protocol which may be used to offset increases in emissions elsewhere, these sinks must result from „direct human-induced land-use change and forestry activities" (art. 3.3 and 3.4).

Though the topic of this study is the carbon cycle on land, for the purpose of completeness a brief excursus on the oceanic part of the global carbon cycle follows:

About one third of the anthropogenic released CO_2 is taken up by the ocean (Feely et al. 2004). Oceanic carbon uptake is principally driven by ocean circulation and carbonate chemistry and provides this large sink for atmospheric CO_2. A recent study of ocean tracer observations and the carbon system by the World Ocean Circulation Experiment (WOCE) and the Joint Global

Ocean Flux Study (JGOFS) indicates a total ocean uptake of anthropogenic CO_2 of about 118 ± 19 PgC between 1800 and 1994 (Wallace 2001, Feely et al. 2004, Sabine et al. 2004). The calculations of different ocean carbon-cycle models range between 1.6 and 2.4 PgC yr^{-1} for the 1980s (Orr et al. 2001, Prentice et al. 2001). For the 1990s a mean oceanic sink based on O_2 observations is estimated to be 1.9 PgC yr^{-1} (LeQuéré et al. 2003).

Rising atmospheric CO_2 -content and rising temperature influence the ocean's carbon uptake capacity. Uptake mechanisms are on the one hand based on ocean-atmosphere CO_2 partial pressure difference. Therefore, the uptake capacity declines with increasing CO_2 concentration due to reduced buffer capacity of the carbonate system. On the other hand, CO_2 solubility is also temperature dependent, e.g. warming reduces the solubility of CO_2 and therefore reduces uptake of CO_2 by the ocean (Watson et al. 1995). Also vertical stratification will increase with global warming followed by reduced outgassing of upwelling CO_2 and a reduced transport to the deep ocean which may be followed by changes in biological productivity (Sarmiento et al. 1998, Matear & Hirst, 1999). Furthermore, no significant fertilization effect could be detected, but a lower ocean pH could increase ocean CO_2 uptake by a few percentage points (Prentice et al. 2001).

It is also important to note that although the global atmospheric CO_2 growth rate shows a high interannual variability (Bousquet et al. 2000), the ocean flux variability remains relatively stable (Rayner & Law 1999, LeQuéré et al. 2000). Thus, the variability of the growth rate is mainly determined by changes of the terrestrial biosphere and its carbon pools (Conway et al. 1994, Battle et al. 2000). This will be discussed in detail in chapter 5.

2.1.2 Terrestrial carbon processes and components

Without disturbances or anthropogenic influences the net carbon balance of the biosphere is in a dynamic equilibrium of carbon uptake and carbon release, and is called net ecosystem production (NEP). Processes of carbon acquisition and storage are composed of photosynthesis, tree growth, plant aging and carbon accumulation in soils. Processes of carbon release are mainly the respiration of living biomass, decomposition of litter and organic soil components by microbial activity, oxidation of soil carbon, tree mortality, degradation and disturbances like fire, wind throw, diseases or animal influences.

Higher plants absorb up to about 40% of the carbon in the atmosphere by stomatal diffusion (Ciais et al. 1997). Based on ^{18}O measurements of atmospheric CO_2, an amount of 16 % (or about 120 PgC yr^{-1}) is assimilated through the process of photosynthesis to gross primary production (GPP) (Farquhar et al. 1993, Knorr & Heimann 1995, Ciais et al. 1997). One half of GPP is transferred into living biomass giving the net primary production (NPP) or annual plant

growth, the other half is respired by plant tissues and is released back to the atmosphere (Lloyd & Farquhar 1995, Waring et al. 1998).

Global terrestrial NPP is estimated to be about 60 PgC yr^{-1} (Ajtay et al. 1979, Cramer et al. 1999, Potter et al. 1999, Roy et al. 2001). Several methods contribute to these estimations: biomass measurement methods based on sequential harvesting (Hall et al. 1993, Dong et al. 2003, Zheng et al. 2003), as well as carbon flux estimations based on remote sensing (Potter et al. 1993, Ruimy et al. 1994, Knorr & Heimann 1995, Prince 1995, Prince & Goward 1995, Goetz et al. 2000, Cao et al. 2002, Zeng et al. 2005), or atmospheric CO_2 data based methods (Bousquet et al. 1999, Law 1999, Peylin et al. 1999, Rayner et al. 1999, Bousquet et al. 2000, Enting 2002, Rödenbeck et al. 2003a, Peylin et al. 2005). However, all of them imply large uncertainties.

Balancing the global carbon cycle, the carbon stored in vegetation is released to the atmosphere mainly by two processes: heterotrophic respiration (Rh) by decomposers, and disturbances such as natural or human-induced fires, wind-throw, diseases and insects.

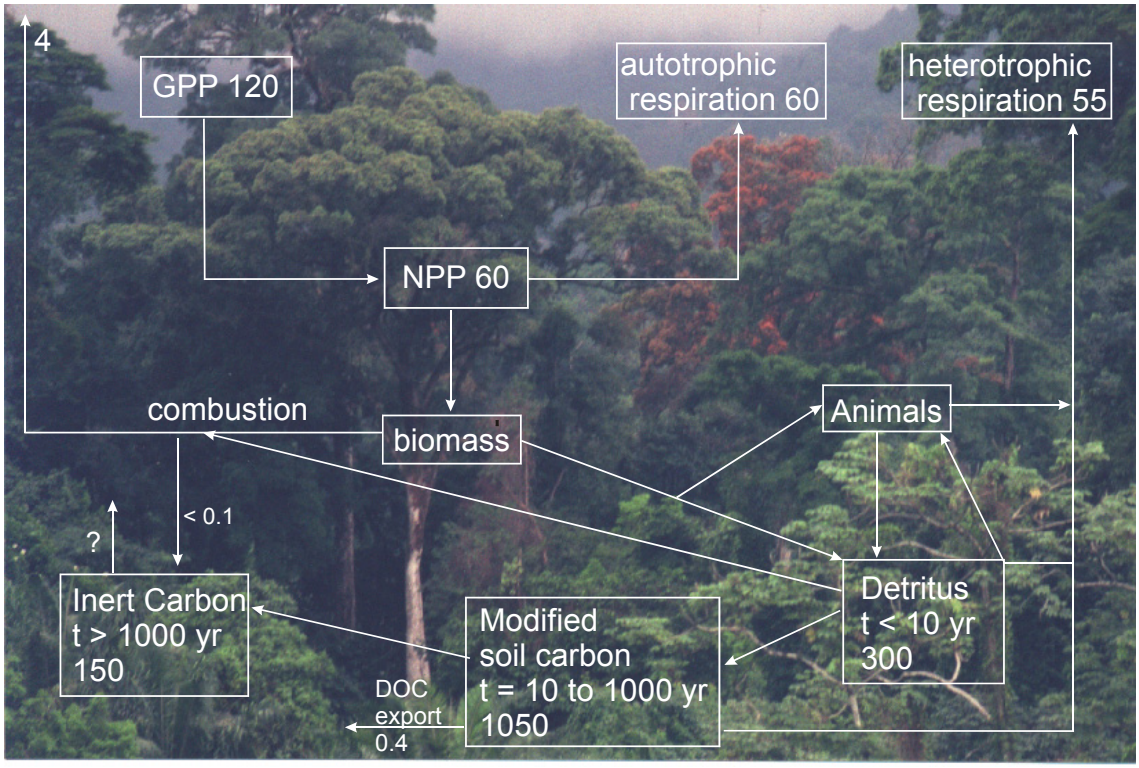

Fig. 2.2. Carbon cycling on land. Figures are given in PgC yr^{-1}.

By contrast with the ocean most carbon cycling on the land takes place locally within ecosystems. About half of GPP is respired by plants. The remainder (NPP) is approximately balanced by heterotrophic respiration with a smaller component of direct oxidation in fires (combustion). Through senescence of plant tissues, most of NPP joins the detritus pool: some detritus decomposes quickly (i.e. is respired and returned to the atmosphere as CO_2) while some is converted to modified soil carbon, which decomposes more slowly. The small fraction of modified soil carbon that is further converted to compounds resistant to decomposition, and the small amount of black carbon produced in fires, constitute the "inert" carbon pool. It is likely that biological processes also consume much of the "inert" carbon as well but little is currently known about these processes. Estimates for soil carbon amounts are from Batjes (1996) and

partitioning from Schimel et al. (1994) and Falloon et al. (1998). The estimate for the combustion flux is from Scholes and Andreae (2000). "t" denotes the turnover time for different components of soil organic matter (IPCC, 2001).

Decomposition of soil organic matter is temperature and soil-moisture dependent as well as controlled by the chemical composition of the dead tissues (Parton et al. 1993). Based on different turnover times soil organic matter is stored in several carbon pools. Short-term pools with a turnover time of less than 10 years consist of detritus and microbial biomass. The medium- to long-term pools with a decadal to centennial turnover time contain modified organic carbon. The inert fraction, although a very small fraction of the overall soil carbon, is composed of stable molecules resistant to further decomposition (Schlesinger 1990, Kuhlbusch et al. 1996).

Anthropogenic and climatic influences may alter the portion of carbon storage within the different pools, e.g. land management may modify soil organic matter and decomposition rates, or wood used for furniture can be seen as having a time-delay in decomposition. Most difficult and challenging to determine is the net ecosystem production (NEP), which is the difference between yearly NPP and Rh and other carbon losses, such as fire disturbances, harvesting, erosion and export of dissolved organic carbon (DOC) (IPCC, 2001). Under equilibrium conditions Rh and other carbon losses equal NPP (i.e. NEP = 0). Several studies show that the terrestrial carbon cycle currently acts as a sink, which means that the terrestrial biosphere accumulates more carbon than it releases (NPP > Rh + disturbances), on a global scale and over periods of decades (e.g. IPCC 2001, Schimel et al. 2001, Cao et al. 2002). Studies based on atmospheric measurements of CO_2 and O_2, as well as modelling experiments suggest a net terrestrial uptake of 0.2 to 0.4 ± 0.7 PgC yr^{-1} in the 1980s and 0.7 to 1.4 ± 0.7 PgC yr^{-1} in the 1990s (IPCC 2001, Schimel et al. 2001, Bopp et al. 2002, Plattner et al. 2002, Houghton 2003a, House et al. 2003).

Thus, the global terrestrial biosphere is currently acting as a sink of carbon, although human impacts such as deforestation contribute significantly to carbon release from the biosphere (see chapter 2.3). This sink removes a fraction of the anthropogenic CO_2 in the atmosphere, reducing the climate change impact of human activity. Therefore, it is important to understand the underlying mechanisms, as well as the spatial distribution of the sinks and their temporal variability.

This thesis contributes to meeting this scientific challenge by analysing and quantifying the spatial and temporal distribution of sources and sinks of the earth's biosphere using a validated global carbon model and direct earth observation data covering 21 years. A detailed modelling strategy is given in chapter 3.

2.1.3 Anthropogenic Impacts

Since ancient times the terrestrial biosphere has been subject to often intense human influences (Houghton 1991, Ramankutty & Foley 1998, Houghton 1999, Houghton 2000a, IPCC 2000, House et al. 2002, Houghton 2003c). Ten thousand years ago the earth's land surface was covered by half with forests (62 Mio. km²), whereas today the remaining area is only 28 Mio km² of closed forest and 12 Mio km² of open or disturbed forest (FAO 1992).

Direct anthropogenic impacts on vegetation include deforestation, land-use (mostly for farming and grazing), land-use change and (forest) management. Main contributor to atmospheric CO_2 rise besides fossil fuel emissions is land-use change. Houghton (2003c) estimates a long-term release of carbon to the atmosphere of about 156 PgC over the period 1850 to 2000. Almost 90 % of these emissions are due to deforestation and result in a 20 % decrease of global forested area (Houghton 1999). 60 % of the deforestation occurred in tropical areas, with a slight deceleration during the last years (Houghton 2000a), whereas in parts of Europe and North America abandoned agricultural land is reforested (FAO 1997, Reid et al. 2005). Forest management and land-use changes profoundly affect the capacity of soils and vegetation to store carbon. Regenerated forests store less carbon than undisturbed ecosystems, even if they are mature (Buchmann & Schulze 1999).

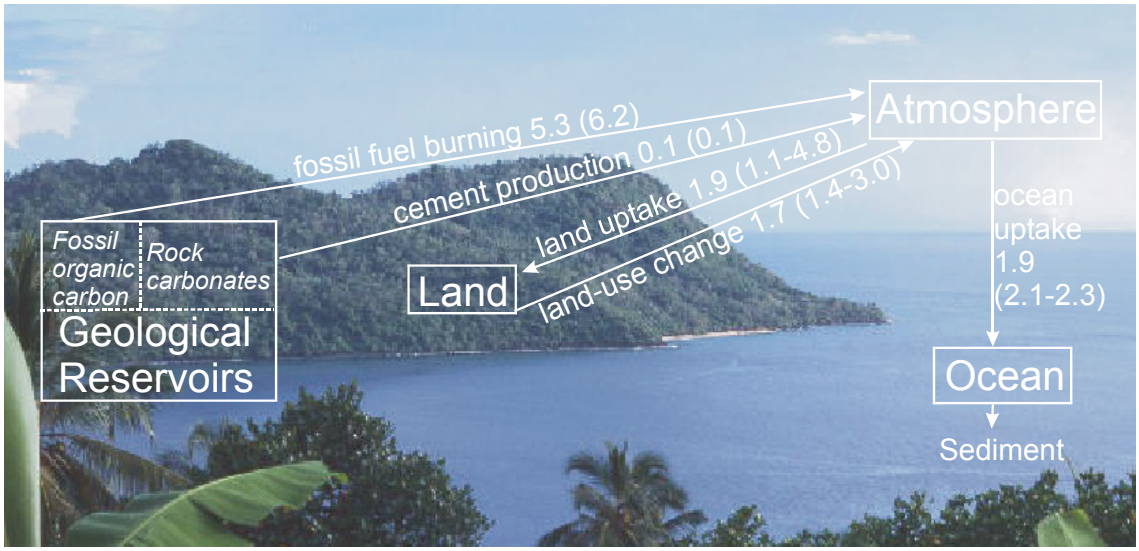

Fig. 2.3. The human perturbation (after IPCC 2001, enhanced with new figures).

Fossil fuel burning and land-use change are the main anthropogenic processes that released CO_2 to the atmosphere in the 1980s. Only a part of this CO_2 stays in the atmosphere; the remainder is taken up by land (plants and soil) or by the ocean. These uptake components represent imbalances in the large natural two-way fluxes between atmosphere and ocean and between atmosphere and land. (IPCC 2001). Figures for the 1990s are shown in brackets (derived from Plattner et al. 2002, House et al. 2003, Houghton 2003c, Bopp et al. 2003).

IPCC (2000) (from Houghton 1991) gives the following types of land-use change and management: conversion of natural ecosystems to permanent croplands, for shifting cultivation,

or to pasture, abandonment of croplands or pastures, harvest of timber and establishment of tree plantations. All those practices influence the carbon release more or less strongly. Management practices also affect soil conditions through slash-and-burn agriculture, tillage, erosion, overgrazing (negative effects, i.e. reduced carbon storage), or fertilization, crop rotation, preservation of wetlands, special forms of harvesting to retain organic matter (positive effects, i.e. enhanced carbon storage).

Indirect effects of anthropogenic impact on the carbon cycle include effects of climate change as well as fertilization effects on vegetation caused by rising atmospheric CO_2 content (Friedlingstein et al. 1995, IPCC 2001), and effects of anthropogenic nitrogen deposition (Townsend et al. 1996, Holland et al. 1997). Due to climate change, NPP may increase especially in marginal ecosystems and ecosystems with strong climatic constraints. Rising temperature may enhance water-stress in dry ecosystems, leading to a reduced NPP (Gerten et al., 2005). Arid and semi-arid regions are furthermore affected by changes in precipitation amount and patterns. Also the high latitudes are of distinct interest: In boreal and arctic regions, rising temperatures lead to an enhanced growing season and an increase in available growing degree days (Lucht et al. 2002). Boreal ecosystems store about 49 % of the world's carbon, of which 84% are stored as soil organic matter in their permafrost and seasonally-thawed soils (Malhi et al. 1999, White et al. 2004). Rising temperatures may advance thawing and increase thawing depth, increase heterotrophic respiration and contribute to an additional rise of atmospheric green-house gases, such as methane. On the other hand, a trend of a greening of the boreal zone is observed by remote sensing data and phenological observations (Myneni et al. 1997, Menzel & Fabian 1999, Myneni et al. 2001, Tucker et al. 2001) indicating a longer growing season and enhanced NPP, but which is nevertheless not enough offsetting enhanced soil respiration (Oechel et al. 1993, Schulze et al. 1999, Oechel et al. 2000, Lucht et al. 2002).

Another effect of rising atmospheric CO_2 is the so-called CO_2 fertilization effect, i.e. the enhanced photosynthesis due to an increased CO_2-uptake through the plant's stomata, which also allows an increased water-use efficiency, because transpiration and therefore water loss is reduced as a result of partially closed stomata (Field et al. 1995, Farquhar 1997, Körner 2000, Gerten et al. 2004)

2.1.4 Future projections

Climate change and rising atmospheric CO_2 concentration will significantly affect the future carbon cycle. GCMs driven by different emission scenarios simulate a global temperature rise in a range from +1.8°C to +6.4°C within a century, with strongest emphasis on the northern hemispheric high latitudes (IPCC 2001). Increases in rainfall over land amount between 6.5 % and 13.9 % until 2100 (Schaphoff et al. 2006). Possible response of the ecosystems can be

predicted by using DGVMs driven with climate change scenarios simulated by GCMs. During the first half of the 21st century most simulations predict increasing NPP and terrestrial carbon uptake due to the CO_2 fertilization effect (Cramer et al. 2001). Additionally, the magnitude of interannual variability of the carbon fluxes increases (Schaphoff et al. 2006). But after 2050 the ability of the terrestrial ecosystems to uptake carbon is reduced and the terrestrial biosphere is becoming a source (Cox et al. 2000, White et al. 2000, Joos et al. 2001, Dufresne et al. 2002, Jones et al. 2003). This is thought to be an effect of increased Rh and regional reductions of precipitation, which is followed by a shift in vegetation zones, e.g. some tropical forest areas will probably be replaced by grasslands (Cramer et al. 2001). Friedlingstein et al. (2003) suggest the climate impact on carbon cycle to release an amount of additional 280 ppmv of CO_2 into the atmosphere until 2100. But there are significant differences among the models concerning magnitude of the predicted changes and regional patterns. In the study of Schaphoff et al. (2006) the LPJ model was driven with several climate change scenarios and some regional patterns occur among all simulations: the boreal forest regions will become a source, whereas the Arctic and high-altitude ecosystems show increased carbon uptake due to a shift of vegetation zones into the cold regions. Tropical rainforest does not show a collapse across all simulations, but in the study of Cramer et al. (2004) some climate models produce a large carbon flux to the atmosphere due to increased drought stress caused by rising temperature and decreasing precipitation.

2.2 Satellite Earth observation of global vegetation

Since the 1960s, when astronauts had the first synoptic view of our blue planet, the use of space-based observations to understand the processes and patterns governing life on earth had been developed intensively, even though initially for military purposes. In the past two decades, satellite remote sensing methods have shown that land surface parameters can be remotely estimated from space with sufficient accuracy, providing a global view with a relatively high spatial and temporal resolution, which is not feasible from surface measurements or modelling. The development of vegetation indices, offering a relationship between spectral photon counts measured by an optical sensor and vegetation activity and status, has contributed substantially to different disciplines, including global change science. The approach pursued in this study adds a surplus to current knowledge as it transcends the deficiencies of remote sensing data and carbon cycle modelling: Satellite data only survey the above-ground conditions without considering any soil processes, while anthropogenic influence is included. A process-based global carbon cycle model accounts for all above- and below-ground carbon dynamics, but as it is based on climate and soil data input alone, it only represents a potential world without any human influence. The current approach utilizes the potentials of both techniques by combining the knowledge obtained by earth observation from space with a process-based global carbon cycle model, offering a synergistic use of a DGVM and remote sensing data. The results provide global, spatially and temporally explicit quantification of the earth's carbon cycle and its variability.

2.2.1 Instruments for vegetation monitoring from space

For the purpose of global vegetation observation and modelling a high spatial and temporal resolution of the acquired data is crucial. Several sensors have been developed in the last 20 years for vegetation monitoring. Especially optical systems with multiband-capability allow the detection of spectral properties of living or burnt vegetation. After more than three decades of optical systems, these properties are well known and data can be interpreted with sufficient reliability. Major disadvantages of all optical systems are cloud cover and effects from aerosols, which block or scatter the reflected radiance from the surface (see chapter 2.2.2). In the following section a selection of the most important passive satellite remote sensing systems appropriate for vegetation monitoring and operating in the visible part of the solar spectrum is discussed.

The *Landsat Multispectral Scanner (MSS)* was the world's first earth observation satellite sensor, launched onboard of Landsat-1 in July 1972. Over the following 21 years Landsat-1 to 5 continued the measurements of the earths spectral surface reflectance in four spectral bands

(visible and near-infrared at 80m spatial resolution) providing one of the longest and most extensive historical archives of satellite earth observation data. Landsat 6 failed to achieve orbit during launch, and forced the continued operation of Landsat 4 and 5. After 1982 the Landsat MSS was augmented by the new sensor *Landsat Thematic Mapper (TM),* which increased the data acquisition capability by providing three additional spectral bands (infrared and thermal) and a higher spatial resolution of 30 m (http://landsat.gsfc.nasa.gov/ project/satellite.html; http://landsat7.usgs.gov/outreach.html)). Landsat-7 orbits the earth at an altitude of 705 km with a sun-synchronous inclination at 98.3 degrees and a descending node at 10:00 a.m. (± 15 minutes equatorial crossing time). The repeating cycle is 16 days with 233 orbits/cycle, therefore total coverage of the earth is accomplished every 16 days. Therefore it produces data at lower temporal frequency as e.g. the AVHRR sensor, but at a higher spatial resolution. Thus, Landsat scenes are mainly applied in studies on local scale, and are widely used for vegetation mapping and monitoring, e.g. studies on land-use change (e.g. Cardille et al. 2002), vegetation structure (e.g. DeFries et al. 2002) and state (e.g. Sader et al. 1989, Steyaert et al. 1997), or for estimations of yields (e.g. Bach 1998) or timber volume (e.g. Trotter et al. 1997).

The National Oceanic and Atmospheric Administration's (NOAA) ***Advanced Very High Resolution Radiometers (AVHRR),*** of which data are used in this study, provide the required features such as global coverage, high spatial and temporal resolution.

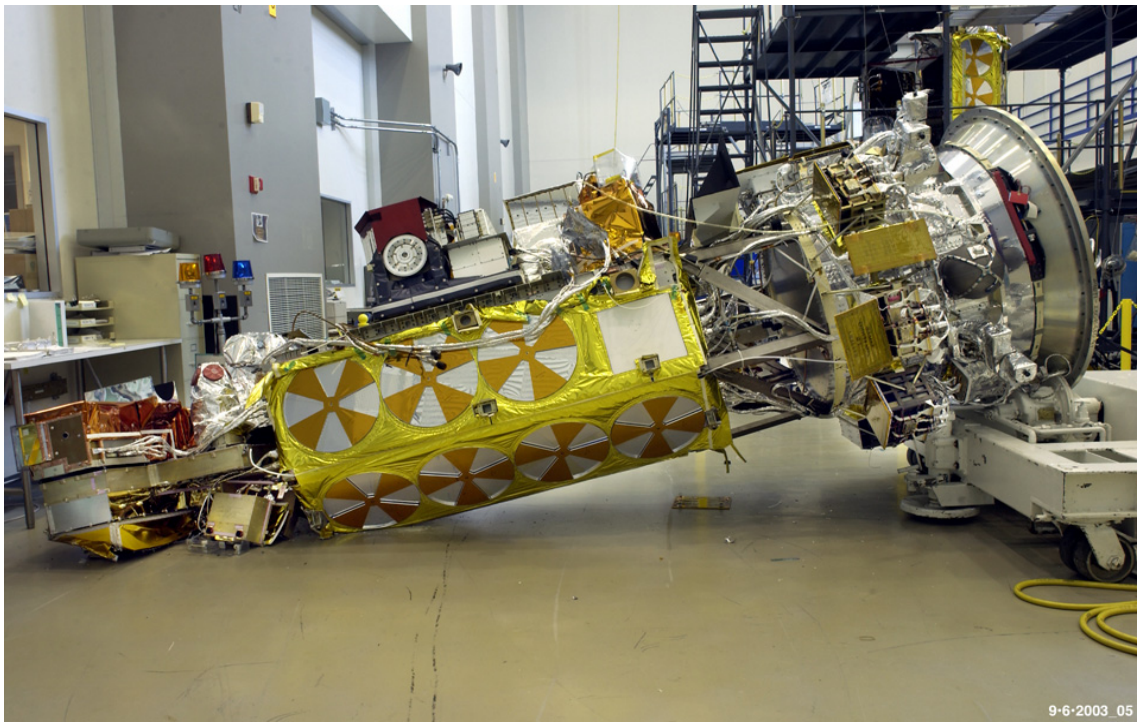

Fig. 2.4. One satellite of the NOAA-series with AVHRR sensor onboard, unfortunately broken down before launch.

The first AVHRR sensor useful for vegetation monitoring was launched on the NOAA-6 satellite in June 1979, featuring five visible, near-infrared and thermal infrared spectral bands (see table 2.1). Data series are available since 1981. The NOAA satellites carrying the AVHRR sensor orbit the earth sun-synchronously at an altitude of 833 km with an inclination of 98.9 degrees. It offers a 110.8° cross-track scan with a swath width of about 2,700 km, providing overlapping coverage. The repeating cycle is daily, and ground resolution is approximately 1.1 km at nadir. The daily cycle is possible with both daily and nightly coverage because usually NOAA maintains two operational satellites in complementary orbits. One crosses the equator at 07:30 a.m. and 7:30 p.m., and the other at 02:30 a.m. and 2:30 p.m. AVHRR provides data for mapping of day- and night-time cloud distribution, land-water boundaries, snow and ice extent, sea and land surface temperatures. The thermal infrared channels are calibrated in flight, whereas the channels 1 and 2 have no onboard calibration capabilities. They are calibrated only before launch and drift in sensitivity during operation. As the AVHRR was designed primarily as a meteorological sensor for NOAA's operational needs, observations of vegetation are not its original mission.

Channel	Resolution at Nadir	Wavelength (µm)	Typical Use
1	1.09 km	0.58 – 0.68	Daytime cloud and surface mapping
2	1.09 km	0.735 – 1.00	Land-water boundaries
3A	1.09 km	1.58 – 1.64	Snow and ice detection
3B	1.09 km	3.55 – 3.93	Night cloud mapping, sea surface temperature
4	1.09 km	10.30 – 11.30	Night cloud mapping, sea surface temperature
5	1.09 km	11.50 – 12.50	Sea surface temperature

Table 2.1. AVHRR/3 channel characteristics, first carried on NOAA-15, launched in May 1998 (http://noaasis.noaa.gov/NOAASIS/ml/avhrr.html)

Vegetation mapping and analysis from AVHRR data is based on a redefinition of the near-infrared and the visible red bands to correspond more closely with the absorption regions of vegetation, enabling suitable computation of the Normalized Difference Vegetation Index (NDVI, for a detailed description see chapter 2.2.4) (NOAA 1981, NOAA, 1985, Kidwell, K. et al. 1991, NOAA, 1994; http://edc.usgs.gov/guides/avhrr.html; http://noaasis.noaa.gov/NOAASIS/ml/avhrr.html). The NDVI computed on the basis of the AVHRR red and NIR channels has widely been used for vegetation analysis (Tucker et al. 1984, Box et al. 1989, Ruimy et al. 1994, Botta et al. 2000, Tucker et al. 2001). Besides the primary meteorological application of the AVHRR sensor, one main usage in environmental monitoring is global land

cover determination (Loveland et al. 2000). Although the AVHRR sensor only provides five spectral bands at coarse resolution, its high temporal resolution with daily global coverage and long time series and its low cost has made AVHRR-data the favored data used for monitoring seasonal and interannual changes in land cover mapping, vegetation analysis, agricultural assessment and land use change (Friedl et al. 2000, Hansen et al. 2000). Furthermore AVHRR data is suitable for the estimation of biomass and primary production on local and global scales (e.g. Box et al. 1989), seasonal patterns of vegetation (e.g. Spanner et al. 1990), or for monitoring of fires and its effects (e.g. Kasischke et al. 1993, Steyaert et al. 1997).
Nevertheless, substantial post-launch calibration and correction of the data is necessary (Slater et al. 1987, Rao 1993, Rao & Chen 1995). Most important source of error is aging of the satellite sensors causing degradation of sensitivity and loss of data accuracy.
However, AVHRR data is favourable for global use, because of its long-term availability, which cannot be provided by the improved but later sensors, and, compared to the Landsat product, its more practicable data volume. After having demonstrated its usefulness for ecosystem monitoring and analysis for over a decade, several similar sensors have been constructed in the 1980s and later, as follows:

The French Government started in 1986 the *Système Probatoire d'Obsérvation de la Terre (SPOT)* which carries a vegetation monitoring instrument since 1998. The sensors are two High Resolution Visible (HRV) imaging sensors with three visible and near-infrared spectral bands and an independent sensor for vegetation monitoring in the wavelength range of 0.43 to 0.47 µm. They acquire data with a wide-field scanning system similar to that used by the AVHRR, giving a daily global coverage with 1km ground resolution at nadir. The other sensors acquire data at 20 m resolution, and an additional panchromatic band provides 10m resolution and can be fused with Landsat Thematic Mapper data to combine the advantages of both systems into one image. SPOT observes the whole planet surface within a day, and orbits the earth at an altitude of 820 km and an inclination of 98.7°. It is also sun-synchronous and passes the equator at 10:30 a.m. local solar time. The orbit repeat cycle is daily, and off-nadir viewing is possible (http://www.spot-vegetation.com/home/quick/quick.html, Saint 1994, Saint 2000). SPOT-Vegetation data is particularly often used for fire monitoring (e.g. Tansey et al. 2004), further usual applications are land-use change and land cover type mapping (e.g. Bartalev et al. 2003, Stibig et al. 2003).

Aboard the Aqua and Terra Satellites of the Earth Observing System (EOS) initiated by the NASA the Moderate Resolution Imaging Spectroradiometer (MODIS) was launched in 1999 (Terra) and 2002 (Aqua). The two satellites orbit the earth sun-synchronously at an altitude of 705 km at 55 degrees with an ascending node at 1:30 p.m. (Aqua) and a descending node at 10:30 a.m. (Terra), providing global coverage every one to two days. The MODIS instruments scan 36 bands covering wavelengths from 0.4 µm to 14.4 µm. The first two bands have a

ground resolution of 250 m, five bands are imaged at 500 m, and the remaining bands have a ground resolution of 1 km. (http://modis.gsfc.nasa.gov/about/specs.html, http://modis-land.gsfc.nasa.gov/; http://cliveg.bu.edu/modismisr/index.html, Justice et al. 1998, Salomonson 1988). Evaluation of MODIS data is ongoing with a first focus on validation of the algorithms, indices and products (e.g. Cohen & Justice 1999, Townshend & Justice 2002). MODIS data is predominantly applied for snow cover mapping (e.g. Bussieres et al. 2002, Klein & Barnett 2003), and for meteorological purposes like temperature, cloud cover, atmospheric water vapour, aerosol and ozone detection (e.g. , Seeman et al. 2002, King et al. 2003). Terrestrial applications are measurements of surface albedo (Schaaf et al. 2002, Gao et al. 2005), fire location and monitoring (Justice et al. 2002, Giglio et al. 2003). The MODIS daily photosynthesis and annual NPP product (Running et al. 1999) was designed for practical applications like the measure of crop yield, range forage and forest production, and other economically and socially significant products of vegetation growth such as vegetation indices, leaf area and fPAR (e.g. Hansen et al. 2002, Huete et al. 2002, Myneni et al. 2002). Geobotanical applications focus on vegetation productivity in high spatial and temporal resolution (e.g. Reeves et al. 2001), or forest succession and regeneration (Lucas et al. 2002).

In 1996 and 2002 Japan launched the ADEOS-1, which was lost in 1997, and ADEOS-2 satellites (Advanced Earth Observing Satellite) carrying the *POLDER (Polarization and Directionality of the Earth's Reflectances)* and *GLI (Global Imager)* sensors. ADEOS orbits the earth sun-synchronously at an altitude of 802.9 km with a inclination of 98.69 degrees. Its descending node occurs at 10:30 a.m. and it has a repeating cycle of 4 days. The French POLDER sensor is a multi-spectral imaging radiometer/polarimeter and spans a wide field of view with 114 degrees and 2400 km swath width. POLDER was designed to achieve data about polarization, directional and spectral characteristics of solar radiation reflected by aerosols, clouds, oceans and land surface, as a basis for discrimination of the scattered radiation in the atmosphere from the radiation actually reflected by the earth's surface. It provides new opportunities in earth observation by measuring polarized reflectances from up to 14 directions along a single satellite pass (e.g. Lieferman et al. 1995). The sampled data contributes to research on aerosol-cloud-radiation interactions (e.g. Mukai & Sano 1999), global atmospheric water vapour content (e.g. Mukai et al. 2002), albedo effects (e.g. Jacob et al. 2002). Studies on the terrestrial biosphere predominantly consider research about the bidirectional reflectance distribution of land surfaces (e.g. Lacaze et al. 1999, Takemata et al. 2000). The GLI sensor was designed to observe oceans, lands and clouds with high accuracy with six 250-m-resolution channels and further 30 channels with a resolution of 1 km. In addition to the common visible and near to thermal infrared channels, GLI possesses also a near ultraviolet channel (0.38 μm), an oxygen absorption channel (0.76 μm) and the water vapour absorption channel (1.4 μm), which are used for atmospheric correction (http://sharaku.eorc.jaxa.jp/ADEOS2/sensor/

sensor.html; http://smsc.cnes.fr/POLDER/GP_satellite.htm; http://sharaku.eorc.nasda.go.jp/GLI/ov/sensor.html). Although the operation of ADEOS-II has stopped in October 2003, interesting data on vegetation dynamics, density and vitality for the northern hemisphere has been obtained (Yamamoto et al. 2005).

The sensor dedicated to vegetation monitoring aboard the European Space Agency satellite ENVISAT-1 (Environmental Satellite) is *MERIS (Medium Resolution Imaging Spectrometer*). The satellite was launched in 2002, orbiting the earth sun-synchronous at an altitude of 782 km with a 35-day repeat cycle and an inclination of 98 degrees. Its ground spatial resolution is 300 m, providing 15 spectral channels including visible and near-infrared spectral bands. MERIS allows global coverage of the earth every 3 days (http://www.esa.int/export/esaEO/SEMWYN2VQUD_index_0_m.html; http://envisat.estec.esa.nl/Satellite/instrument/MERIS/). MERIS was primarily designed for the monitoring of oceans and coastal areas, e.g. for oceanic water qualities through observing water color, leading to a greater understanding of the role of oceans and their productivity in the climate system (e.g. Rast & Bezy 1999). Additional objectives are atmospheric measurements of e.g. cloud cover, water vapor content and aerosols and it can also be used for land surface monitoring (e.g. Gobron et al. 2004).

This list of widely used optical sensors gives an impression of how broad the spectrum of earth observation is, even in the small field of vegetation monitoring. For the present study, the AVHRR sensor was chosen because of its long temporal availability associated with good spatial resolution and long-term experiences in post-processing procedures, as it is the only system that provides daily global coverage since the early 1980s.

2.2.2 Spatial and radiometric corrections of the satellite data

As already indicated, interactions between solar radiation and the atmosphere, target-sensor geometry, sensitivity degradation of the sensor over its lifetime, and changing orbital parameters of the satellite bias the measurements. These distortions are minimized by post-processing procedures, which are applied to the data before analysis and interpretation:

(1) Atmospheric effects

Atmospheric effects are absorption and scattering by gases and aerosols (Rayleigh scattering), affecting the surface reflectance measured by the satellite. Atmospheric aerosols increase atmospheric scattering and reduce the surface signal to the sensor, which also reduces the NDVI. Ozone and water vapour absorption affect the visible and NIR channels. Rayleigh scattering mainly influences the signal recorded in the visible channels and is more pronounced on low sun elevations and larger view angles. Aerosol scattering has an effect both on visible and NIR channels (Zhou et al. 2001). Therefore, during post-processing atmospheric correction is necessary, requiring data about vertical gaseous

contents and the optical depth of the atmosphere, which are based on measurements of atmospheric transmission under clear-sky conditions (Rahman & Dedieu 1994).

A main influencing atmospheric substance is water vapor: although the chemical composition of the atmosphere is relatively stable and its influence on scattering and absorption can be modelled and corrected, it is difficult to quantify the influence of atmospheric moisture, e.g. clouds and haze. Climate variations influence the water vapor content of the atmosphere, which is linked to temperature through evaporation and transpiration. Daily coverage and wide-angle view support increasing likelihood of obtaining a clear-sky view of the surface, but compositing procedures are necessary to create mostly cloud-free datasets. Usually, maximum NDVI-value compositing is used, where single images are combined over a period of 10 or 15 days, retaining only the most cloud-free pixel (max. NDVI) obtained in this period (James & Kalluri 1994).

(2) Land surface effects

Reflectances fluctuate depending on the viewing angles and on the surface cover types and season: e.g. reflectances at the margins of the swath are 2-4 times larger than at nadir (Cihlar et al. 1997). The amount of radiation received and reflected by the surface also varies dependent on the terrain relief: as the sensor scans across the swath, the top and side of objects are imaged and appear to lean away from the nadir point in each scan line. Reflected radiation fractions also vary due to the bidirectional anisotropy characteristic of most natural targets, which means that most surfaces reflect the radiation in various directions depending on surface properties. Therefore corrections using the seasonal bidirectional reflectance distribution function (BRDF) can be applied for each land cover type (Roujean et al. 1992, Wu et al. 1995).

(3) Sensor effects

As data values vary with the solar and observational angle of the sensor, which may also change during the period of satellite operation due to orbital drift, a geometric distortion requires correction. The data is calibrated using an orbit model with correction parameters for spacecraft orbit, attitude, velocity and altitude, earth rotation and curvature (Kaufman et al. 2000). Also variations in the sensitivity of the sensor to radiation influence the sensed data, but usually they are already calibrated onboard the satellite (Rao & Chen 1996). In order to correct the degradation of sensor sensitivity over time, the AVHRR data are calibrated against a desert target (Libyan desert and Takla Makan desert) with radiometrically stable conditions.

2.2.3 Remote Sensing of vegetation and spectral vegetation indices

An important objective of remote sensing analysis is to derive important vegetation and canopy characteristics from the measured radiance such as vegetation type, percentage of plant cover, absorbed photosynthetically active radiation (APAR), leaf area index (LAI), or biomass. The development of these parameters is guided by measurements of local "ground truth", also demonstrating that the underlying models are applicable on local and larger scales. Every surface has reflective properties distributed over a range of wavelengths. Ratios of reflectances at different wavelengths are used to detect e.g. the presence of vegetation and its status. Plants show a specific spectral behaviour, depending on their physiological status and photosynthetical activity.

As shown in Figure 2.5 healthy plants absorb light for their photosynthesis predominantly in the visible part of the spectrum (0.4 – 0.7 μm), especially red and blue light with a small reflectance maximum in the green light (0.5 μm). Vegetation strongly reflects light in the near-infrared part of the spectrum (0.7 – 1.3 μm). Mainly, the green chlorophyll and an array of related "antenna pigments" in the leaves absorb a large fraction of the visible light, and the mesophyll cells scatter light in near-infrared wavelengths. Inactive vegetation (winter deciduous trees) or dry vegetation does not show this spectral response, because of different water and pigment content and surface characteristics of the leaves (Albertz 1991, Barret & Curtis 1992).

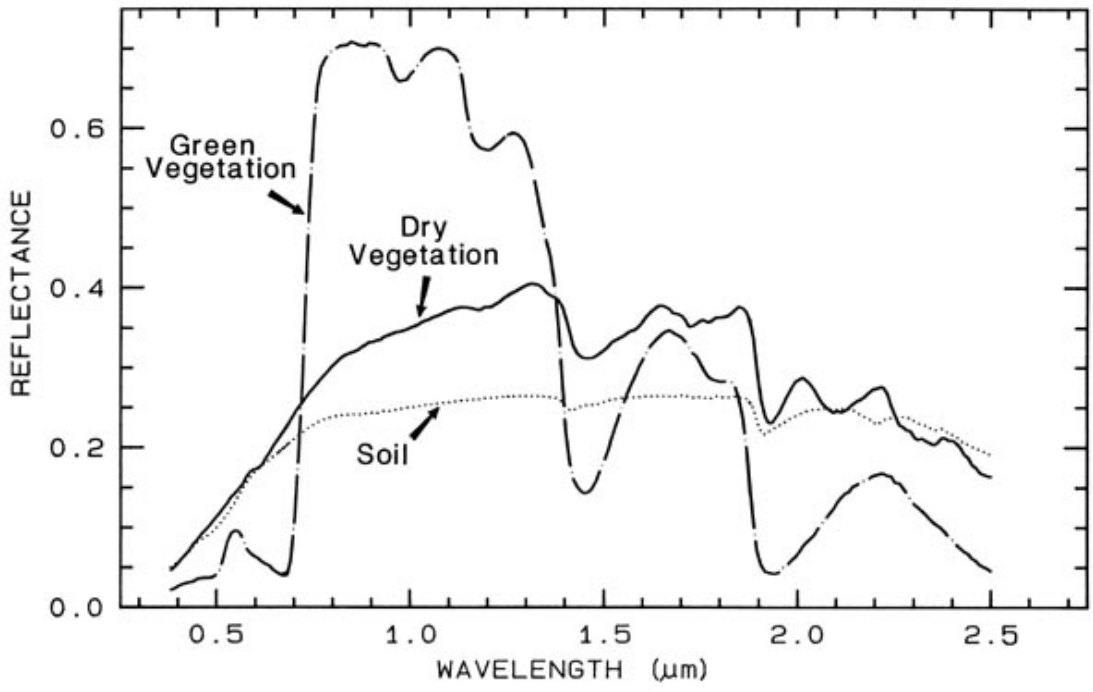

Fig. 2.5. Spectral reflectance of natural surfaces (Lillesand & Kiefer 1994).

Particularly, the canopy's Leaf Area Index (LAI), which is defined as the one sided green leaf area per unit ground area in broadleaf canopies, or as the projected needleleaf area per unit ground area in needle canopies (Monteith & Unsworth 1990, Scurlock et al. 2001), and other ecological variables are strongly correlated with vegetation indices (Cihlar et al. 1991). Spectral vegetation indices use the above-mentioned spectral characteristics of living plants by employing various techniques (summarizing, differencing, rationing, etc.) by combining two or more wavelengths. The Simple Ratio (SR) is computed as the ratio of AVHRR channel 2 (NIR) over channel 1 (red) reflectances (Rouse et al. 1974, Heimann & Keeling 1989, Potter et al. 1993). Huete (1988) proposed a Soil-Adjusted Vegetation Index (SAVI), which minimizes the influence of soil reflectance. It was developed to describe and quantify changes of vegetation status. Kaufman and Tanré (1992) developed a vegetation index that incorporates the effects of scattering of radiation within the atmosphere, the Atmospherically Resistant Vegetation Index (ARVI). The Global Environment Monitoring Index (GEMI) was developed by Pinty and Verstraete (1992) to specifically investigate AVHRR data. It corrects atmospheric influence by a non-linear combination of red and near-infrared wavelengths, and provides increased independence of atmospheric disturbances. Empirical evidence supports the hypothesis that the vegetation indices are related to vegetation parameters such as leaf area index (LAI), vegetation cover, radiation absorption, canopy photosynthesis and conductance (Hall et al. 1992).

2.2.4 The Normalized Difference Vegetation Index (NDVI) and FPAR

The most widely used vegetation index is the Normalized Difference Vegetation Index (NDVI) (Rouse et al. 1974, Tucker 1979, Justice et al. 1985). It is a measure of the greenness of vegetation, and it is related to a number of ecological variables, e.g. the fraction of vegetation cover and leaf area index (Cihlar et al. 1991). It is defined as a non-linear transformation of the red and near infrared (NIR) channels:

$$NDVI = \frac{\rho_{NIR} - \rho_{\mathrm{Re}\,d}}{\rho_{NIR} + \rho_{\mathrm{Re}\,d}} \qquad (1)$$

Where ρ is the reflectance in either the red (channel 1: 0.54-0.68 µm) or near-infrared (channel 2: 0.73-1.10 µm) spectral band of the AVHRR sensor, respectively. As shown in fig. 2.5 green vegetation absorbs most of the red light and NIR reflectance is very high. Almost all other surface types do not exhibit this spectral signature. The values of the NDVI range from -1 to +1, the NDVI for green active vegetation is higher than 0.4, highly vegetated surfaces are characterized by values of NDVI ~ 0.8. Soil and snow have NDVI values of -0.2 to 0.2, stressed or minimal vegetation has an NDVI of about 0.2 to 0.4.

The combination of the red and infrared channels in a ratio or difference allows the separation of vegetation growth from the background signal, as it enhances the contrast between soil and vegetation and reduces the influence of scattering radiation (Baret & Guyot 1991, Gutman & Ignatov 1998), although variations in soil brightness may produce variations in NDVI from one image to another (Liu & Huete 1995). Moreover, the NDVI ratio between bands reduces variations caused by surface topography and viewing geometry (Holben & Justice 1981). Effects that influence the satellite images such as atmospheric effects and geometric distortion tend to reduce the NDVI. Therefore NDVI maximum value compositing is a method for selecting the best observation (highest value) over a given compositing period.

A large number of models base on the relationship of NDVI to leaf area and leaf reflectances depending on the horizontal and vertical distribution of leaves in a canopy as well as the reflective properties of the underlying soil (Asrar et al. 1984) providing the amount of radiation intercepted by the photosynthesis process in plants (Asrar et al. 1984, Cihlar et al. 1991). Theoretical considerations by Myneni et al. (1995b, 1997) show that the NDVI within a canopy is directly connected to leaf chlorophyll content in the canopy, providing a causal explanation for the empirical findings.

Not all incoming radiation is absorbed by vegetation for biomass production and photosynthesis. The portion of the electromagnetic spectrum useful for photosynthesis (400-700 nm) is called photosynthetically active radiation (PAR). PAR is linearly related to the NDVI (Asrar et al. 1984). FPAR (the fraction of photosynthetically active radiation), the amount of light absorbed by the canopy for photosynthesis, is related to the productivity of vegetation and is an important variable of most biosphere-atmosphere models (Bonan 1995). In remote sensing, fPAR depends on architecture and optical conditions of the canopy and the background reflectance. Two major estimation techniques for deriving fPAR from satellite data have been developed. The first is the use of empirical relationships between LAI/fPAR and vegetation indices like the NDVI (Asrar et al. 1985, Sellers et al. 1992, Chen and Cihlar, 1996). E.g. Asrar et al. (1992) have been suggested the NDVI to be linearly related to FPAR, but depending on the soil background brightness and view and sun zenith angles. Empirical methods are easy to use, but they are often site- and sensor-specific and therefore not applicable for global evaluation (Tian et al. 2000). An empirical relationship does not necessarily imply a causal relationship (Myneni et al. 1995b). The second category of techniques includes radiative transfer models, which describe the radiative regime of canopies, including the distribution of vegetation elements, i.e. canopy architecture on the leaf-level. Their limitations are the relatively complicated application and these models do not account for the hot-spot effect, which has to be calculated separately (Zhang 2001). (A hot-spot effect occurs, when the scanning vector of the sensor is in the same direction as the position of the sun, followed by stronger reflectances from the surface so that parts of the satellite image appear to be brighter

than others.) Myneni and Williams (1994) found a causal relationship between NDVI, LAI and the fPAR depending on vegetation class and ground cover, respectively. Their transfer model is dependent on pixel heterogeneity, plant leaf area, and variations in leaf orientation, and sensitive to background, atmospheric, and bidirectional effects. Myneni et al. (1997b) developed an enhanced three-dimensional radiative transfer model to convert atmospherically corrected NDVI datasets into fPAR. It is based on the assumption that NDVI is related to the derivative of surface (or canopy) reflectance depending on the wavelength (Myneni et al. 1995a). Additionally, it accounts for the fact that light decays exponentially with deeper penetration into the canopy through successive absorption and scattering depending on vegetation type.

Based on the above mentioned assumptions and models, Myneni et al. (1997b) developed the dataset of global fPAR dataset used here, using the long-term time series of the AVHRR satellite derived with their radiative transfer model based on the relationship between NDVI and the photosynthetically active radiation.

2.3 Computer modelling of global vegetation

A number of approaches is used in the literature to estimate the terrestrial release and uptake of atmospheric CO_2. They are based either on measurements or on computational modelling, and vary in their ability to estimate the different flux components as well as in their spatial and temporal coverage.

(1) **Forest inventories** provide local estimates of biomass and NPP, but require dense spatial sampling if larger areas are to be quantified, and their temporal coverage is only intermittent (Dong et al. 2003, Zheng et al. 2003).
(2) Measurements of **eddy-fluxes** provide data with a high temporal resolution of all important carbon cycle components (NEP; NPP and Rh inferred), but these are taken only at a limited number of sites and at certain biomes around the world, and are difficult to generalize (Valentini et al. 2000, Barford et al. 2001).
(3) **Inverse modelling** of global measurements of atmospheric CO_2 content provides estimations of continental-scale NEP as a highly resolved time series since the 1980s, but only with a coarse spatial resolution of several thousand kilometers (Bousquet et al. 1999, Law 1999, Peylin et al. 1999, Rayner et al. 1999, Bousquet et al. 2000, Enting 2002, Rödenbeck et al. 2003a, Peylin et al. 2005).
(4) **Remote sensing approaches** combine light use efficiency (LUE) formulations for vegetation with earth observations and therefore utilize satellite data's high spatial resolution and time series since the 1980s. This combination of modelling and observational data allows to estimate all important carbon cycle fluxes (Potter et al. 1993, Knorr & Heimann 1995, Prince & Goward 1995, Ruimy et al. 1996, Potter et al. 1999, Goetz et al. 2000, Potter et al. 2003).
(5) **Biogeochemical modelling** based only on climate input variables also provides high spatial and temporal resolution, but it lacks quantification of the human influence on the carbon cycle. An advantage of biogeochemical models is that they can be forced with GCM scenarios (General Circulation Model scenarios) to give estimates of potential future developments of the terrestrial carbon cycle (e.g. Foley et al. 1996, Kindermann et al. 1996, Friend et al. 1997, Cao & Woodward 1998b, Cramer et al. 2001, Knorr & Heimann 2001, Sitch et al. 2003, Zeng et al. 2005).

In this thesis an approach is developed which combines using a biogeochemical model and remotely sensed earth observation data. By combining these two approaches improved estimates of global carbon fluxes are expected from a determination of the terrestrial carbon uptake and release and its spatio-temporal variability.
As mentioned above, three modelling approaches, relevant to this study, are discussed in detail in the following section, two different modelling systems account for global carbon pools and

fluxes, based either on remote sensing or biogeochemical modelling, and a third branch uses CO_2 flux measurements in combination with atmospheric transport models to detect regional sources and sinks of atmospheric CO_2.

2.3.1 Remote-sensing approaches

In the light use efficiency (LUE) approach, satellite observations, specifically the satellite-derived fraction of canopy-absorbed photosynthetically active radiation (fPAR) or various vegetation indices, are related to biological productivity on a global scale by semi-empirical functions. Monteith (1977) found that throughout several crop types and environmental conditions, the relationship between NPP and absorbed solar radiation during a growing season is linear. These findings have led to a generation of 'efficiency' NPP models combining LUE with various environmental parameters. Supplementary, some models presume that the fraction of incoming PAR absorbed by the vegetation is determined by the direction of incoming radiation, the proportion of diffuse radiation in the global radiation and its hemispheric distribution, the spectral properties of the optical elements (leaves) and the spatial distribution of these elements and the structure of the canopy (leaf area index, leaf angels) (Ruimy et al. 1994). Nevertheless, often the more simple linear relationship between fPAR and vegetation indices is used (Potter et al. 1993).

In the production efficiency concept, NPP is defined as the product of intercepted solar radiation used by the vegetation for photosynthesis (Monteith 1972, 1977), which is additionally modified by several reduction factors such as temperature or water stress. At first, a potential conversion efficiency or carbon yield is applied, which is expressed by the fraction of PAR converted into dry organic matter:

$$NPP\ (t) = e\ (t) * fPAR\ (t) * PAR\ (t) \qquad (2)$$

where t = time; PAR = incoming photosynthetically active radiation, $fPAR$ = fraction of photosynthetically active radiation absorbed by the canopy, and e = conversion efficiency of absorbed fPAR into dry organic matter. e differs among vegetation types and environmental conditions, and is usually derived from literature and often systematically adapted (Running & Hunt 1993, Ruimy et al. 1994). E.g., mean e is lower for forests than for grasslands in the same latitudinal zone, and e for forests increases from the equatorial to the boreal zone. Furthermore, e decreases with increasing biomass and temperature, which could result from an increasing fraction of assimilates lost through autotrophic respiration (Ruimy et al. 1996). In the modelling process, the maximum possible efficiency is then further reduced by temperature and water stress. The calculation of these reductions ranges from simple reduction factors to differentiated modelling approaches. Thus, temperature stress can be expressed as reduction

terms at very high and very low temperatures (e.g. described by an asymmetric bell shape) with an optimum temperature defined as the air temperature in the month when NDVI reaches its maximum (Potter et al. 1993). The water stress factor can be derived using reduction factors determined by potential and actual evapotranspiration. Some models additionally account for below-ground NPP or biomass by either using a ratio of above-ground NPP or applying a fully coupled soil carbon model.

The different modelling approaches vary in the way they handle the different processes. TURC (**T**errestrial **U**ptake and **R**elease of **C**arbon; Ruimy et al. 1996) only accounts for above-ground biomass and NPP. It is based on the hypothesis that the variation of the relationship between NPP and absorbed radiation is mainly determined by the loss of assimilates through autotrophic respiration, whereas the relationship between GPP and absorbed solar radiation is constant.

GLO-PEM (**Glo**bal **P**roduction **E**fficiency **M**odel; Prince & Goward 1995, Goetz et al. 2000) derives a canopy photosynthetic efficiency from leaf-level measurements. GPP is derived from absorbed PAR and a potential carbon yield of absorbed energy following the approach of Kumar & Monteith (1982). This model does not consider below-ground biomass. Among all remote-sensing based models GLO-PEM is unique, because all input variables are satellite-derived (PAR, water vapour, AVHRR channels 1, 2, 4, and 5, mean air temperature).

The SDBM (**S**imple **D**iagnostic **B**iosphere **M**odel, Knorr & Heimann 1995) also uses satellite data for determining vegetation greenness and phenology, and a one-layer bucket model which enables to calculate evapotranspiration and a drought-stress indicator. The model was tested against CO_2 measurements and a coupled photosynthesis-hydrology scheme, which detects feedbacks between drought-stress and photosynthesis through modelling of the soil water.

One primary purpose of BETHY (**B**iosphere **E**nergy-**T**ransfer **Hy**drology Scheme, Knorr 1997, 2000) was to test the performance and uncertainties of a number of different model setups by using different modelling strategies, input datasets and parameters (Knorr & Heimann 2001a & b). In order to explore the differences in NPP calculations, the model can be run with two photosynthesis schemes, either based on the approach of Farquhar et al. (1980) and Collatz et al. (1992), or on a light use efficiency approach based on Monteith (1965). Satellite data is used for a basic vegetation map and a vegetation index (GEMI) is translated into fPAR by a radiative transfer model.

SiB2 (**Si**mple **B**iosphere Model vers. **2**, Sellers et al. 1996a, 1996b) was specifically designed to revise vegetation parameters derived from remote sensed data. It is based on a SVAT scheme (Soil-Vegetation-Atmosphere-Transfer) which simulates matter and energy transfer in a "bottom up" approach, integrating processes on the organ level into a model of vegetation structure, microclimate, soil and hydrological exchanges. This vertical multi-layer approach is mainly suited for local investigations and requires a wide range of measured input parameters. By using remote sensing data as input, SiB2 calculates the fluxes at the leaf level, which are

afterwards integrated over the canopy. The use of satellite data here is to calculate surface parameters determining spatial and temporal dynamics of phenology. In contrast to most of the LUE models, no linear relationship between canopy light APAR and NPP is presumed.

A more sophisticated approach is the CASA model (**C**arnegie-**A**mes-**S**tanford-**A**pproach) which is also based on the LUE concept of Monteith (1972), but it is enhanced by a soil model (Parton et al. 1993, Randerson et al. 1997) which calculates Rh as a climate-dependent function of carbon in the system (Potter et al. 1993, Field et al. 1995, Thompson et al. 1996, Potter et al. 1999, 2001). It has been improved continuously since its first development in 1993. E.g., the LUE term has been calibrated against NPP measurements (Potter et al. 1993) and satellite data (Sellers et al. 1994); evapotranspiration has been connected to water content in the soil profile layers (Potter 1999); soil fertility factors have been implemented (Potter 1999), and the fPAR derivation by using a linear NDVI relationship has been replaced by canopy radiative transfer algorithms (Potter et al. 2003).

Advantage of these models is their direct relation to vegetation observation by satellite. Therefore, they are based on realistic figures of seasonality, intensity of vegetation activity and surface coverage. Their disadvantage is their temporal restriction to available satellite images and their sensors; the earliest global coverage began with the AVHRR sensors in 1981. Furthermore the observations are restricted to above-ground information. The second major component determining the land carbon balance, the soil carbon processes, are not accessible to direct observations. If at all, statistical relationships or process-based formulations are used.

2.3.2 Global biogeochemical models

The global carbon cycle can also be modelled by considering biogeochemical fluxes and processes explicitly.

All existing models vary in their approach how they account for photosynthesis and net primary production, in their complexity and their focus on different questions. In most models photosynthesis is calculated following either the biogeochemical approach of Farquhar et al. (1980) and Collatz et al. (1992) (SiB2, DOLY, IBIS-2, HYBRID, CEVSA, LPJ, BIOME-4), or a simplified version without the parameterization of enzyme kinetics (TEM, BIOME-BGC, FBM), or the models follow the concept of Monteith (1965) or Monsi & Saeki (1953), where the photosynthetic capacity of a canopy is dependent on leaf nitrogen distribution and light transmissivity (CASA, TURC, GLO-PEM, SDBM). TRIFFID uses a modified approach following Cox et al. (1998), where the photosynthetic rate is related to PAR, relative humidity, temperature and CO_2 concentration at the leaf surface. BETHY uses an approach after Asrar et al. (1992), where NPP is the product of absorbed solar radiation and a LUE, with the degree of absorption estimated from satellite data. Furthermore, NPP can be simulated as an empirical correlation to temperature and precipitation after Lieth (1977) (HRBM, SLAVE).

Two main branches can be distinguished: models of seasonal biogeochemical fluxes (or terrestrial biosphere models (TBMs)) and process-based dynamic global vegetation models (DGVMs). The first group simulates carbon, water and nutrient interactions within ecosystems and incorporates descriptions of all key processes. The approaches encompass the range from empirical regressions to models capturing photosynthesis and respiration via explicit mechanistic formulations, but their disadvantage is that they rely on prescribed vegetation distribution maps, hence do not consider changes in environmental conditions that lead to dynamic (e.g. time-lag) effects.

Some examples of such models are GTEC (**G**lobal **T**errestrial **E**cosystem **C**arbon; Post et al. 1996, King et al. 1997), HRBM (**H**igh **R**esolution **B**iosphere **M**odel; Esser et al. 1994), FBM (**F**rankfurt **B**iosphere **M**odel, Luedeke et al. 1994), TEM (**T**errestrial **E**cosystem **M**odel, McGuire et al. 1995, 1997, Tian et al. 1999), CENTURY (Parton et al. 1992, Metherall, 1993), CARAIB (**CAR**bon **A**ssimilation **I**n the **B**iosphere, Warnant et al. 1994, Nemry et al. 1996), SLAVE (**S**cheme for **L**arge scale **A**tmosphere **V**egetation **E**xchange, Friedlingstein et al. 1995), and CEVSA (**C**arbon **E**xchanges in the **V**egetation-**S**oil-**A**tmosphere System, Cao & Woodward 1998b, Cao et al. 2002). For a full listing of all mentioned models, their approaches and input variables see tab. 4.1.

These models simulate carbon and water fluxes (some of them also nitrogen fluxes) on an hourly or daily time scale. But they vary strongly in their approaches, having been developed for different purposes. The CENTURY model, e.g., was designed to simulate soil organic matter dynamics and nitrogen processes of grasslands and agro-ecosystems, and as this is not feasible without modelling the above-ground biomass, a vegetation module was incorporated. CARAIB, HRBM, and TEM have been developed to calculate the impacts of climatic changes and rising CO_2 on carbon fluxes at the ecosystem level. HRBM takes into account the human factor in the carbon cycle by using land-use, land-use change, and population density maps as input. It is based on relations derived from regression analysis after the MIAMI model of Lieth (1975), who related annual NPP to mean annual temperature and annual precipitation. Soil and litter carbon is calculated using depletion coefficients based on monthly values of temperature and humidity. TEM applies plant physiological relations and differs in the way it combines carbon and water fluxes using the inputs of a separate water balance model. GPP is calculated as a function of light availability, air temperature, atmospheric CO_2 concentration, moisture availability and nitrogen supply.

The models also differ in their structure of calculating biospheric carbon: the HRBM model provides two pools of ‘living’ and eight pools of ‘dead’ biomass, whereas the FBM only has two pools of ‘living’ and one pool of ‘dead’ carbon, and TEM one pool each. However, two pools of ‘living’ biomass including woody and herbaceous plants are the minimum requirement for a realistic consideration of the carbon cycle and the effects of climate and CO_2 rise on the

biosphere. SLAVE particularly focuses on the long-term response of the biosphere to elevated CO_2 and therefore it contains a fertilization factor submodel. NPP is calculated empirically correlated to temperature and precipitation after Lieth (1975), and it is further limited by nitrogen, phosphorus and soil moisture availability. The CEVSA model of Cao et al. (2002) is designed in a modular form accounting for biophysical and biogeochemical processes including a photosynthesis scheme after Farquhar et al. (1980) as well as carbon allocation and turnover, decomposition of organic materials and nitrogen input, and vegetation distribution. It only lacks a dynamic component.

Most of the models were designed to generally enhance understanding of the role of terrestrial ecosystems in the global carbon cycle. They differ in the way they treat assimilation of carbon by plants, water cycle, and soil carbon processes, as well as in their temporal resolution, and whether they take into account snow cover, nitrogen or seasonality.

2.3.3 Dynamic global vegetation models (DGVMs)

DGVMs equally contain numerically descriptions of processes, but they additionally consider changes in ecosystem structure and composition over time. The reason why DGVMs have been developed is that in view of a changing and varying climate and rising atmospheric CO_2, it became obvious that transient changes in vegetation structure and distribution need to be accounted for (Cramer et al. 1999). This new challenge is handled with plant functional types (PFTs), which compete with each other for water, light and nutrients, and which respond to disturbances like fire. Thus, they simulate a mosaic where different PFTs establish, grow and die again or which could be displaced by other types under changing conditions.

The LPJ-DGVM used in this study is a DGVM of intermediate complexity applicable to a wide range of global problems. It computes terrestrial carbon and water fluxes on a pseudo-daily basis, including feedbacks between photosynthesis and transpiration through canopy conductance based on the concept of Farquhar et al. (1980) and Collatz et al. (1992). The approach follows principally the light use efficiency concept, but internally predicts *e* from environmental variables (Sitch et al. 2003). Ecosystem-level processes are interactively coupled on a yearly time step, including primary production (GPP, NPP), carbon allocation to above- and below-ground carbon pools, turnover of tissue, soil and litter carbon, competition between plant functional types (PFTs) for light and water, population dynamics, and the natural fire regime (Sitch et al. 2003). The nitrogen cycle is not explicitly modelled, but it is implicitly accounted for by the ‘strong optimality’ hypothesis, which assumes that maximum NPP is dependent on variations in plant nitrogen content (Dewar 1996). A more detailed model description is given in chapter 4.2.1.

In the following, other DGVMs based on mechanistic coupling of water and carbon cycle processes are briefly mentioned.

IBIS-2 (**I**ntegrated **Bi**osphere **S**imulator, Kucharik et al. 2000), is an improved version of the prototype model IBIS-1 developed by Foley et al. (1996). In contrast to most TBMs and DGVMs, the photosynthesis-stomatal conductance module (after Farquhar et al. 1980 and Ball et al. 1986) is based on a big-leaf-approach calculated for a leaf at the top of the canopy, which is then scaled up proportional to the vertical profile of APAR within the canopy (Kucharik et al. 2000). The diurnal cycle is resolved in 60 min time-steps. IBIS-2 represents vegetation cover as a collection of 12 plant functional types, including eight tree, two shrub and two grass types. The soil biogeochemistry is based on a eight soil layer formulation with four carbon pools including microbial biomass determining heterotrophic respiration. Additionally, nitrogen cycling is calculated based on carbon-nitrogen ratios. Disturbances such as fire, herbivory or wind-throw are not explicitly simulated. IBIS-2 has been enhanced by a crop growth simulation module (Kucharik 2003, AGRO-IBIS) to investigate how future climate changes may affect crop yield and land management.

DOLY (Dynamic Global Phytogeography Model, Woodward et al. 1995) is also designed to analyse how vegetation responds to global changes, in particular to rising atmospheric CO_2. It is based on a global productivity and phytogeography model. It does not have an inherent soil model but can be coupled to a model of soil carbon and nitrogen cycling, e.g. as proposed by Parton et al. (1993). HYBRID 3.0 (Friend et al. 1997, Friend & White 2000) is based on a gap model describing the radiation transformation of a forest canopy with competition for light of individual trees (after Leemans 1991). Soil carbon processes are modelled as in the CENTURY model (Parton et al. 1993). Main difference is the spatial resolution: because of limited computational space, this model is mainly used for investigations concerning a certain plot.

In order to investigate carbon fluxes on a global scale including human-induced land-use change, the simplified version HyLand has been developed (Levy et al. 2004). Within HyLand the individual tree simulation of the gap model has been removed, the water cycle and nitrogen dynamics have been simplified, while retaining the vegetation and soil compartments.

BIOME-3 (Haxeltine & Prentice 1996) is a precursor of the LPJ-DGVM and its design shows very similar basics. It is an equilibrium-model, designed to simulate vegetation development and distribution without a dynamic component like competition of plants under changing climatic conditions. Competition is restricted to a competitive balance between woody plants and grasses competing for available soil water. Light competition is not mechanistically modelled. As its emphasis is more on vegetation development and distribution, the soil module only accounts for soil water and its effects on vegetation. Heterotrophic respiration is not considered, therefore no global carbon sources and sinks carbon can be determined. Additionally, no disturbances, such as fire are considered.

Model	type	Input	Resolution	Time steps	Strategy	N?	Disturbances	References
CASA	PEM	t, prec, cld, lat, NDVI, soil, Ninput	Dep on input 8km..1°	monthly	NPP based on LUE (empirically), enhanced by a soil C model	YES	As detected by sat	Potter et al. 1993, Field et al. 1995
GLO-PEM	PEM	PAR, wv, t, AVHRR ch 1,2,4,5	8 km	10-15 days	NPP based on LUE (mechanistically), no below-ground biomass, only soil water	NO	As detected by sat	Prince & Goward 1995
SDBM	PEM	t, prec, cld, lat, NDVI, soil	Dep on input 8km..1°	monthly	NPP based on LUE (empirically), and mechanistic model are compared until best fit of parameters	NO	As detected by sat	Knorr & Heimann 1995
TURC	PEM	T, lat, cld, NDVI, vegt	Dep. on input 8km..1°	monthly	NPP based on LUE (empirically)	NO	As detected by sat	Ruimy et al. 1996
BETHY	PEM + Rh	t, prec, wetd, swr, soil, vegt, GVI, fPAR	Dep. On input (2°)	hourly/ daily	process-based model and mechanistic model (fPAR input) are compared until best fit of parameters	NO	As detected by sat	Knorr 1997, 2000
SIB2	SVAT	t, prec, wsp, swr, lwr, wvpd, NDVI, canh, LAI, fracgl, cr, soil, vegt	1°	daily	SVAT model, coupled to GCM, mechanistic process model, using climate, soil and NDVI data to estimate C and H_2O fluxes	NO	Large-scale dist. Parameterized	Sellers et al. 1996a+b
BIOME-BGC	TBM	trange, prec, topo, lat, soil, rd, Ninput,	Dependent on input	daily	Estimates LAI from water balance, process-based, no phenology	YES	Fire, mortality, harvest	Running & Hunt 1993
CARAIB	TBM	t, trange, prec, cld, wsp, rh, soil, rd	1°	daily	Leaf level photosynthesis model, C and H_2O balance integrated over the canopy, phenology internal	NO	NO	Warnant et al. 1994
CENTURY	TBM	tmax, tmin, prec, soil, plantNPSL, Ninput	Individual ecosystems	monthly	Mechanistic soil C and N model with above-ground vegetation processes, calibrated against observations	YES	Fire, harvest, grazing, cultivation	Parton et al. 1993
CEVSA	TBM	T, prec, wvp, wetd, trange, swr, CO2, soil, landcover	0.5°	monthly	Vegetation structure and physiological processes, coupled C and H_2O balance, no dynamic component.	YES	Land cover	Cao & Woodward 1998b
FBM	TBM	prec, lat, t, trange	?	daily	Leaf level photosynthesis model, C and H_2O balance integrated over canopy, phenology internal	NO	NO	Luedecke et al. 1994
GTEC	TBM	cld, t, rh, prec,LAI, vegt, soil	1°	hourly/ daily	Mechanistic process model, using climate and soils data to estimate c and H_2O fluxes	NO	NO	King et al. 1997
HRBM	TBM	T, prec, cld, soil, LUm, RAP, LUC, pop,	0.5°	monthly	Regression of annual NPP on climate, seasonality driven by AET, influenced by land-use, LUC and population density	NO	Land-use, fire	Esser et al. 1994
SLAVE	TBM	T, prec, CO2, vegt,	5°	yearly	empirical: measured NPP is related to temperature and precipitation, limited by N, P and soil water	YES	managed areas	Friedlingstein et al. 1995

Table 2.2. Overview of different terrestrial vegetation models

Model	type	Input	Resolu-tion	Time steps	Strategy	N?	Distur-bances	References
TEM	TBM	T, p, ld, lat, topo, soil, vegt, Ninput, plantNPSL	0.5°	monthly	Mechanistic progress model, hydrological inputs by separate water balance model	YES	NO	McGuire et al. 1995
BIOME3	DGVM	Tmin, t, prec, cld, lat, soil,	0.5°	monthly	Vegetation structure and physiological processes, coupled C and H_2O balance, phenology internal, no Rh	NO	NO	Haxeltine & Prentice 1996
BIOME4	DGVM	Tmin, t, prec, cld, lat, soil,	0.5°	monthly	Vegetation structure and physiological processes, coupled C and H_2O balance, phenology internal, no Rh	NO	NO	Kaplan et al. 2003
DOLY	DGVM	T, prec, rh, cld,	local to global	yearly	Vegetation structure and physiological processes, coupled C and H_2O balance,	YES	NO	Woodward et al. 1995
HYBRID	DGVM	Tmax, tmin, prec, wvp, swr	Plot based	daily	Vegetation structure and physiological processes, coupled C and H_2O balance, phenology internal, gap model based	YES	NO	Friend et al. 1997
HyLand	DGVM	Tmax, tmin, prec, wvp, swr, CO2, LUC,	0.5° (dep. on input)	daily	Simplified Hybrid model, not gap model based, no phenology, simple empirical competition	Prescribed concentr.	Land-use	Levy et al. 2004
IBIS-2	DGVM	Cld, t, tmin, trange, prec, rh, soil, surf, topo, wetd, wsp	1°	hourly	Vegetation structure and physiological processes, coupled C and H_2O balance, phenology based on GDD	YES	Fract. of biomass removed	Kucharik et al. 2000
LPJ	DGVM	Cld, t, prec, soil, lat, CO_2	0.5°	daily/ yearly	Vegetation structure and physiological processes, coupled C and H_2O balance, phenology based on GDD and water stress	NO	Fire	Sitch et al. 2003
ORCHIDEE	DGVM	T, tmin, tmax, dpt, prec, wsp, swr, press	0.5°	Daily/ yearly	Based on SVAT scheme coupled with vegetation dynamics processes via photosynthesis, Coupled with GCM	NO	Fire, herbivory	Krinner et al. 2005
TRIFFID	DGVM	T, prec, soil, LUm, swr, CO_2	Dep. On input (2°)	hourly/ daily	Vegetation structure and physiological processes, coupled C and H_2O balance, agricultural regions prescribed as grasslands	NO	Disturb. rate for each PFT	Cox 2001, Jones & Cox 2001
VEGAS	DGVM	T, prec, rh, wsp, swr, topo	2.5°	monthly	Vegetation structure and physiological processes, coupled with ocean, land surface and atmospheric model	NO	Fire	Zeng 2003, Zeng et al. 2004

Table 2.2. Overview of different terrestrial vegetation models

Abbreviations of Table 2.2:

canh	canopy height
ch	channel
cld	monthly mean cloudiness
CO2	yearly global CO2 concentration
cr	canopy roughness
dpt	dew point temperature
fracgl	fraction of green leaves
GVI	global vegetation index
LAI	leaf area index
LUC	change of agriculturally used areas (1860-1980)
LUm	land-use map
lwr	long wave radiation
NDVI	Normalized Difference Vegetation Index
Ninput	atmospheric and soil nitrogen inputs
PEM	Production Efficiency Model, based on the light use efficiency approach
plantNPSL	plant nitrogen, phosphorus, sulfur and lignin content
pop	population parameters
prec	monthly mean precipitation
press	surface air pressure
RAP	relative agricultural net primary productivity
rd	rooting depth
rh	relative humidity
soil	soil texture
surf	surface type
SVAT	soil-vegetation-atmosphere-transfer model
swr	short wave radiation
t	monthly mean temperature
tmax	average temperature of the warmest month
tmin	average temperature of coldest month
topo	topography
trange	monthly mean temperature range
vegt	vegetation type
wetd	wet days per month
wsp	monthly mean wind speed
wv	water vapor
wvpd	water vapor pressure deficit

BIOME-4 (Kaplan et al. 2003) is the enhanced version of BIOME-3 and now implicitly simulates competition between 12 plant functional types, but still lacking explicit simulation of Rh.

TRIFFID (Jones & Cox 2001) only simulates five PFTs (broadleaf and needleleaf trees, C3 and C4 grasses and shrubs). Photosynthesis is calculated after Cox et al. (1998, 1999), – where photosynthesis of C3 plants is a function of PAR and leaf temperature – and the scheme of Collatz et al. (1992) (for C4 plants). Computational time-steps are every 30 min, while the carbon pools are updated every 10 days. Competition follows the Lotka-Volterra approach (Huntingford et al. 2000) and a tree-shrub-grass dominance hierarchy. The Lotka-Volterra approach is a population model which links favourable environmental conditions with population sizes and the species' ability to reproduce under certain conditions (Hughes et al. 2004). Heterotrophic respiration is a function of soil moisture and temperature after McGuire et al. (1992) and Raich & Schlesinger (1992). Agricultural areas are prescribed, where only grasses are allowed to grow.

VEGAS (Vegetation-Atmosphere-Global-Soil, Zeng et al. 2004, 2005) uses a very coarse resolution of 2.5°, but it is coupled to the Hamburg Ocean Carbon Cycle Model (HAMOCC (Six & Maier-Reimer 1996) through a mixed atmosphere. 4 PFTs (broadleaf and needleleaf trees, C3 and C4 grasses) compete for climatic constraints, temperature tolerance and height-dependent shading. The calculation of a height dependent maximum canopy is a unique feature of this model useful for decadal simulations of variability, e.g. in soil carbon fluxes. Soil carbon processes occur in three carbon pools depending on temperature and moisture conditions. The model accounts for wetlands and fire disturbances. The isotope carbon 13 is modelled providing a diagnostic tool for differentiating oceanic and terrestrial carbon fluxes.

ORCHIDEE (ORganizing Carbon and Hydrology in Dynamic EcosystEms, Krinner et al. 2005), is a DGVM designed as an extension of an existing surface-vegetation-atmosphere transfer scheme which is included in a coupled ocean-atmosphere GCM. Based on a combination of three submodels, an energy and water exchange module, a model that simulates the phenology and carbon dynamics of the terrestrial biosphere, and a dynamical component based on the vegetation dynamics scheme of LPJ, it can be run in several modes, with dynamical or prescribed vegetation distribution.

The great disadvantage of this model family is that most of them simulate potential vegetation only without consideration of human influences. This effect can be simulated by a model when land-use and agriculture is included in the modelling code. Such code is currently in the development phase in several modelling groups.

2.3.4 Atmospheric inversion

Another approach to detecting regional sources and sinks of atmospheric CO_2 is inverse modelling. It is based on atmospheric CO_2 concentrations measured at different stations around the globe. The measured atmospheric concentrations are then related to concentration gradients and atmospheric transport and linked to inferred surface exchange fluxes (Keeling et al. 1989, Tans et al. 1990, Peylin et al. 1999, Enting 2002, Roedenbeck et al. 2003b). The concentrations and their spatial differences serve as input for an inverse modelling with three-dimensional atmospheric tracer transport models driven by global meteorological data to derive both the seasonal cycle of carbon sources and sinks and their interannual variability (Bousquet et al. 1999, Rayner et al. 1999, Gurney et al. 2002, Roedenbeck et al. 2003a).

The inversion methods are applied on continental scale, thus their spatial resolution is on the scale of several thousands of kilometers. Furthermore, the limited number of monitoring stations leads to a high uncertainty in the mathematical inversion process. Therefore additional information has to be included, such as maps of air-sea exchange of CO_2 and of terrestrial CO_2 fluxes, inferred from modelling or data (Prentice et al. 2001). Additionally, a consensus in results has not been reached so far, due to the use of several different atmospheric transport models, so that there exists a high variation of outputs (Gurney et al. 2002, Gurney et al. 2004).

One of the main contribution to the source and sink discussion by this approach was the detection that the mean latitudinal gradient of CO_2 concentration between the northern and the southern hemisphere was not as large as it should be as predicted from the geographical distribution of fossil fuel burning. This fact indicated a large extratropical land carbon sink in the terrestrial northern hemisphere, because air-sea flux measurements showed no extended oceanic uptake (Keeling et al. 1989, Tans et al. 1990, Ciais et al. 1995, Fan et al. 1998, Janssens et al. 2003). The estimated land-atmosphere flux is –2.3 to 0.6 PgC yr^{-1} in the northern extratropics and –1.0 to +1.5 PgC yr^{-1} in the tropics for the 1980s (IPCC 2001). For the period 1992 to 1996 Gurney et al. (2004) found a northern hemispherical sink of 2.5 +-1.2 PgC yr^{-1}. The whole terrestrial biosphere acted in general as a stronger sink in this period than in the 1980s. Bopp et al. (2002) give the following land-atmosphere flux: 0.3 +- 0.9 PgC yr^{-1} for the 1980s and 1.2 +- 0.9 PgC yr^{-1} for the period 1990 to 1996.

3. OBJECTIVES AND METHODS

3.1 Objective of this thesis

The objective of this study is the derivation of the global terrestrial carbon balance, by combining the mechanistic process functions of a DGVM with the real-world observations of vegetation provided by satellites. Above- and below-ground carbon pools and fluxes are to be quantified to better understand the interannual variations of terrestrial sources and sinks of atmospheric CO_2.

The interpretation of satellite data in terms of land surface carbon dynamics has hitherto largely been based upon so-called light use efficiency (LUE) models of various complexity. The observed satellite signal is transformed into carbon uptake rates through a conversion factor, moderated by limitations caused by temperature or soil water availability (Veroustraete et al. 2002, Nemani et al. 2003). In the most advanced versions, the passage of carbon into soil carbon pools is also computed (Potter et al. 2003). With the current approach the satellite data is assimilated into a fully developed mechanistic model of the carbon and water balances of vegetation and soil, the Lund-Potsdam-Jena Dynamic Global Vegetation Model (LPJ-DGVM), which in its standard mode computes the terrestrial carbon cycle from climate, CO_2 and soil data alone (Sitch et al. 2003). A coupling of these two approaches, performed in this study, allows to combine 'real world' observations with a model that is capable of simulating the carbon cycle's primary processes. This fills a gap in current research in the way that a process-based dynamic carbon-cycle model has not before been coupled with a 21 years time series of satellite data. Comparable investigations are merely produced by the CASA model approach (Potter et al. 1993, Field et al. 1995, Thompson et al. 1996, Potter et al. 1999, 2001), which does not account for fire disturbances and dynamic vegetation development. The BETHY model (Knorr & Heimann 2001 a & b, Rayner et al. 2005) is only applied for single years, although being based on process-based estimations and including a dynamic component.

This approach provides the following deliverables additionally contributing to the current knowledge. The results will be discussed in detail in the chapters 4 and 5:

- A full, observation-based accounting of all relevant carbon cycle components for the last 20 years (1982 to 2002), i.e. not only of NPP as is the case with published approaches, but also of Rh, soil carbon, biomass, net ecosystem production, and natural and anthropogenic ecosystem disturbances.
- Improvement of the biogeochemical simulations due to the assimilation of global spatio-temporal earth observation data into the model.

- An analysis of the temporal variability of the carbon cycle components (NPP, Rh, carbon released by fire, biomass and soil carbon) and its main drivers (climatic variables such as precipitation and temperature and distinct atmospheric circulation patterns) for global and regional scales
- The detection of global spatio-temporal variability of terrestrial carbon sources and sinks for 21 years (1982-2002).
- An analysis of distinct singular events like the El Niño-Southern Oscillation (ENSO) or volcanic eruptions (Pinatubo) and their regional and global effects on the terrestrial carbon cycle, specifically its sources and sinks.

The results will be realized pursuing the following workflow: The input satellite datasets had to be prepared for use in the LPJ-DGVM by closing data gaps in the satellite data input and had to be scaled to fit the models magnitudes (chapter 3.2.2). Elimination of incorrect backscattering of the signal due to low solar angle and snow cover was carried out by substitution of values below a temperature threshold. Within the framework of the LPJ-DGVM a stepwise assimilation of monthly fPAR data into the model has been developed. The fPAR value represents pivotal variables of the model, e.g. foliage projective cover, phenology, and the distinction between evergreen and deciduous physiology, contributing to a more 'realistic' view on the vegetation activity and the distribution of vegetation types. Agricultural areas, respectively croplands and pasture, have been adopted by using a global cropland map derived from the MODIS global land cover product (Strahler et al. 1999, Friedl et al. 2002) and a pasture and fodder production map provided by RIVM (IMAGE Team 2001), crops have been represented by herbaceous PFTs with satellite phenology. Several simulations comprising various setups provide an analysis of the different input datasets and different model results. Model runs with and without agricultural areas highlight e.g. the loss of biomass due to deforestation and land-use change. The application of different satellite datasets allows detection of major discrepancies and failures of the satellite data. A detailed modelling protocol will be given in chapter 3.3.1. The results will be highlighted and discussed in the chapters 4 , 5 and 6.

3.2 Data and modelling basis

3.2.1 The LPJ-DGVM (Lund-Potsdam-Jena Dynamic Global Vegetation Model)

I assimilated satellite data into a fully developed mechanistic model of the carbon and water balances of vegetation and soil, the LPJ-DGVM, which in its stand-alone normal mode computes the terrestrial carbon cycle from climate and soil data alone. A detailed model description is given in Sitch (2000) and Sitch et al. (2003). Model inputs are observed monthly data of temperature, precipitation and cloudiness from the CRU05 database covering the period of 1901 – 2002 on a 0.5° * 0.5° global grid provided by the Climate Research Unit, University of East Anglia (New et al. 1999a; New et al. 1999b). Monthly data were interpolated to pseudo-daily values to serve the photosynthesis and water balance modules. Soil texture classes were based on the FAO soil data set (FAO 1991, Zobler 1986). A dataset of CO_2 concentrations for 1901 – 1995, extended by interpolation up to 2002 (Keeling & Whorf 2004), was obtained by the Carbon Cycle Model Linkage Project (Kicklighter et al. 1999, McGuire et al. 2001).
Based on 0.5° * 0.5° grid cells, vegetation is interpreted as a combination of fractional coverage of ten different plant functional types (PFTs), the global distribution of which is determined by bioclimatic limits as introduced in the BIOME-models and inter-PFT competition for resources (Prentice et al. 1992, Haxeltine & Prentice 1996, Haxeltine et al. 1996, Kaplan 2001), see table 3.1.

PFT	**$T_{c,min}$ (°C)**	**$T_{c,max}$ (°C)**	**GDD_{min} (°C)**	**$T_{w\text{-}c,min}$ (°C)**
Tropical broadleaved evergreen	15.5	-	-	-
Tropical broadleaved raingreen	15.5	-	-	-
Temperate needleleaved evergreen	-2.0	22.0	900	-
Temperate broadleaved evergreen	3.0	18.8	1200	-
Temperate broadleaved summergreen	-17.0	15.5	1200	-
Boreal needleleaved evergreen	-32.5	-2.0	600	-
Boreal needleleaved summergreen	-	-2.0	350	43
Boreal broadleaved summergreen	-	-2.0	350	-
Temperate herbaceous	-	15.5	-	-
Tropical herbaceous	15.5	-	-	-

Table 3.1. Bioclimatic limits of the PFTs (Sitch et al. 2003)

Bioclimatic limits reflect differences in the cold tolerance mechanisms of woody plants as described by Prentice et al. (1992) and Woodward (1987), and co-determine the global distribution of the different vegetation formations. Sufficiently high temperatures are a major determinant for photosynthesis in temperate and boreal ecosystems. Therefore, the GDDs (growing degree days, which are defined as the minimum degree-day sum for plant

establishment with a temperature above 5°C) are also a criterion for vegetation activity and establishment of certain plant types (Long 1991, Malhi et al. 1999). The PFTs of the model represent the average individual of functional groups of higher plant species, given by their physiological, morphological, phenological, bio-climatic and fire-response attributes. They differ in potential geographic distribution (tropical, temperate, boreal), structure (eight woody and two herbaceous), and function, subdivided by leaf morphology (broadleaved, needle-leaved) and phenology (evergreen, deciduous).

Function	Symbol	Value	Units	Description
Structure	CA_{max}	15	m²	Maximum woody PFT crown area
	lr_{max}	1 (0.75)	-	Leaf-to-root ratio under non-water stressed conditions (value for herbaceous)
Phenology	T_{base}	5 (2)	°C	Minimum temperature for summergreen PFT leaf growth
	ω_{min}	0.35	-	Minimum water stress factor for drought deciduous PFTs
Photosynthesis	$p0_2$	20.9	kPa	0_2 partial pressure
	p	100.0	kPa	Atmospheric pressure
	$\Lambda_{max,C4}$	0.4	-	Optimal ci/ca for the tropical herbaceous
	$\Lambda_{max,C3}$	0.8	-	Optimal ci/ca in C3 plants (all PFTs except tropical herbaceous)
	a_{C3}	0.015	-	Leaf respiration as a fraction of Rubisco capacity in C3 plants
	a_{C4}	0.02	-	Leaf respiration as a fraction of Rubisco capacity in C4 plants
Plant Respiration	r	0.066 (0.011)	$gCgN^{-1}d^{-1}$	Tissue respiration rate at 10°C (value for trop. broadleaved evergreen & raingreen PFTs)
Mortality	$fuel_{min}$	200.0	gCm^{-2}	Minimum fuel load for fire spread
	m_e	0.3 (0.2)	-	Litter moisture of extinction (value for herbaceous PFTs)
	r_{fire}	0.12 (0.5)	-	Fire resistance (value for trop. broadleaved evergreen & raingreen PFTs)
Establishment	est_{max}	0.24	m^{-2}	Maximum sapling establishment rate
	$prec_{min}$	100	mm yr^{-1}	Minimum annual precipitation for successful sapling establishment
Soil and litter decomposition	f_{air}	0.7	-	Fraction of the decomposed litter emitted as CO_2 to the atmosphere
	f_{inter}	0.985	-	Fraction of soil-bound decomposed litter entering the intermediate soil pool
	f_{slow}	0.015	-	Fraction of soil-bound decomposed litter entering the slow soil pool
	τ_{litter}	2.86	yr	Litter turnover time at 10°C
	τ_{inter}	33.3	yr	Intermediate soil pool turnover time at 10°C
	τ_{slow}	1000.0	yr	Slow soil pool turnover time at 10°C

Table 3.2. Some relevant parameters and constants in model equations (Sitch et al. 2003)

The ten PFTs are tropical evergreen and raingreen broadleaved forest, temperate broadleaved deciduous (beech, oak) and broadleaved evergreen forest (e.g. oak: *Quercus ilex*), temperate needle-leaved evergreen forest (e.g. pine, fir), boreal needle-leaved deciduous (larch) and evergreen forest (e.g. spruce, pine) as well as boreal broadleaved deciduous forest (e.g. birch, aspen). Two types of herbaceous plants are represented, C3 and C4 plants, differentiated by their photosynthetic pathway. A number of relevant parameters are listed in table 3.2. The parameters are constants which describe certain ratios between functional dependencies applied in the modelling equations. They are defined separately for the ten PFTs, if defining bioclimatic limits, photosynthetical and respiratory processes, fire resistance or phenological dates, or they are global values, if concerning on structure, soil and litter decomposition or establishment.

Daily potential evapotranspiration and monthly soil temperatures are derived from monthly climatological input, soil type and CO_2 concentrations. Terrestrial carbon and water fluxes are computed on a daily basis. Carbon assimilation by plants is a balance between the CO_2 demand by the photosynthetical process and the CO_2 supply by diffusion of CO_2 into the leaves, which is called stomatal conductance. Photosynthesis and stomatal conductance are both affected by environmental factors such as radiation, temperature, air humidity, soil moisture and changing atmospheric CO_2 concentration (Collatz et al. 1992), and they interact with each other. For a flow-chart describing the individual process representations and their exchange of information see fig. 3.1. Photosynthesis is based on the scheme of Farquhar et al. (1980), which has been simplified by Collatz et al. (1991, 1992) for the use in global vegetation models. It is based on a function including absorbed photosynthetically active radiation (APAR), temperature, day-length and canopy conductance and considers the balance of light-limited and Rubisco-limited rates of photosynthesis. The resulting model resembles a LUE model, but the light use efficiency here is determined by environmental variables.

Gross photosynthesis yields gross primary production (GPP) for each PFT population, which is defined as the total amount of carbon assimilated and not lost in photorespiration, which is then reduced through maintenance and growth respiration. The difference between GPP and autotrophic respiration is defined as NPP, which represents the net carbon flux from the atmosphere to the vegetation. Daily phenology is determined by temperature and water stress. Assimilated carbon is further lessened by a reproduction cost. According to a number of scaling and allocation rules the remainder of photosynthates is allocated following a functional balance between the four carbon pools for leaves, sapwood, heartwood and fine roots, as well as for a resulting crown area and individual leaf area index (LAI). The sizes of these four carbon pools and the population density define the average individual of every woody PFT. Grasses only have two carbon pools (leaf and root mass) and population density is set to 1.

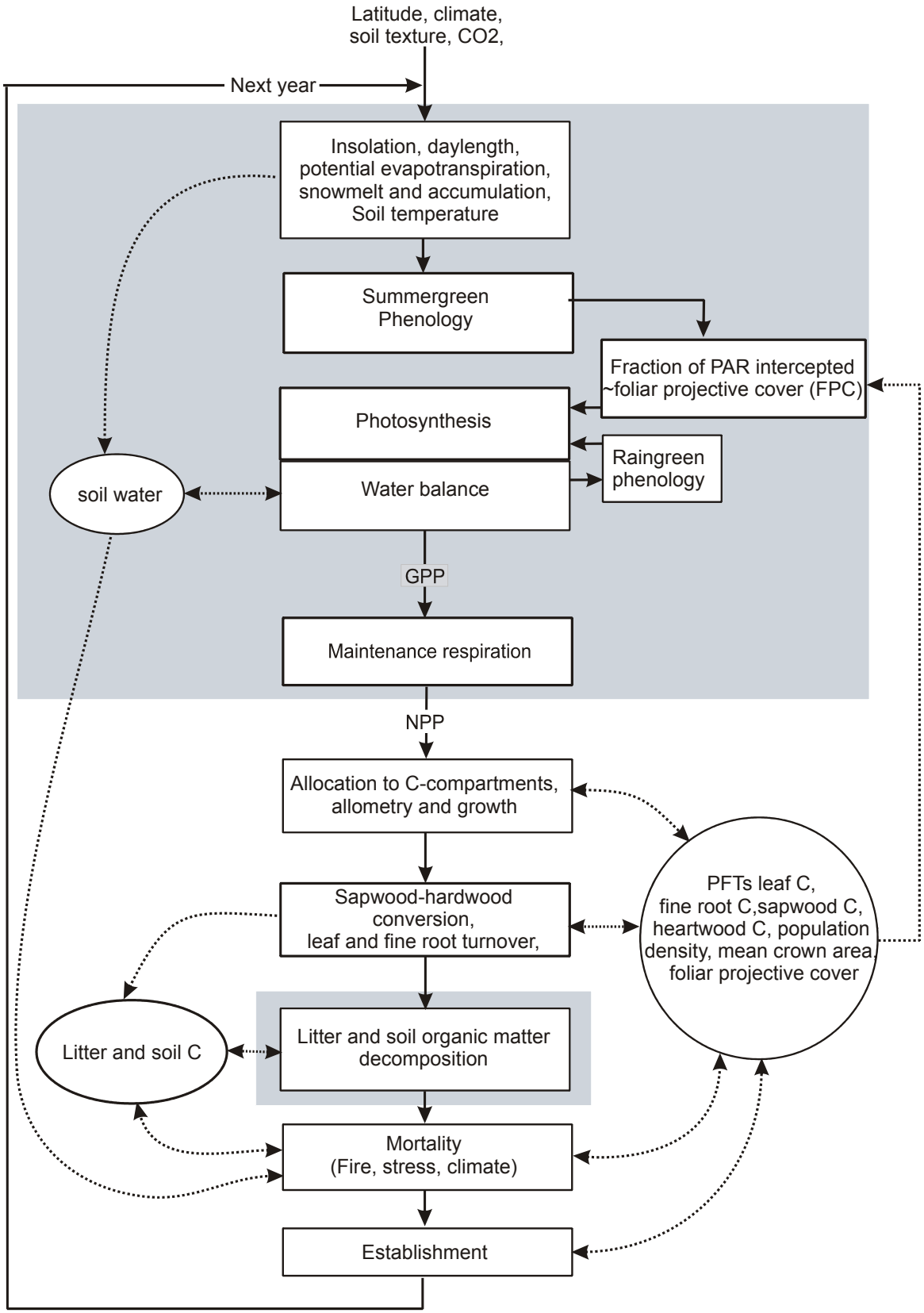

Fig. 3.1. A flowchart describing the order individual process representations (in boxes), known as modules, are performed (solid lines) in all grid cells, during one simulation year. The dashed lines represent exchange of information between vegetation and soil state variables and the individual modules, with arrows representing the direction of information flow. Modules with a shaded background are called on a daily or monthly time step, the remainder called annually (Sitch et al. 2003).

Following seasonality, living biomass is lost to dead leaves, tissue turnover and volatile root tissues that are added to the litter pools. Litter entering soils is transformed into soil organic matter and is decomposed into CO_2 through heterotrophic respiration. Decomposition of litter and soil organic carbon is dependent on soil moisture content and temperature. Finally, the average individual passes through a mortality and establishment routine, followed by an update of the population densities within the grid cell. Disturbances, such as fire and competition for light, additionally affect the population. The overall fractional coverage (FPC – foliage projective cover) of every grid cell is the result of multiplying average individual FPC with crown area and population density.

A LPJ model run in standard mode starts with a thousand years spin-up driven by repeated 1901 to 1930 climate to reach an approximate equilibrium in carbon pools and vegetation cover. It is necessary to use an interannually variable climate as input, otherwise incorrect results e.g. of fire appearance may occur, which depends on the occurrence of drier-than-average years. A transient run using the CRU data for 1901-2002 follows. Model output is composed of stocks and fluxes of carbon and water, e.g. NPP, heterotrophic respiration (Rh), net ecosystem production (NEP), biomass, soil carbon, runoff, and fire carbon for every grid cell and every month (except fire carbon with a yearly output) for the period 1901 to 2002.

The LPJ-DGVM in its original mode has been validated extensively by Sitch et al. (2003) and Peylin et al. (2005). The results show reasonable agreement with measured monthly net fluxes of CO_2 (corresponding to net ecosystem exchange – NEE) for six flux monitoring sites from the EUROFLUX campaign (Heimann et al. 1998). LPJ has also been tested successfully against observations of the seasonal cycle of CO_2 exchange (Dargaville et al. 2002) and atmospheric inversions concerning atmospheric CO_2 growth rate anomalies, showing good agreement in phase and amplitude of major anomalies, even at the latitudinal and regional scales (Peylin et al. 2005). Reliable NPP response to climate variability has also been shown, whereas the performance of Rh in cold regions is discontenting due to inadequate sensitivity of Rh to low temperatures (Peylin et al. 2005). A comparison of soil-moisture data from various sources and locations showed also good agreement (Sitch et al. 2003), except during the early growing season at Russian sites, a bias that may stem from the fact that permafrost is not considered correctly with a too strong emphasis on thawing in spring. A comparison with a satellite-derived dataset of percentage tree cover, phenology and leaf morphology (Defries et al. 2000) showed that the model simulates the vegetation patterns correctly. Lucht et al. (2002) demonstrated good agreement between the LPJ-modelled and satellite (AVHRR)-derived LAI in the circumpolar boreal zone for trends as well as anomalies. LPJ has also been applied to water-related investigations. Wagner et al. (2003) showed good agreement in many regions of the globe between LPJ's modelled global soil moisture anomalies and corresponding data derived from remotely sensed microwave scatterometer data. Water balance and global runoff

has been successfully validated against observations by Gerten et al. (2004a). Furthermore, based on this validation, potential future changes in water limitations of the terrestrial ecosystems have been investigated using five different climate change scenarios (Gerten et al., 2006). LPJ has also been applied for estimating the so-called 'green water', which is defined as the amount of water transpired by plants and therefore used for biomass production. It is an important resource contributing also to human food production as well as to ecosystems productivity (Gerten et al. 2004b). The simulated length of the fire season has been tested for several sites and showed good agreements with the observations except for regions with a length of fire season longer than 160 days. Comparisons to national fire statistics showed that the model simulates the regional fires regimes with moderate to high accuracy. Differences to observations may occur, where modelled PFTs differ from actual vegetation types (Thonicke et al. 2001).

3.2.2 Satellite data and post-processing

Satellite data provide information about vegetation cover on a global scale in high temporal and spatial resolution. In the current study, they are applied to acquire biospheric parameters such as vegetation greenness, green-up and senescence, or forest cover density for extended and remote regions. These parameters serve for further calculations of e.g. NPP based on light-use efficiency of vegetation absorbing a certain fraction of the photosynthetically active radiation (fPAR). In the current study the advantages of satellite data such as high spatial resolution and global availability are used to cope with uncertainties caused by the distinct heterogeneity of land surfaces which cannot be captured by common DGVMs.

The satellite data used in this study to constrain the LPJ-DGVM are monthly data sets of the fraction of photosynthetically active radiation (fPAR) derived from optical reflectance data observed by the National Oceanic and Atmospheric Administration's (NOAA's) Advanced Very High Resolution Radiometer instruments (AVHRR) onboard the afternoon-viewing NOAA series satellites NOAA 7, 9, 11 and 14. The original dataset contains global monthly and 10-day composites of the Normalized Differenced Vegetation Index (NDVI) at 8 km resolution.

Two different versions of these data are used that differ with respect to the post-processing chain. The first time series covers the period from January 1982 to December 2002 and is based on the Global Inventory Modeling and Mapping Studies (GIMMS) version 3 NDVI data set. The second time series is derived from the Pathfinder AVHRR Land (PAL) NDVI data set and covers the period from January 1982 to December 1999. Both NDVI datasets were converted to fPAR by the working group of R. Myneni at Boston University (processing of 2003) by using a three-dimensional radiative transfer model (Myneni et al. 1997). This approach calculates the

reflectance of various vegetation types by taking into account successive adsorption, transmission and scattering effects within the canopy dependent on environmental variables that drive the radiation regime in vegetation canopies. For use with the vegetation model the data were averaged to a spatial resolution of 0.5 degrees.

Differences between the GIMMS and the PAL data sets concern calibration, handling of inter-sensor variations, and atmospheric corrections, particularly of volcanic aerosols (Brown et al. 1985, Gordon et al. 1988, Weinreb et al. 1990, Justice & Tucker 1994, Rao et al. 1994, Vermote & Kaufman 1995, Los 1998). In general, major problems of the AVHRR data series concern the calibration, i.e. the continuous changes in sensor sensitivity and with satellite orbital drift followed by successive changes in sun-target-sensor geometry (Zhou et al. 2001). Additionally, the problem gets more complex, because insufficient knowledge exists about absorption and scattering effects of ozone, water vapour, and aerosols in the atmosphere as well as about the spatially and temporally variable properties of the surface (Gutman 1999). Orbital drift and atmospheric effects are further combined with bidirectional effects of the surface, which differ concerning different atmospheric states and various surface cover types.

For the derivation of the PAL dataset a calibration method after Rao et al. (1993) is used. This method was developed for the use with several different satellites, where data are corrected aboard the satellite using pre-flight calibration constants based on values obtained in the Libyan Desert as a standard surface. Atmospheric correction for PAL includes ozone absorption and pressure level within a Rayleigh scattering correction for the channels 1 and 2 radiance (after Gordon et al. 1988). Topographic data is applied to correct pressure levels for the calculation of the Rayleigh coefficients and the resulting surface reflectances are normalized for solar illumination.

For the GIMMS dataset an inter-satellite calibration method developed by Vermote & Kaufman (1995) is used which is based on data from high cold clouds and the dark ocean. As with this method the NDVI of deserts is not stable, additionally a sensor degradation correction after Los (1998) is applied. Pixels at extreme angles and areas affected by clouds are removed. Then, a normalization after Pinzon et al. (2001) is applied, which accounts for solar zenith angle and therefore provides data with nadir viewing direction. GIMMS additionally applies full radiative transfer correction after Vermote et al. (1992) for every day and every orbit, including stratospheric volcanic aerosol correction for the eruptions of El Chichón (1982-1984) and Pinatubo (1991-1993) (Vermote & El Saleous 1994). Because of these corrections the NDVI values increase with a strong effect in low latitudes and a small effect in high latitudes (Zhou et al. 2001).

The data of both datasets have not been corrected for atmospheric moisture or dust contamination, both of which will reduce NDVI values and therefore the derived fPAR values

in the datasets. In order to minimize residual atmospheric effects only the maximum NDVI value within a 15-day-interval is analyzed in both datasets.

However, published direct comparisons concerning the quality and usefulness of these two datasets are rare. Fig. 3.2 shows the NDVI anomalies (as NDVI is the base for fPAR calculation) for the time period 1982 to 2001 at different latitudes as provided by Compton Tucker (personal communication, 2004). Regarding the years 1984, 1992, 1995 and 2001, the PAL dataset has significantly more extraordinary peaks and data gaps than the GIMMS dataset. On the basis of personal communication with several experts (Compton Tucker, Ranga Myneni, Keith McCloy), I decided to base scientific evaluations primarily on results obtained from the GIMMS data set, which was judged to be of higher and more consistent quality for the following reasons: The high variations are considerably damped in the GIMMS version, it includes corrections for stratospheric aerosols following the eruptions of El Chichón and Mt. Pinatubo, and the calibration method to erase errors when switching from one sensor to the next is more sophisticated. Additionally corresponding values for the widely used PAL data are provided in brackets for comparison.

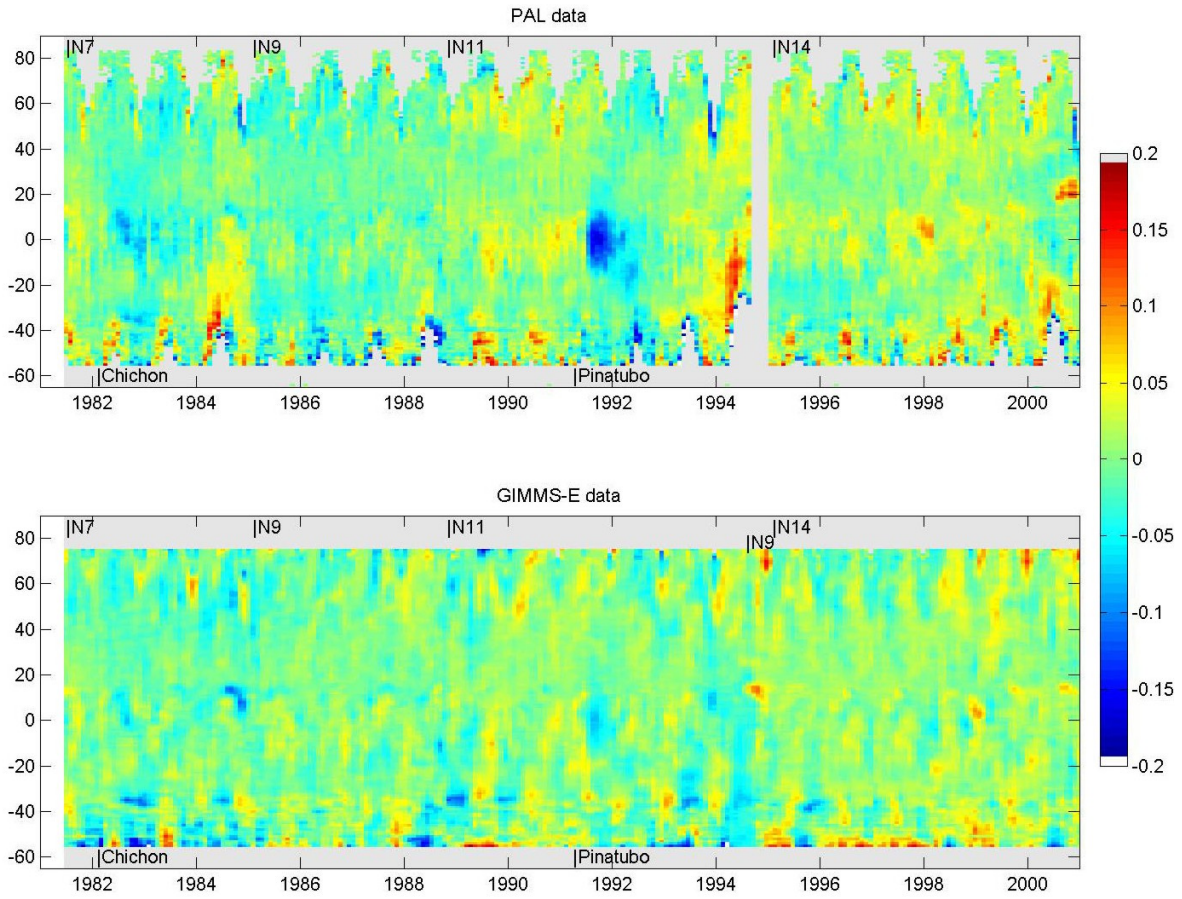

Fig. 3.2. Global NDVI anomalies as given by the PAL and GIMMS datasets as a function of latitude (y-axis) and time period 1982 to 2001 (x-axis) (Tucker 2004, pers. comm.).

In order to illustrate to which extent the choice of data set and differences in data processing affect the biogeochemical interpretation of the data, fig. 3.3 highlights the difference in NPP simulated by the LPJ versions with different satellite data input averaged over the time period 1982 to 1999 and calculated as LPJ-GIMMS minus LPJ-PAL. LPJ-PAL generally produces lower NPP than LPJ-GIMMS, with greatest differences in the south American and African tropics, parts of the African Sahel, the north-eastern American, Norwegian and northern Siberian tundra, as well as parts of Thailand and Vietnam. As already mentioned above, the differences shown originate in different post-processing approaches, i.e. predominantly in the stratospheric volcanic aerosol correction leading to higher fPAR values for the GIMMS dataset. The PAL-based simulation derives global NPP estimations of 1.4 PgC yr^{-1} less than the estimations based on the GIMMS dataset.

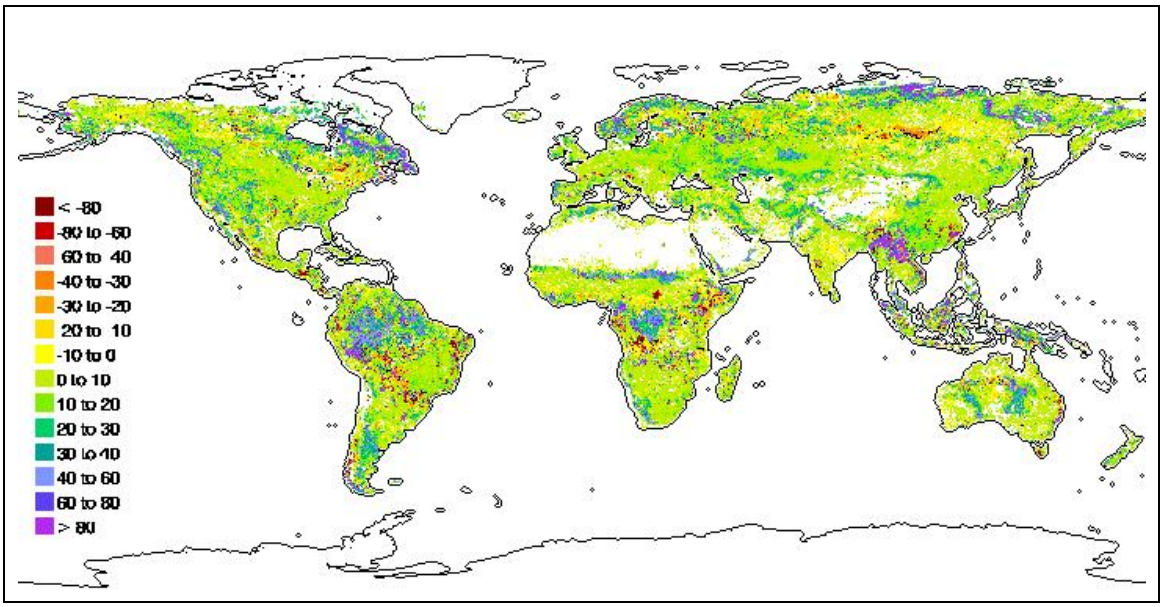

Fig. 3.3. Differences between average NPP output generated with different satellite data input (GIMMS minus PAL, average over 1982 to 1999, in gC m^{-2} yr^{-1})

Before assimilating the datasets into the LPJ-DGVM, additional post-processing was necessary to cancel differences and to close gaps between the modelled and the observed datasets. Several cases may occur that cause differences between the modelled and observed datasets, which require adjustment or substitution:

(1) The two datasets differ in their scaling: the measured fPAR does not exceed values of 0.83, whereas the maximum LPJ-modelled fPAR value is 1, because scattering effects and reduced atmospheric transmission further reduce the signal reaching the satellite, which is not taken into account in the LPJ modelling process. This requires an up-scaling of the satellite data before comparing and substituting the observed with the modelled data.

(2) Data errors, i.e. data exceeding fPAR values of 1 need to be excluded.

(3) Long- and short-term data gaps had to be interpolated or substituted:

- Long-term data gaps were defined as pixels with fPAR values more than half of the time lower than 0.05 and with fPAR values greater than 0.05 for the rest of the time. They occur mainly in tropical south-eastern Asia (e.g. Sarawak), where permanent cloud cover impede a clear view on the earth. Those long-term data gaps were filled with the LPJ-simulated values, rendering these pixels neutral with respect to their effect on LPJ. With the definition marginal desert pixels are not referred to as long-term data gaps, because their interannual fluctuations show a shorter frequency. Core desert pixels are also long-term data gaps per definition, but as the substituting values are taken from the LPJ model, no differences occur. 4.2 % of all pixels belong to long-term data gaps, where the substituting values of LPJ are > 0, and which do not belong to deserts.
- After numerous experiments to differentiate between short term data gaps and marginal desert pixels with fluctuating vegetation cover, short term data gaps were defined as pixels with 18 % of the fPAR values lower than 0.05, but with a maximum value greater than 0.2 for the rest of the time series. 0.4% of all pixels of the GIMMS dataset and 1.2% of the PAL dataset belong to these short-term data gaps. They have been interpolated using concurrent values of temporally adjacent pixels.

3.3 Method of data assimilation into the LPJ-DGVM

3.3.1 Satellite data assimilation into the LPJ-DGVM and modelling protocol

Assimilation of satellite-observed fPAR into the LPJ-DGVM is performed stepwise. First, the LPJ-DGVM is run without constraint for a thousand years to reach an equilibrium state of model-predicted vegetation composition and in each pixel's soil, litter and vegetation carbon pools. A 30-year sequence of climate data from the beginning of the 20th century is repeated in cycles during this spin-up. The final state reached is the result of the model's inherent process-based functional logic without interference from satellite data. It is the starting point for a second spin-up lasting 900 years, during which the model is now additionally forced by a cyclical assimilation of the available 21 (19) years of satellite fPAR data. During this phase, vegetation composition and long-term carbon stores are allowed to re-adjust to the constraint until it reaches a new equilibrium.

Once this is established, the historical period of 1901 to 2002 (1999) is simulated as a transient series using observed climatic data while maintaining the cyclical forcing by satellite data. This sets up the conditions for the time period of interest, 1982 to 2002 (1999), when satellite data and climate data are finally temporally consistent. Only this latter period is subsequently analysed. By this method, carbon pools at the outset (1982) are in a realistic initial state.

The flow chart in fig. 3.4 shows the alterations to data flow in the model code implemented for satellite data assimilation as well as related conceptual enhancements of the model. Additional inputs are the monthly fPAR datasets, which are interpolated to pseudo-daily values, and a global crop and pasture mask file (for a description of derivation and implementation of the agricultural area mask see chapter 3.3.2). Several modules are directly influenced by the additional data. Changes due to satellite data assimilation are implemented primarily for phenology and the calculation of maximum foliage projective cover (FPC). The litter pool is readjusted according to the new vegetation cover fractions. The crop mask mainly influences photosynthesis, phenology, turnover in terms of harvesting, and fire fraction, but only in agricultural areas. Several additional adjustments had to be made to the model. In the first year after the start of the satellite constraint, litter carbon pools are adjusted proportionally to the new maximum FPC of each PFT. Computation of the phenology is omitted as it is now determined by the satellite signal. This particularly concerns the timings of green-up and senescence as well as of drought-deciduous leaf-shedding. In some areas of Siberia the bioclimatic limits used by the model for evergreen needle-leaved trees are lowered to allow observed evergreen fractions in very cold areas to occur. Fire is not allowed to occur on agricultural lands. A detailed description of the changes is given in the following section.

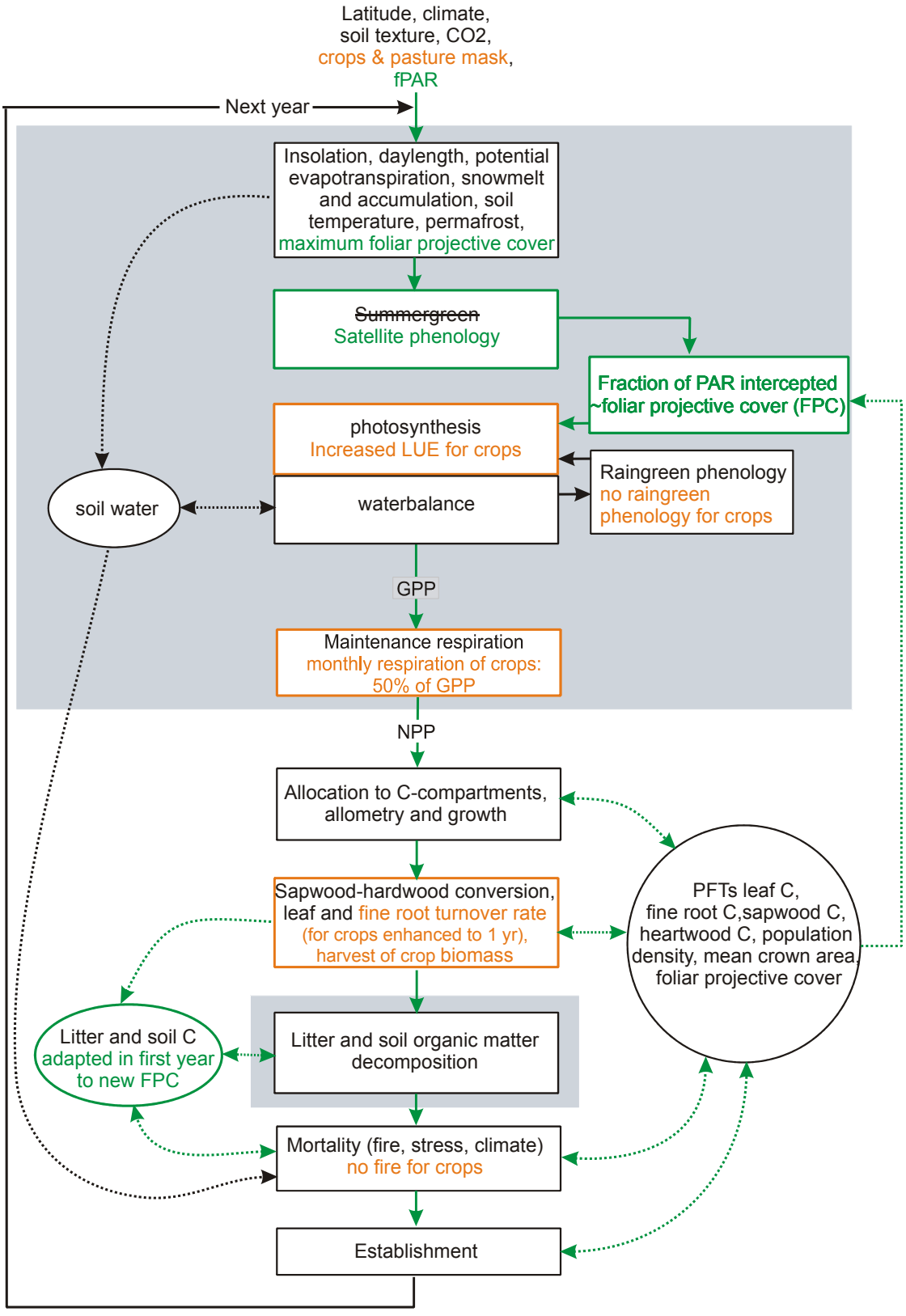

Fig. 3.4. The modified flowchart of the original LPJ-DGVM (Sitch et al. 2003) describing the order of individual processing steps. The dashed lines represent exchange of information between vegetation and soil state variables and the individual modules, with arrows representing the direction of information flow. Modules with a shaded background are called on a daily or monthly time step, the remainder called annually. Changes made for satellite data assimilation due to FPAR assimilation are shown in green, due to crop and pasture simulation in orange. Green arrows specify transfer flow that is indirectly influenced by the fPAR assimilation.

Satellite data are assimilated into the model using the following strategy.

The highest monthly value of fPAR observed during a year is used to determine the maximum vegetation cover (FPC) of a grid-cell, one of the main parameters of the model, which is closely linked to maximum fPAR.

(1) $FPC\ (max) = fPAR_{SAT}\ (max)$

As FPC is defined as the foliage projective cover that can be imagined as the shadow of all leaves projected on the ground, it is functionally related to the amount of photosynthetically active radiation absorbed by the canopy.

The daily "summergreen phenology" module is substituted by the satellite phenology as daily phenology is directly related to the daily absorbed photosynthetically active radiation. Monthly fPAR values are interpolated to daily values for use with this module. As pixels with potential snow cover may pretend less cover of evergreen vegetation than effectively existent, they are recalculated to avoid masking of the vegetation signal in wintertime by snow (see fig. 3.5). Winter values are reconstructed using a maximum-value criterion on periods defined by a +5°C phenological temperature threshold, which is justified because vegetation is inactive below this temperature.

(2) $fPAR\ corr\ (t < 5°C) = fPAR_{SAT}\ (t = 5°C)$

Below this threshold the maximum winter value is substituted with the maximum fPAR value of this period. The maximum value also eliminates biases resulting from low solar angle.

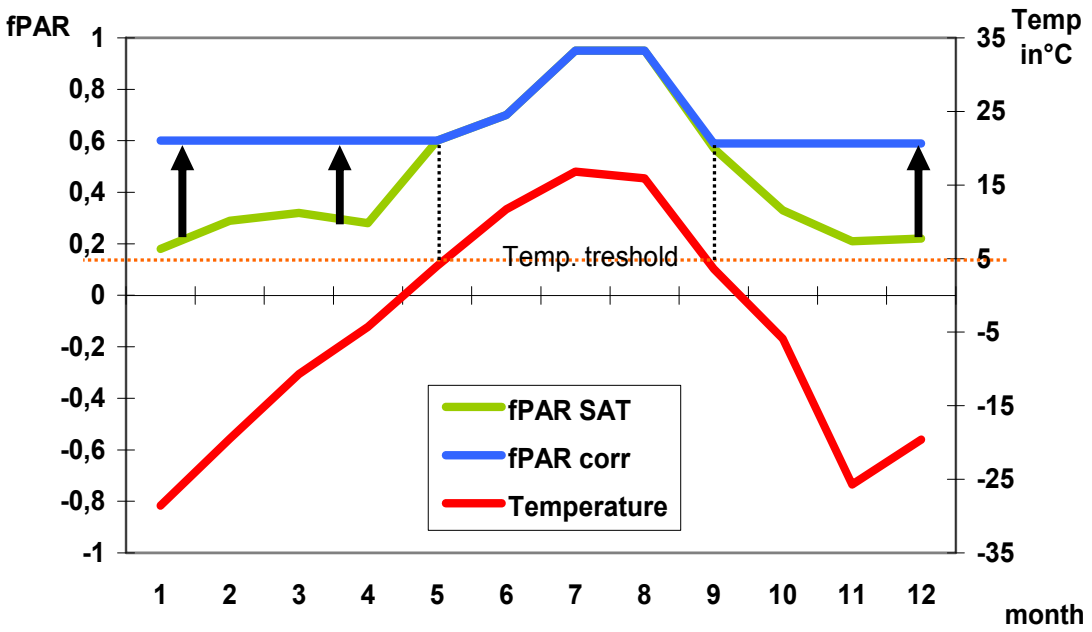

Fig. 3.5. Substitution of observed winter fPAR to eliminate snow effects and low solar angle in satellite data. Pixel at 60°N, 95°E, Siberia.

A main logical problem to solve was to subdivide the single fPAR value per pixel into several occurring PFTs within the pixel. Therefore, the seasonal signal of fPAR during each year is interpreted in terms of fractions of PFTs present in the grid cell contributing to the overall signal. The strategy is illustrated in fig. 3.6. First, the fraction of evergreen versus deciduous vegetation is quantified from the annual fPAR minimum.

(3) $\Sigma FPC\ (evg) = fPARcorr\ (min)$

At boreal and temperate northern and many southern latitudes, the annual minimum fPAR is determined by the maximum fPAR value achieved during the period below a 5°C temperature threshold, at subtropical and tropical latitudes the minimum fPAR is determined by water stress. Within each of the two resulting groups of evergreen and deciduous vegetation types, fPAR was then attributed to individual PFTs by following proportionally the vegetation composition predicted for that pixel by the LPJ-DGVM.

(4) $FPC\ (evg)_{d,y} = fPARcorr\ (min)_y\ * [FPC(evg)_{d,y-1}/\Sigma FPC(evg)_{d,y-1}]$

(5) $FPC\ (dec)_{d,y} = [fPARcorr\ (max)_y - fPARcorr\ (min)_y] * [FPC(dec)_{d,y-1}/\Sigma FPC(dec)_{d,y-1}]$

for everey day (d) of every year (y), and related to the vegetation composition of the previous year (y-1).

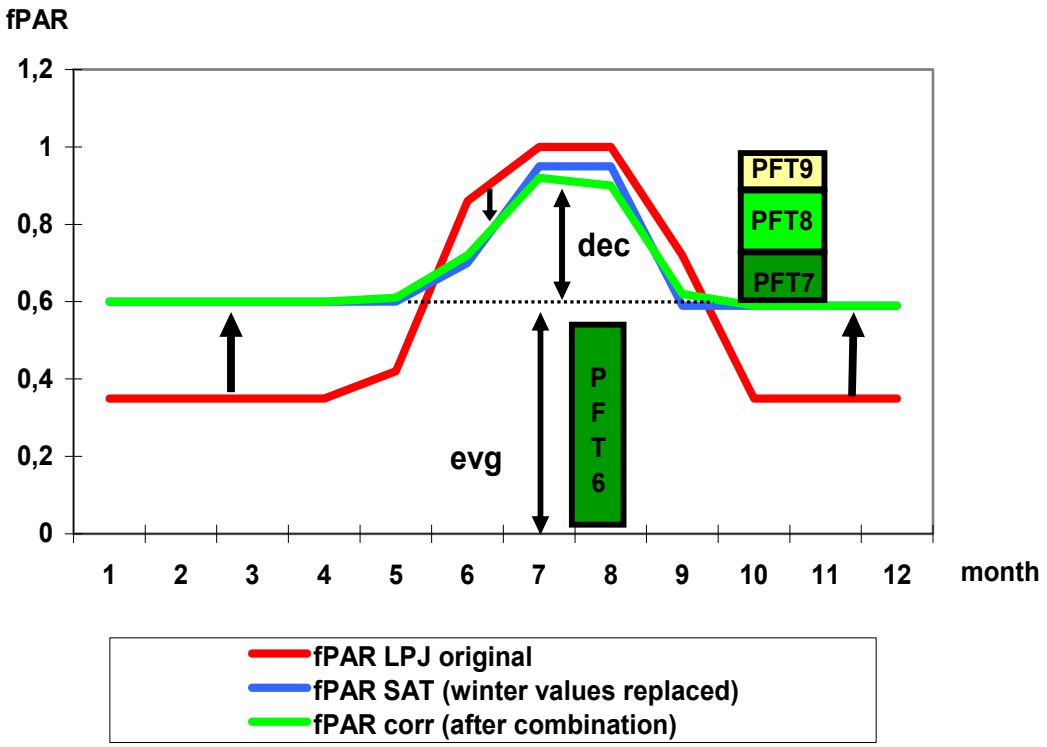

Fig. 3.6. Forcing of LPJ by observed satellite-fPAR. Decomposition of signal into PFTs following LPJ-computed fractional abundance of PFTs

Since the vegetation composition of the model adjusts dynamically to prevailing conditions, it has already adapted to the presence of the satellite data constraint during spin-up.
As a result of this procedure, the ratio of evergreen to deciduous woody vegetation in each pixel is taken from the satellite data while the fractional occurrence of particular PFTs within these two groups is the product of the model's capability to predict vegetation composition from considerations of biogeochemical competition (Fig. 3.6).
The capability of the model to interpret vegetation biogeochemistry is retained as fully as possible while taking into account the satellite data constraint, which concerns only the pixel as a whole. The spatial distribution of PFTs found amounts to an interpretation of the satellite signal in terms of land cover through the model's biogeochemical interpretation.

3.3.2 Agricultural areas

Similar to other current global biogeochemical models, the standard version of the LPJ-DGVM considers only potential natural vegetation, not agricultural land-use. However, about one third of the earth's land surface is currently covered with croplands or pastures (Ramankutty et al. 2002, Leff et al. 2004). Their particular seasonal dynamics are reflected in the satellite data. A simple crop model is therefore implemented into LPJ for pixels that can be identified as either cropland or pasture according to a fixed geographical mask (see Fig. 3.7).
The cropland mask was derived from the 2001 version of the 1 km-resolution global land cover data set from the Moderate Resolution Imaging Spectroradiometer (MODIS) provided by the Department of Geography of the Boston University (Strahler et al. 1999, Friedl et al. 2002, data access: http://duckwater.bu.edu/lc/mod12q1.html).
Cropland areas are defined to be 0.5° grid cells where the MODIS land cover dataset shows major agricultural activity, while ensuring agreement with the total area of global croplands (19 million km²) of the MODIS data set. As a consequence, pixels with a fraction of more than 42.5 % of cropland in the MODIS data are included into the crop mask. Similarly, a mask of areas used for pasture and fodder production was derived (34.5 million km²) using the Special Report on Emission Scenarios (SRES, IPCC 2000) land cover data sets for the year 1970, which were produced with the IMAGE-2.2 model (IMAGE Team 2001). In cases of overlap, the cropland mask takes precedence. In cropland and pasture pixels, only the two vegetation types representing C3 and C4 herbaceous vegetation and grasses are allowed to grow. Cropland phenology is given by the satellite fPAR observations. In the extra-tropics (outside of 20°N and 20°S) the productivity of croplands, but not that of pastures, is enhanced in comparison to that of natural grasslands by increasing the light use efficiency by a factor of 1.65 (Ruimy et al.

1999). Since tropical croplands are often even less productive than corresponding natural vegetation (Dadwhal et al. 1996, Esser, Enquête Kommission 1994), their productivity was not enhanced. Fire occurrence was suppressed in the crop regions, but not in areas with pasture.

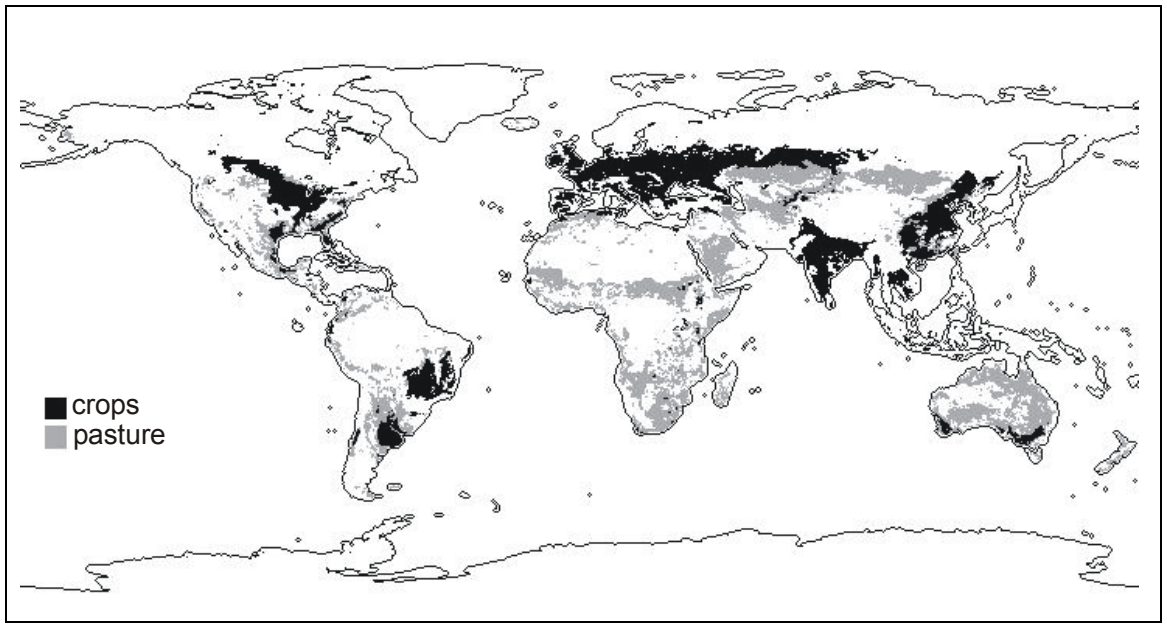

Fig. 3.7. Croplands (derived from MODIS), pasture and fodder production mask (derived from RIVM)

To take account of the modified carbon cycle in an agricultural utilized area, removal of carbon from the system due to harvesting is implemented. At the end of each growing season, 75% of the aboveground biomass carbon is assumed to be harvested for croplands and returned to the atmosphere. The remaining 25% is entered into the litter-pool, where they contribute to the short and long-term soil carbon pools, resulting in a lessened carbon allocation in the soils as well as in the annual calculation of NPP than under natural grasslands. In LPJ in standard mode monthly respiration is defined as the sum of leaf, root and sapwood growth and maintenance respiration. For crops monthly respiration is lowered to 50 % of gross primary production, as considered by Sitch (pers. comm.), to account for the increased growth rate of crops compared to grass and for the removal of crop biomass by harvesting. The root turnover rate is commonly calculated as the reciprocals of tissue longevity. For crops root turnover rates have been changed to one year, in contrast to half a year for grasses according to the differing physiognomy of crops which incorporate various crop types such as cereals, roots and tubers, pulses, or oil and sugar crops.

One main limitation of this approach is that e.g. no dynamic augmentation of agricultural areas over time is applied so that the derived harvest values are only approximations calculated for a steady state of 1970. Additionally, no differentiated crop module is implemented that addresses the distinct physiognomy and phenology of several different crop types, therefore the harvest

values only concern to a cereal/grass type. A sophisticated crop module for LPJ is in development.

Table 3.3 shows a comparison between measured NPP from different agricultural sites, the NPP simulated by LPJ constrained with GIMMS-fPAR data, and the NPP calculated by the original potential vegetation model. LPJ-GIMMS simulated data are of a comparable order of magnitude as the measured values, except for extremely intensively cultivated areas such as the central United States or Germany, where fertilization and irrigation are widely used and higher NPP can be achieved. Obviously, the satellite data implementation has led to a greater magnitude of NPP levels compared to LPJ-potential vegetation, indicating the simulation of a more heterogeneous landscape in the agricultural regions in LPJ-GIMMS.

Country	**Landcover/ crop type**	**NPP measured (gC m^{-2} yr^{-1})**	**NPP LPJ-GIMMS (gC m^{-2} yr^{-1})**	**NPP LPJ-pot. Vegetation (gC m^{-2} yr^{-1})**	**Reference**
Illinois U.S.	Corn, Soybean	2159 to 1180	610 to 1008	757 to 873	Turner et al. (2002)
Austria	Pastures and croplands	558 to 1003	626 to 945	709 to 853	Haberl et al. (2001)
Germany	Rape and Sugar Beats	844 to 1875	603 to 961	669 to 795	Esser, Enquete Kommision (1994)
India	Crops	238	235 to 756	528 to 663	Dadwhal et al. (1996)
Central U.S.	Crops (corn, soybean, wheat, barley)	239 to 760	241 to 940	425 to 945	Prince et al. (2001)
Japan	?	634	476 to 766	583 to 647	Matsushita & Namura (2002)

Table 3.3. Comparison of measured and simulated NPP of agricultural lands

4. SPATIAL PATTERNS OF TERRESTRIAL CARBON FLUXES AND POOLS

4.1 Introduction

The primary objective of this study (see chapter 3) is to achieve an improvement of the model's quantification of the terrestrial carbon cycle due to more realistic spatial and temporal data input obtained by earth observation. The subsequent sections are devoted to investigating the extent to which this improvement can be demonstrated.

The current chapter 4 will investigate the spatial patterns of carbon fluxes and pools obtained from coupling the LPJ-DGVM with satellite data giving an improved insight into the terrestrial carbon cycle, into uptake and release of carbon, both on a continental to global scale and for a long time period of more than 20 years. Their year-to-year temporal variability will be investigated subsequently (chapt. 5).

The effect of assimilating satellite data into a process-based global vegetation model is analyzed by comparing the results obtained by three versions of LPJ with and without satellite data assimilation. Table 4.1 lists these three modelling approaches, while table 4.2 presents the resulting global carbon pools and fluxes. The results have been compared to other model results and observed data, which is presented in the following chapters, differentiated for the different carbon cycle components NPP, Rh, fire carbon, harvest, biomass and soil carbon.

The following three different LPJ versions will be distinguished:

(1) LPJ-P: LPJ in original mode representing the potential natural vegetation (Sitch et al. 2003)

(2) LPJ-C: An enhanced LPJ-P which additionally accounts for croplands and areas with pasture in a simplified way in order to be able to divide the carbon pools in potential natural vegetation and areas influenced by humans (crops are parameterized as grasses with LPJ phenology, see chapter 3.3.2)

(3) LPJ-S: The combined version, incorporating satellite fPAR and considering cropland and pasture, which represents the actual vegetation influenced by humans (crops are parameterized as grasses with observed fPAR phenology, see chapter 3.3.2)

Modelling approach	Abbreviations used in the following chapters
LPJ-potential vegetation	LPJ-P
LPJ potential vegetation with forced cropland spatial pattern	LPJ-C
LPJ with observed fPAR phenology from GIMMS dataset – Actual vegetation including agricultural areas	LPJ-S_{GIM}
LPJ with observed fPAR phenology from PAL dataset – Actual vegetation including agricultural areas	LPJ-S_{PAL}

Table 4.1. Modelling approaches of LPJ and used abbreviations

4.1.1 Vegetation cover

The satellite-observed time series of fPAR values is used to constrain the model while largely preserving the model's ability to predict occurring plant types as a function of climate and competition between types. Since LPJ-P computes both vegetation parameters and composition, alterations in conditions by the satellite constraint, for example in the seasonality of plant production, can lead to shifts in competitive advantages that alter simulated vegetation composition. To the extent that the joint system of satellite data and vegetation model (LPJ-S) is more powerful than the model itself, the resulting PFT distribution should be more realistic than that predicted by the model alone. The model with satellite-data constraint therefore can also be used as a land cover classifier predicting vegetation composition from the fPAR signal. This also applies to vegetation patterns due to human interference, which the stand-alone model, of course, cannot predict by itself.

In order to support this hypothesis, fig. 4.1 shows a composite highlighting comparisons between different types of vegetation in various areas simulated with different LPJ versions compared to a satellite-derived vegetation cover map (from MODIS 2000/2001). In North America, the spatial distribution of deciduous broadleaf trees is much improved in comparison with the MODIS land cover data when the model is constrained by satellite data. The fraction of deciduous broadleaf forest is reduced for the benefit of grasses and boreal needle-leaved forest. This indicates that the fPAR-induced shifts in vegetation competition have led to a more realistic simulation (Tab. 4.2). Though, a prevalence of deciduous forests along the Eastern US Seaboard is not correctly simulated, suggesting a review of associated model parameterization. The overall quality, however, has improved, including effects of the crop mask. The pattern of tropical evergreen forests in South America and South East Asia is greatly improved by constraining the model with satellite data. The new distribution includes effects of human influence and an improved seasonal cycle, leading to a distinct differentiation between tropical evergreen and deciduous forests.

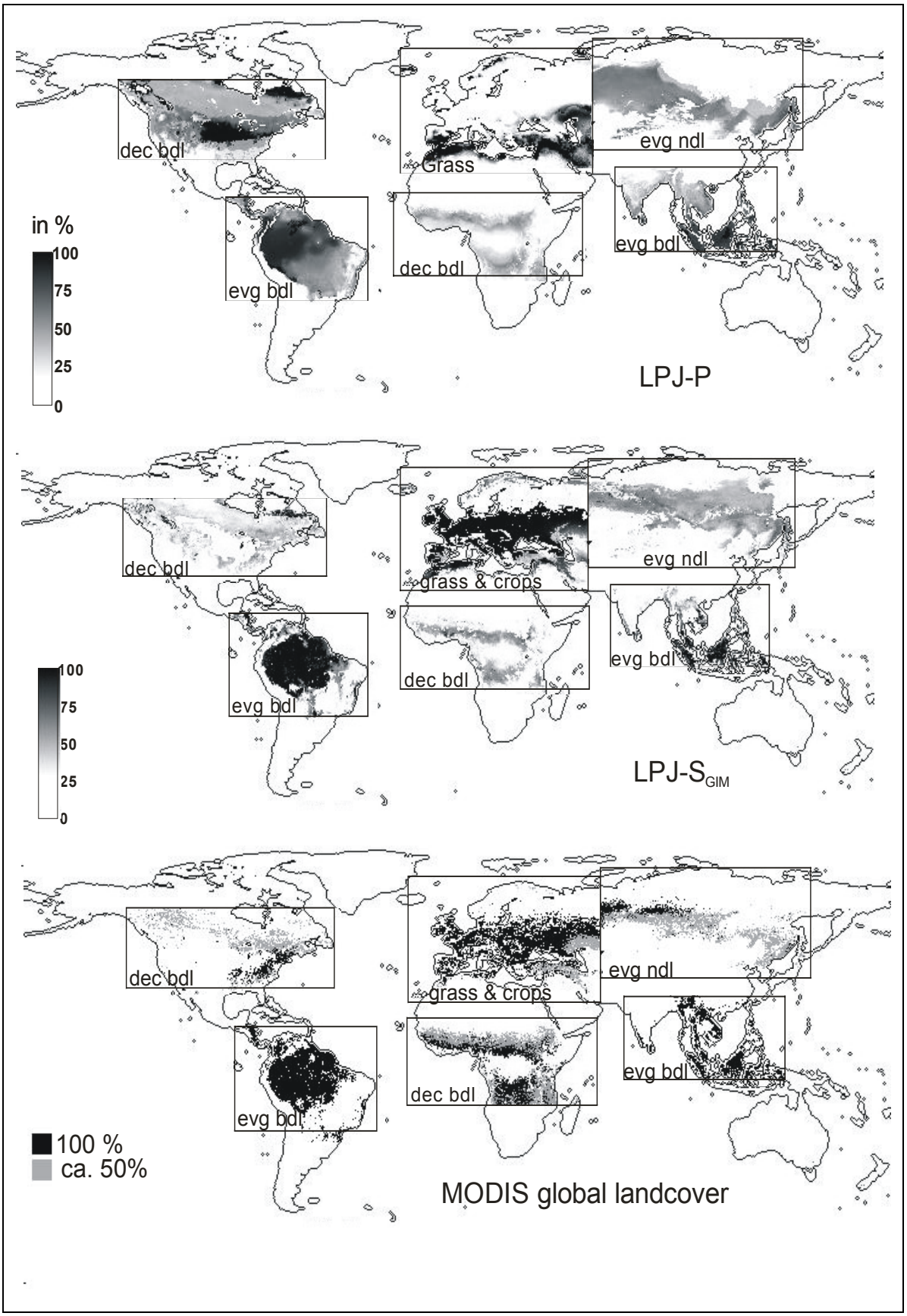

Fig. 4.1. Distribution of selected PFTs modelled by LPJ with and without satellite data constraint and of MODIS landcover (2000/2001).

Regarding the tropical deciduous forest in Africa, it shows also an improvement in distribution whereas its density is still not simulated correctly and therefore the parameterization of this PFT should be further revised. But as the MODIS data only captures the physiology, such as deciduous or evergreen, and not the size of the trees, the dense cover with deciduous broadleaved vegetation in the MODIS data is probably due to a dense bush vegetation which cannot be modelled by LPJ, which only differentiates between herbaceous and tree vegetation. This might explain the difference of 3.73 Mio km² between the LPJ-S_{GIM} and MODIS derived land cover (Tab. 4.2).

The distribution of evergreen needle-leaf trees in Siberia is also greatly improved, on the one hand due to the implementation of the crop mask, on the other hand due to the satellite induced seasonality which ameliorates the ratio between deciduous and evergreen trees and grass (Tab. 4.2). A more realistic simulation of grass and croplands in Europe is mainly due to the introduction of the cropland mask.

Concluding, vegetation cover has changed blatantly between the modelled world with potential vegetation and the model incorporating satellite observations, in particular for deciduous forests and grasses. It shows that the application of potential vegetation models to predict carbon fluxes is inadequate as the 'real' world' immensely deviates from the 'potential vegetation world'.

	LPJ-P	**LPJ-S_{GIM}**	**MODIS**	**LPJ-S_{GIM} minus LPJ-P**	**LPJ-S_{GIM} minus MODIS**
trop evg bdl	18.74	17.74	16.98	- 1.00	+ 0.76
trop dec bdl	11.37	3.83	7.56	- 7.54	- 3.73
temp & bor dec bdl	22.20	5.60	5.23	- 16.6	+ 0.37
temp & bor evg ndl	17.67	16.95	15.83	- 0.72	+ 1.12
grass (& crops)	20.59	49.44	52.95	+ 28.85	- 3.51
bor dec ndl	4.48	2.56	6.22	- 1.92	- 3.66
temp evg bdl	5.04	3.21	n.a.	- 1.83	n.a.
barren	32.84	34.84	34.16	- 2.02	- 1.30
total area	132.95	134.17	138.93		

Table 4.2. Land cover area for different vegetation types as derived by LPJ-P, LPJ-S and MODIS (in Mio km²). trop=tropical, temp=temperate, bor=boreal, evg=evergreen, dec=deciduous, bdl=broad-leaved, ndl=needleleaved. Differences in total area are a result of different inputs for total terrestrial surface (CRU-data for LPJ-P, AVHRR-fPAR for LPJ-S, both without Antarctica, MODIS including Antarctica)

4.1.2 Carbon fluxes

The model with satellite data constraint produces generally smaller carbon fluxes than the purely climate-based stand-alone simulation of potential natural vegetation. The implementation of the crop-mask into the original model enhances NPP and Rh, whereas biomass is reduced to a more realistic size compared to studies based on forest inventories (WBGU 1988, Mooney et al. 2001).

Parameter	**Unit**	**LPJ-P**	**LPJ-C**	**LPJ-S_{GIM} (LPJ-S_{PAL} in brackets)**	**Difference LPJ-P–LPJ-S_{GIM} (LPJ-P–LPJ-S_{PAL})**	**Addressed in chapter**
NPP	PgC yr^{-1}	70.6	73.1	60.0 (59.2)	-10.6 (-11.4)	4.2
Rh	PgC yr^{-1}	60.9	63.6	52.3 (51.7)	-8.6 (-9.2)	4.3
Fire C	PgC yr^{-1}	8.4	4.9	4.3 (4.1)	-4.2 (-4.3)	4.4
Harvested C	PgC yr^{-1}	0	3.3	2.7 (2.7)	2.7 (2.7)	4.5
NEE	PgC yr^{-1}	1.3	1.3	0.7 (0.8)	-0.6 (-0.5)	4.8
Biomass	PgC	910	667	638 (615)	-272 (-295)	4.6
Soil C	PgC	1670	1597	1371 (1341)	-299 (-329)	4.7
Runoff	km^3 yr^{-1}	35.750	40.700	44.015 (45.420)	8.265 (9.670)	-

Table 4.3. Comparison of global carbon pools and fluxes, 18-year average (1982 to 1999)

The results shown in table 4.3 can be interpreted as follows and will be discussed in more depth in the following sections:

- Regarding NPP it is obvious that the implementation of crops in LPJ-C enhances NPP compared to LPJ-P. In contrast, NPP is strongly reduced after implementation of both fPAR and agricultural areas (LPJ-S). Despite an enhancement of NPP due to the crop mask a strong reduction of NPP in comparison to LPJ-P is found (10.6 PgC yr^{-1}). A detailed analysis of the possible causes is given in chapter 4.2.
- Rh shows a behaviour similar to that of NPP, because it is strongly coupled to NPP, although its total fluxes are lower than NPP. Rh is reduced after implementation of the satellite data, even though soil respiration is enhanced in LPJ-C (chapter 4.3).
- Carbon released by fires is reduced after implementation of agricultural areas in LPJ-C, because fire is suppressed on croplands (see chapter 3.3.2). An additional slight reduction of fire carbon occurs in LPJ-S. Fire return intervals are reduced in natural areas due to a lower biomass and accordingly lower litter carbon available for fire fuel (chapter 4.4).
- Harvested carbon is reduced by 0.6 PgC yr^{-1} comparing LPJ-S with LPJ-C. Causes might lie in the better and shorter reproduced seasonality of crops by LPJ-S which influences NPP, biomass and therefore harvested carbon (chapter 4.5).

- NEE does not alter between LPJ-P and LPJ-C, but it is reduced by 0.5 PgC yr^{-1} after implementation of the fPAR data due to an asymmetric reduction of the relevant components NPP, Rh and fire carbon (chapter 4.8).
- A strong reduction due to the implementation of agricultural areas (LPJ-P compared to LPJ-C) occurrs for biomass (243 PgC). This figure can be taken to represent the total biomass removed by human agricultural activities. Input of fPAR data reduces biomass by 29 PgC additionally including effects in the satellite data of naturally lower vegetation density and removal of biomass by humans within the natural areas (chapter 4.6).
- On the contrary, only 73 Pg of soil carbon loss occur after implementation of the crop mask (LPJ-C), but 226 Pg are lost additionally due to satellite data input (LPJ-S). The reduction mainly occurs in agricultural areas where less carbon is stored in the soils due to harvesting and the occurrence of bare soils in winter as observed by satellite. Nevertheless, natural areas also contribute to this reduction due to a smaller amount of biomass and therefore input into the litter carbon pool (chapter 4.7).
- As a consequence of more open vegetation runoff is enhanced. After implementation of the crop mask global annual runoff increases by 5 km^3, additionally rising by further 4 km^3 after implementation of the satellite data. This is a consequence of reduced transpiration in a landscape with generally less vegetation. This compares better with global runoff data (42.353 km^3) as published by Cogley (1998) (Gerten et al. 2004).

In order to understand the spatial patterns that underlie these results, the following sections present the different carbon flux components in more detail and resolved for spatial patterns.

4.2 Net primary production (NPP)

NPP is defined as the net gain of organic matter by plants in an ecosystem. It is calculated from gross primary production (GPP) - the total amount of carbon taken up in photosynthesis - minus autotrophic respiration, which is determined as the cost of assimilation, maintenance and growth of the plants. Global NPP is estimated to be 60 PgC yr^{-1} (Cramer et al. 1999, IPCC 2001), which is about half of GPP. This value has been determined by integrating the results of field measurements (Ajtay 1979, Saugier & Roy 2001), and comparing them to remote sensing data and atmospheric inversion modelling. Nevertheless it has to be taken into account that each of these methods taken apart contains large uncertainties.

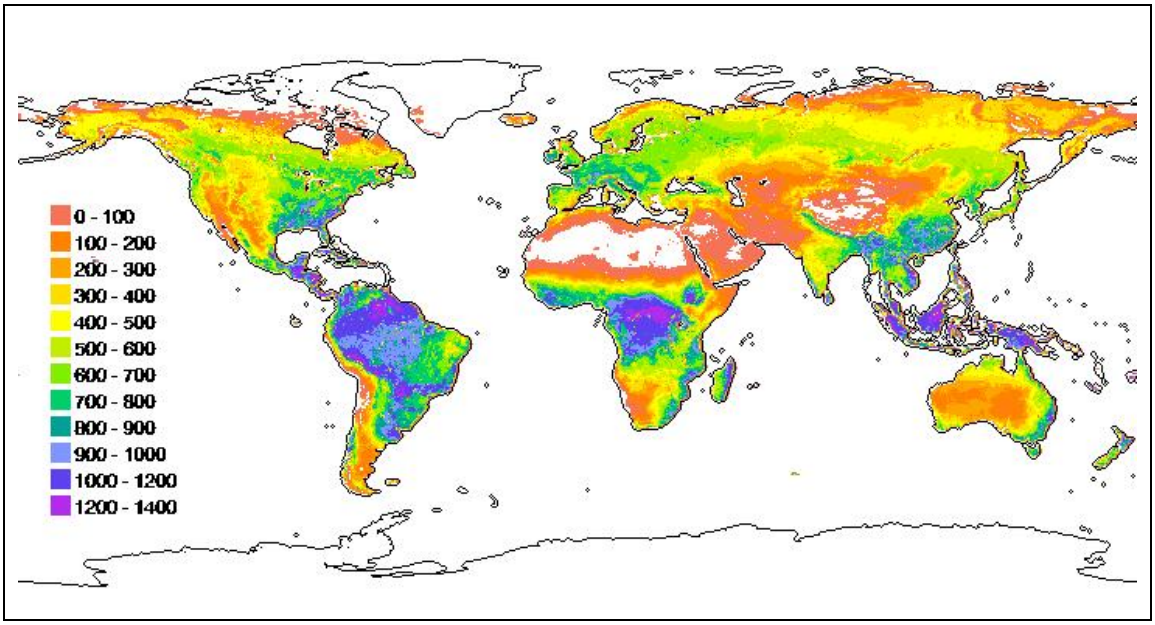

Fig.4.2. Mean NPP for the period 1982 to 2002 as derived from a LPJ-S_{GIM} simulation run with satellite fPAR data (in gC m^{-2} yr^{-1})

NPP is mainly climate-driven, temperature-limited at higher latitudes (boreal and northern temperate regions), whereas at lower latitudes precipitation is the limiting factor (Schultz 1995, Malhi et al. 1999, Nemani et al. 2003). A pronounced interannual variability is found at higher latitudes as well as in semiarid ecosystems (for more analysis of the interannual variability of various regions see chapter 5). Fig. 4.2 shows the average spatial patterns for the time sequence of 1982 to 2002 of the simulated NPP based on satellite observations (LPJ-S). As expected, NPP is highest in the tropics and lowest in arid and semi-arid areas as well as in very high latitudes or in high altitudes where tundra vegetation predominates.

NPP is often overestimated by vegetation models (Cramer et al. 1999). Its simulation of plant productivity is based on generalization of the photosynthetic process estimated for a whole grid cell and where leaf area, incoming radiance, temperature, rainfall and soil parameters are assumed to be homogenous. Without consideration of heterogeneous conditions which have

been shown to influence plant productivity significantly by numerous experiments, NPP may be overestimated up to 30% (Pierce & Running 1995). In fact, LPJ-P overestimates NPP by about 10 PgC yr^{-1} (Tab. 4.3). With this combined approach global NPP is found to be 60.0 PgC yr^{-1} (LPJ-S_{GIM}), significantly lower than the NPP of potential vegetation (70.6 PgC yr^{-1}). This result fits better with other estimates inferred by different modelling and measurement approaches, although inventory data are still significantly lower (Zheng et al. 2003) (see table 4.4). This reduction is not the consequence of implementation of the crop mask, rather application of a crop-mask based on grass-phenology increases NPP in LPJ-C compared to LPJ-P from 70.6 PgC yr^{-1} to 73.1 PgC yr^{-1}. The significant reduction of NPP is a consequence of the assimilated satellite data, leading to a more realistic vegetation distribution and seasonality. As grass may have a NPP as high as that of trees, a more productive grass PFT representing crops, as described earlier, increases global NPP by 2.5 PgC yr^{-1}. Nevertheless, biomass on cropland pixels is reduced to a more realistic size.

In contrast to the findings of the model intercomparison project of Cramer et al. (1999), which showed that the results of almost all modelling approaches exceed the global inventory data, the present results from LPJ-S converge noticeably with the IPCC estimates (IPCC 2001). Our estimates are also in the same order of magnitude as the yearly results simulated by the approach of Potter et al. (1999), which is a combination of a light use efficiency model with satellite data (CASA model).

Year/ period	Potential vegetation (LPJ-P)	Forced Cropland Spatial Pattern (LPJ-C)	Actual Vegetation (LPJ-S_{GIM})	IPCC 2001	Prince & Goward 1995	Knorr & Heimann 2001	Potter et al. 1999	Cramer et al. 1999	Zheng et al. 2003
1982-99	70.6	73.1	60.0	59.9 /62.6	-			44.4 – 66.3	
1983	68.1	70.9	57.0				56.1		
1984	69.6	71.7	58.5				54.0		
1985	69.5	71.5	59.5				58.8		
1986	70.4	72.4	59.9				58.9		
1987	68.6	71.4	58.4		68.97	67.1-82.9	59.7		
1988	69.4	72.1	59.1				59.0		
1983-88	69.3	71.7	58.7				57.75		
1989-93	71.4	73.6	60.7						41.7-49.5

Table 4.4 Comparison of NPP estimates derived by different approaches (in PgC yr^{-1})

The comparable approach of Prince & Goward (1995, GLO-PEM), driven with satellite data, shows too high values compared to the IPCC results and the current study. Knorr & Heimann (2001a) developed a global vegetation model that can be run in two modes: a process-based

modelling of photosynthesis and a version, where fPAR is used to calibrate and adjust the modelling parameters stepwise. They derive a difference map for NPP on the basis of the two different approaches. This comparison shows partly similar patterns to our results, whereas their simulated global NPP for 1987 is 75.8 to 82.9 PgC yr^{-1} in the potential vegetation version and 67.1 to 73.6 PgC yr^{-1} in the satellite-calibrated version depending on which photosynthesis scheme they apply (Knorr & Heimann 2001b). Compared to other results (Tab. 4.4) these figures are rather high and the satellite data input does not reduce NPP by the same order of magnitude as our approach.

Table 4.2 shows that the reduction of NPP by LPJ-S is not caused by implementation of the crop mask, as the presence of growth-enhanced grasses/herbaceous does not reduce global NPP in comparison to the NPP achieved when potential woody vegetation is growing. In the following it will be discussed which regions and reasons contribute to the reduction in NPP. Several causes are likely, which will be investigated and quantified in the following section:

(1) Human influence (deforestation, forest management, selective logging, small agricultural areas) in the natural vegetation regions
(2) Reproduction of a more heterogeneous landscape with more open vegetation in natural vegetation regions due to the implementation of the fPAR data
(3) Changes of PFT distribution in the LPJ-S version leading to a reduction in NPP
(4) Improved seasonality within both the crop regions and the natural areas due to the implementation of the fPAR data

In order to divide between the influence of the satellite fPAR input and the application of the crop mask on changes in NPP, several model runs with and without agricultural areas have been performed. Besides the different versions LPJ-P (potential vegetation), LPJ-C (potential vegetation + agricultural areas) and LPJ-S (actual vegetation + agricultural areas), two additional model runs have been simulated only taking into account the satellite fPAR without considering agricultural areas (LPJ-Snocrops with GIMMS and PAL-fPAR input).

(1) Human influence in regions with natural vegetation

Human influence is assumed to appear in areas outside the crop mask, occurring as forest management, deforestation and land-use change, small-size logging activities or small agricultural areas which are not captured by the crop mask.

To prove this hypothesis, fig. 4.3 illustrates the distribution of pixels which incorporate less than 42.5 % crops, which are not included in the crop mask (see chapter 3.3.2), but which may contribute to the natural area's smaller NPP result. This figure shows that almost all pixels with residual crop fraction are situated at the borders of the great agricultural regions, and they do

not exceed an area of 11 % globally. These residual crop pixels have an NPP of 9.1 (9.0) PgC yr^{-1}, contributing with about 23 % to the reduction of NPP in these areas classified as natural but containing a small fraction of cropland (Tab. 4.5). The remainder of 77 % or 30.8 (29.9) PgC yr^{-1} represents the NPP of the natural areas which is reduced due to implementation of satellite data alone, according to a combination of effects such as improvement of seasonality, reduction of vegetated area and shifts in PFT distribution.

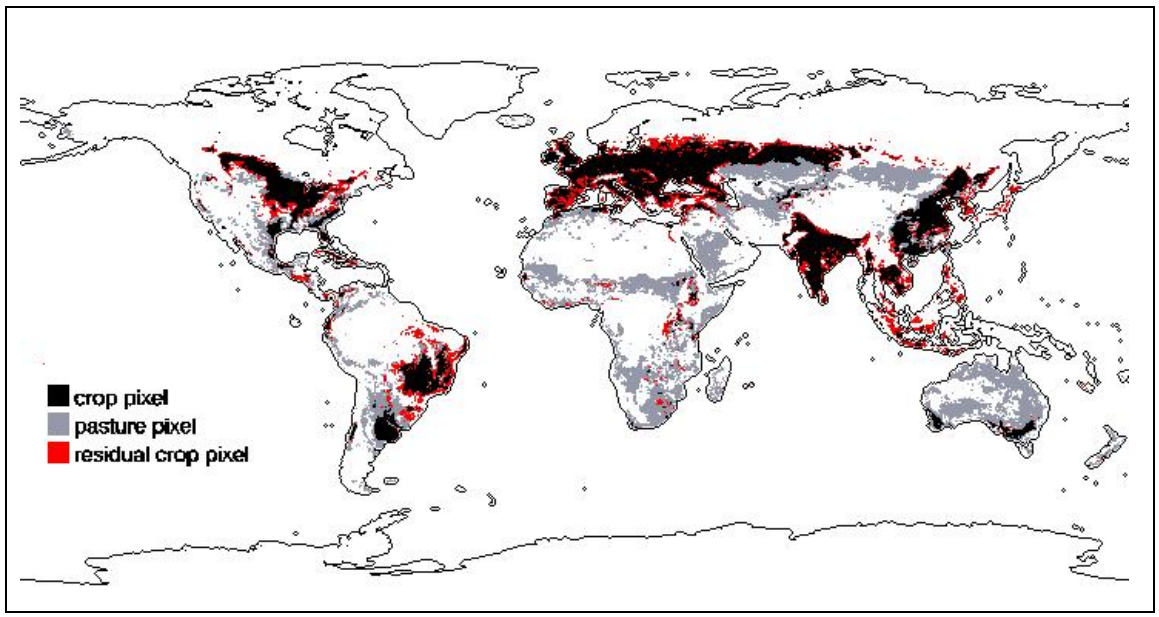

Fig. 4.3. Map of residual crop pixels (red) within the natural regions

The reduction of NPP due to residual crop pixels within the natural areas only constitutes 0.8 (0.9) PgC yr^{-1}. The satellite induced reduction of NPP in natural areas therefore amounts to 4.6 (5.3) PgC yr^{-1} and can be traced back to a more realistic modelling of seasonality as well as the reduced vegetation cover provided by the satellite data. This effect is also found within the agricultural areas. As NPP for the agricultural areas increases by 2.5 PgC yr^{-1} when comparing LPJ-P with LPJ-C (Tab. 4.5), the reduction of NPP in agricultural areas after implementing the satellite data (GIMMS: 5.2 $PgCyr^{-1}$; PAL: 5.3 $PgCyr^{-1}$) must be the consequence of the fPAR induced seasonality of crops as well as a more open vegetation (see hypothesis 2).

	LPJ-P	**LPJ-C**	**LPJ-S_{GIM}**	**LPJ-S_{GIM} no crops**	**LPJ-S_{PAL}**	**LPJ-S_{PAL} no crops**
All pixels	70.6	73.1	60.0	59.5	59.2	58.6
Agricultural areas	25.6	28.1	20.4	19.9	20.3	19.7
Natural areas	45.0	45.0	39.6	39.6	38.9	38.9
Residual crop pixels	9.9	9.9	9.1	9.1	9.0	9.0

Table 4.5. NPP (average 1982 to 1999 in PgC yr^{-1}) for different LPJ versions for agricultural and natural regions

In order to analyze whether the differences between the two versions (LPJ-P and LPJ-S_{GIM}) might be traced back to model deficiencies or to implementation of agricultural areas, I regarded the latitudinal patterns of NPP for the different model versions (LPJ-P and LPJ-S), divided into natural and agricultural areas.

As noted, total NPP is reduced after implementation of the satellite data, particularly north of 15°S. Strongest reduction occurs in the northern latitudes (30° to 60° N) and in the tropics which can be deduced to a more realistic vegetation cover in both the natural and agricultural regions (cf. Fig. 4.1). Only in a small band between 20° and 30° N, the semi-arid areas simulated by LPJ-S show a slightly higher NPP which can be attributed to a greening trend in the Sahel throughout the 1990s (Eklundh & Sjöström 2005, Hickler et al. 2005). South of 15°S NPP of both versions is nearly the same. There, neither the natural nor the agricultural areas show an appreciable difference between the two versions, because human influence is small and the NPP of the cropland is nearly as high as the NPP of the natural vegetation. Regarding the natural tropical areas north of 15°S (dark and light green), the difference between the two versions indicates a modelling deficiency concerning the seasonal cycle modelling, likely due to a shift in PFT distribution from tropical evergreen to deciduous forest (see hypothesis 3).

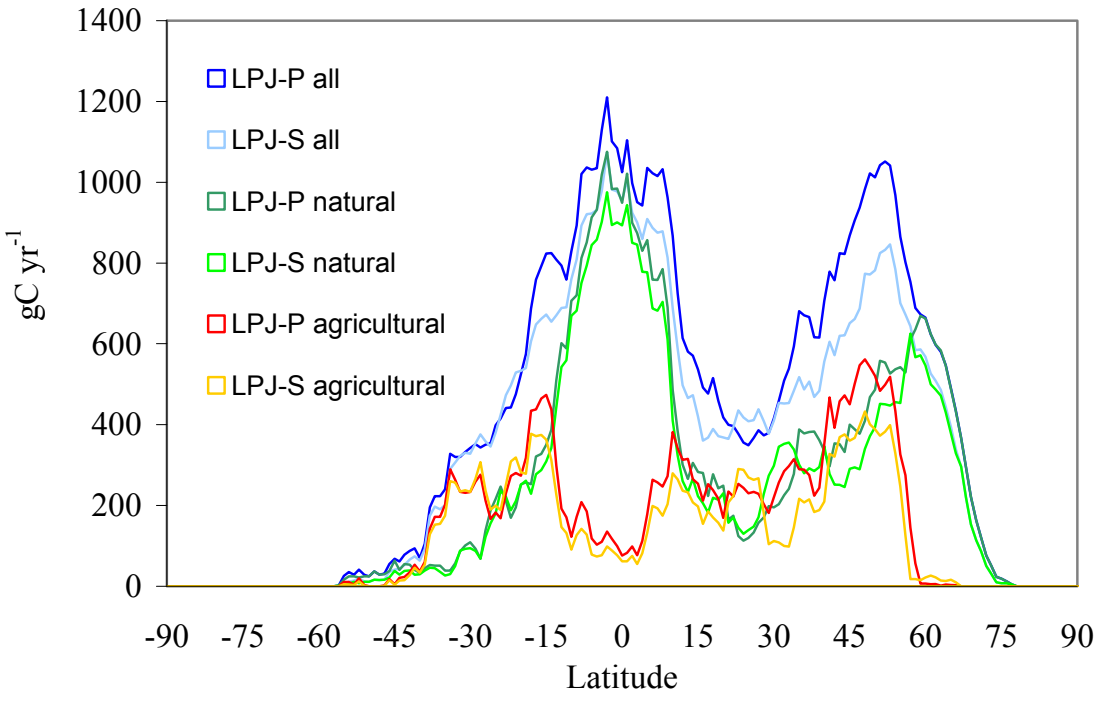

Fig. 4.4. Latitudinal distribution of NPP for LPJ-P (darker colours) and LPJ-S_{GIM} (lighter colours) for 1999. Agricultural Pixels are all pixels within the crop & pasture mask (reddish), and natural areas are defined as the pixels outside the crop mask (greenish).

However, as table 4.4 shows, the satellite data captures human influences within the natural areas due to deforestation, land-use change, forest management or selective logging, since the

strongest differences occur in the northern temperate and boreal zone and in the tropics, where a strong human impact can be assumed. As human influence is followed by a loss in forest biomass, also the NPP is reduced. A small fraction of reduction can be deduced to the residual crop pixels which are classified as natural. The two curves recording the agricultural regions show only a slightly lower NPP of crops compared to the potential natural forest, due to the enhanced NPP of the crops.

(2) Reproduction of a more heterogeneous landscape with more open vegetation in natural vegetation regions due to the implementation of the fPAR data

The global reduction of NPP after implementing the satellite data is partly the consequence of a reduction of vegetated areas as well as of changes of vegetation cover from forest to grassland, resulting in a more heterogeneous landscape with more open vegetation. Fig. 4.5 shows, that in wide regions vegetated area is reduced after implementing the satellite data.

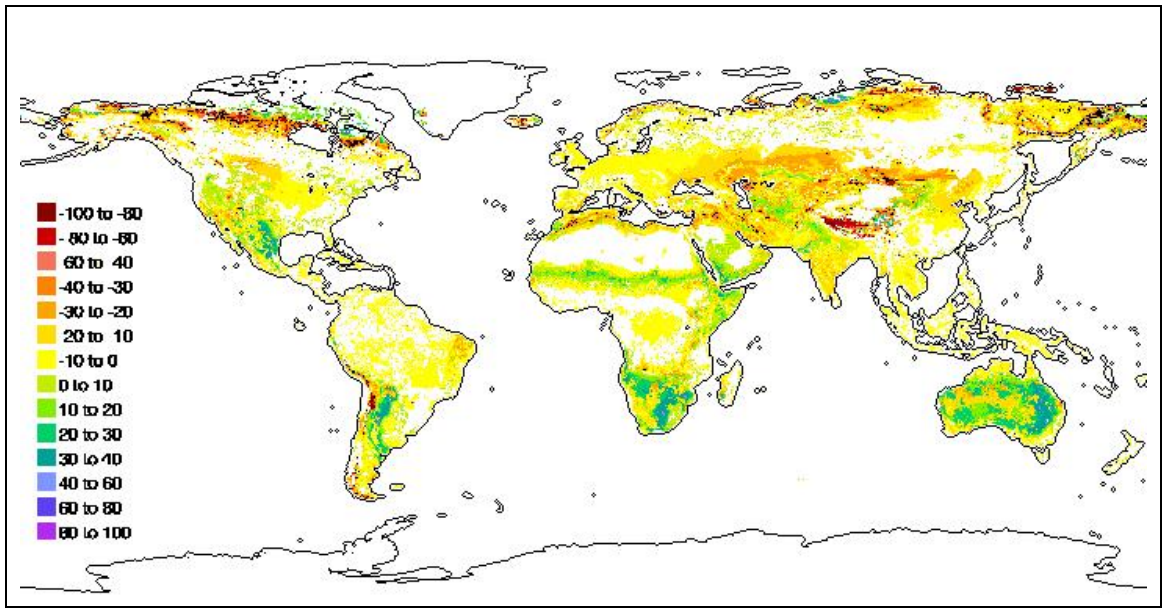

Fig. 4.5. Changes in vegetated area after implementation of fPAR data (LPJ-S_{GIM} minus LPJ-P) - decrease (negative) and increase (positive) in % of total foliage projective cover.

Most of the reduction of vegetated area is around 20 %, although in some areas in the North American and north Siberian tundra region, particularly near the tree line, as well as in some marginal regions of the Himalaya and the South American Andes the reduction exceeds 60%. This conclusion was already drawn by Sitch et al. (2003), showing a forest-tundra border located too far north, which is now improved by assimilation of the satellite data. For the semiarid regions of Africa (the Sahel region and southern Africa) as well as for Australia and the grasslands of America and Asia an increase in vegetated area is simulated by LPJ-S. In these regions both, the grassland and the forest fraction, increases with a stronger emphasis on

grasslands (Figs. 4.6 and 4.7). This reflects the inability of LPJ-P to correctly reproduce particularly the vegetation of semi-arid regions with extreme climatic conditions such as frequent droughts. In these regions very specialized vegetation grows, which likely is not captured adequately by the PFTs. Sitch et al. (2003) stated that LPJ-P tends to overestimate the woody components in the African Sahel and the North American Prairie, which is now modelled more correctly by LPJ-S (cf. fig. 4.1).

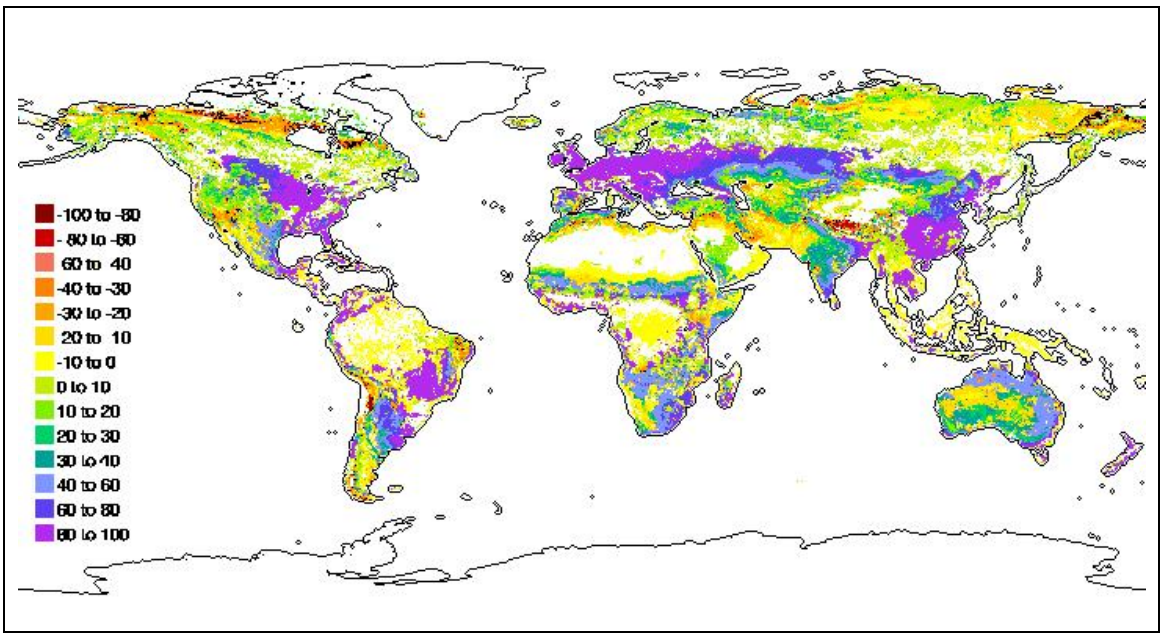

Fig. 4.6. Changes in grass area after implementation of fPAR data in % of total foliage projective cover (LPJ-S_{GIM} minus LPJ-P)

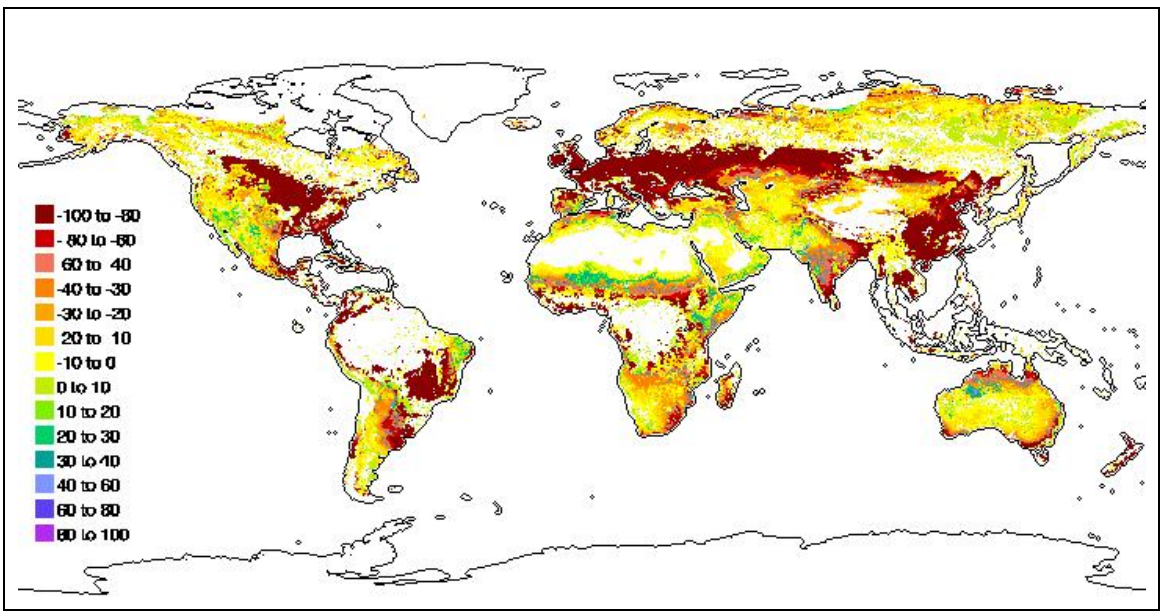

Fig. 4.7. Changes in forest area after implementation of fPAR data in % (LPJ-S_{GIM} minus LPJ-P) - decrease (negative) and increase (positive) in % of total foliage projective cover

A global increase of the barren fraction is observed, due to the reduction of grasslands, in particular in the polar and high altitude regions (fig. 4.6). Areas with strong grassland increase predominantly belong to cropland or pasture areas (see chapter 3.3.2). As a matter of course, the forests disappeared in the agricultural regions (fig. 4.7). Several regions in the boreal zone and Northern America show a slight increase of grasslands, underlining the fact that the boreal forests are more heterogeneous and open than modelled by LPJ-P.

The question arises which spatial patterns emerge when comparing the NPP simulated by the different approaches of LPJ. Which regions contribute most to the differences in NPP? Is the implementation of the satellite data followed by a global reduction or is it possible to specify regional differences in NPP increase and decrease? Fig. 4.8 shows the differences in NPP output between LPJ with agricultural regions (LPJ-P) and LPJ constrained by satellite data (LPJ-S). Yellow and red colors indicate higher values for LPJ-C, whereas green and blue colors refer to a larger NPP computed by LPJ-S.

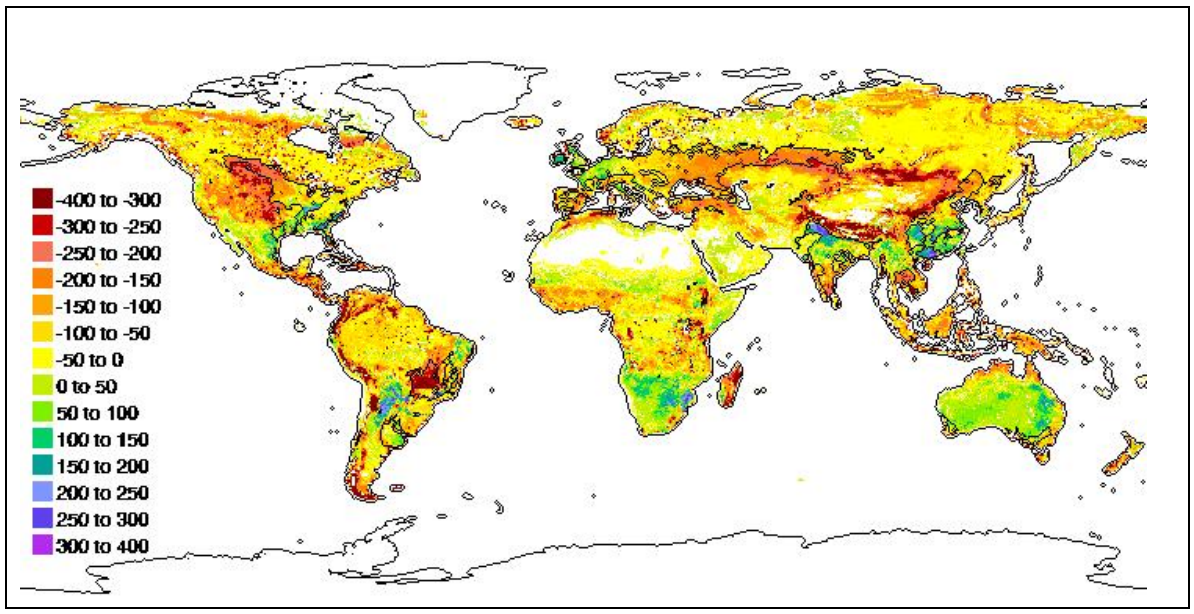

Fig. 4.8. Differences of NPP between LPJ-S_{GIM} and LPJ-P in gCm^{-2} yr^{-1}(LPJ-S minus LPJ-P), averaged over 1982 to 2002, agricultural areas are marked by a black line.

LPJ-P generally slightly overestimates the productivity of almost all ecosystems. Regions with greatest reduction in NPP are mainly located at the northern margin of forest occurrence, and at the margins of great mountain ranges such as the Himalaya or the Andes, indicating that – as already stated above – LPJ-P does not correctly reproduce the forest-tundra. In contrast, some semi-arid regions are underestimated. The overestimation of NPP by LPJ-P might be due to the following reasons:

(1) The LPJ-P model overestimates NPP due to its inherent structure, or

(2) LPJ-S incorporates also human influence in natural forests such as management or selective logging.

Presumably, the lower NPP of forests originates in a combination of both effects. Predominantly, the reduction of NPP is an effect of less vegetation, as the changes from forest to grassland or barren suggest (Figs 4.5 to 4.7). Areas with increase of vegetation and consequently of NPP are results of an inadequate model capacity to capture very specialized or adapted ecosystems.

Further reduction of NPP might be caused by the contribution of open water (rivers and small lakes) and swamps, glades, and rocky sites which are not considered in LPJ-P (except great lakes), but which might lead to a more open vegetation in the satellite-driven version.

(3) Changes of PFT distribution in the LPJ-S version leading to a reduction in NPP

Different regions have quite different responses in terms of NPP increase or reduction after implementation of the satellite data (Fig. 4.8). In the following, changes in NPP between the two versions (LPJ-S_{GIM} and LPJ-P) are analyzed regarding the shifts in PFT distribution for regions with greatest differences. As the amounts of carbon allocation vary among the PFTs changes in PFTs must affect NPP results. It will be addressed to the question for which regions major differences occur due to the satellite data constraint, consequently showing the significant variations between the 'real world' and the world with modelled potential vegetation. Furthermore, the main reasons for these differences will be analyzed.

The following regions contribute most for the reduction in NPP due to various reasons:

A reduction of NPP in LPJ-S is observed for North America and Northeastern Siberia due to a reduction of broadleaved deciduous forest (fig. 4.1). At the same time the fraction of grasses and boreal needle-leaved forest increases. As needle-leaved forests tend to have a lower NPP than broadleaved forest (Lieth 1975), the changes in PFT distribution lead to a reduced NPP. This shift in fractional coverage reflects the satellite-derived determination of evergreen and deciduous forest fractions based on the fPAR's seasonal behavior. This result can be confirmed by Sitch et al. (2003) who showed an overestimation of boreal deciduous broadleaved vegetation in Canada and Eurasia by comparing the LPJ-P modelled vegetation cover with satellite-derived maps achieved by DeFries et al. (2000). A comparison with the map of forests and woodlands of Russia provided by IIASA agrees with the reduced distribution of broadleaved forest in LPJ-S (Stolbovoi et al. 1998, Strahov 1998, http://www.iiasa.ac.at/Research/FOR/russia_cd/for_maps.htm#for)

Major overestimation of NPP simulated by LPJ-P appears in central North America. This can be attributed to an increase of the barren fraction within the agricultural areas. Within the natural areas NPP is reduced due to a shift in PFT distribution. The mid-western and southern parts (Texas) show a decrease in forest to the benefit of the grass fraction (Figs. 4.6 and 4.7). In the Canadian and Siberian tundra the barren fraction increases by about two thirds at the

expense of grasses. Compared to the MODIS global land cover dataset and Friedl et al. (1999), these shifts lead to more realistic conditions.

For the southern margin of the Himalayan Mountains and the Andean region an increase of the barren fraction occurs at the cost of boreal broad-leaved deciduous forest and grasses leading to a considerably reduced NPP. The MODIS global land cover map shows that, in fact, these regions are dominated by grasslands and open shrub lands with actually a more open landscape than simulated by LPJ-P.

In the pasture regions of Northern Africa and Mongolia the barren fraction significantly increases within the satellite-constrained version at the cost of grasses. This indicates a strong degradation in these regions (20 to 30 %) which could not be captured by the original model even though the pasture mask is implemented.

Some small regions obtain increased NPP after satellite data input. Regions with a surplus up to 50 to 80 gC m^{-2} yr^{-1} are located at the southern margin of the Amazon basin, Southwest Africa, and Australia. In the Amazon region a shift of tropical evergreen broad-leaved forest further southwards replacing deciduous forest leads to the slight increase in NPP. In Australia the grass fraction is reduced while the evergreen types, both needle-leaved (needle-leaved evergreen trees are represented by Eucalyptus forms in Australia) and broad-leaved, are expanding. Furthermore, some regions with a surplus up to 200 gC m^{-2} yr^{-1} can be observed in Southern Brazil/Argentina, Eastern Brazil and Southern China/Northern Thailand. In Brazil the tropical evergreen forest spreads out into the southern and the eastern parts which increases NPP. In South China the fraction of temperate needle-leaved evergreen and broad-leaved deciduous forests decrease at the benefit of temperate broadleaved evergreen forest while the total fraction of plant cover remains unchanged.

NPP increased within some agricultural areas, i.e. in Northern India and Southern China, likely due to irrigation (Döll & Siebert 2002). The increase in agricultural NPP as observed for Western Europe and Southeastern United States can be attributed to intensive cultivation and fertilization. The higher NPP observed for the South African and Australian pasture regions in LPJ-S indicates that the forced grass growth is better adapted than the potential natural savanna, likely because no competition with trees occurs.

(4) Improved seasonality within both the crop regions and natural areas due to the implementation of the fPAR data

A testing of several agricultural pixels showed a significant reduction of the maximum fPAR values, but no distinct harvesting date could be detected. In fact, the winter values of fPAR in agricultural areas range mostly up to 0.5, indicating an intensive cultivation during wintertime with winter wheat or green manuring. Additionally, no comparable results are existent in the

literature, as all studies about crop seasonality are site-specific or they investigate crop production and yield but without linking it to seasonality (e.g. Moulin et al. 1998, Abrol et al. 1996, Prince et al. 2001, Unsworth et al. 1996). Therefore, this hypothesis remains unproved.

Concluding, implementation of agricultural areas and assimilation of the fPAR data contribute by nearly the same extent to the NPP reduction with 5.2 and 4.6 PgC yr^{-1}, respectively. For all regions the opening of the landscape mainly causes the reduction while in the natural areas additional effects due to shifts in PFT distribution can be observed. Changes in seasonality due to the fPAR data could not be ascertained.

4.3 Heterotrophic respiration (Rh)

Rh is the carbon released to the atmosphere through the process of decomposition of organic carbon, mainly by soil micro-organisms. The patterns of Rh look similar to those of NPP (Fig. 4.2), but are slightly lower in magnitude (Fig. 4.9). Highest values are found in the tropical forest, lowest in the arid and semi-arid regions as well as in the sparely vegetated tundra regions at high latitudes. Comparing LPJ-P to LPJ-S, Rh is globally reduced by 8.6 (9.2) PgC yr^{-1} due to the lower biomass input into soils (Tab. 4.3). Annual amount of Rh is found to be 52.3 (51.7) PgC yr^{-1} (LPJ-S), as an average of the period 1982 to 1999.

Fig. 4.10 shows the difference of Rh between LPJ-P and LPJ-S. Comparable to NPP (Fig. 4.8), Rh is reduced within the agricultural areas due to a general decrease in vegetation cover (Fig. 4.4), and due to the amount of harvested carbon that does not enter the soil pool. Only some parts in India show an increase due to more vegetated area (Fig. 4.5) followed by higher NPP (Fig. 4.8) and Rh levels. This might be an effect of irrigation which can indirectly be observed by the satellite, as the occurrence of more green vegetation leads to increased soil respiratory processes. For the western Siberian region some areas with increased Rh can be observed. Some of the semi-arid regions in southern Africa and Australia also show a higher respiration in the satellite-constrained version, as a consequence of more dense vegetation with a higher litter input and enhanced respiration activity in the soils.

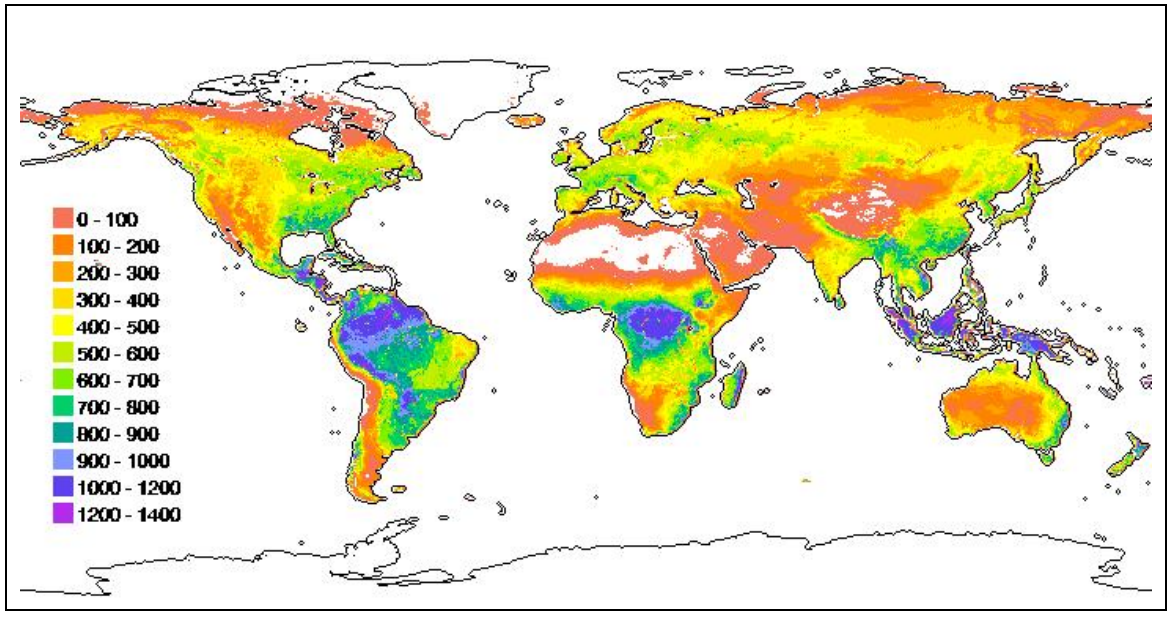

Fig. 4.9. Average Rh for the period 1982 to 2002 as derived from a LPJ-S_{GIM} simulation run with satellite fPAR data (in gC m^{-2} yr^{-1})

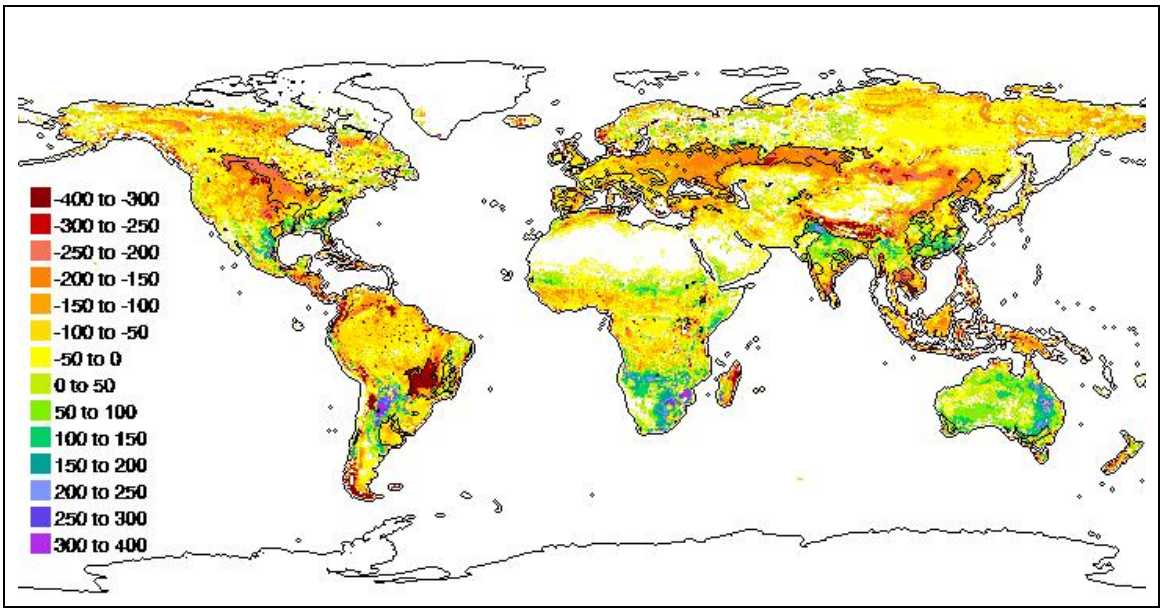

Fig. 4.10. Differences of Rh between LPJ-S_{GIM} and LPJ-P in gCm^{-2} yr^{-1}, averaged over 1982 to 2002 (LPJ-S minus LPJ-P), agricultural areas are marked.

Global data on Rh for an independent comparison is rare in the literature, either as model results or as measurement-based estimates. Compared to global regression-based model results of Rh by Raich et al. (2003), our figures are significantly lower (see table 4.5). But given a global uptake of 0.8 to 1.3 PgC yr^{-1}, as well as a global NPP of 60 PgC yr^{-1} (IPCC 2001), and regarding the fact that Rh could not exceed NPP globally under carbon sink conditions, the estimate of Raich et al. (2003) must be considerably much too high. In comparison with other vegetation model results collected by the Potsdam model intercomparison project (Cramer et al. 2001) our estimates are of a similar magnitude. Compared to these figures the implementation of satellite data has improved the results significantly.

	LPJ-P	**LPJ-C**	**LPJ-S_{GIM}**	**LPJ-S_{PAL}**	**Raich et al. (2003)**	**Cramer et al. (2001)**
Time period	(1982-94)	(1982-94)	(1982-1994)	(1982-94)	(1980-1994)	
Rh in PgC yr^{-1}	61.2	63.1	51.80	51.32	79.3-81.8	~ 46-61

Table. 4.6. Mean annual global soil CO_2 emissions 1980/1982-1994

4.4 Fire Carbon

Carbon released by fire is calculated in the LPJ-model as a combination of fire occurrence and its effects (Thonicke et al. 2001). A combination of observed and statistical data (daily litter moisture status, length of fire season, burnt area) and modelled processes gives fire occurrence based upon fuel load, litter moisture and PFT specific fire resistances. Fire effects are driven by length of fire season and fire return interval.

Average global fire carbon for the period 1982 to 2002 calculated with LPJ-S_{GIM} is shown in Fig. 4.11.

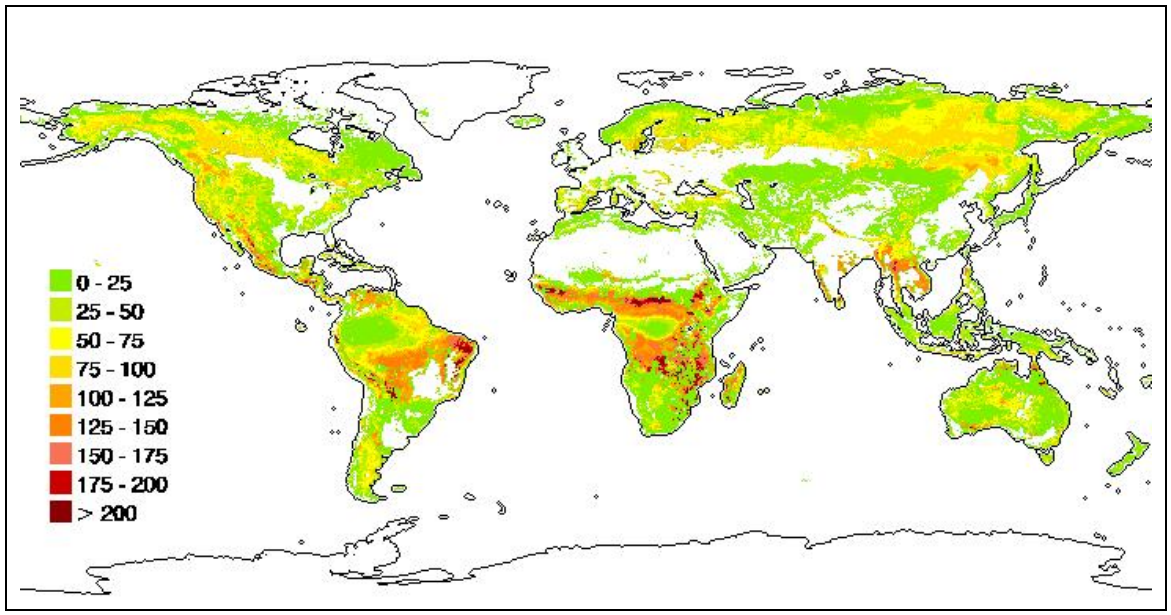

Fig. 4.11. Average carbon released by fire for the period 1982 to 2002 as derived from LPJ-S_{GIM} (in $gCm^{-2}\ yr^{-1}$)

Highest fire carbon release is found in the semi-arid areas of Africa and South America where the occurrence of deciduous forest provide more fire carbon load than grasslands. The wide-spread areas in Europe, North America and South-East Asia without any fire carbon release refer to the agricultural areas (i.e. croplands) where fire is suppressed in the LPJ-S simulation. Global fire carbon of LPJ-P is 8.4 PgC yr^{-1}, more than double the values found in literature. Andreae & Merlet (2001) estimate global burnt biomass for the late nineties to have been 8.6 Pg yr^{-1}. Converted to carbon mass (factor: 0.45, Schultz, 1995), this leads to 3.9 PgC of annual global carbon burnt by fire. Implementation of the satellite data should lead to a more realistic fire carbon due to reduced NPP and biomass. Comparing LPJ-P with LPJ-C (see table 4.6), fire carbon was significantly reduced (from 8.4 to 4.9 PgC yr^{-1}) due to the implementation of the crop-mask. This is the result of fire suppression for agricultural areas (croplands). With LPJ-S global fire carbon is found to be 4.3 (4.1) PgC, presenting an additional decrease of 0.6 (0.8) PgC yr^{-1}. This figure agrees much better with the estimate given by Andreae & Merlet (2001).

The reduction of fire carbon when assimilating the satellite data can be traced back to several processes:

(1) Reduction of combustive material in pasture areas where fire was not suppressed due to a reduction in total vegetation cover,
(2) Reduction of total burnt area due to fire suppression in agricultural areas, or
(3) Reduction of combustive material and fire occurrence in natural regions
(4) Reduction in total burnt biomass due to less vegetation cover (if fires occur, less biomass to be lost)

In order to investigate these hypotheses, table 4.6 shows the itemization of the fire carbon fractions for agricultural and natural areas, as well as for the residual crop pixels not captured by the agricultural masks.

	LPJ-P	**LPJ-C**	**LPJ-S_{GIM}**	**LPJ-S_{GIM} no crops**	**LPJ-S_{PAL}**	**LPJ-S_{PAL} no crops**
All pixels	8.4	4.9	4.3	7.0	4.1	6.6
Agricultural areas	3.7	0.6	0.2	2.9	0.2	2.7
Natural areas	4.3	4.3	4.1	4.1	3.9	3.9
Residual crop pixels	1.2	1.2	0.7	0.7	0.6	0.6

Table 4.7. Carbon released by fire (average 1982 to 1999 in PgC yr^{-1}) for different LPJ versions for agricultural and natural regions

In agricultural areas fire carbon is reduced significantly (by 3.5 PgC yr^{-1}) after satellite data assimilation; the remainder of 0.2 PgC yr^{-1} is associated to fire occurrence in pasture regions. In natural areas fire carbon has only decreased by 0.2 (0.4) PgC yr^{-1} with a total amount of 0.7 (0.6) PgC yr^{-1} in residual crop pixels indicating a stronger reduction of fire carbon in natural areas. This results from combined effects of an opening of the landscape providing less biomass for fire fuel in the natural areas and a shift of PFTs to grass domination with a high flammability in the residual crop pixels.

Another relevant parameter for investigating changes of fire occurrence and fire carbon release is the average fire return interval (FRI) (Fig. 4.12). FRI is defined as the expected return time of fire in a certain region, which is the inverse of the annual fractional area burnt, averaged over a sufficiently long time period, according to the fire history concept of Johnson & Gutsell (1994) (Thonicke et al. 2001). In order to analyze whether an increase of fire return interval contributes to the reduced fire carbon (hypothesis (3)), fig. 4.13 shows differences in FRI. Positive values refer to a decrease in fire occurrence.

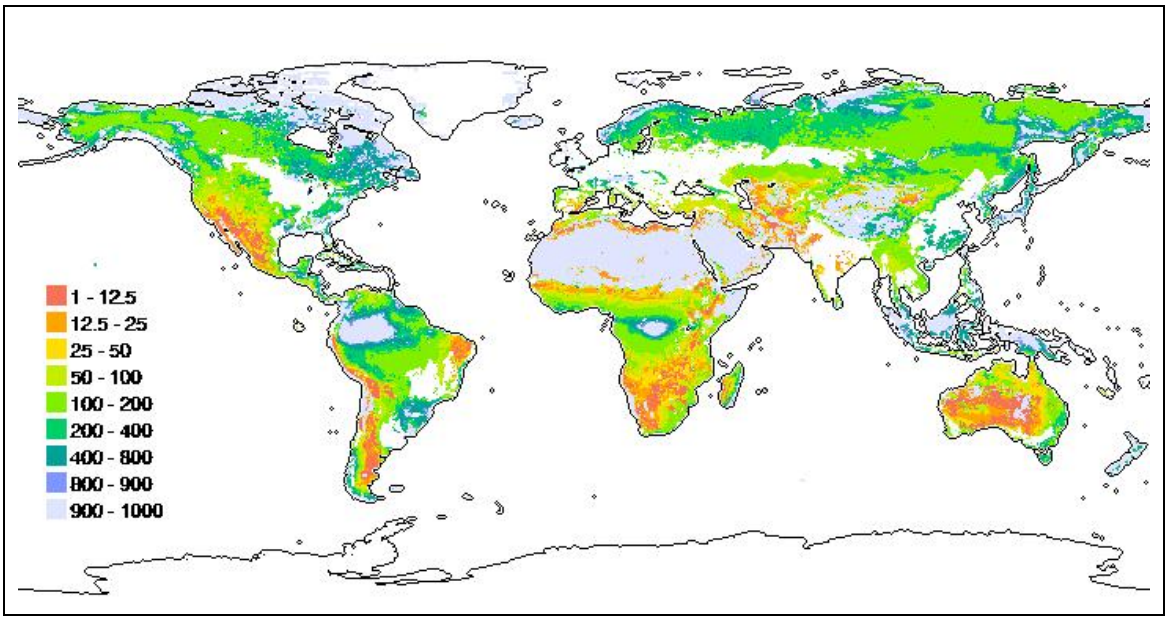

Fig. 4.12. Average fire return interval (FRI) in years (LPJ-S_{GIM}, average over 1982 to 2002).

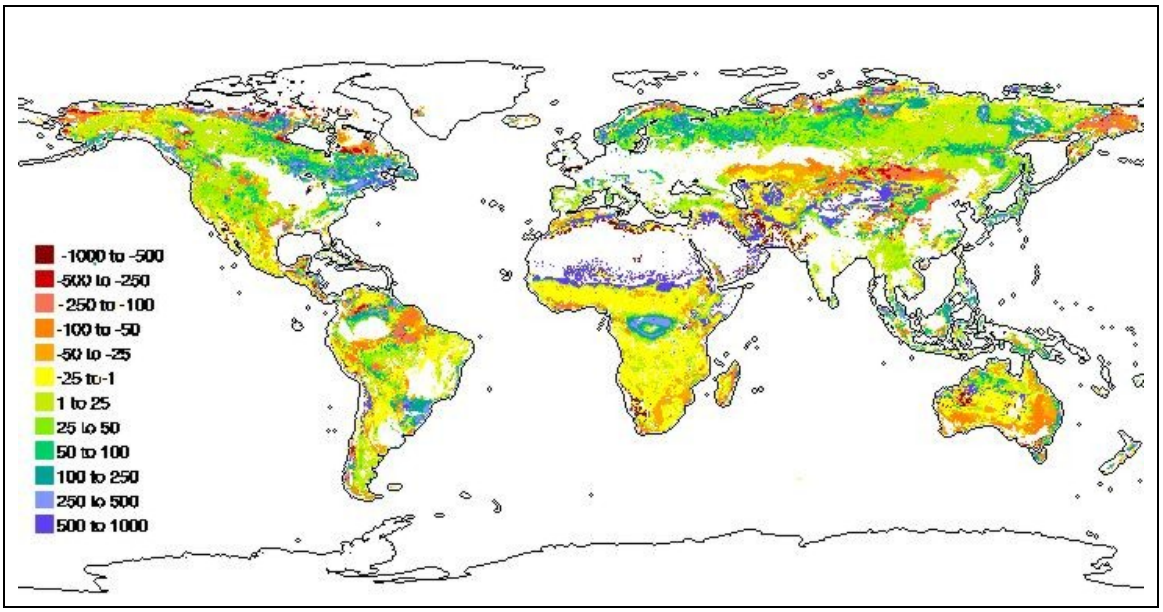

Fig. 4.13. Comparison of FRI (in years) for different versions (LPJ-S_{GIM} minus LPJ-C) in years, averaged over 1982 to 2002

Fire frequency particularly decreased in eastern North America, the entire boreal zone and in some small parts of the tropical forests. Probably this is due to less combustive material following a lower amount of biomass and less litter input. FRI of the Siberian boreal forests is simulated too short by LPJ-P (Thonicke et al. 2001). After the satellite data assimilation, the fire frequency decreased in these regions except for the far eastern Siberian region. Biomass and therefore combustive material of the boreal zone is dependent on permafrost, which reduces soil moisture and increases fire occurrence (Beer 2005). Unfortunately, consideration of permafrost was still in development when producing the current results with LPJ-S. A small increase of fire occurrence is associated with a small increase of fire carbon, especially in the African tropical and subtropical zone, as well as in southern Australia, the southern Eurasian

regions and the semi-arid regions of Central America. This can be attributed to the change from forest to more grasslands, which have a higher flammability. Fig. 4.14 highlights the spatial differences and patterns of carbon released by fire between LPJ-C and LPJ-S.

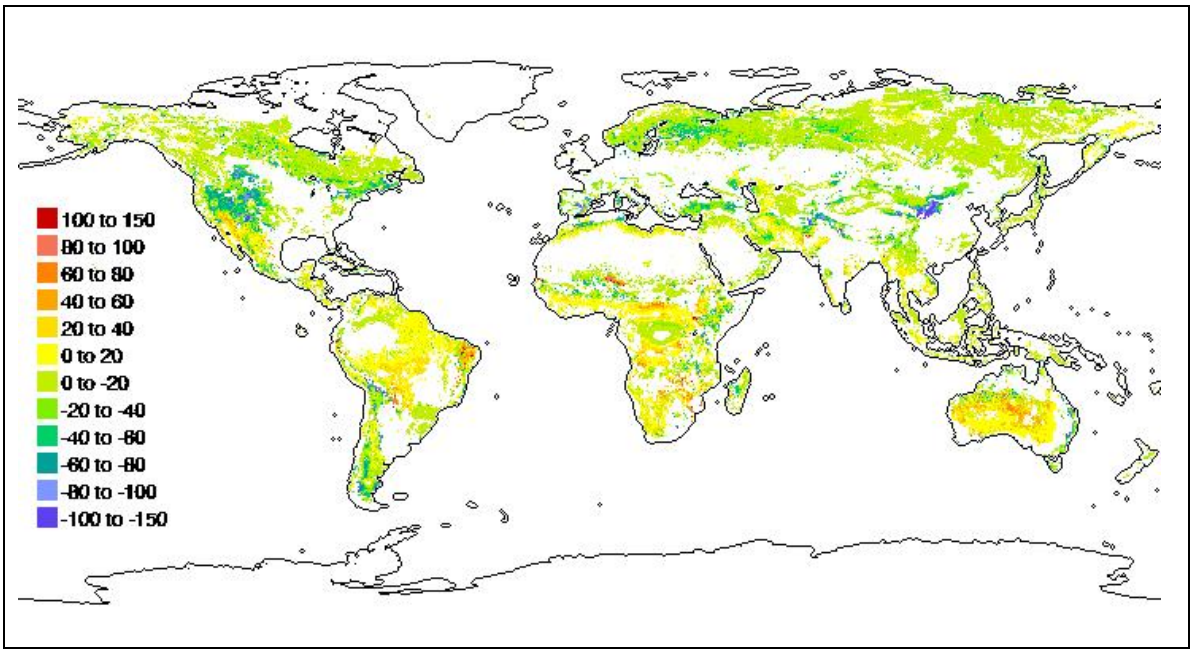

Fig. 4.14. Differences of fire carbon between LPJ-S_{GIM} and LPJ-C in gCm^{-2} y^{-1}, averaged over 1982 to 2002 (LPJ-S_{GIM} minus LPJ-C)

Due to assimilating the satellite data fire carbon was reduced in the temperate and higher latitudes, whereas it somewhat increases in the tropics and the semi-arid regions of Africa and Australia. Occurrence of fires is dependent on available litter carbon; it has to exceed a threshold of 200 gCm^{-2} of litter carbon (Thonicke et al. 2001). Therefore, the reduction of fire carbon in Northern America and East Asia is due to reduced litter carbon. However, increase of fire carbon as a consequence of increasing litter carbon only occurs in Australia. In the southern Amazon region and in Africa neither litter carbon nor NPP are enhanced. An increase of tropical evergreen forest with higher biomass at the expense of less-productive rain-green forest might be the cause for this fire carbon increase.

The significant reduction of fire carbon is obviously when plotting the latitudinal means (Fig. 4.15). LPJ-P shows doubled fire carbon compared to both LPJ-C and LPJ-S. Strongest reduction occurred in the northern latitudes between 30 and 60°N where also fire return interval decreased strongest. Differences between LPJ-C and LPJ-S occur mainly within the agricultural regions between 30° and 50°N, i.e. in pasture regions, where fire is not suppressed, whereas the remaining regions show only small differences. Therefore, the additional reduction between LPJ-C and LPJ-S is only due to implementation of the satellite data within the pasture regions, leading to grass-dominated vegetation with higher fire frequency.

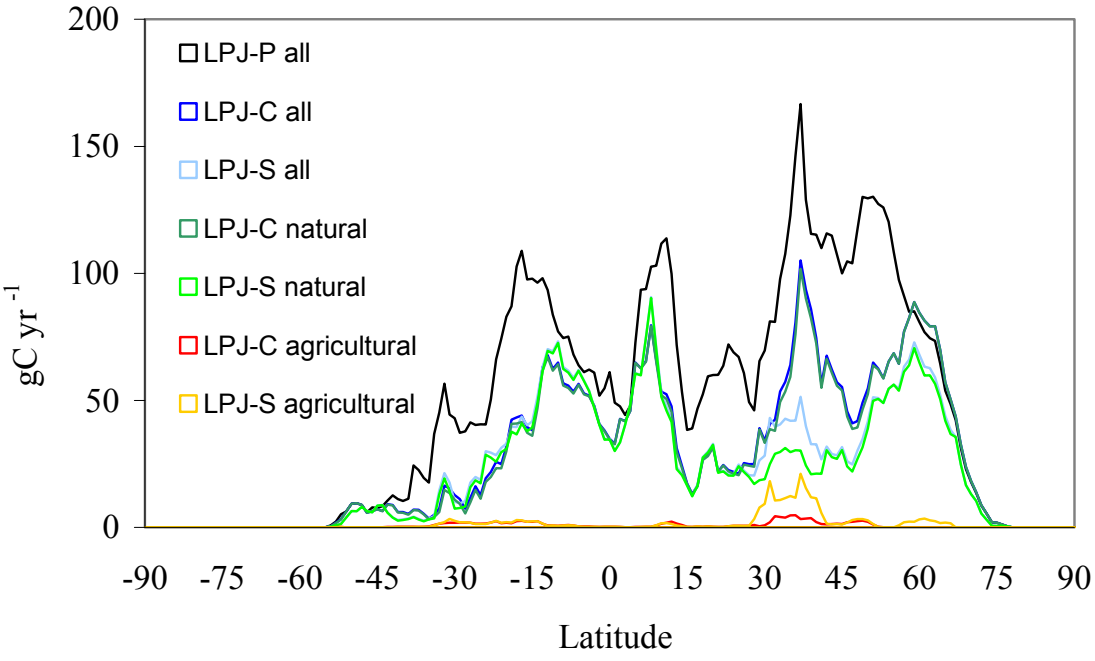

Fig. 4.15. Latitudinal distribution of fire carbon (1999) for LPJ-C (darker colours) and LPJ-S_{GIM} (lighter colours). Agricultural Pixels are all pixels within the crop & pasture mask (reddish), and natural areas are defined as the pixels outside the crop mask (greenish).

4.5 Harvest

As described in more detail in chapter 3, 75 % of annual growing aboveground biomass on agricultural lands is harvested. Grazing of pasture has not been considered. Global figures on annual harvested carbon are rarely found in the literature. For comparison, I estimated global harvested carbon based on global annual yield production for 176 crop-types published by the FAO (2001). Based on this dataset, I calculated dry matter depending on conversion factors derived from measurements of water content for different crops (Kirchgeßner 1987). Finally, the amount of carbon is set as 45 % of dry matter as proposed by Schultz (1995) and Carvalho et al. (1998). It has to be noted that the achieved results must be seen as guiding values, as yield does not exactly corresponds to harvested material, which additionally includes e.g. straw. Comparison with FAO global yield data shows that the simulated amount of harvested carbon is within the same order of magnitude: the FAO dataset reports 1.99 PgC annual harvested carbon, LPJ both with GIMMS and PAL calculates 2.7 Pg of annual harvested carbon. Taking into account that the FAO value is based on yield data and therefore too low, the LPJ value seems to be plausible. IPCC (2000) estimates global annual NPP of croplands to be 5.1 to 6.8 PgC yr^{-1}. Subtracting the value of 75% harvested material which is assumed here to return to the atmosphere, these figures are reduced to 3.1 to 4.1 PgC yr^{-1} which is close to the estimate of the present study. The global comparison between the different approaches shows a reduction of harvest from LPJ-C to LPJ-S from 3.3 to 2.7 PgC yr^{-1} due to a further reduction in total vegetated area.

4.6 Biomass

Several attempts have been made to estimate global vegetation biomass, and their results range between 450 and 1395 PgC (see table 4.7). They base on statistical approximations of forest inventories, and on process- or remote sensing-based modelling. E.g., IPCC (2001) gives 466 or 654 PgC global carbon stocks of plants, depending on the analysis they refer to (WBGU 1988, Mooney et al. 2001). The wide range of values results from using different definitions of the term 'biomass' and the terrestrial surface. I.e., Smil (2003) defines 'biomass' as the entirety of all living organisms including their non-metabolizing tissues, whereas 'phytomass' as used in table 4.7 is the amount of biomass stored above-ground. Global forest carbon stocks as discussed in the IPCC report (2001) encompass all above- and below-ground tree components (stems, branches, leaves, and roots) including standing dead biomass (WBGU 1988).

Study	**Phytomass/Biomass**
Ajtay et al. (1979)	560
Amthor et al. (1998)	486
Baes (1976)	680
Bazilevich et al. (1971)	1080
Bolin (1970)	450
Bolin et al. (1979)	590
Bowen (1966)	507
Brown & Lugo (1982)	500
Cao & Woodward (1998b)	640
Esser (1987)	657
Field et al. (1998)	500
Foley (1994)	801
Goudrian & Ketner (1984)	594
Hall & Scurlock (1993)	560
Holmen (1992)	560
Kovda (1971)	1395
Matthews (1984)	734
Mooney et al. (2001), IPCC (2001)	654
Olson et al. (1983)	559
Post et al. (1997)	780
Potter (1999)	651
Siegenthaler & Sarmiento (1993)	550
Sitch et al. (2003)	910
Smith et al. (1992)	737
WBGU (1988), IPCC (2001)	466
Whittaker & Likens (1975)	827
This study (LPJ-S_{GIM})	638

Table 4.8. Estimates of global phytomass (above-ground biomass, from Smil, 2003) and biomass (including below-ground biomass, additional values from other studies shaded in gray) (in PgC).

In the current approach, biomass is calculated as the sum of all above- and below-ground biomass, including leaf mass, sapwood mass, heartwood mass and root mass for each individual, extrapolated to the area by multiplication with population density. Global biomass of vegetation (including root mass) is found to be 638 (615) PgC derived by LPJ-S, 272 (295) Pg lower than LPJ-P (Tab. 4.3), now comparing better with the results of IPCC (2001). If phytomass is assumed to be 25 % of total above- and below-ground biomass (House & Hall 1999, Jackson et al. 1996, 1997), LPJ-S now is situated at the lower end of the range giving 479 PgC of above-ground biomass.

Fig. 4.16 shows global carbon storage in terrestrial biomass with the tropical forests achieving highest accumulation of vegetation carbon (15 to 25 kg m^{-2}), followed by the boreal forests (6 to 15 kg m^{-2}). The figures for the tropical forests compare well with data collected by the FAO using forest inventories (Brown 1997), giving 15-35 kg m^{-2} for moist forest, but using a different biomass definition (biomass is defined as the total amount of aboveground living organic matter in trees expressed as oven-dry tons per unit area). Considering the amount of carbon in dry matter (-45 %, Schultz 1995) as well as in root mass and above-ground dead biomass (+50%), the FAO figures remain comparable to the model output.

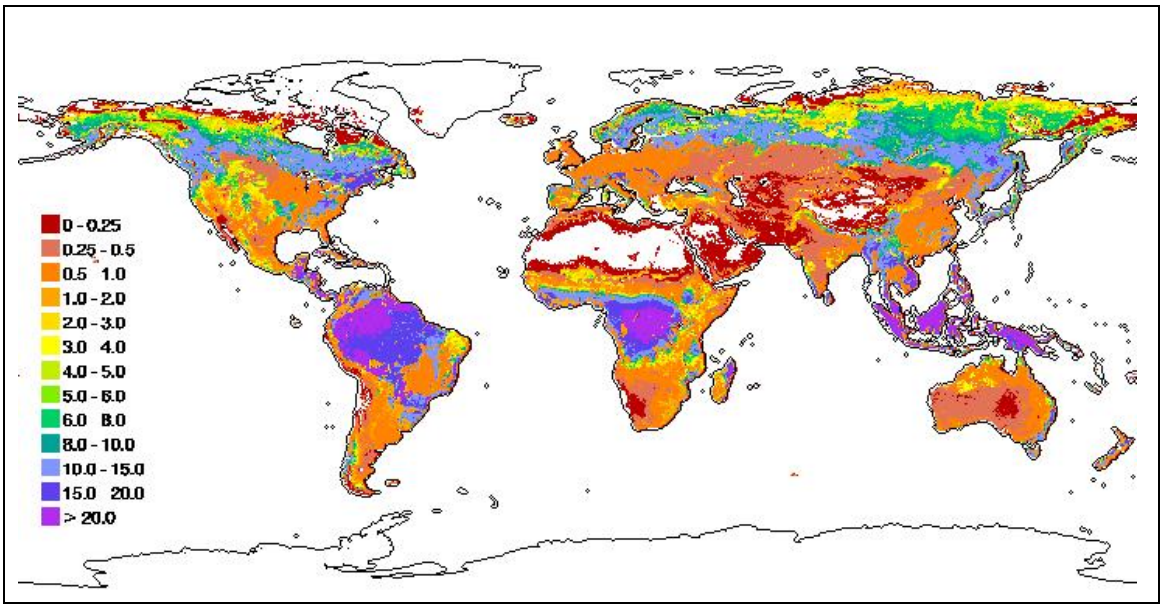

Fig. 4.16. Average biomass (above- and below-ground) for the period 1982 to 2002 as derived from LPJ-S_{GIM} (in kg m^{-2} yr^{-1}), please notice that the legend is nonlinear.

As stated before (see table 4.3), a significant reduction of global biomass occurs comparing LPJ-P with LPJ-S. Biomass of LPJ-S is 272 (295) Pg lower than LPJ-P. The question arises which regions contribute most to the reduction in global biomass after implementing the satellite data. Is there a general reduction leading to the global figures or are there regions where biomass increases or strongly decreases after implementation of the satellite data? Table 4.9 indicates that strongest reduction occurs due to the implementation of the agricultural areas.

	LPJ-P	LPJ-C	LPJ-S_{GIM}	LPJ-S_{GIM} no crops	LPJ-S_{PAL}	LPJ-S_{PAL} no crops
All pixels	910	667	638	837	615	796
Agricultural areas	274	31	35	234	33	214
Natural areas	636	636	603	603	582	582
Residual crop pixels	121	121	95	95	92	92

Table 4.9. Average Biomass in PgC (1982 to 1999) for different versions for agricultural and natural regions.

Regarding spatial patterns (fig. 4.17), implementation of the crop mask produces the strongest differences, mostly higher than 5 kg $m^{-2}yr^{-1}$. The difference between LPJ-P and LPJ-C of 243 PgC refers to the reduction due to the implementation of grass instead of woody PFTs representing the total carbon loss due to deforestation and land-use. The historical carbon loss due to land-use change was estimated to be 180 to 200 PgC up to the 1990s (DeFries et al. 1999), and 156 PgC for the period 1850 to 2000 (Houghton 2003c). House et al. (2002) estimate the emissions due to land-use change to have been 200 to 220 PgC since ancient times up to the year 2000. Assuming LPJ to overestimate vegetation biomass by 33 to 54 PgC (according to the difference between LPJ-P and LPJ-S in the natural areas), the remaining carbon loss due to human influence is found to be 239 (241) PgC until 1999 with the approach used in this study. Our figures only slightly exceed the above-mentioned figures.

The reduction of 33 (54) PgC between LPJ-C and LPJ-S in the natural areas indicates that LPJ-P overestimates biomass of natural vegetation of about 5 to 10%. Compared to other modelling studies and inventory data, overestimation of the natural areas appears to be somewhat higher. E.g., Dong et al. (2003) calculate a carbon storage of 61 ± 20 PgC for 1.42 billion ha of temperate and boreal forest (including biomass of wood, bark, braches, twigs, stumps and roots of trees, but no dead biomass). LPJ-P simulates a biomass of 95.6 PgC for 1.7 billion ha of temperate and boreal forest including dead biomass, which is reduced to 67.5 PgC after satellite data assimilation, now comparing better with the inventoried data.

As forest inventories provide relatively accurate measurements of forest growth and stock volume for natural areas on regional scales, Table 4.10 compares biomass per unit area as derived by different LPJ-model versions applied on local scales with forest inventory data for Europe and a region in central Siberia. The LPJ approach of Beer (2005) includes permafrost simulation and assimilation of satellite-derived land cover data in Siberia, while Zaehle (2005) considers changes of allocation rules to a tree-size dependent allocation for Europe. Table 4.10 shows that model improvements as proposed by Zaehle (2005) and Beer (2005), as well as assimilation of fPAR data (this study) lead to significant reduction of biomass compared to the LPJ-P model.

Region	Modelled Biomass	Approach	Reference	Forest Inventory	Reference	LPJ-S	LPJ-P
Europe	7.4	LPJ size dependent allocation	Zaehle (2005)	6.0	Goodale et al. (2002)	4.9	10.0
Siberia	5.2	LPJ permafrost	Beer (2005)	3.5	McCallum & Shvidenko, Beer (2005)	6.3	8.2
	2.8	LPJ permafrost +Landcover					

Table 4.10. Biomass density as derived by different modelling approaches and forest inventories on regional scales. Values are given in kg m^{-2}

One reason for overestimation of biomass in LPJ-P is an age-related decline in forest growth influencing biomass volumes as suggested by Zaehle (2005). It is based on the hydraulic acclimation theory (Magnani et al. 2000) that considers tree size-dependent allocation of carbon, since plants allocate more carbon to fine roots with increasing tree height to maintain water supply for transpiration as path length and hydraulic resistance increases. As a consequence, forest growth declines with increasing age, as it would be too costly for the plants to allocate biomass far away from photosynthetic tissues. Additionally, the model does not account for regional differences in soil fertility, causing major spatial variations in forest growth (Zaehle 2005).

Beer (2005) considers the following reasons for the overestimation of boreal biomass in LPJ-P: Biomass of the boreal zone is dependent on consideration of permafrost, causing a reduction of soil moisture during the growing season, and a shortening of season with available water for plants (Frolking et al. 1999; Hollinger et al. 1999). Additionally, a reduction of soil moisture is followed by an increase in fire occurrence which further reduces biomass. Simulation of more frequent fire occurrence leads to a shift in PFT distribution which influences biomass production due to differences in carbon allocation of the different PFTs. Beer (2005) showed in test runs with permafrost simulation that implementing permafrost reduces leaf mass by about 60 % due to enhanced water-stress, leading to a reduced leaf production and NPP, enhanced mortality of saplings and juvenile plants, followed by a generally decelerated forest growth (according to the studies of Jarvis & Jarvis 1964, Woodward 1995, Black & Bliss 1980). Unfortunately, an elaborate permafrost and soil moisture consideration as well as the improvements of Zaehle (2005) were still in development when producing the current results with LPJ-S. Therefore, LPJ-P and LPJ-S basically overestimate biomass in the boreal zone, although the value calculated for Siberia (table 4.10) compares well with forest inventory data. The reason for this accordance can be engaged regarding fig. 4.17, showing a strong decrease of biomass in the northern tundra regions. Beer (2005) additionally considers water surfaces, limitations in nutrient availability (Woodward, 1995) and unfavourable soil conditions to further reduce biomass, which can indirectly be fetched by the fPAR data.

However, it should be noted, that the analyses of Beer (2005) and Zaehle (2005) are regional studies and their applicability on global scales has not been tested yet.

In order to investigate how the assimilation of the satellite data influences spatial changes of biomass distribution in natural areas, fig. 4.17 records the differences between LPJ-S and LPJ-P. Within the natural temperate and boreal forest areas LPJ-P overestimates biomass in some regions, particularly in the European and the Northeast American boreal forest. Most likely for the reduction in LPJ-S is a shift in PFT distribution after implementing the satellite data. In fact, the PFT distribution changes from a dominance of boreal evergreen needle-leaved forest to more boreal broad-leaved summer-green forest. In contrast to this reduction, a broad band in Canada, as well as a region in Northeastern Siberia show a biomass increase, with opposite vegetation changes: boreal needle-leaved evergreen trees expand at the expense of boreal broad-leaved deciduous trees.

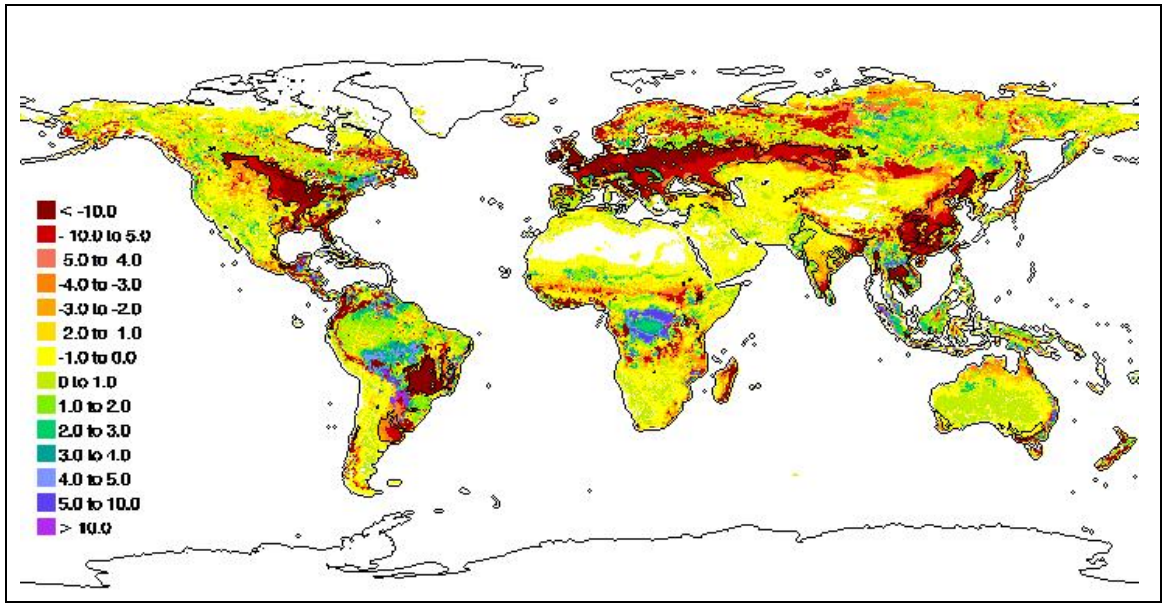

Fig. 4.17. Differences of biomass between LPJ-S_{GIM} and LPJ-P in $kgCm^{-2}yr^{-1}$. (LPJ-S minus LPJ-P), Agricultural areas are marked.

Zaehle (2005) reported that the overestimation of biomass in old forest stands is larger for conifers, explaining the increase of biomass in regions, where a change of PFT to needle-leaved forest occurrs. Although there is no persistent pattern in PFT distribution or shifting, a higher fraction of boreal needle-leaved forest occurs in most cases when biomass rises. If it decreases the fraction of boreal broadleaved deciduous forest and grasses increases. A very distinct deviation from the general pattern of overestimating biomass by LPJ occurs in tropical regions: for African, Amazon and south-east Asian tropical forest LPJ-S calculates a higher biomass than LPJ-P. This is again due to a shift in PFT distribution, as LPJ-S produces a higher fraction of tropical evergreen broad-leaved forest, at the expense of tropical deciduous broad-leaved forest. Additionally, a narrow band at the northern border of the Sahel shows a higher biomass

production with LPJ-S. These areas are not situated within the regions captured by the crop or the pasture mask. As already mentioned in chapter 4.2, PFT comparisons between the two versions show a decrease of grasses and of the barren fraction, but an increase in tree PFTs, indicating the change to a greener Sahel than expected, which is in agreement with recently published studies (Eklundh & Olssen 2003, Eklundh & Sjöström 2005, Hickler et al. 2005). Further southwards in the Sahel region biomass decreases, representing a more grass dominated ecosystem than LPJ-P predicts, suggesting that the borders of different savanna types are poorly captured within the unconstrained version. Nevertheless, those differences can also be a result of the limits of model parameterization, with difficulties to capture marginal regions or regions with plants that are highly adapted to extreme climatic conditions. This explication remains hypothetically, as it is hardly to be quantified.

Table 4.9 additionally highlights the portion of biomass captured in residual crop pixels within the natural areas. It shows that the residual crop pixels capture a lot of the reduction of the biomass total (26/29 PgC) for the natural areas when comparing LPJ-P and LPJ-S. Consequently, overestimations and underestimations approximately balance out in the global average. In fig. 4.18 the latitudinal distribution of biomass calculated by the different versions (LPJ-P and LPJ-S_{GIM}) is shown. It reflects the reduction of biomass due to the satellite data assimilation illustrated for natural and agricultural regions. The small difference between LPJ-P and LPJ-S in the natural vegetation areas can be assigned to the residual crop pixels.

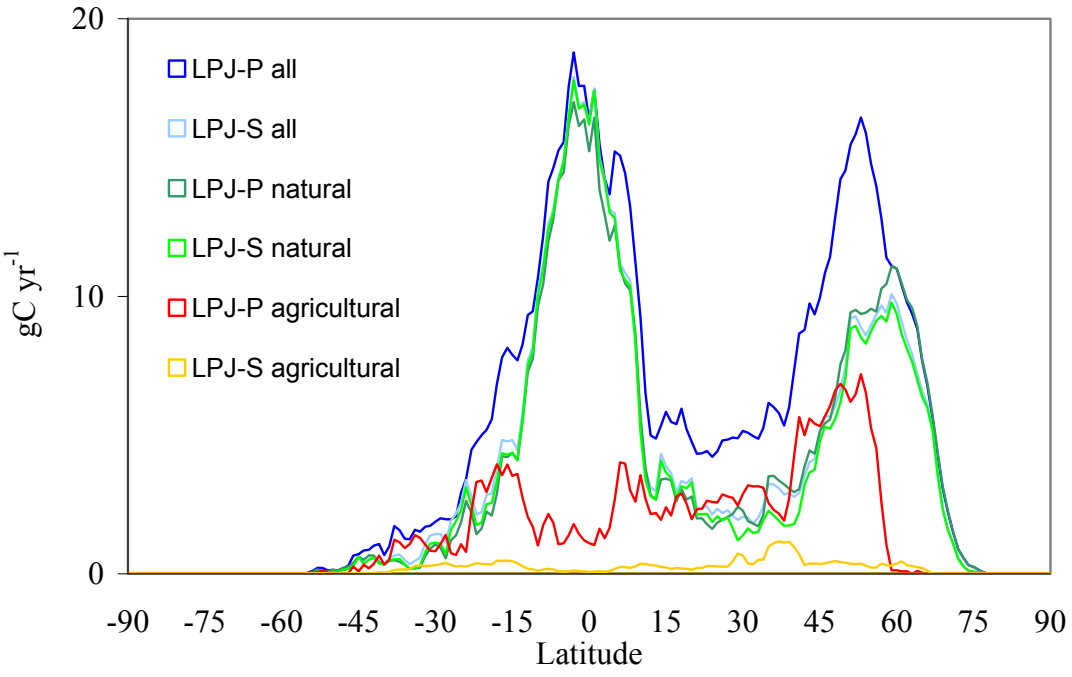

Fig. 4.18. Latitudinal distribution of biomass for LPJ-P (darker colours) and LPJ-S_{GIM} (lighter colours) for 1999. Agricultural pixels are all pixels under the crop & pasture mask (reddish), and natural areas are defined as the pixels outside of the crop mask (greenish).

The difference between the biomass within agricultural areas is very significant, pointing out the difference between the undisturbed world (~ LPJ-P simulating forests in the nowadays agricultural used regions) and the world with human action (simulations with agricultural mask). Thus, this difference can be seen as the biomass removed for agriculture, as already stated above.

4.7 Soil carbon

Soils play a major role in maintaining the balance of the global carbon cycle, i.e. as they contain approximately two thirds of the carbon in terrestrial ecosystems (Baes et al. 1977, Post et al. 1982). Because of the large size and long residence time of the carbon pools in soils, increased carbon sequestration in soils is one proposed method to reduce atmospheric carbon dioxide. However, human disturbance is one of the main contributors to a decrease in soil carbon storage (Schlesinger 1977). Published estimates of global soil carbon storage vary widely between 700 and 2946 PgC (see tab. 4.11), based on different inventory and modelling methods and remain highly uncertain. The estimates of Schlesinger (1977) and Post et al. (1982) seem to be based on the most extensive data bases and therefore provide the most reliable figures, which are close to the results simulated by LPJ-S.

Study	Soil carbon (PgC)	Comments
Ajtay et al. (1979)	2070	Estimates based on published inventories
Baes et al. (1977)	1080	Estimates based on published inventories
Bazilevich (1974)	1392	Estimates based on published inventories
Bohn (1976)	2946	Estimates based on published inventories
Bolin (1970)	700	Estimates based on published inventories
Cox et al. (2000)	1180	Modelled
Dixon et al. (1994)	787	Estimates based on published inventories
Goldewijk et al. (1994)	1499	Modelled
Houghton (2003 b)	1500 – 2000	Within first top meter
IPCC (2001)	1567	
Jobbaggy & Jackson (2000)	2300	Within top 3 m
Kirschbaum (2000)	1500	within first top meter
	2400	within top 2 meter
Melillo et al. (1995)	1301	Modelled
Post et al. (1982)	1395	Inventory
Schlesinger (1977)	1456	Inventory
WBGU (1988)	2011	Based on Ajtay et al. (1979), Dixon et al. (1994), Shvidenko & Nilson (1998)
Xiao et al. (1997)	750	reactive soil carbon
Sitch et al. (2003) LPJ-P	1670	Modelled
This study LPJ-S	1371 (1341)	Modelled

Table 4.11. Estimates of global carbon sequestered in soils.

In the current approach, soil carbon is computed as the sum of the PFT specific below-ground litter pools, the slow and the fast soil carbon pools. Debris enters the litter pools every year. Litter and soil carbon decay depends on soil temperature- and moisture-dependent decomposition rates. The soil carbon pools differ in their turnover rates of 33 and 1000 years (see table 3.2 in chapter 3). Soil carbon is generally reduced in the satellite-constrained version. LPJ-S computes 1371 (1341) PgC global soil carbon, 299 (220) Pg lower than LPJ-P (Tab.

4.3). These figures compare well with the estimates of Post et al. (1982) and Schlesinger (1977).

Climate is found to be the major determining factor for soil carbon density (Post et al 1996). Generally, soil carbon density increases with wetter conditions, as well as with cooler temperature regardless of precipitation level. These findings are supported by fig. 4.19. Highest soil carbon storage is simulated in the boreal zone, where slow decomposition rates allow high accumulation rates (according to Malhi et al. 1999). Although biomass and litter carbon is highest in the tropics, fast turnover rates and strong eluviation lead to relatively low soil carbon accumulation. However, the values of LPJ-S for tropical moist forests with 4 -7.5 kg m^{-2} are too low compared to the World soil organic carbon map (USDA 1997) giving soil carbon storage of 12 – 20 kg m^{-2}. This difference can be attributed to the occurrence of tropical moor land in Indonesia and seasonally water-covered regions in the Congo and Amazon river basin, which cannot be modelled by LPJ. In the boreal zone, largest differences occur in eastern Siberia, where carbon stocks given by USDA (1997) range between 8 and 16 kg m^{-2}, whereas LPJ-S calculates 30 to 45 kg m^{-2}. (For the USDA global soil carbon map see Annex). In Canada and western Siberia simulation of LPJ-S ranges between 30 and 50 kgC/m², whereas the mapped data encompass 120 kg m^{-2}. This might be the effect of permafrost which enhances soil carbon accumulation. The high range differences in the USDA map mostly result from merging different soil carbon inventories using different methods. Modelled and mapped soil carbon densities in the temperate zone are similar (8-16 kg m^{-2}) in LPJ-S and the USDA map.

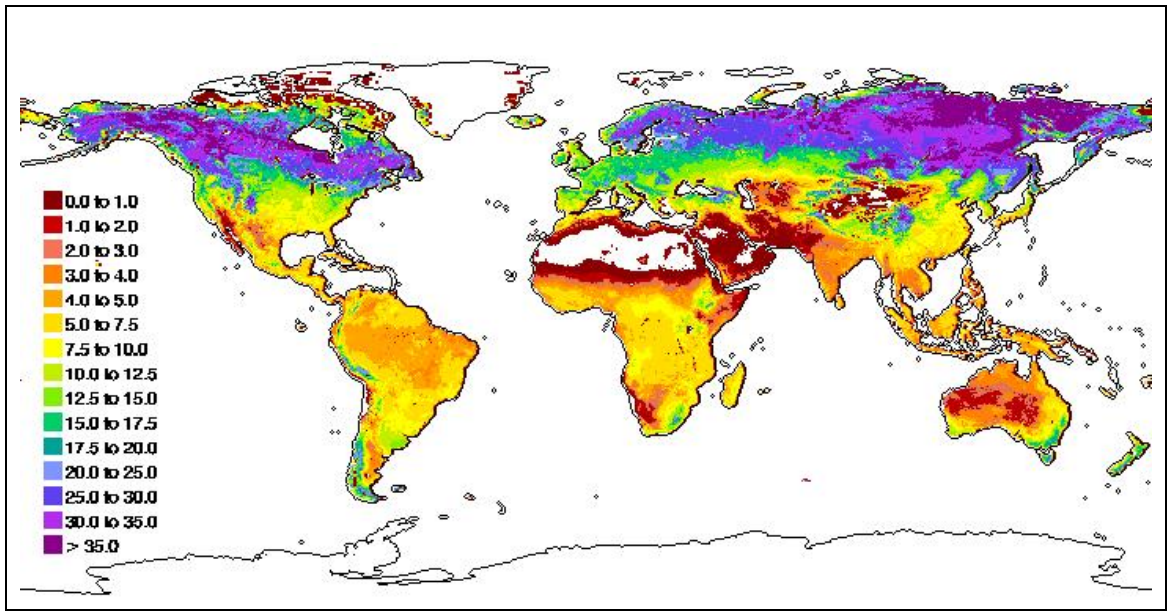

Fig. 4.19. Average soil carbon for the period 1982 to 2002 as derived from LPJ-S_{GIM} (in kg m^{-2}), please notice that the legend is nonlinear.

In addition to estimating the world soil carbon pool, it is important to visualize the differences between the satellite-driven version and LPJ-P in order to assess the influence of human

deforestation and conversion of forest to agricultural land on soil carbon density and distribution (Fig. 4.20). Additionally, it can be investigated whether input of satellite data and therefore consideration of human influence has led to significant changes in the soil carbon pools in the natural areas.

	LPJ-P	**LPJ-C**	**LPJ-S_{GIM}**	**LPJ-S_{GIM} no crops**	**LPJ-S_{PAL}**	**LPJ-S_{PAL} no crops**
All pixels	1670	1597	1371	1405	1341	1376
Agricultural areas	489	416	355	389	348	383
Natural areas	1181	1181	1016	1016	993	993
Residual crop pixels	170	170	143	143	143	143

Table 4.12. Soil carbon (average 1982 to 1999 in PgC) for different versions for agricultural and natural regions

The reduction of 299 PgC between LPJ-P and LPJ-S (Tab. 4.12) can be attributed to conversion of forest to agricultural land, where harvesting reduces the litter and soil carbon pools significantly. The second reason for reduction is a result of the occurrence of more bare soil in winter on croplands. The reduction between LPJ-P and LPJ-C is much lower (73 PgC).Within LPJ-C the agricultural areas are parameterized as grasses with the potential grass phenology, whereas in LPJ-S the satellite phenology prescribes more bare soil in winter after harvest. Strikingly, the soil carbon reduction in agricultural areas shows a particular pattern with stronger decrease to the east in Eurasia and to the Northwest in North America (Fig. 4.20).

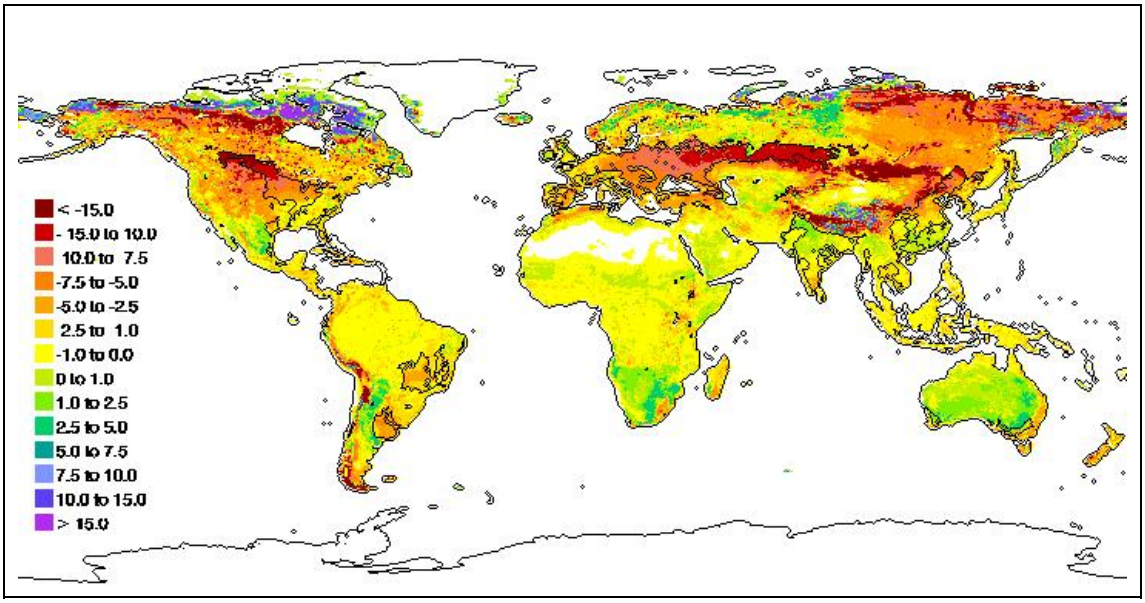

Fig. 4.20. Differences of soil carbon between LPJ-S_{GIM} and LPJ-P in kg $m^{-2}yr^{-1}$ averaged over the time period of 1982 to 2002. Agricultural areas are masked.

This can be attributed to an increase in bare soil up to 40 % (see figs. 4.4 and 4.5) in these regions as a result of the significantly lower fPAR values in the satellite data.

Additional 165 PgC are lost in the natural regions, whereof 27 PgC can be related to residual crop pixels within the natural areas. The remainder of 138 PgC is predominantly assoicated to an over prediction of soil carbon in the northern boreal zone and in high-altitude regions such as the Himalayan mountains. The changey in PFT distribution from LPJ-P to LPJ-S suggest that the strong soil carbon decrease is due to a higher barren fraction at the expense of grasses and boreal broadleaved and needle-leaved deciduous trees. From this a more realistic simulation of the tree-line further to the south can be inferred, according to Sitch et al. (2003), who reported the simulation of a forest-tundra border located too far north. Further north LPJ-P underestimates soil carbon as a consequence of underestimating the vegetated area. The barren fraction is reduced in the satellite-constrained version, and is converted to grass and shrub-land or tundra vegetation. This increase in cover can be related to the lack of a specific shrub simulation in LPJ-P. These findings are underlined by the latitudinal comparison of soil carbon (Fig. 4.21).

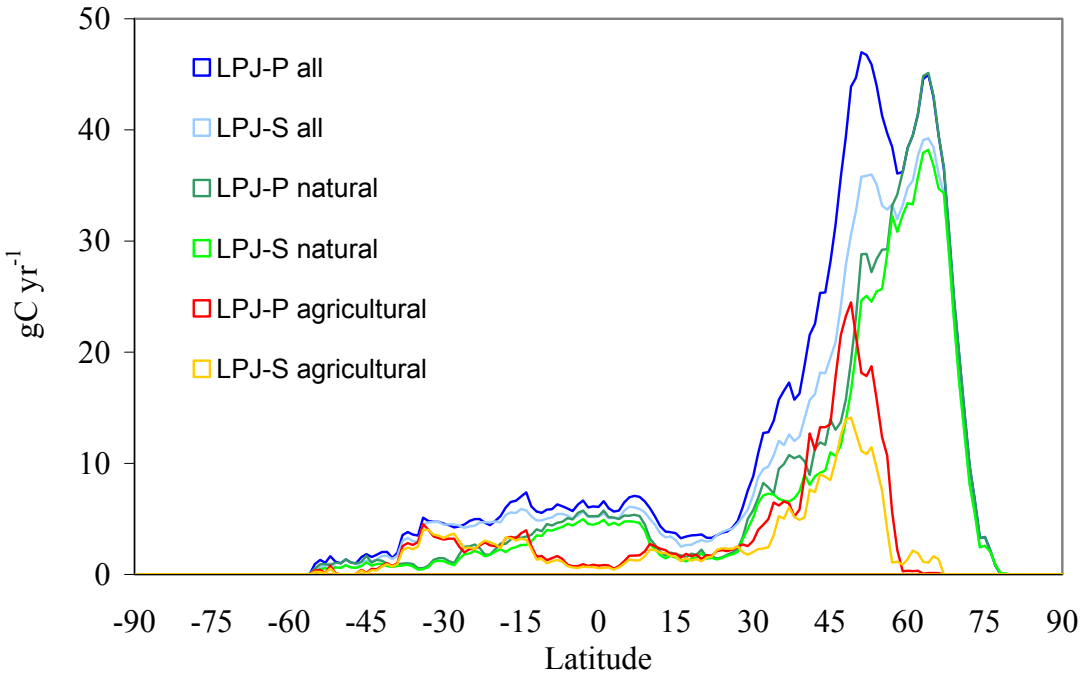

Fig. 4.21. Latitudinal distribution of soil carbon for LPJ-P (darker colours) and LPJ-S_{GIM} (lighter colours) for 1999. Agricultural Pixels are all pixels within the crop & pasture mask (reddish), and natural areas are defined as the pixels outside the crop mask (greenish).

It shows the strongest differences between 30°and 60°N, especially in the regions where the majority of agricultural areas occurs. The main proportion of decrease appears in the crop areas, but nevertheless a small fraction of decrease is present also in the natural areas. As

already stated, this is due to residual agricultural pixels within the natural areas, as well as a result of shifts in PFT distribution and a reduction of vegetated or forested area.

Concluding, the global total of soil carbon storage now compares better with inventoried data. Strongest reduction of soil carbon is due to deforestation and conversion of forest to agriculture. A smaller fraction of decrease can be attributed to a more realistic simulation of the boreal tree-line. Generally, the changed PFT distribution after satellite data implementation has led to a more open landscape and reduced soil carbon. However, as inventoried data is still fragmentary and highly uncertain a reliable comparison remains challenging.

4.8 Net ecosystem exchange (NEE)

Terrestrial net ecosystem exchange (NEE) is a key parameter in the global carbon balance and the atmospheric green-house gas budget. Here defined as

NEE = NPP – Rh – fire carbon – harvested carbon,

the calculation of NEE enables the detection of temporally and spatially highly variable terrestrial sources and sinks of carbon dioxide and to obtain an insight into the behavior of the earth's land surface concerning carbon uptake and release.

For both input datasets LPJ-S simulates a global sink of -0.7 PgC averaged for the period 1982 to 1999 (negative values indicate atmospheric reduction or land sink, positive values indicate atmospheric increase or land source). Compared to the non-constrained version (LPJ-P and LPJ-C), NEE is reduced by 0.6 PgC yr^{-1} due to the stronger reduction in NPP as opposed to a weaker reduction of Rh, which is a result of a generally reduced vegetation cover.

In the following I compare these results with published estimates to ascertain if implementing the satellite data has led to any improvements. Recently several recalculations have been published for land-atmosphere carbon fluxes separated for the 1980s and the 1990s, which are listed in table 4.12 and compared to the present results derived for the LPJ-versions. Most of them are based on analysis of atmospheric O_2 and CO_2 concentration to partition between terrestrial and oceanic uptake of carbon (e.g., see Keeling et al. 1996, Battle et al. 2000). As only 50 to 60 % of the carbon dioxide emitted from fossil fuel combustion and cement production remains in the atmosphere, and 30 % is taken up by the oceans, the remainder of 10 % is taken up by terrestrial ecosystems, called the net land-atmosphere flux. It is determined by several mechanisms such as land-use change, forest management, disturbances such as fire, effects of climate change, increasing atmospheric CO_2 concentration, and the fertilization of N deposition. As the emissions caused by land-use change are estimated to be 0.6 to 2.2 PgC yr^{-1}, the residual terrestrial sink (formerly the so-called 'missing sink') is evaluated by difference to be -0.9 to -3.0 PgC yr^{-1}, with a very high range of uncertainty (± 2.0 PgC yr^{-1}) (IPCC 2001, De Fries et al. 2002b, Houghton 2003c). Table 4.13 gives an impression of the high range of figures obtained by different authors, especially concerning the amount of land-use change, showing the very large uncertainty still present in the estimations of the residual terrestrial sink.

IPCC (2001) stated that the land-atmosphere flux has decreased significantly in the 1990s, that is net uptake of the terrestrial biosphere has increased notably. In the 1980s only -0.3 ± 0.9 PgC yr^{-1} were taken up by the terrestrial biosphere. In the 1990s this amount increased to -1.4 ± 0.7 PgC yr^{-1}. Including a yearly carbon release by land-use change of 1.3 and 1.6 PgC yr^{-1} for the 1980s and the 1990s respectively (but these values are also highly uncertain, see below), the terrestrial vegetation assimilated -1.6 PgC yr^{-1} in the 1980s and -3.0 PgC yr^{-1} in the 1990s

(hence also highly uncertain). Thus, the global terrestrial sink has increased by -1.1 PgC yr^{-1}. Table 4.13 and Figure 4.22, including the estimations derived by other approaches such as oceanic modelling (Bopp et al. 2002, Plattner et al. 2002), approaches which combine satellite data and modelling (Cao et al. 2002, DeFries et al. 2002b) or land-use change modelling (Houghton 2003a&c) show that not all approaches agree on this terrestrial sink enhancement.

Plattner et al. (2002), for example, recalculated the partitioning between land and sea uptake, considering a larger outgassing of the oceans due to enhanced heat uptake than estimated by IPCC (2001). They showed a larger oceanic sink in the 1990s than in the 1980s, suggesting a smaller terrestrial uptake in the 1990s (+0.3 PgC yr^{-1}). As these revised estimates are in consistence with oceanic modelling and various measurements (for a detailed discussion see Plattner et al. 2002), they are more reliable. According to this, Bopp et al. (2002) consider outgassing of the ocean to be related to long-term warming trend and decadal variability. Their revised carbon budget also suggests lower terrestrial uptake rates for the 1980s, but higher rates for the 1990s than Plattner et al. (2002) (+0.9 PgC yr^{-1}), even though showing a small downward revision compared to IPCC (2001).

A highly uncertain factor in carbon cycle estimations is the amount of carbon released by land-use change, such as deforestation, reforestation, and regions recovering from agricultural abandonment. Published and methodologically credible estimates of tropical deforestation rates show discrepancies of up to a hundred percent (Cramer et al. 2004) and figures on carbon released by LUC include uncertainty ranges higher than 1 $PgCyr^{-1}$ (Tab. 4.13 and Fig 4.22). Estimations of Houghton (2003c), e.g., based on agricultural and forestry statistics obtain figures of around 2 PgC yr^{-1} of carbon released from LUC, whereas the study of De Fries et al. (2002b), combining satellite data with a terrestrial carbon model, suggests only 0.6 PgC yr^{-1} and 0.9 PgC yr^{-1} for the 1980s and 1990s, respectively. The results of Achard et al. (2002) (0.64 ± 0.21 PgC yr^{-1} for 1990 to 1997), also using a remote sensing approach, support the findings of DeFries et al. (2002b). These discrepancies can be traced back to the different methods used which all carry their own problems and uncertainties. Differences may occur as different definitions of ‘forested area’ as well as ‘intact’ and ‘disturbed’ forest are used. Studies based on forestry statistics are based on regional figures which are then up-scaled to global values, including different evaluation methods in different countries. Additionally, estimations of how the density of carbon in the removed vegetation is determined can also vary strongly. With this high uncertainties within the single compartments of the carbon budget a reconstruction of the overall carbon balance remains highly uncertain. Small changes within one factor such as the carbon released by land-use change can strongly affect the net land-atmosphere flux (Fig. 4.22). This has to be kept in mind when discussing the figures in comparison to the results of this study. Within this context the new figures presented here amount to providing an additional estimate that may be considered when assessing the overall picture.

	IPCC 2001 (TAR rev.)	Bopp et al. 2002	Plattner et al. 2002	Cao et al. 2002	De Fries et al. 2002b	Houghton 2003a&c	House et al. 2003	LPJ-S_{GIM} (LPJ-S_{PAL})	LPJ-C	LPJ-P
	1980s							**1982-1989**		
Emission (fossil fuel, cement)	**5.4±0.3**	**5.4±0.3**				**5.4±0.3**				
atmospheric increase	**3.3±0.1**	**3.3±0.1**				**3.3±0.1**				
Oceanic uptake	**-1.8±0.8**	**-1.8±0.8**	**-1.7±0.6**							
land-atmosphere flux	**-0.3±0.9**	**-0.3±0.9**	**-0.4±0.7**	**-0.2**	**-0,3 ±0.9**	**-0.4±0.7**	**-0.3±0.9**	-0.1 – 0.9 (-0.5–0.5)	0.2	0.2
→ release from land-use change (LUC)	**1.3** (0.3-2.8)	**1.3**	**1.3**	**1.3**	**0.57 (0.32-0.84)**	**2.0±0.8**	**0.9-2.8**	0.3 – 1.3[2]	1.3	1.3
→ Residual terrestrial sink	-1.6 (-4.0-0.3)	-1.6	-1.7	-1.53	0.3	-2.4±1.1	-4.0 to -0.3	**-0.4[1] (-0.8)**	**-1.1**	**-1.1**
1990s		**1990-96**	**1990s**							
Emission (fossil fuel, cement)	**6.3±0.4**	**6.2±0.4**				**6.3±0.4**				
atmospheric increase	**3.2±0.1**	**2.7±0.1**				**3.3±0.2**				
Oceanic uptake	**-1.7±0.5**	**-2.3±0.7**	**-2.4±0.7**							
land-atmosphere flux	**-1.4±0.7**	**-1.2±0.9**	**-0.7±0.8**	**-1.1**	**-1.0±0.9**	**-0.7±0.8**	**-1.0±0.9**	-0.4 - 0.7 (-0.3–0.8)	0.3	0.2
→ release from land-use change	**1.6** (0.5-2.8)	**1.6**	**1.6**	**1.6**	**0.91 (0.50-1.36)**	**2.2±0.8**	1.4-3.0	0.5-1.6[2]	1.6	1.6
→ Residual terrestrial sink	-3.0 (-1.2 - -4.9)	-2.8	-2.3	-2.7	-1.9	-2.9±1.1	-4.8 to -1.6	**-0.9[1] (-0.8)**	**-1.3**	**-1.4**
differences between the decades (1990s minus 1980s)										
Land-atmosphere flux	-1.1	-0.9	-0.3	-0.87			-0.9	-0.5 (0.0)	-0.1	0.0

Table 4.13. Carbon uptake rates (in PgC yr^{-1}) by the terrestrial biosphere (bold figures: observed/modelled, simple black figures: evaluated by difference, blue figures: inserted), global figures for all carbon fluxes derived by LPJ-S are attached as Annex

---

[1] NEP as derived by LPJ-S (NEP=NPP – Rh – fireC – harvest), no explicit LUC, but implicit due to vegetation changes as seen by the satellite within the 10 years of the decade. But as during spin-up, those pixels have been already deforestated before, the LUC can only capture the small amount of vegetation that has been able to regrow during the short period of modelling.

[2] LUC span is derived as follows: maximum value: average LUC from all estimations (IPCC 2001, De Fries et al. 2002, Houghton 2003 a&c); minimum value: to account for a possible residual LUC during the 10 years when deforestation of young regrowth may occur .

[3] Span of land-atmosphere flux dependent on the amount of LUC captured by LPJ-S

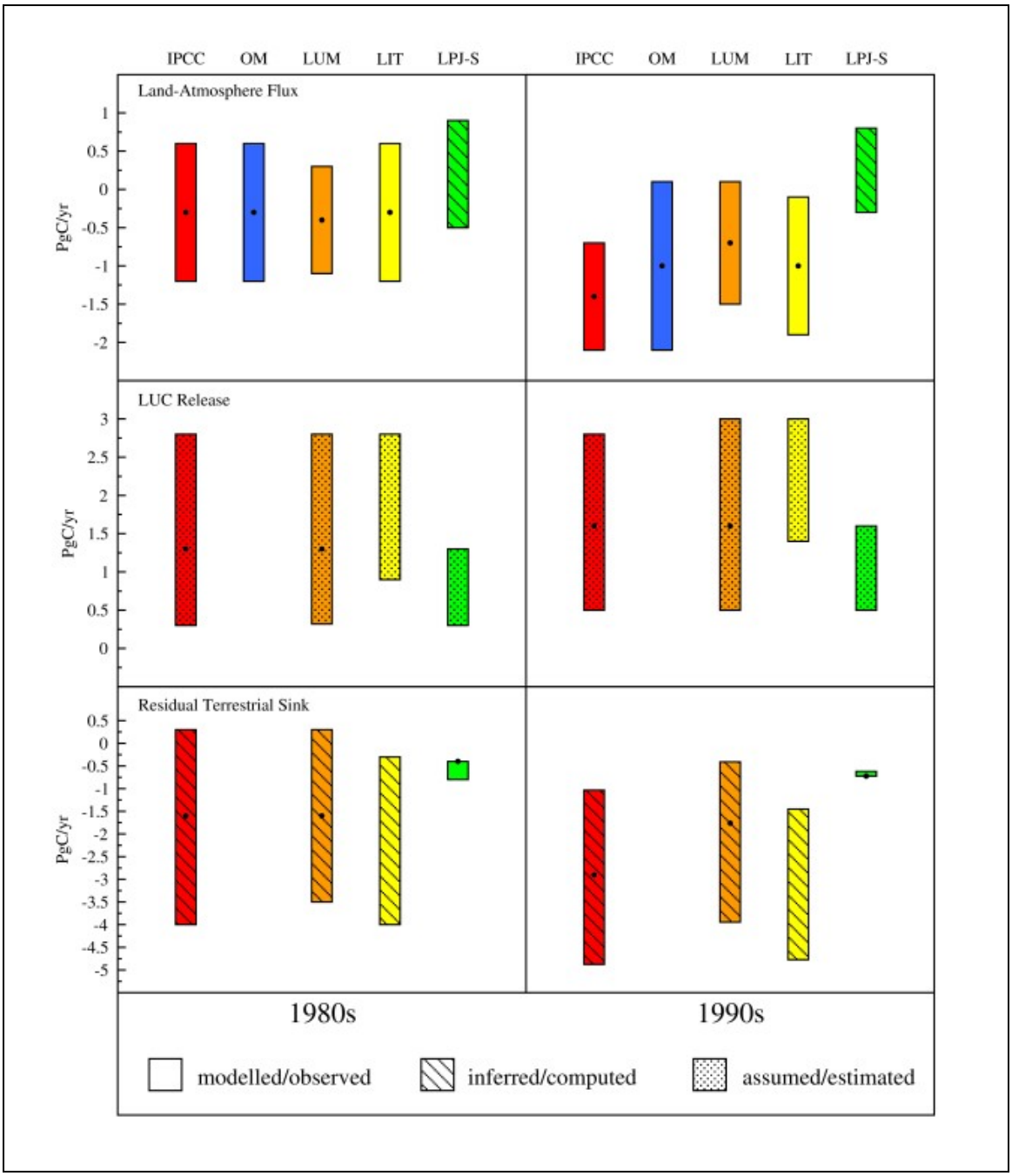

Fig. 4.22. Carbon balance estimates for the 1980s and 1990s derived by different approaches. (IPCC 2001,revised version, OM – Oceanic Modelling (Plattner et a. 2002, Bopp et al. 2002), LUM – Land-use change modelling based on remote sensing or inventory data (DeFries et al. 2002b, Houghton 2002a&c), LIT – literature research (House et al. 2003)

The results of LPJ-P and LPJ-C approximately represent the residual terrestrial sink, as they do not account for any land-use change. The results obtained by LPJ-S are also assigned to the residual terrestrial sink, as LUC during the last two decades of the 20th century was not explicitly modelled. Changes in vegetation cover such as due to regrowth and deforestation operate within a decade, but are difficult to quantify as fractional changes with spatial detail. We therefore decided to not use a dynamic land-use change mask, as these masks imply large uncertainties, which would have been even more intensified by the conversion into a half-

degree-grid. A reasonable expedient surplus of knowledge by inserting a dynamic LUC mask could not be expected, but rather an enhancement of uncertainties. Additionally, the satellite data have been already used during spin-up, so that the majority of deforestation effects have already been accounted for when the transient simulations begin. Additional changes in vegetation cover that occur due to regrowth and deforestation within the given period are not precisely quantifiable. Therefore, I present a range of possible carbon release from land-use change in order to account for the span found between the following model runs: from LPJ-S under the bracketing assumption that it does not account for any LUC (with a figure for carbon released from LUC derived as an average from all cited approaches, adding 1.3 and 1.6 PgC yr^{-1} for the 19980s and 1990s, respectively), up to LPJ-S under the bracketing assumption that it partially accounts for LUC (resulting in a small additional carbon release of 0.3 and 0.5 PgCyr^{-1}, for the 1980s and 1990s, respectively). Fig 4.22 visualizes the uncertainties within all approaches in determining the LUC. Regarding fig. 4.22, the evaluated land-atmosphere flux of LPJ-S agrees with the other approaches for the 1980s when including their uncertainty ranges. For the 1990s, even if the range of uncertainty of 1.0 PgC yr^{-1} is considered, most of the studies consider a stronger terrestrial uptake than LPJ-S. Compared to this, the values of LPJ-S are too high, even though they are still within the uncertainty ranges of some studies. Evidently, differences in the outputs of LPJ-S_{GIM} and LPJ-S_{PAL} occur. LPJ-S_{GIM} definitely shows differences between the two decades, which seems to be more reasonable. Additionally, the magnitude of difference between the two decades is reflected better with the LPJ-S_{GIM} version compared to the observations. Plattner et al. (2002) present a terrestrial uptake more similar between the decades, with a net terrestrial uptake of -0.4 and -0.7 PgC yr^{-1} for the 1980s and 1990s, respectively, which is closer to the estimates of the current approach. Regarding the results of Houghton (2003c)., it has to be taken into account that he only considers the carbon fluxes related to land-use change as a result from direct human influence such as deforestation and regrowth, ignoring other sinks and sources of carbon as caused by climate change or CO_2 fertilization. Therefore, the carbon fluxes from land-use changes are not necessarily the same as the net terrestrial flux from all terrestrial processes. Similar to the current approach, Cao et al. (2002) estimated net carbon fluxes via ecosystem modelling based on remote sensing data to be -0.2 and -1.1 PgC yr^{-1}, for the 1980s and 1990s, respectively. Their approach also includes land-use change as ‘seen’ by the satellite, comparing well with the estimates of Bopp et al. (2002), although their difference between the decades is too high compared to the revised calculations of Plattner et al. (2002). The discrepancy to our results can be explained by differences in accounting for additional fluxes, as they do not consider fire disturbance or harvesting.

Concluding, looking at all these estimates it has to be kept in mind that the differences between the modelled and observed results usually are smaller than their very wide range of uncertainty.

I.e. the net ecosystem exchange is the most sensitive factor in carbon cycle modelling, as it may vary strongly when only small changes in NPP, Rh, carbon released by land-use change or by other disturbances occur. The review of House et al. (2003) concerning different approaches to determine the net land-atmosphere flux concludes that the inconsistencies in results are mainly due to considering different processes, pools and methods. The different results should rather be seen complementary than inconsistent, supporting the understanding of the different processes contributing to the terrestrial carbon budget. Additional carbon exchange accounted for in atmospheric studies but not in LPJ are the transport of dissolved organic carbon by rivers (of ill-known magnitude, but surely 0.2 PgC yr^{-1}) and the effects of forest management and fire prevention. These may also contribute to the atmospherically observed NEE and could explain a fraction of the remaining differences.

Regarding the spatial patterns of the differences in NEE between LPJ-S_{GIM} and LPJ-P averaged over 1982 to 1999 (Fig. 4.22), LPJ-S_{GIM} shows in some mid- to high latitudes as well as in semi-arid regions a higher NEP than LPJ-P, indicating stronger sinks (green colors). The red colors in the North American tundra denote a relatively stronger source in the satellite-driven model caused by lower NPP due to a lower grass and higher barren fraction. Caused by the averaging over 21 years, the overall differences in sources and sinks are small. The net terrestrial balance is not evenly distributed over the land surface. In order to investigate which regions contribute most to the change between the decades, fig. 4.23 illustrates differences of NEP between the 1980s and the 1990s. As this figure only denotes relative changes, positive values indicate strengthened uptake or reduced sources in the 1990s, whereas negative values imply reduced uptake or weakened sinks.

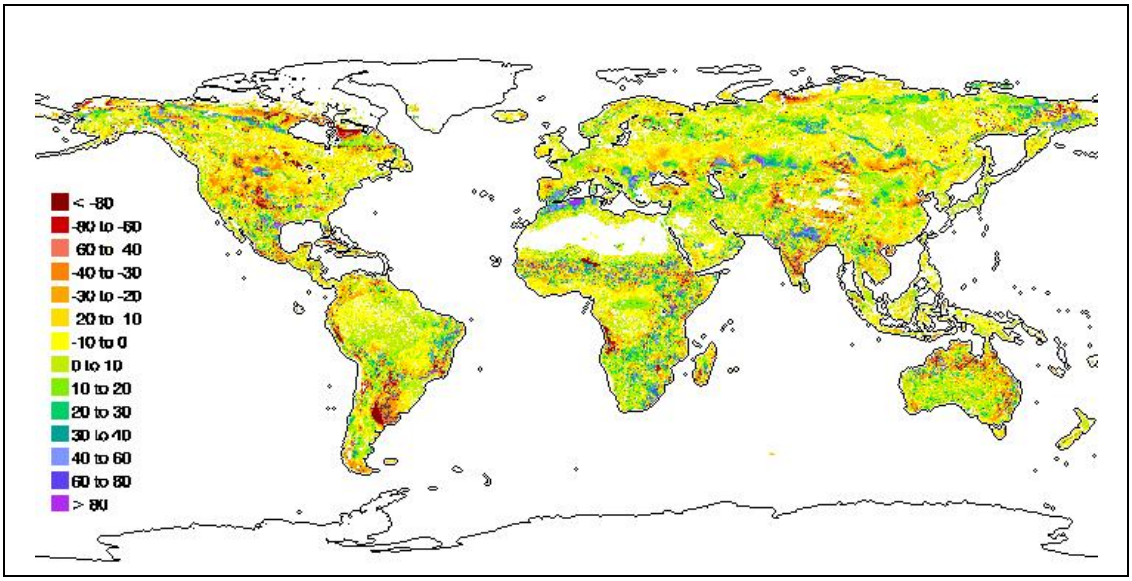

Fig. 4.23. Differences of NEE between LPJ-S_{GIM} and LPJ-P in $gCm^{-2}yr^{-1}$, averaged from 1982 to 2000

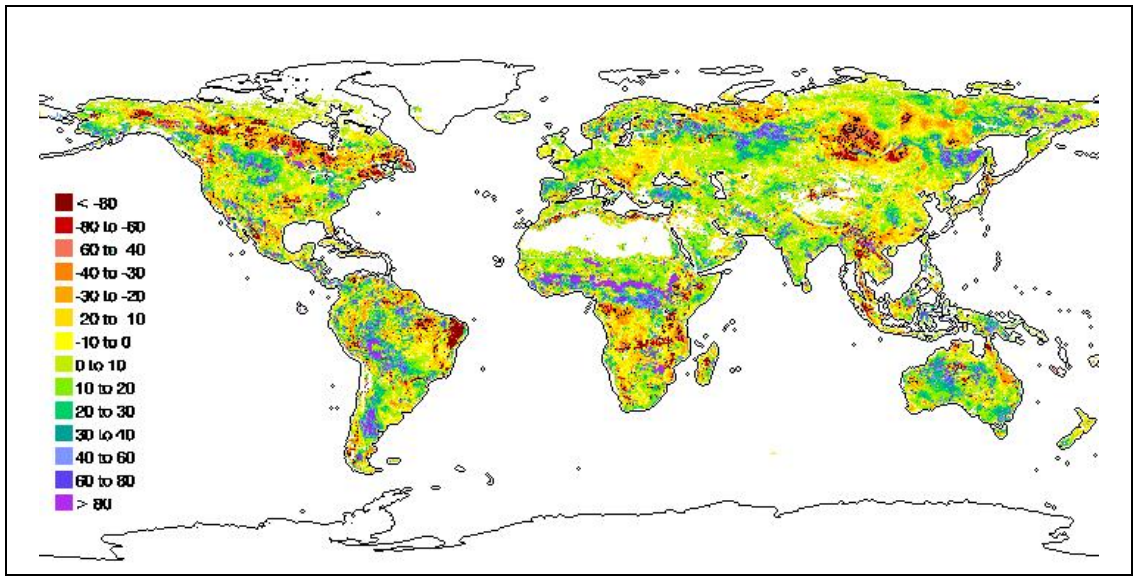

Fig. 4.24. Difference of average NEP (LPJ-S_{GIM}) between the 1990s and 1980s (avg. NEP 1990s minus 1980s, in $gCm^{-2}yr^{-1}$)

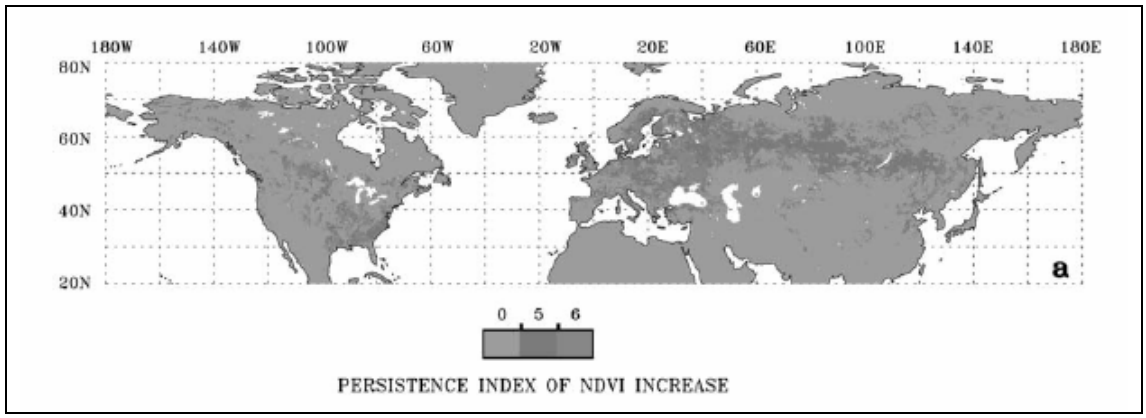

Fig. 4.25. Spatial presence of persistent NDVI increase in the northern latitudes. Zones of long-term greening, characterized by five or six periods of growing season average NDVI increase. (Bogaert et al. 2002)

Boreal zone: Inversion and modelling studies indicate a strong greening trend in the northern hemispheric biosphere, especially the boreal forest zone (Myneni et al. 1997, Schulze et al. 1999, Myneni et al. 2001, Lucht et al. 2002, Dong et al. 2003, Hicke et al. 2002). As a consequence of a warming trend most pronounced in the high latitudes, Eurasia and North America show a vegetation greening trend evinced by a positive trend in averaged NDVI (Myneni et al. 1997, Zhou et al. 2001, Bogaert et al. 2002, Slayback et al. 2002). Plant metabolism is not only stimulated directly by the warmer temperatures, but also indirectly as the CO_2 fertilization effect is enhanced under warmer conditions (Kirschbaum 1994). But as these studies mostly address the enhanced forest growth and NPP, NEP may show a different picture. Beyond the above mentioned studies, although reflecting a generally positive trend in NPP for the boreal zone (increase of 0.4 PgC yr^{-1}, figures of all carbon fluxes for the latitudinal zones are attached as Annex), the current model results show in some regions (Central Siberia,

Canada) a relative reduction of net fluxes during the 1990s (Fig. 4.23). These regions are subject to change from a net sink in the 1980s to a weak source in the 1990s, mainly driven by a reduction in NPP. This is in agreement with the findings recently made by Angert et al. (2005), who demonstrated that the boreal greening trend as a result of advanced spring budburst is offset by a reduced uptake in summer due to warmer and drier conditions in the period 1994 to 2002. Additionally, disturbances such as insect attacks and fire activity have increased recently, i.e. in Canadian and Russian forests (Kurz & Apps 1999, Kasischke & Stocks 2000, Nilsson et al. 2000, Shvidenko & Nilsson 2002). Unfortunately this cannot be tested with the current simulation, since in LPJ-S fire activity is dependent on the amount of biomass and NPP, it increases with increasing NPP and vice versa. A switch from carbon sink to carbon source may also be caused by increases in decomposition rates and soil respiration as a consequence of increased surface air temperatures (Savage et al. 1997, Goulden et al. 1998, Lindroth et al. 1998, Rayment & Jarvis 2000, Bergner et al. 2004). As Rh has not decreased as much as NPP, the net fluxes have changed towards a weak source. The TransCom 3 project, an intercomparison of 16 atmospheric transport models (Gurney et al. 2004) showed a weak net sink (-0.16 PgC yr^{-1}) for the entire boreal zone (split in + 0.2 PgC yr^{-1} for boreal North America and -0.36 PgC yr^{-1} for boreal Asia) for the period 1992 to 1996, which agrees with the current model estimates of -0.24 PgC yr^{-1} for the same period.

Northern temperate zone: Gurney et al. (2004) calculated a strong net terrestrial sink of -2.26 ± 0.75 PgC yr^{-1} for northern mid-latitudes for the period 1992 to 1996 (Europe: -0.96 ± 0.27 PgC yr^{-1}; temperate North America: -0.89 ± 0.32 PgC yr^{-1}; temperate Asia: -0.41 ± 0.74 PgC yr^{-1}). Houghton (2003a) additionally considers river transport and subsequent oceanic release, which is not captured by the inverse modelling, to reduce the northern terrestrial sink by about 0.3 PgC yr^{-1} (Aumont et al. 2001) resulting in a net sink of -1.96 ± 0.75 PgC yr^{-1}. Houghton (2003a) calculates a northern mid-latitude sink inferred from forest inventories to be 0.7 PgC yr^{-1} for the years around 1990 (Goodale et al. 2002), which is significantly lower than the inversion estimates. The processes contributing to this sink are thought to be CO_2 and N fertilization, increased temperature, and the regrowth of forests on abandoned agricultural land (Houghton 2000a). Generally, the model results derived by LPJ-S reflect the same patterns of positive trends in NDVI as obtained by Bogaert et al. (2002) (see fig. 4.24). LPJ-S shows only a small net terrestrial sink (-0.2 PgC yr^{-1} for the period 1992 to 1996), being even lower than the uncertainty range of the inversion estimates. The lower values might be a result of the model's inability to reflect rapid changes in land-use change. Results of Potter et al. (2003) derived by a satellite data driven ecosystem model show similar low values between -0.2 and -0.3 PgC yr^{-1} for the period 1982 to 1999 for North America and Eurasia, respectively.

For all these comparisons it has to be noted that discrepancies between figures obtained from different methods (forest inventories, inverse modelling, ecosystem modelling) might be a

result of different measurement and modelling periods, because the averaged estimations are sensitive to year-to-year variations which may be very large.

Sahel: A noticeable increase in terrestrial uptake occurs in the Sahel region. Recent analyses done by Eklundh & Olssen (2003), Eklundh & Sjöström (2005), and Hickler et al. (2005) examining NDVI and precipitation data indicate that the Sahel has recovered from the severe droughts of the 1980s showing a definite greening trend throughout the 1990s. Increased precipitation permits vegetation changes from barren to sparse or even more densely vegetation. Agricultural areas also have expanded implying improved conditions for cultivation. Additionally, increasing atmospheric CO_2 concentration allows enhanced vegetation growth due to an increasing water use efficiency of the plants. Hence, conditions for establishment of vegetation being unfavourable until now are improved.

Absolute values of net terrestrial fluxes obtained by LPJ-S indicate that the Sahel region has turned from a strong source of carbon in the 1980s (0.4 PgC yr^{-1}) to a relatively pronounced sink in the 1990s (-0.2 PgC yr^{-1}). Unfortunately no comparable values derived by inverse modelling or measurements exist for this region in the literature.

Tropical regions: Generally, the carbon balance of the tropics is very uncertain due to a lack of measurements of all types, such as inverse analyses, forest inventories and eddy flux measurements. Phillips et al. (1998) suggested undisturbed tropical forest to be a sink of carbon, at least in the neotropics with accumulation rates of 0.62 ± 0.3 PgC yr^{-1}, but this uptake is more than offset by emissions from deforestation and decomposition, resulting in a net source of carbon for the tropics with 1.5 ± 1.2 PgC yr^{-1} for the period 1992 – 96 (Aumont 2001, Gurney et al. 2002, Houghton 2003a). These figures are based on rates of deforestation obtained by FAO, which might be too high, as two remote sensing studies of tropical deforestation suggest (Achard et al 2002, DeFries et al. 2002). Their estimated carbon flux for the 1990s is 0.96 and 0.9 (range 0.5–1.4) PgC yr^{-1}, respectively, but they do not account for soil carbon losses which often occur after deforestation. House et al. (2003) compiled net tropical fluxes reported by several studies ranging between +1.95 ± 0.6 PgC yr^{-1} (Houghton 2003c), +1.65 ± 0.4 PgC yr^{-1} (Dixon et al. 1994), and -1.0 to +1.5 PgC yr^{-1} (Heimann 2001) for the 1980s. Those reported figures imply that the net carbon source of the tropics has weakened during the 1990s, according to fig. 4.23 which indicates that the relative changes of NEP between the decades are positive in terms of carbon accumulation or less carbon release. LPJ-S simulates an increase from -0.2 PgC yr^{-1} in the 1980s to -0.9 PgC yr^{-1} in the 1990s denoting the tropics to be a moderate sink. Regarding the fact, that LPJ-S underestimates land-use change by at least 1.4 PgC yr^{-1}, we get a tropical source that has weakened from 1.2 PgC yr^{-1} (1980s) to 0.5 PgC yr^{-1} (1990s). A reason for the increase of tropical net fluxes between the decades is predominantly an enhanced NPP (increase of 1.8 PgC between the decades), which exceeds the

weaker increase of soil respiration (1.0 PgC). Further analysis on the changes in terrestrial uptake and its causes is given in chapter 5.

The LPJ-simulated estimates still lie within the uncertainty ranges of the inverse analyses, albeit at the very low end of the range. Gurney et al. (2004) estimated a tropical source to be 0.5 ± 0.8 PgC yr^{-1} for the period 1992 to 1996 (split up to 0.74 ± 0.77 PgC yr^{-1} for tropical America, 0.27 ± 0.94 PgC yr^{-1} for Asia, and -0.51 ± 0.6 PgC yr^{-1} for Africa). The net carbon uptake of African tropical regions underlines the currently found positive fluxes in the Sahel region. Enhanced carbon release occurred in Northeastern Brazil, South Africa, California, and Indonesia. These patterns hint at the persistent strong El Niño event between 1991 and 1994, and 1997/98, which came along with severe droughts these regions (Philander 1990, Dai & Wigley 2000).

5. TEMPORAL VARIATIONS AND TRENDS OF THE TERRESTRIAL CARBON CYCLE

As the global atmospheric CO_2 growth rate shows a high interannual variability (Conway et al. 1994, Lloyd 1999, Bousquet et al. 2000, Fung 2000, Schaefer et al. 2002), but the ocean fluxes do not (Rayner & Law 1999, Le Quéré et al. 2000, Le Quéré et al. 2003), the growth rate variability is mainly determined by changes in the terrestrial biosphere and its carbon pools (Conway et al. 1994, Kaduk & Heimann, 1996, Houghton et al. 1998, Lloyd 1999, Tans & Wallace 1999, Battle et al. 2000, Houghton 2000b, Prince et al. 2000, Rödenbeck et al. 2003a, Murayama et al. 2004). Additionally, about half of the anthropogenic fossil fuel emissions are absorbed by land and oceans. Several inversion and modelling studies indicate a significant carbon sink in the northern hemispheric biosphere, especially the boreal forest zone (Myneni et al. 1997, Schulze et al. 1999, Goetz et al. 2000, Myneni et al. 2001, Dargaville et al. 2002, Hicke et al. 2002, Dong et al. 2003). Nonetheless, it is difficult to determine the regional distribution of this 'missing sink' and the long-term trends in its variability (Fung, 2000). Schaefer et al. (2002) investigated the effect of climate on the interannual variability of terrestrial CO_2 fluxes based on the SiB2 model (see table 4.1), and demonstrated strong regional differences: while precipitation is dominating NEP interannual variability in the tropics, temperature drives the terrestrial carbon fluxes in the extratropics. Many of the biogeochemistry models suggest that temperature and precipitation are the main drivers of interannual variability, but they differ in their description of the underlying mechanisms (Dickinson 2000, Houghton 2000b, Lloyd 1999, Kaduk & Heimann 1996). While some consider respiration to be the dominating factor in some regions (Houghton 2000b), others suggest photosynthesis to be the leading driver (Kaduk & Heimann 1996). The present study provides additional insight into the spatio-temporal interactions between net CO_2 exchange of the terrestrial ecosystems and climate variability, and their underlying mechanisms.

Furthermore, the global CO_2 growth rate and biospheric source-sink behaviour are usually stated as global means. In contrast, here global maps were generated to demonstrate complex spatial structures, which are not temporally constant. The different processes, as well as the variety of different carbon pools and fluxes that determine much of the yearly growth rate are resolved at a high spatial resolution (0.5°).

Earth observation data were assimilated into the LPJ-DGVM in an effort to identify controls on the net carbon exchange of the terrestrial biosphere bearing the following question: which drivers contribute most to the interannual variability of NEP, climate anomalies or biogeochemical processes? And which feedbacks and interactions can be determined?

5.1 Long-term interannual variability of global NEP

The standard deviation of simulated global NEP serves here as a measure for interannual variability (IV). For the time period from 1982 to 1994, an interannual variability of 0.87 PgC yr^{-1} was computed by the LPJ satellite-based simulations. This estimate compares slightly lower to results by Conway et al. (1994) who estimated 1.1 PgC yr^{-1}, Houghton (2000b) with 1.0 PgCyr^{-1}, and Schaefer et al. (2002) with 1.3 PgC yr^{-1}. But as already stated in chapt 4.8, LPJ-P simulates smaller net fluxes and consequently smaller interannual variability than derived from other analyses. This might be a consequence of the model spin-up based on data input of a 1901 to 1930 monthly climatology and a pre-industrial concentration of atmospheric CO_2.

LPJ simulation results visualized on a global map (Fig. 5.1) indicate strong regional differences in the average interannual variability of NEP over 1982 to 2002. Areas that considerably contribute to a high fluctuation of NEP are the semi-arid grasslands of Southern America, Africa and Australia. This compares well with results of Schaefer et al. (2002). The influence and contribution of climate and individual carbon flux variability on NEP on global and regional scales will be investigated in the following sub-chapters.

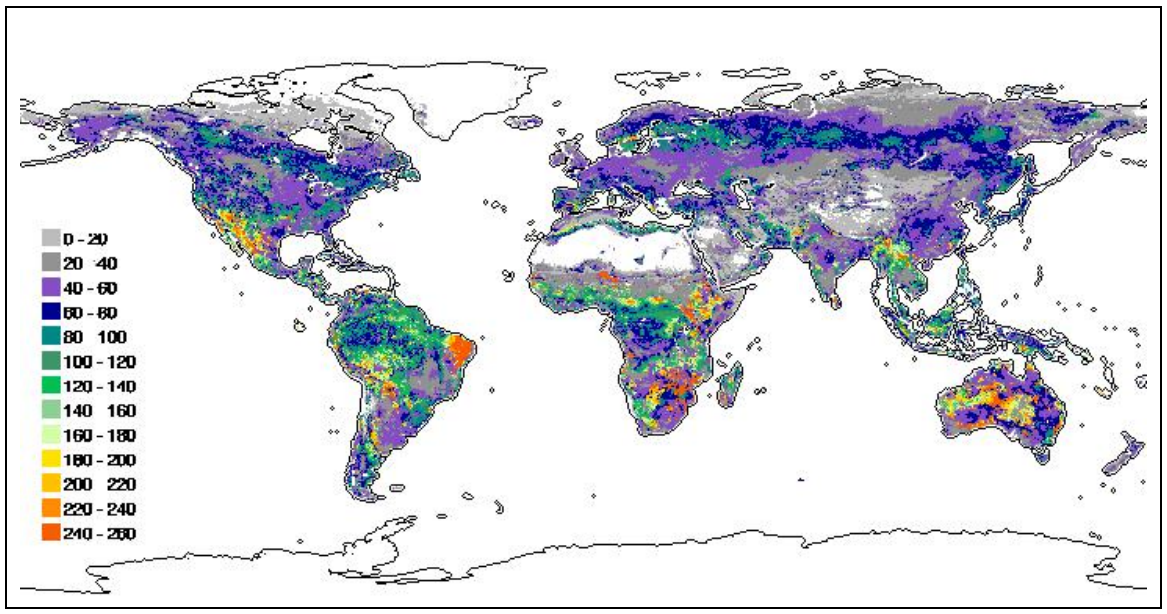

Fig. 5.1. Mean interannual variability of NEP (standard deviation in gC m^{-2} yr^{-1}) for the period 1982 to 2002.

5.1.1 The influence of climate on NEP variability

Cao et al. (2002) reported climate variability to be the most important factor for variations in terrestrial carbon uptake. Braswell et al (1997) found that on a global scale warm years are

followed by a reduced atmospheric CO_2 growth rate with a time lag of two years, concluding that climatic variability is correlated with changes in the carbon budget.

During the modelled time period of 1982 to 2002, climate variability on global and regional scales is dominated by anomalous climate events and a significant warming period that occurred in the 1990s with the seven warmest years recorded since instrumental climate recording started in 1860. Its average global temperature exceeded the long-term average by 0.63°C (Mann et al. 1998, WMO 1999, Folland et al. 2001). The year 2005 was reported as the warmest year on record (NASA 2006) and the years 2002 and 2003 followed as the second-warmest years (NOAA 2004).

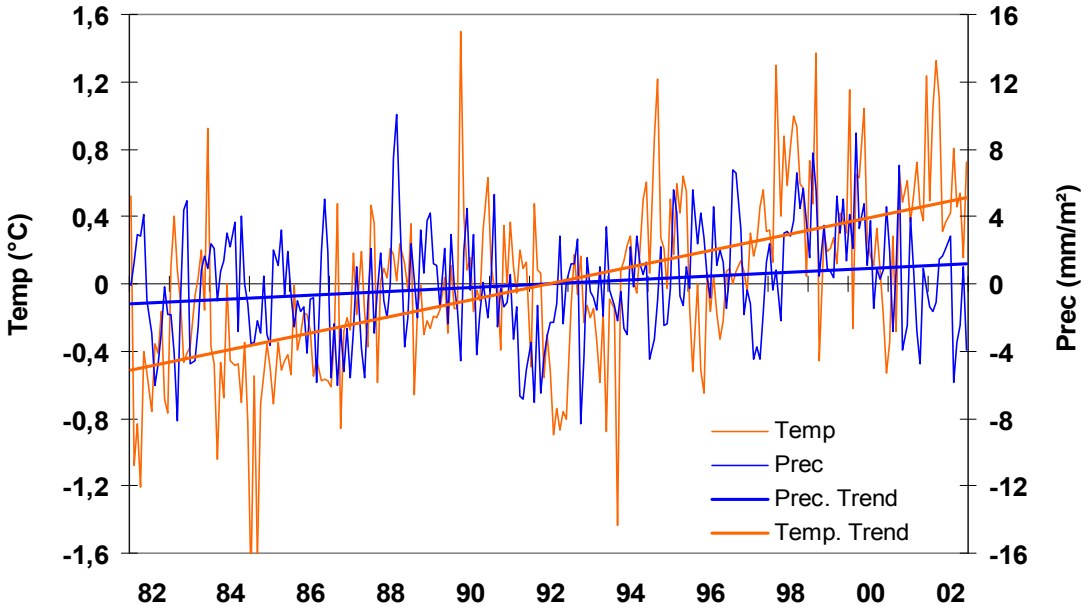

Fig. 5.2. Monthly global anomalies of temperature and precipitation for the time period 1982 to 2002 (CRU dataset, New et al. 1999a & b)

Fig. 5.2 presents the global monthly anomalies of temperature and precipitation as deviations from their mean values from 1982 to 2002. The 1990s featured noticeably more warm years than the 1980s, causing a definitive positive trend over this period. The global precipitation trend only shows a very slightly positive trend. Mean temperature variability for the same period (Fig. 5.3) is highest in the northern extra-tropics with a maximum in north-eastern Siberia, whereas pronounced precipitation variability (Fig. 5.4) is observed in the tropics and sub-tropics. Although precipitation variability is observed highest in the tropics, carbon flux variability does not respond linearly (Fig. 5.1), because usually sufficient amounts of precipitation are available to provide constant vegetation productivity.

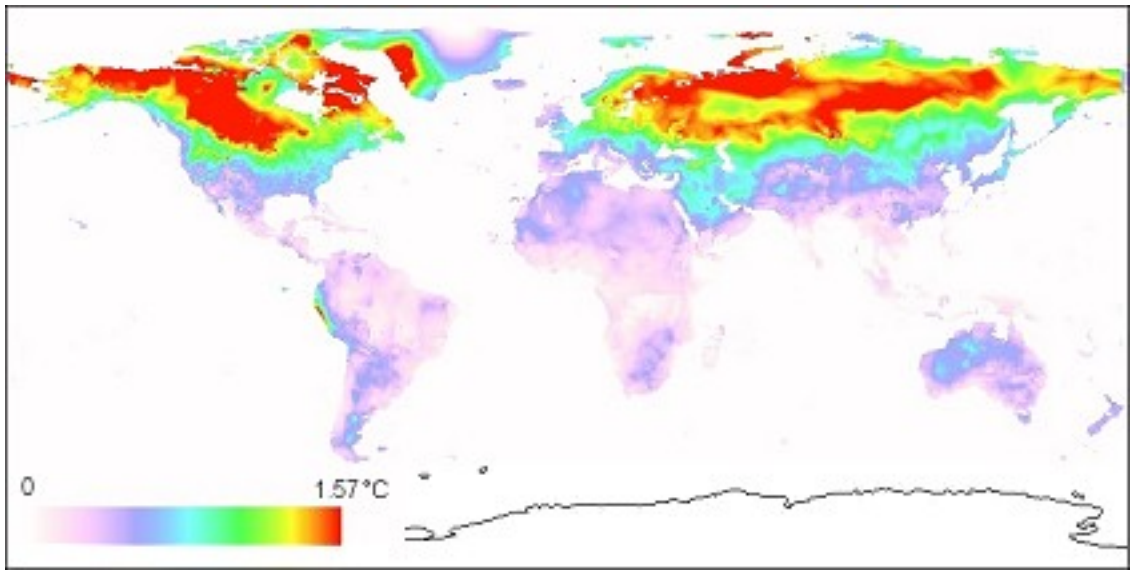

Fig. 5.3. Mean interannual variability of temperature (standard deviation in °C) for the time period 1982 to 2002

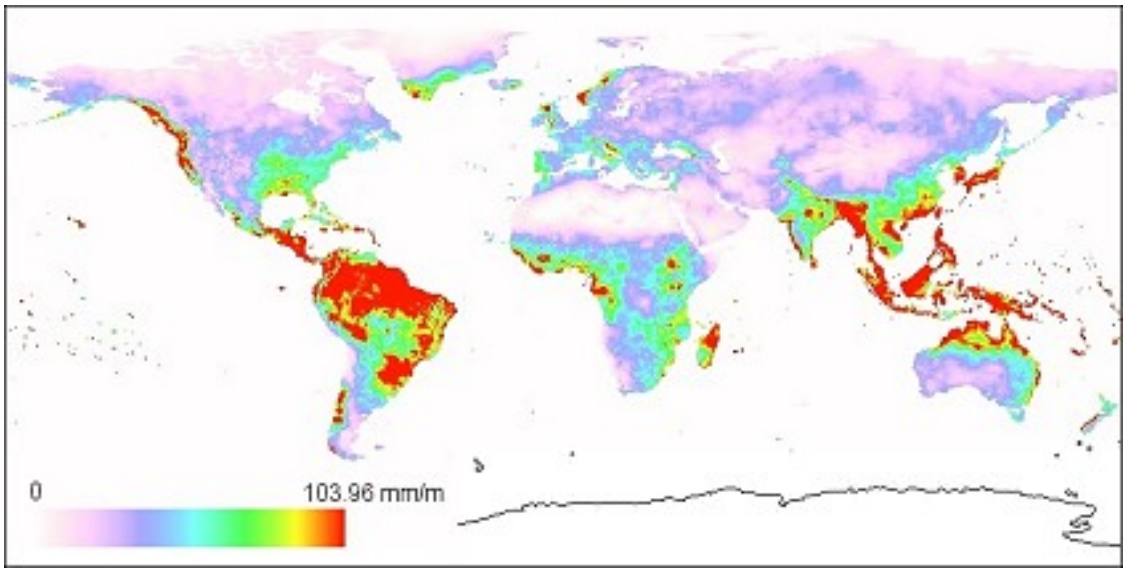

Fig. 5.4. Mean interannual variability of precipitation (standard deviation in mm m^{-1}) for the time period 1982 to 2002

Mean estimated NEP variability of northern temperate and boreal regions, and semiarid and arid regions of central Australia and South Africa (Fig. 5.1) does not reflect the regional mean precipitation variability. Therefore some other influence factors on interannual variability need to be investigated, such as fire occurrence or widespread climatic signals as e.g. the El Niño-Southern Oscillation (ENSO). Increasing trends may also be determined by increasing atmospheric CO_2 acting as a stimulant on NPP. The spatial distribution of the regions with high variability indicates a possible influence of ENSO, controlling the precipitation patterns in Australia, South East Asia and Africa as well as in the Amazon regions and North-East Brazil. The influence of ENSO on interannual variability of NEP will be investigated in chapter 6, discussing individual El Niño events of the late 1990s.

Tropical forests show low NEP variability, indicating a stable behaviour of the climatic drivers as well as of carbon fluxes and fire disturbance there. Schaefer et al. (2002) reported enhanced NEP variability in the western Amazon region, resulting from ENSO precipitation variability, but which might also be traced back to problems with the input ECMWF precipitation data set. Since the LPJ simulation does not show this anomalous NEP variability, this is probably an effect of different used climatic input datasets.

As NEP is the result of different carbon fluxes, now the question arises in which way the climate parameters do influence the carbon cycle components? Neither temperature nor precipitation variability (figs. 5.3 and 5.4) show the particular patterns found in NEP variability. Biospheric activity is linked non-linearly to climate events in a complex system of biogeochemical feedbacks, e.g. evapotranspiration, microbial activity in the soils etc. The following section investigates in more detail selected carbon cycle components their response to specific regional climatic patterns.

5.1.2 Interannual variability of carbon fluxes determining NEP

Interannual fluctuations in NEP are a function of variability in NPP fluxes, soil respiration and ecosystem disturbances. Variations in climate can affect the seasonal and annual fluctuations in carbon fluxes, but differentiating the influence of particular climatic variables on NEP is difficult, as they are not independent of each other. Regarding the NEP-influencing carbon fluxes separately, the image gets more complicated. E.g., the NPP of the higher latitudes is mainly determined by temperature, while in lower latitudes NPP is influenced by precipitation variability (Churkina & Running 1998, Cao et al. 2002). In addition, elevated atmospheric CO_2 concentration supports photosynthetical processes in higher latitudes, which is more pronounced at higher temperatures, while in the tropics stress due to warmer temperatures might be compensated by the CO_2 fertilization effect (Kirschbaum 1994, Cao & Woodward 1998a, Tian et al. 1998). Fig. 5.5 shows the fluctuations of LPJ-simulated global monthly carbon fluxes NPP, Rh and NEP.

NPP shows considerably strong interannual variations with a coefficient of variation of 45 % (mean NPP is 5.03 PgC month^{-1} with a range of 2.3 PgC month^{-1}) for the time period 1982 to 2002. These estimates compare slightly higher to results of Cao et al. (2002), who reported a coefficient of variation of 34 %, and a mean NPP of 4.32 ± 1.48 PgC month^{-1}. Rh calculated by LPJ shows less monthly variations with a coefficient of variation of 39 %, and a mean of 4.37 ± 1.73 PgC month^{-1}. These Rh estimates compare slightly higher to results of Cao et al. (2002), who reported a coefficient of variation of 25%, and a mean of 4.26 ± 1.08 PgC month^{-1}.

LPJ global estimates for NEP show a stronger variability (-0.78 to 2.09 PgC month^{-1}) than model results of Cao et al. (2002) (-0.73 to 1.23 PgC month^{-1}). The FBM model estimates of Kindermann et al. (1996) range between -2.51 to +2.55 PgC yr^{-1} for the time period 1980 to 1994. The LPJ results compare well to the simulated NEP of Potter et al. (2003), derived by the CASA model, that varies between -0.9 and +2.1 PgC yr^{-1}. However, it has to be noted that the mentioned approaches are all based on satellite data input, so that the comparison is limited, since the approaches mainly vary in their way to model carbon fluxes. Independent inverse modelling studies vary in their estimates for peak-to-peak amplitude of net terrestrial fluxes without specifying the absolute peak values as they are reporting flux anomalies. Bousquet et al. (2000) observed a NEP peak-to-peak amplitude of 5 PgC yr^{-1}, while Peylin et al. (2005) reported an amplitude of ± 2 PgC yr^{-1}.

LPJ estimates of NPP, NEP and Rh show considerable seasonal fluctuations (Fig. 5.5). For all carbon fluxes maxima are observed in spring and summer while minima occur during the autumn and winter season. Monthly fluctuations of NEP are mainly a function of variability in NPP and Rh. Simulated monthly Rh shows considerably less interannual variations than monthly NPP. In early spring model predictions for Rh exceed those for NPP when temperature is already high enough for decomposition processes, whereas budburst occurs later in spring. A minor second maximum of NEP in autumn is caused by vegetation greening during the southern hemispheric spring.

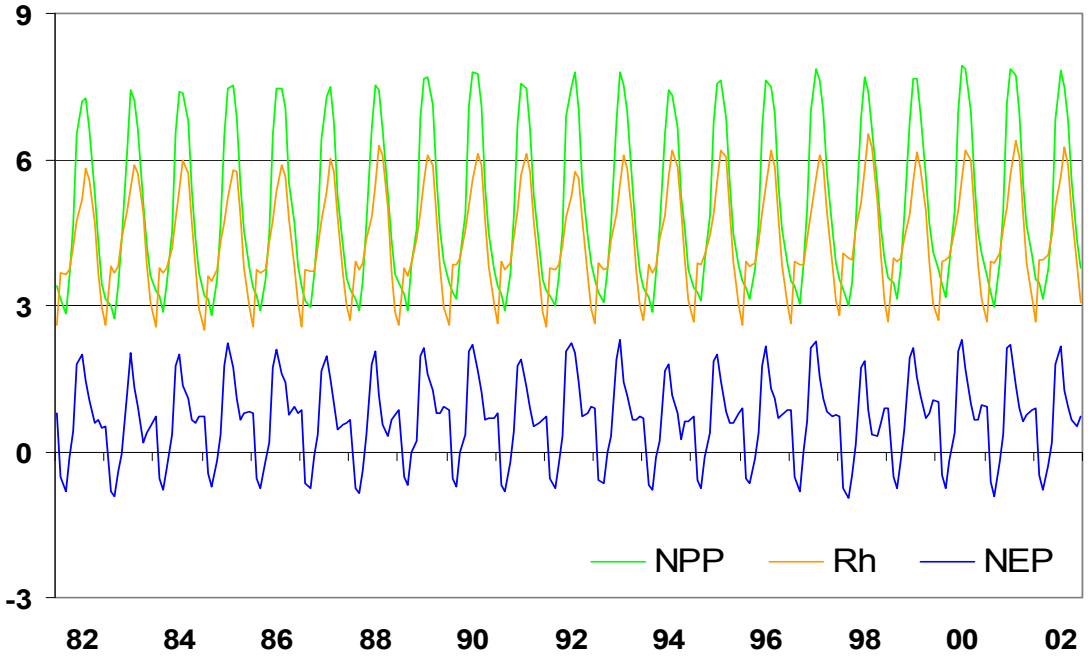

Fig. 5.5. LPJ model estimates of monthly global carbon fluxes for NEP, NPP, and Rh (PgC month^{-1}) for 1982 to 2002

Figs. 5.6.A to C show the global distribution of LPJ mean monthly results for the interannual variability of NPP, Rh and carbon released by fire during the time period between 1982 and 2002. NPP is the main regional contributor to interannual variability on a global scale (Fig. 5.6.A), whereas fire carbon shows the highest magnitude in variation, but only in very few regions (Fig. 5.6.C). In tropical and subtropical regions the interannual variability of NPP is mainly controlled by precipitation variability (Fig. 5.4). Temperate regions show relatively small fluctuations of NPP (< 60 $gCm^{-2}yr^{-1}$) compared to the boreal zone where NPP variability is moderate (60–120 $gCm^{-2}yr^{-1}$). However, the moderate boreal NPP fluctuations significantly contribute to the annual seasonal changes in global NEP. Reason is the global distribution of land with more vegetated area on the northern hemisphere, dominating the seasonal cycle of NEP with high NPP in spring and summer, and Rh exceeding NPP in the fall. For the temperate zone, the weak interannual variability of NEP is a result of small year-to-year fluctuations of NPP, RH and fire.

The modelling results demonstrate a high interannual variability of NPP in regions of the Southern Amazon, as well as in North-Eastern Brazil, along the North American West-Coast, in South East Africa, areas in Asia, particularly in Thailand and central and eastern Australia. In these regions the pronounced interannual variability of NPP is an effect of El Niño events. They particularly cause reduced rainfall and/or increased temperatures influencing changes in evapotranspiration, i.e. plant and soil respiration.

Fluctuations of soil respiration mainly occur in the Amazon boundary regions, the semi-deciduous areas of the African Tropics, within a small band of the boreal forests in the northern latitudes, and in South-East Asia, but generally showing less year-to-year variations than annual NPP. In the tropics, heterotrophic respiration is driven by soil moisture variability that depends predominantly on the availability of precipitation and less on temperature there. In the boreal zone concurrent patterns of temperature variability and soil respiration cannot be identified. But as soil respiration activity responds exponentially to increasing temperature (Lloyd & Taylor 1994), small changes in soil temperature can produce large soil respiration anomalies, as observed during summer when soil respiration exponentially increases during peak temperatures. Apparently, the storage of large carbon pools of slowly decomposing litter with residence times of many years buffers the interannual effect of climate variability on Rh over large areas.

No interannual variability of fire carbon flux occurs in agricultural zones, originating from the suppressed fire in these regions. Consequently, the generally low IV of NEP in the temperate zone is an effect of the lacking fire carbon variability in agricultural areas as broad regions of the temperate zone are cultivated. Natural fires occur most frequently and show largest variability in the semiarid grasslands of south-western North America, North-Eastern Brazil, Patagonia, within the Mediterranean Region, the Sahel, and central Australia (Fig. 5.6.C).

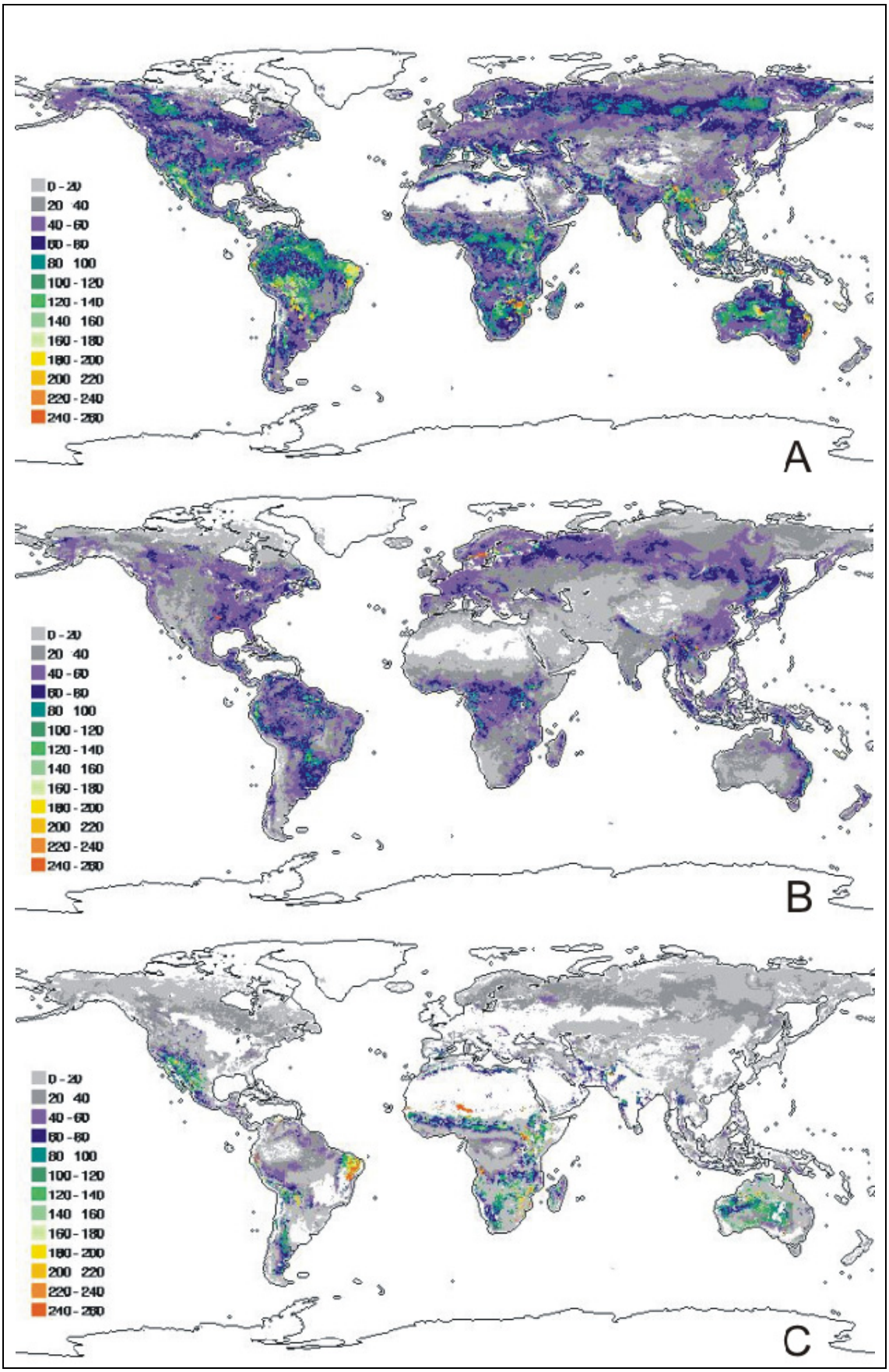

Fig. 5.6. LPJ model estimates for the interannual variability of mean NPP (A), Rh (B) and carbon released by fire (C) (standard deviation in $gCm^{-2}yr^{-1}$) for the time period 1982 to 2002

In these regions the interannual variability of NEP is mainly a function of variability in fire carbon fluxes (Fig. 5.7).

Fig. 5.7 identifies the carbon fluxes significantly influencing the interannual variability of NEP. Classes are based on the interannual variability of a particular carbon flux, which has to exceed 60 $gCm^{-2}yr^{-1}$ (representing one third of maximum annual variation) to be determined as influencing factor on the interannual variability of NEP. White regions represent low interannual variability for all carbon fluxes with fluctuations of less than 60 $gCm^{-2}yr^{-1}$.

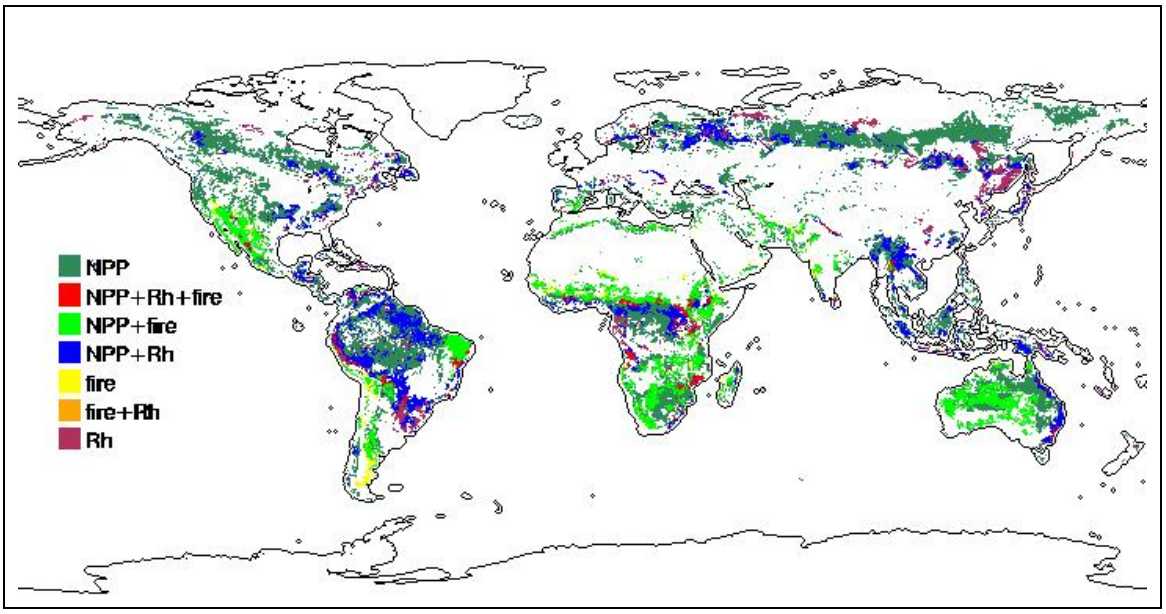

Fig 5.7. Regional distribution of the main influence components on NEP variability

NPP variability as main driver dominates the boreal zone (which is temperature driven) and the central tropical forests, where it is determined by precipitation and therefore soil moisture. NPP and Rh variability together dominate the boundaries of the tropical moist forests and some small areas in the boreal zone. While fire alone only dominates the interannual variability of NEP in Southern Patagonia, fire together with NPP variability influences broad regions of semi-arid grasslands all over the world. Concluding, interannual variability of NEP is mainly determined by fluctuations in NPP, which is controlled by temperature in the high latitudes and by precipitation variability in the lower latitudes. Fire occurrence affects strongest the total magnitude of NEP variability. The influence of soil respiration is most pronounced in tropical regions, where precipitation variability controls soil moisture status.

5.1.3 Response of global carbon fluxes to anomalous climate events

Temporal variations of global monthly carbon fluxes can be affected by global anomalous climate events such as the El Niño-Southern Oscillation (ENSO), and the North Atlantic Oscillation (NAO). The de-seasonalized time series of NEP anomalies (Fig. 5.8) indicate

distinct episodes of increase and decrease. Fig. 5.8 presents a measure of the world's most prominent climate cycle, the Southern Oscillation Index (MEI – Multivariate ENSO index), to identify correlations between terrestrial carbon fluxes and anomalous climate events. Positive MEI values indicate El Niño events, while negative MEI values represent La Niña periods (Bradley et al. 1987, Diaz & Markgraf 1992, Philander 1990). The global time series suggest no correlation between NEP anomalies and MEI values ($r^2 = 0.04$). In contrast, Prince & Xue (2001) found that the interannual variability of global NPP is closely related to ENSO years. In fact, in the years 1983 and 1987 NPP decreased while in years with La Niña events (1984, 1994 and 1996) an increase in NPP was observed. The correlation between NPP and MEI seems to be small ($r^2 = 0.21$, see table 5.1), but considering the fact that the comparison associates global carbon fluxes with a regionally occurring climate signal, it can be interpreted as moderately significant.

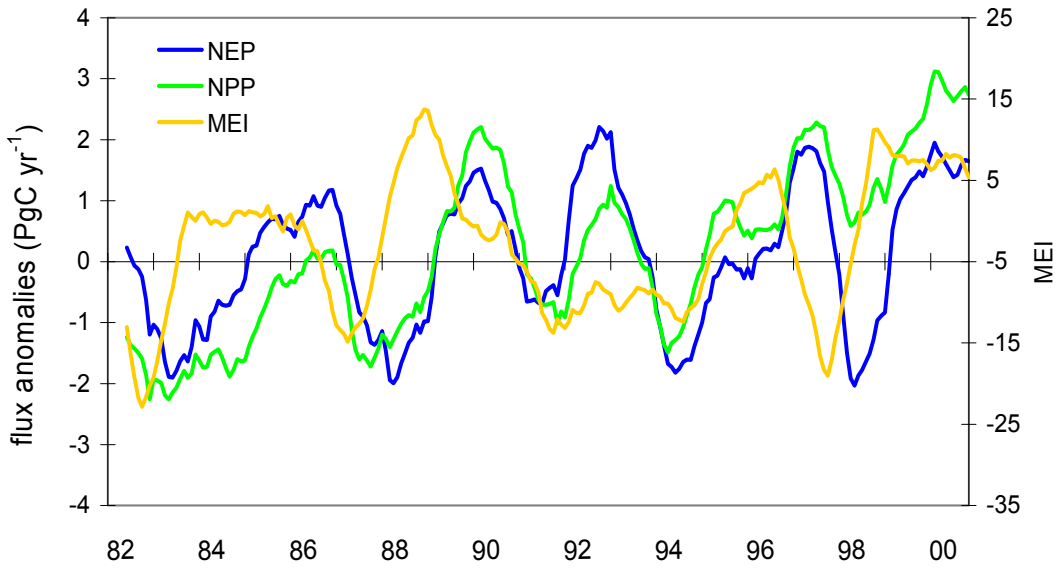

Fig. 5.8. Global anomalies for net ecosystem production (NEP), net primary production (NPP), and the Multivariate ENSO index (MEI)

NPP correlates better with MEI than NEP, because rainfall is strongly reduced throughout the tropics during an El Niño event, followed by a reduction in NPP. According to the results of Cao et al. (2002), soil respiration also reacts by decrease to the reduced precipitation and dry soil moisture status, which partly cancels out the NPP reduction, leading to a weak response of NEP. Both, NEP and NPP react with a time-lag of approximately 12 months to the MEI, corresponding to the results of Reichenau & Esser (2003) who reported varying time lags of up to 11 months for global NEP responding to El Niño events. If the investigation is confined to the Amazon basin, NPP reacts with a time-lag of three months to fluctuations in MEI (Foley et al. 2002).

	Net Ecosystem Production (NEP)	Net Primary Production (NPP)	Heterotrophic Respiration (Rh)
MEI	0.04	0.21	0.23
Temperature	-0.18	0.34	0.69
Precipitation	-0.10	0.26	0.47

Table 5.1. Correlations between monthly global anomalies of carbon fluxes and climate variables (numbers represent correlation coefficients, p = 0.05)

Globally, NEP shows a weak negative correlation to both, temperature and precipitation. NPP and soil respiration show a more pronounced relation to climate, particularly they correlate to temperature. But as correlations do not imply necessarily a causal relationship further analysis has to be done. Regional correlations between carbon fluxes and ENSO will be discussed later (chapter 5.2).

5.1.4 Global carbon fluxes and CO_2 growth rate anomalies

In the following, various global carbon fluxes, including their trends and interannual variability, are compared to investigate the role of terrestrial vegetation on global net carbon exchange. Fig. 5.9 highlights interannual changes in different global carbon fluxes including anthropogenic emissions from fossil fuel burning (Marland & Rotty 1983, ORNL 1990, BP 2004) and land-use change (Houghton 2003c), the ocean uptake (Buitenhuis et al., in prep.), the modelled land uptake of this study (NEP and NPP) as well as the atmospheric CO_2 increase (Keeling & Whorf 2004). Emissions from fossil fuel burning, land-use change, and ocean uptake do not show a strong interannual variability, and they show adversative time series. Thus, the yearly CO_2 growth rate anomalies are clearly determined by changes in terrestrial biospheric sources and sinks as reflected in the annual rates of net land uptake (NEP).

In order to quantify the interrelation between the net CO_2 growth rate anomalies and NPP variability, Nemani et al. (2003) estimated global NPP for the years 1982 to 1999. Based on climate and satellite data input, their approach is similar to Production Efficiency Models (PEMs) following Prince et al. (1995), Potter et al. (2001), and Field et al. (1995), upgraded by a number of key parameters derived from the BIOME-BGC (Running et al. 2000, White et al. 2000, Thornton et al. 2002). Similar to the current study, vegetation greenness parameters were estimated by assimilating global AVHRR-PAL and -GIMMS NDVI, LAI and fPAR input datasets, but generated by different algorithms. Therefore, congruent comparison with the results obtained by this study is not strictly possible, but suitable for general comparisons. Predicted estimates for carbon fluxes over 1982 to 1999 compared well to model results of this study.

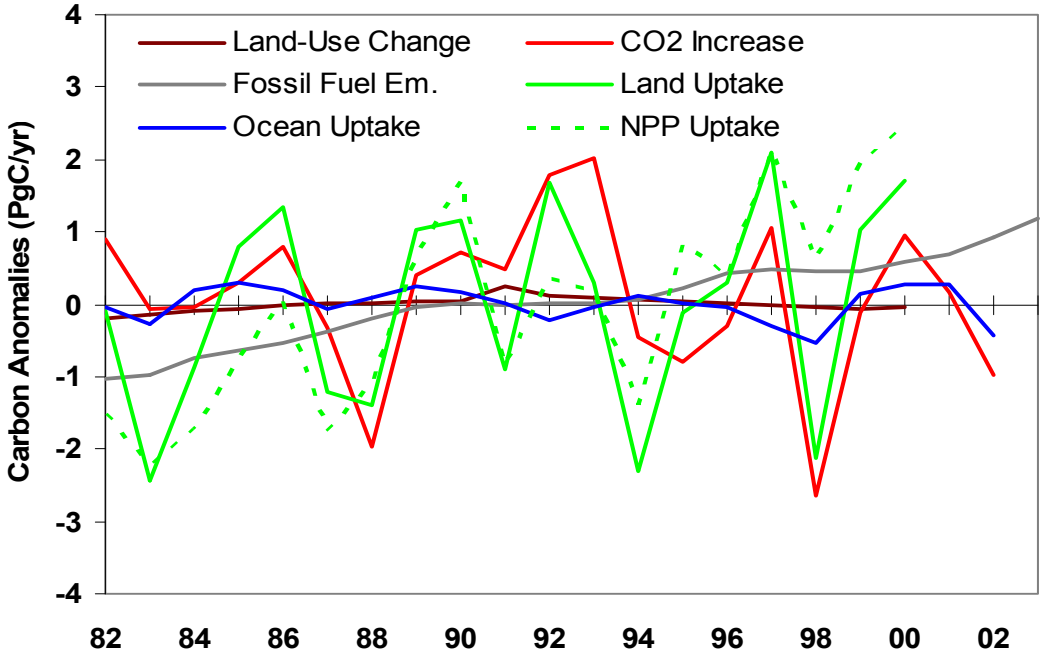

Fig. 5.9. Annual global carbon flux anomalies after Lucht et al (in prep.); (data from: BP, 2004; Houghton, 2003c or http://cdiac.ornl.gov/ftp/ndp050/ndp050.dat; Buitenhuis et al., in prep; Keeling & Whorf, 2004).

Nemani et al. (2003) estimated a mean global NPP of 54.5 PgC yr^{-1} that compares lower to LPJ-simulated NPP with 60.6 PgC yr^{-1} for LPJ-S_{GIM} and 59.2 PgC yr^{-1} for LPJ-S_{PAL}. However, the global increase of NPP over 18 years is similar: Nemani et al. (2003) reported an increase of 3.42 PgC, the present approach shows an increase in NPP of 3.45 PgC (LPJ-S_{GIM}) and 4.39 PgC (LPJ-S_{PAL}). LPJ satellite-derived model estimates are close to the findings of Nemani et al (2003) (Fig. 5.10.B). Both approaches estimate an NPP increase of 0.2 % per 1 ppm-increase of CO_2, which is close to measurements (Curtis & Wang 1998).

Nemani et al. (2003) relates annual NPP anomalies (PgC yr^{-1}) to annual CO_2 growth rates (ppmv) observed at Mauna Loa, Hawaii (Keeling & Whorf 2004) (Fig.5.10A) (Data access: http://cdiac.esd.ornl.gov/ftp/trends/co2/maunaloa.co2). A comparison of satellite-derived observations (Fig. 5.10.A) and LPJ model results (Fig. 5.10.B) in relation to the atmospheric CO_2 growth rate suggest that interannual variations of NPP are strongly related to global increases in atmospheric CO_2 growth rate. Nemani et al. (2003) stated that terrestrial NPP strongly controls the anomalies of the CO_2 growth rate, even though it accounts for only a part of the carbon exchange with the atmosphere. Consequently, regarding the figures, there are still some inconsistencies, i.e. in the 1990s, after the Mt. Pinatubo eruption and the long extraordinary El Niño event from 1991 to 1994. Also the 1998/99 El Niño shows are strong difference between NPP and CO_2 growth rate.

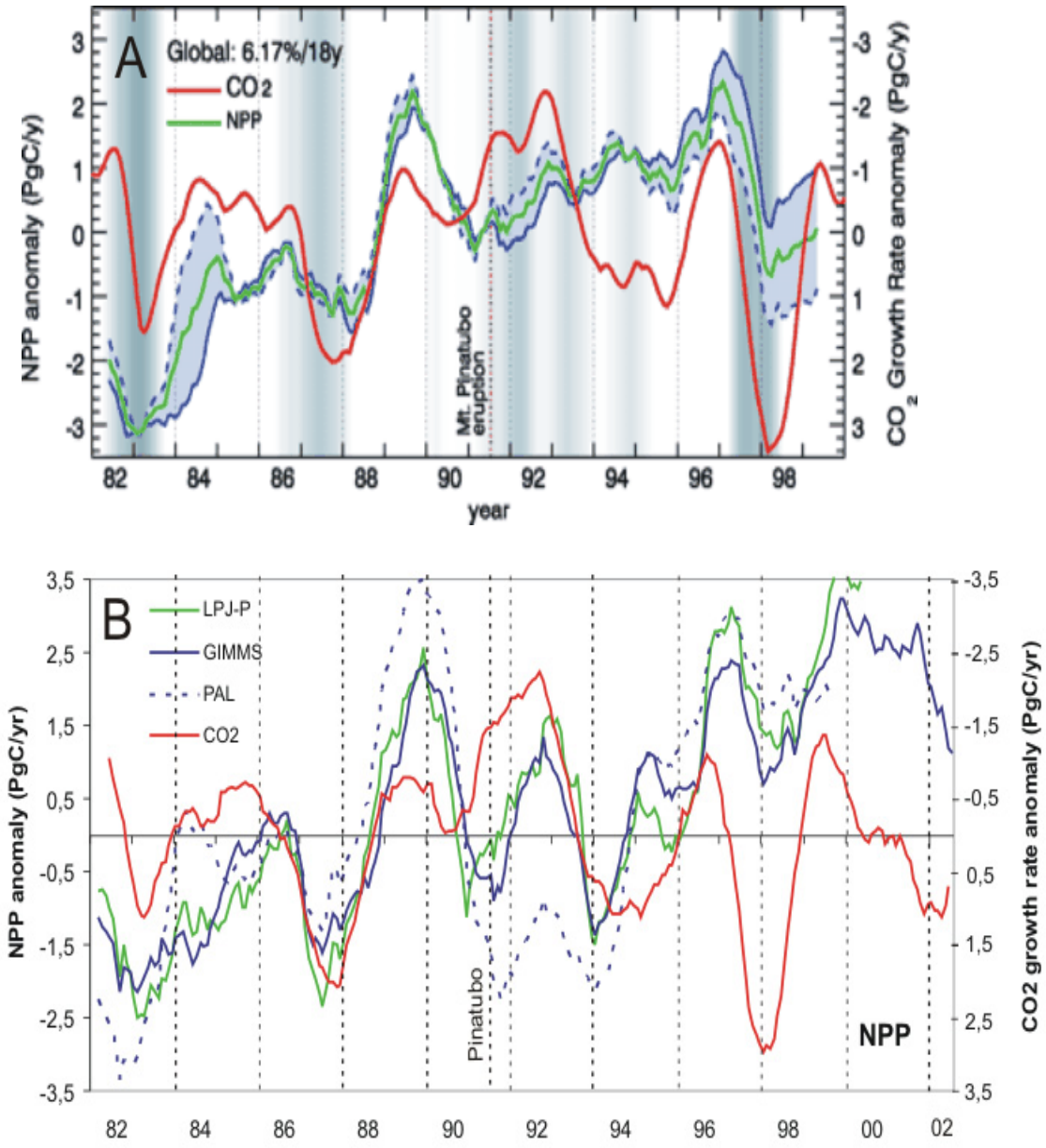

Fig. 5.10. A) Interannual variations from 1982 to 1999 in global NPP in relation to atmospheric CO_2 growth rate, from Nemani et al. (2003). Trends in global NPP anomalies for GIMMS (solid blue line), PAL (dashed blue line), and their average (green line), CO_2 growth rate (inverted) in red; a multivariate ENSO index (MEI) in gray scale, darker shades represent higher MEI values. B) Interannual variations from 1982 to 2002 in global LPJ-simulated NPP in relation to atmospheric CO_2 growth rate. Trends in global NPP anomalies result from different satellite information, GIMMS (solid blue line), PAL (dashed blue line), and their average (green line), CO_2 growth rate (inverted) in red.

These inconsistencies cannot be explained by the LUE-approach of Nemani et al. (2003), because a full carbon accounting needs to include soil carbon processes and heterotrophic respiration, as well as other carbon sources such as fire disturbance. With the present approach full carbon cycle estimation is possible. Fig. 5.11 shows the interannual variability of the simulated NEP derived by LPJ with different satellite input datasets compared to the annual

CO_2 growth rate anomaly. It indicates that the variability of modelled NEP is much closer to the variability of atmospheric CO_2 than NPP. While LPJ-S_{GIM} modelled NEP has a good fit (r = 0.76) to the annual atmospheric CO_2 growth rate, a strong deviation occurs with the PAL data input (r = 0.19). A time lag of about two to several months between LPJ-modelled NEP and the observed CO_2 growth rate reflects the delayed onset of heterotrophic respiration following NPP also with a time lag of several months (Fig. 5.12).

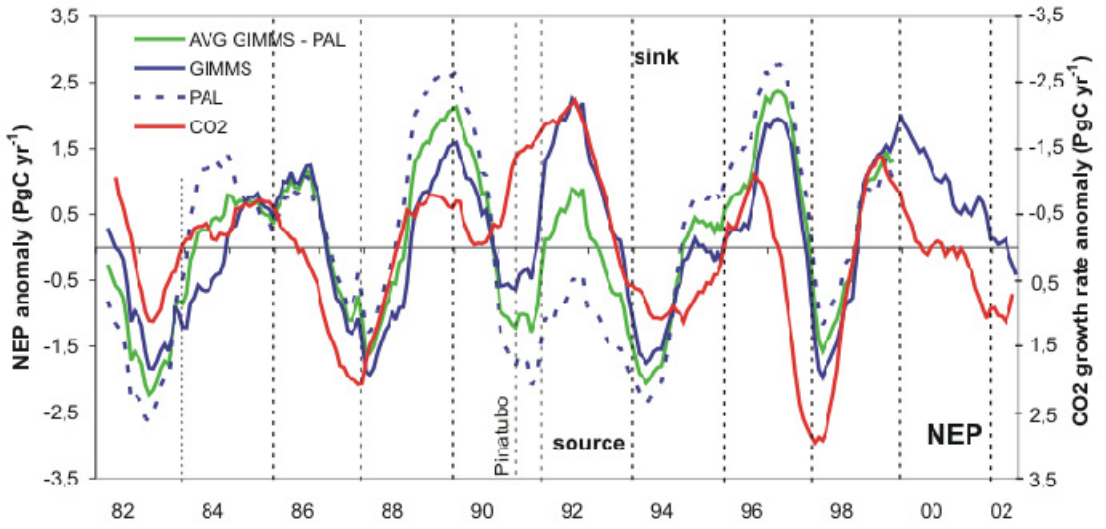

Fig. 5.11. Interannual variability from 1982 to 2002 in global NEP in relation to annual atmospheric CO_2 growth rate. Trends in global NEP anomalies for GIMMS (solid blue line), PAL (dashed blue line), and their average (solid green line), CO_2 growth rate (inverted) in red.

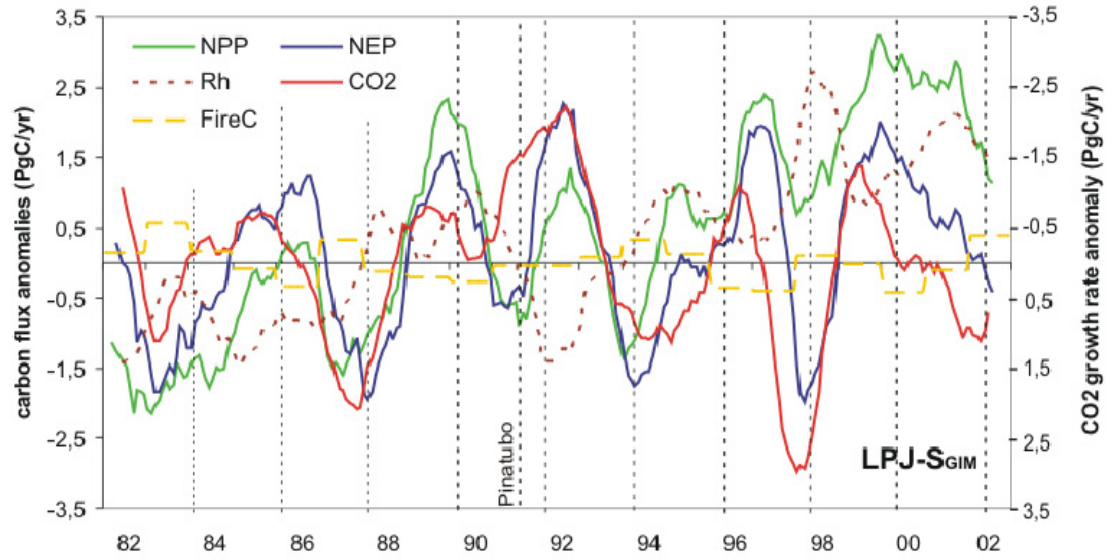

Fig. 5.12. Global terrestrial net carbon flux anomalies simulated with LPJ-S_{GIM}. Please note that the CO_2 growth rate anomalies are inverted.

NPP corresponds directly to changes in atmospheric CO_2 and climate fluctuations, while soil respiration responds gradually to environmental changes, for example as plant production only successively adds organic material to soil pools. This indicates that the temporal lapse of the CO_2 growth rate is mainly determined by NPP, but its magnitudes and timings are shaped by Rh. Fire carbon also shows a shape following NPP, balancing the offset determined by the influence of Rh. During the ‘‘post-Pinatubo’’ period, the mean atmospheric CO_2 growth rate was relatively low during 1991– 1993 and recovered in 1994–1995. The observed cooling of 0.6°C between late 1991 and mid-1992 drove a decrease of Rh in LPJ only. Peylin et al. (2005) reported a good agreement between LPJ-P-modelled carbon fluxes, atmospheric inversion derived fluxes and atmospheric CO_2 growth rate anomalies supporting the necessity of accounting other processes than NPP.

Concluding, interannual variations in terrestrial carbon fluxes include other factors than NPP, which can be detected by combining high resolution remote sensing information with a process-based vegetation model. The modelled carbon fluxes can help to better explain differences between the model estimates of Nemani et al. (2003) and the atmospheric CO_2 growth rate as seen in 1983, 1987 and following the Pinatubo eruption in 1991. Thus, it can be reported here that the annual CO_2 growth rate is dominated by fluctuations in NPP, but further shaped and balanced by soil respiration changes and fire occurrence.

5.2 Regional influences on interannual variability of net ecosystem production

5.2.1 NEP controlling factors on regional scales

In order to illustrate the relative influence of different components on NEP variability on regional scales, four sites were selected representing different ecosystems (Table 5.2).

Ecosystem	Region	Lat	Lon	NPP	Rh	fireC	Tem	Prec	NEP
Boreal forest	Asia / Siberia	60°N	110°E	51.4	30.1	24.4	17.0	21.1	69.8
Temperate savanna	North America West Coast	30°N	109°W	32.6	12.2	111.9	6.7	46.2	205.7
Subtropical savanna	Africa / Sahel	18°N	8°E	68.4	19.8	73.9	1.9	96.3	138.7
Tropical moist forest	South America Amazon	0°N	57°W	23.9	33.4	30.1	1.0	120.7	123.8

Table 5.2. Ranges of interannual fluctuations of carbon cycle and climatic components for four sites representing different ecosystems (standard deviation of carbon fluxes in gC m^{-2}, prec. in mm, temp. in °C)

These results support the findings, that NEP interannual variability is mostly a function of fire in ecosystems with high fire frequencies such as the northern American West coast region, and subtropical savanna. In subtropical savanna regions also highest variability in NPP occurs, caused by the high amount of biomass of a dense grass layer, which is highly sensitive to precipitation variability. At the northern boreal forest site, NEP variability is predominantly a function of NPP and to a weaker extent influenced by Rh, since both strongly depend on temperature. In the South American tropics NEP variability is mainly determined by variations in soil respiration. Since the annual temperature cycle shows almost no variability, rainfall governs Rh variability and associated soil processes.

NEP variability is highest in ecosystems with high influence of fire. Rh variability is mainly lower than NPP variability except in the humid tropics, where it exceeds NPP variability and where it is determined by rainfall variability. Neither temperature nor precipitation variability could be confidently determined as the sole contributor to NEP variability on terrestrial carbon fluxes and needs further investigation.

5.2.2 Response of regional carbon fluxes to climate variability

In order to upscale the findings derived by looking at individual grid cells onto regional scales and to further investigate the influence of climate on regional carbon flux variability, four latitudinal bands were selected representing the boreal, the northern and southern temperate zones, and the tropics (Fig. 5.13).

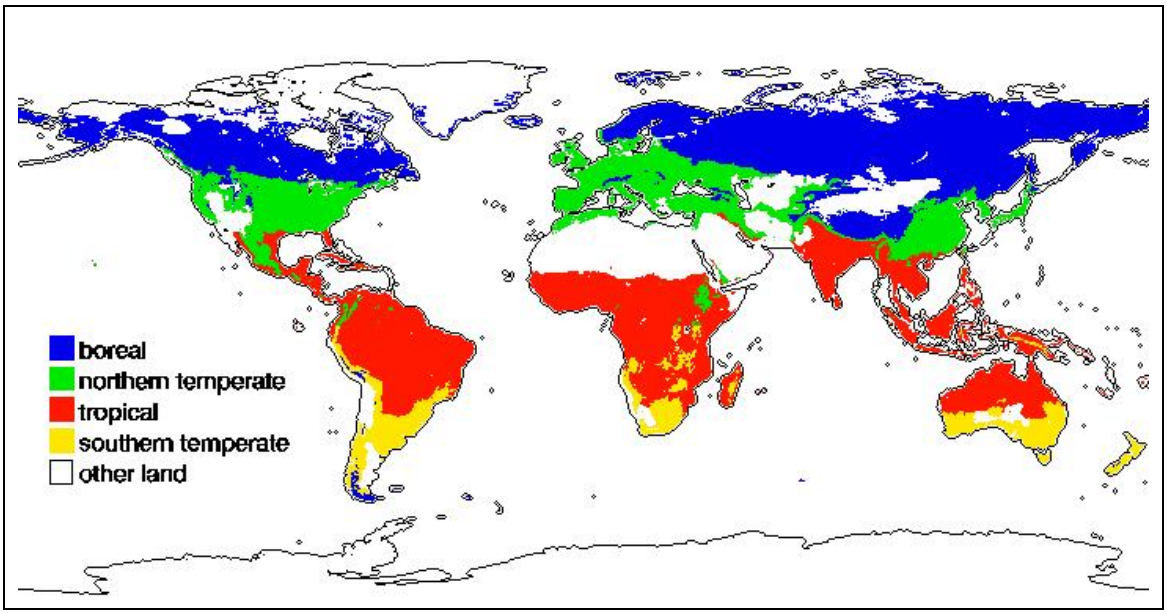

Fig. 5.13. Different climatic zones used for the following analysis

The four selected latitudinal zones differ in their patterns of temperature and precipitation as described below:

- Boreal zone: mean annual precipitation > 200 mm, mean annual temperature < 5°C
- Northern temperate zone: mean ann. precipitation > 200 mm, mean ann. temp. > 5 < 20°C
- Tropical / subtropical zone: mean ann. precipitation > 200 mm, mean annual temp. > 20°C
- Southern temperate zone: mean ann. precipitation > 200 mm, mean ann. temp. > 5 < 20°C
- Other land regions (and water): mean ann. precipitation < 200 mm

Carbon fluxes of NPP, RH, and NEP have been correlated to climatic parameters to characterize specific eco-climatic relationships for each of the latitudinal zones (Table 5.3). Monthly anomalies of mean monthly carbon fluxes and temperature/precipitation have been used to minimize the effect of co-influence of subsequent monthly values and to eliminate seasonal effects. The analysis was based on 228 monthly values for each carbon flux and climatic variable. For sampling 228 values a correlation of $r = 0.132$ (for $p = 0.05$) is statistically significant.

Latitudinal zone	Carbon fluxes	Temperature Anomalies	Precipitation Anomalies
Boreal	NEP	-0.22	-0.22
	NPP	0.25	0.10
	Rh	0.52	0.36
Northern temperate	NEP	-0.14	-0.29
	NPP	0.35	0.05
	Rh	0.69	0.48
Tropics	NEP	-0.44	0.17
	NPP	-0.17	0.43
	Rh	0.43	0.58
Southern temperate	NEP	-0.60	-0.08
	NPP	-0.43	0.43
	Rh	0.21	0.79

Table 5.3. Relation between climate variability and carbon fluxes for the latitudinal zones are shown in blue for a negative correlation, in red for a positive correlation and in black for a weak correlation.

In most regions NEP is negatively correlated with temperature, particularly in the tropical and southern temperate regions. For all regions, except for the southern temperate zones, soil respiration is a function of temperature, thus determining the negative correlation between NEP and temperature. Additionally, for tropical and southern temperate regions, high temperatures predominantly affect transpiration producing negative correlations between plant production and temperature. For the northern extratropical regions, warmer temperatures trigger plant productivity, balancing the diminishing effect of enhanced soil respiration on terrestrial uptake. Changes in the amount of precipitation have the most pronounced effect on both NPP and soil respiration in the tropics and southern temperate regions. For regions northwards of the equator, precipitation variability dominates Rh, while NPP is mostly affected by temperature changes.

As the correlation analysis in table 5.3 records wide latitudinal zones comprising different spatial and temporal patterns, the nonparametric, rank-based Spearman correlation coefficient was chosen to demonstrate the regional relations between mean annual carbon fluxes and climate variability for every pixel on a yearly basis (Figs. 5.14 and 5.15). Values of $r \geq 0.3994$ (for $p = 0.05$) are defined to be statistical significant. The maps demonstrate that the picture is more differentiated which cannot be captured by the large-scale latitudinal zones, i.e. for NEP, even though latitudinal patterns can be observed for NPP and soil respiration when correlated to temperature.

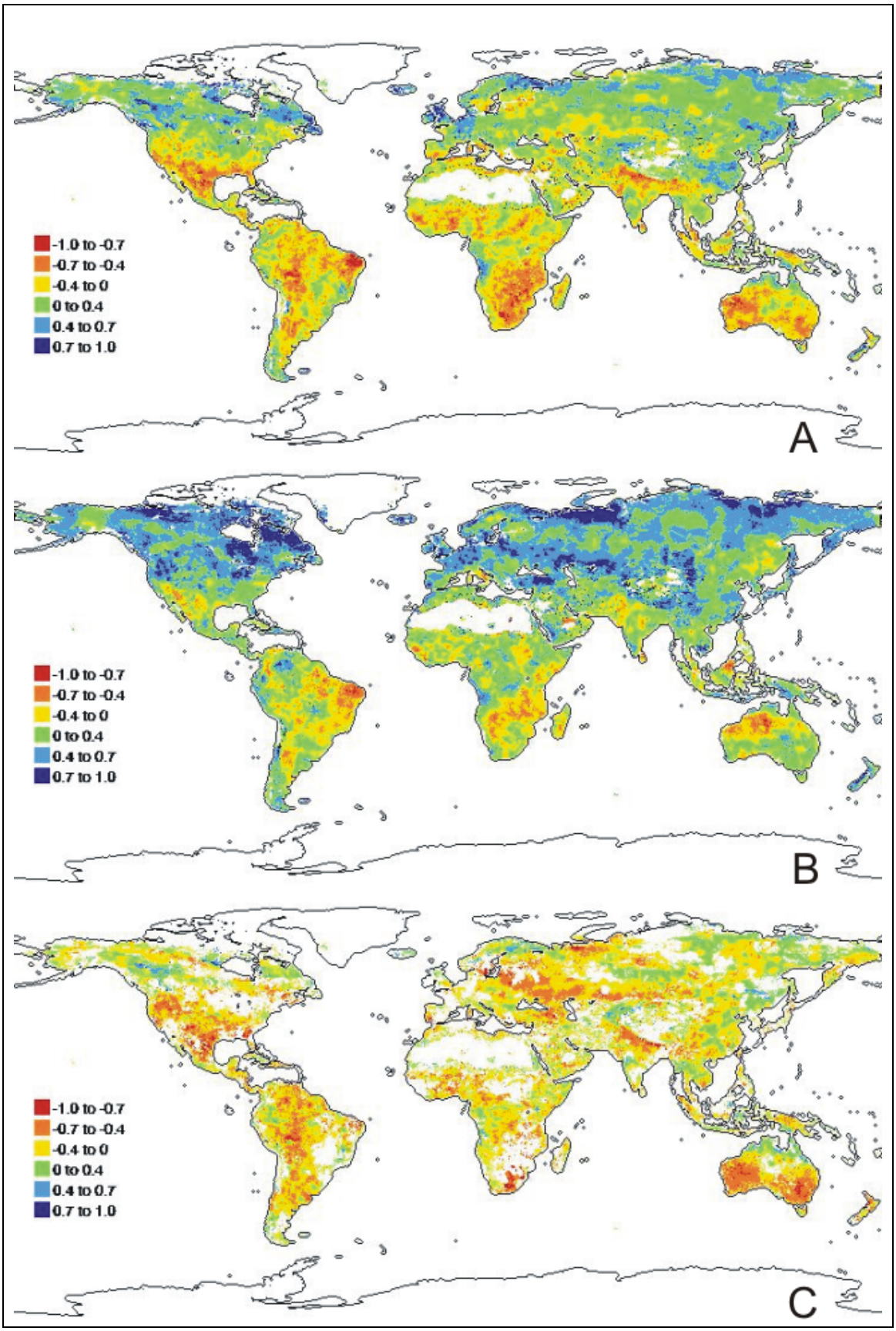

Fig. 5.14. Correlation of monthly mean carbon fluxes and temperature. (A) temperature and NPP, (B) temp. and Rh, (C) temp. and NEP.

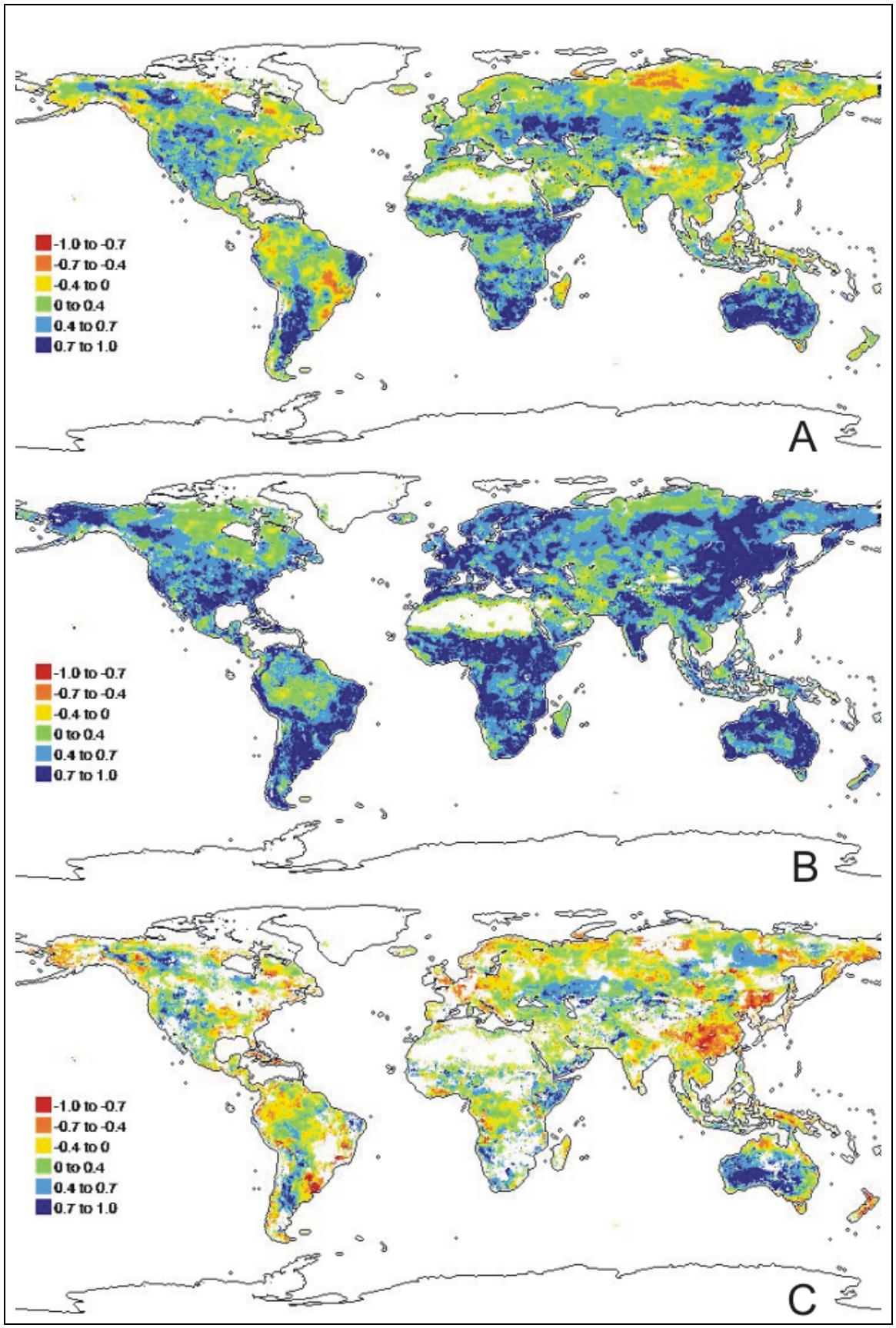

Fig. 5.15. Correlation of monthly mean carbon fluxes and precipitation. (A) precipitation and NPP, (B) prec. and Rh, (C) prec. and NEP.

Globally, for most regions NEP is negatively correlated to temperature as a response to changes in soil respiration (Fig. 5.14B and C). There is a distinct latitudinal response of NPP to temperature with a positive correlation for the northern extra-tropics when warmer temperatures enhance plant productivity and growing season is elongated. Additionally, photosynthesis is enhanced under elevated atmospheric CO_2 concentration with greater responses at warmer temperatures (Kirschbaum 1994). A negative correlation occurs southwards of 30°N (Fig. 5.14A), when transpiration is enhanced due to warmer conditions and carbon losses increase with rising temperatures due to enhanced photorespiration (Schultz 1995).

Precipitation variability has a high influence on NPP and even more pronounced on soil respiration, but it strongly differs regionally. For arid regions a positive correlation between NEP and precipitation variability can be demonstrated as these ecosystems are dependent on sufficient amounts of rainfall. The correlation between NEP and precipitation becomes negative when NPP responds inversely to precipitation (China, Northern Siberia, South America). This might be an effect of an oversupply of rainfall in monsoon regions (China) or water logging in regions with permafrost (Siberia), where a reduction of precipitation may lead to an enhanced plant growth. However, this relation does not necessarily imply a causal interrelationship.

The contribution of interannual variability of carbon fluxes and the impact of climate variability to the total land-atmosphere carbon flux also differs temporally. The following graphs (Fig. 16 to Fig. 19) compare time series of carbon flux anomalies to temperature and precipitation for the four selected latitudinal zones. Negative values of NEP indicate a relative source flux from the vegetation to the atmosphere, whereas positive values account for a terrestrial uptake anomaly.

Boreal and northern temperate zone:

For all northern latitudinal zones, Rh is strongly related to changes in temperature and precipitation, with the relation between soil respiration and temperature being more pronounced (with r = 0.69 for the temperate and r = 0.52 for the boreal zone). The short-term variability in rainfall and temperature shows a positive relation (in contrast to the tropics), because precipitation is mostly a result of condensation as a response to dynamic baroclinic instability dependent on relative humidity that increases with rising temperatures (Zeng et al. 2000). Therefore, rising temperature is often followed by enhanced rainfall raising the water content of the soils, which indicates that soil respiration is strengthened by both higher temperatures and higher soil moisture status. Peylin et al. (2005) compared model results of the LPJ and the SLAVE model concerning differences in modelling carbon flux variability. The study found that the simulated Rh response to climate variability varies significantly with the formulation used to model soil respiration. The LPJ model applies a modified Arrhenius formulation (Lloyd & Taylor 1994) that responds very sensitive to temperature changes. In contrast, the “Q10”

modelling approach used by the SLAVE model shows almost no relation between Rh and temperature. However, Peylin et al. (2005) considered the results of LPJ to be more reliable as they are closer to the inversion results of Rayner et al. (1999). LPJ model results are also supported by a study of Woodwell et al. (1998) who found that soil respiration generally is more sensitive to temperature changes than are photosynthesis rates.

All northern ecosystems show a moderately positive correlation between NPP levels and changes in temperature.

For the boreal zone, NEP variability shows no direct relation either with levels of NPP or with Rh (fig. 5.16). The curves indicate that temperature and precipitation together form the shape of NPP variability. This implies that in the boreal zone, vegetation growth is more determined by climate variations, i.e. by soil moisture status and temperature thresholds than in the temperate regions. The reason might be that species are closer to the limits of their ecological amplitude than in warmer regions.

In contrast, in the temperate regions climate conditions are basically more favourable for plant growth and not the main limiting factor. Therefore, changes in soil conditions become more important. For the northern temperate regions Rh variability appears to be more closely related to temperature and precipitation compared to NPP levels. Generally, anomalies in the temperate zone are less pronounced than in the boreal zone. The study of Goulden et al (1996) at a temperate deciduous forest demonstrates that mean annual variations in temperature and precipitation do not cause carbon flux variability. Moreover, the authors stated that short-term weather anomalies, such as dry or cool springs or long-lasting snow cover that appear simultaneously with sensitive periods of forest growth are responsible for terrestrial carbon flux variability. The NEP variations of the northern temperate regions are mostly determined by low NPP variability during the 1980s when Rh is relatively stable. During the 1990s increased fluctuations of soil respiration can be observed that are reflected in the increased variability of NEP (fig. 5.17). This leads to the conclusion that changes in soil respiration determine NEP variability in the temperate zone.

Over the 20 years of investigation the anomalies of both NPP and soil respiration show an increasing trend of 4.08% and 3.96% per year, respectively. Temperature shows also an increasing trend while precipitation remains nearly stable. Increasing temperature leads to a elongated growing season. Additionally, rising atmospheric CO_2 concentration causes enhanced plant growth as the plant water use efficiency increases which is expressed by an increase in NPP. This process is even enhanced under warmer conditions (Kirschbaum 1994). Soil respiration is stimulated by higher temperatures and an additional litter input into the soils caused by the enhanced vegetation productivity. The net effect of these increasing trends is almost zero as they more or less cancel out each other, therefore the net flux remains stable.

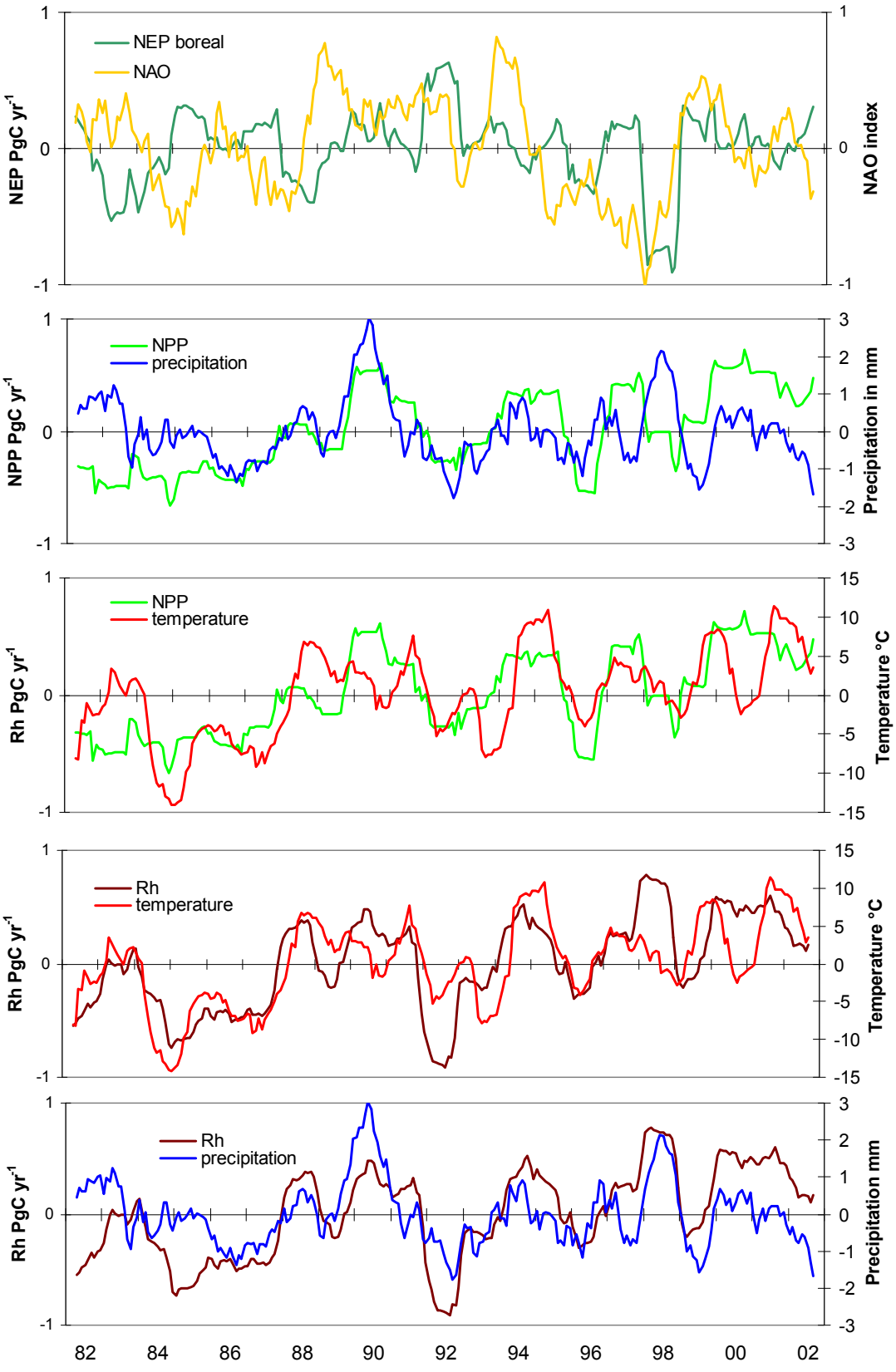

Fig. 5.16. Interannual variability of modelled boreal carbon flux compared to climatic parameter anomalies (positive values of NEP indicate enhanced uptake or reduced release)

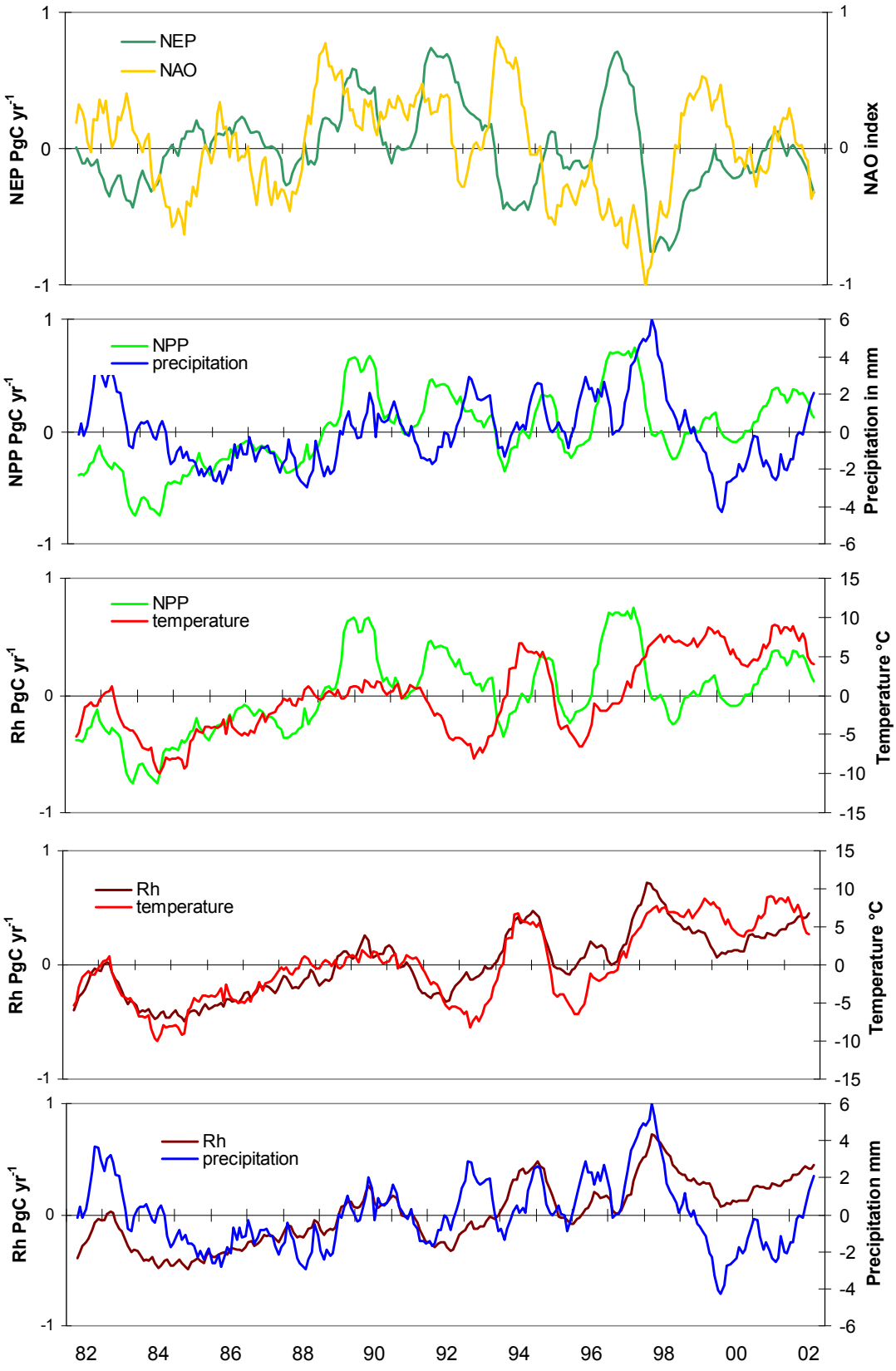

Fig. 5.17. Interannual variability of modelled northern temperate carbon flux compared to climatic parameter anomalies.

The study of Schaphoff et al. (2006), analyzing future carbon pool development under changing climatic conditions until 2100 derived by several GCMs, reported that this balance will change to a carbon source due to increased respiratory processes of the soil carbon storage. This shows, that the still existing balance is vulnerable to further warming and additional increase of atmospheric CO_2 concentration.

Tropics: Fig. 5.18 shows that the global land atmosphere flux variability is dominated by contributions from the tropics. In the tropics, NEP variability is mainly determined by NPP variability. NPP correlates moderately with precipitation (r = 0.43). But regarding fig. 5.18 the time series of NPP and precipitation coincide with a time-lag of several months, which can be confirmed by studies of Potter et al. (1999), Prince & Xue (2001), and Foley et al. (2002). This effect is caused by the delayed response of soil moisture content to precipitation amounts which determines the photosynthesis rate of plants. NPP and temperature are negatively correlated, determined by the soil moisture content which declines with increasing temperature. This temperature stress effect is likely to be balanced by the CO_2 fertilization effect (Cao & Woodward 1998a, Tian et al. 1998).

The NPP of tropical and subtropical arid regions show also distinct positive response to enhanced precipitation (Fig. 5.15.A) due to several reasons: vegetation growth is enhanced following wetter conditions as rising atmospheric CO_2 content improves the water use efficiency of plants. This process also advances the conditions for new plant establishment.

The time series of Rh correlates well with both precipitation (r = 0.58) and temperature (r = 0.43). It is determined by two processes: increasing temperature leads to dieback of vegetation and thus, initially to an increase in litter fall. Higher amounts of decomposing plant material along with increasing temperatures and soil moisture content can lead to intensified soil respiration. Low soil moisture content and droughts followed by subsequent fire events can additionally cause a net carbon flux from the terrestrial biosphere to the atmosphere. Thus, NEP anomalies consequently correlate negatively to temperature. Moreover, NEP variability is determined by a combination of several effects: A positive MEI (La Niña) followed by increased amounts of precipitation can lead to enhanced NPP and a net sink, responding with the same time delay as NPP, even though it can be counterbalanced when soil respiration activity is decreasing. Rh is determined by both, temperature and precipitation. Both can adversely affect soil respiration through changes in litter fall and soil moisture status. During La Niña litter fall is small but soil moisture status is higher restricting soil respiration when the organic material is used up. During El Niño, litter fall is strengthened but soil moisture status is small leading to reduced soil respiration which balances the reduced NPP. Additionally, the occurrence of fires can intensify the land-atmosphere carbon flux.

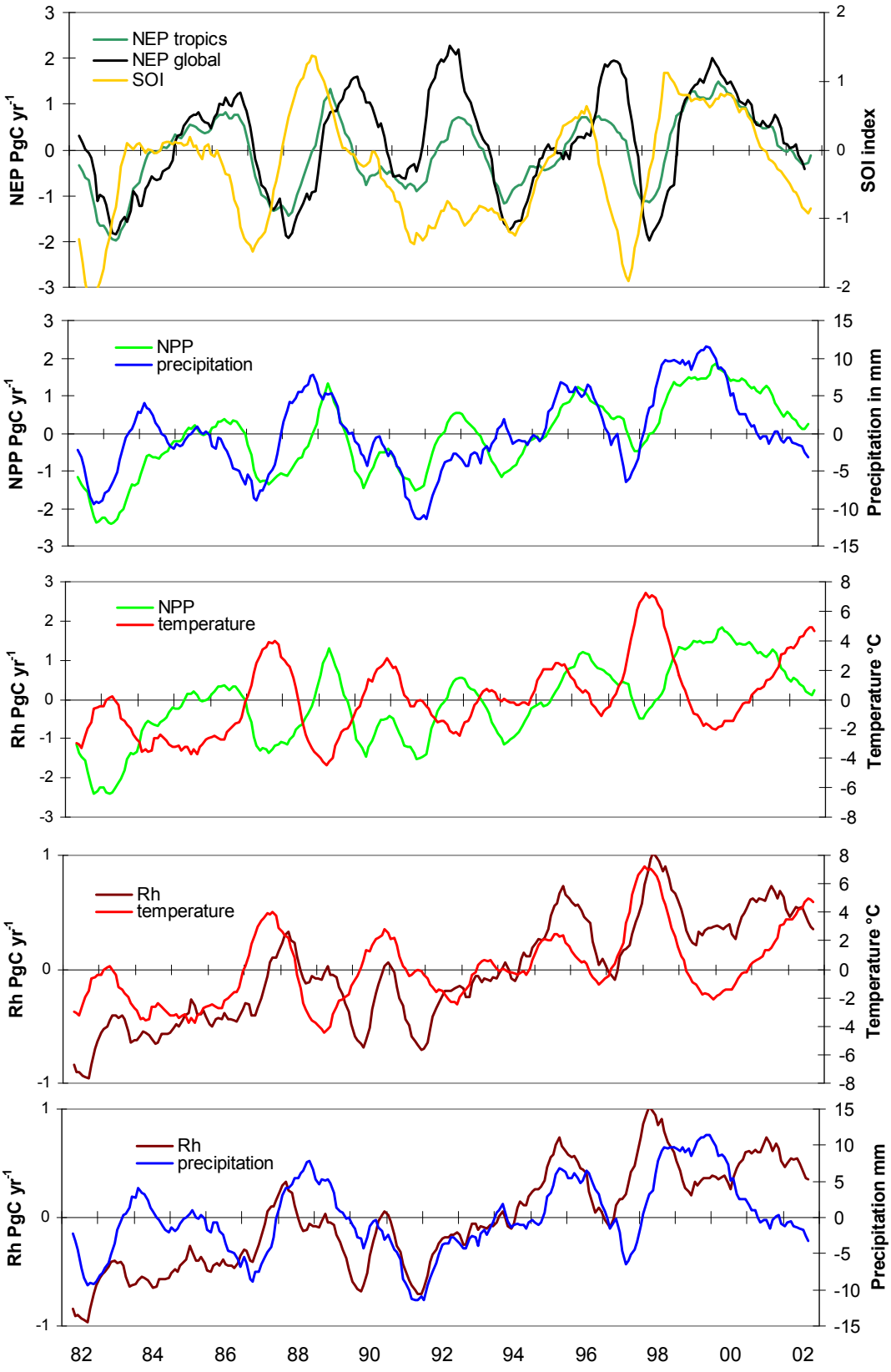

Fig. 5.18. Interannual variability of modelled tropical carbon flux compared to climatic parameter anomalies.

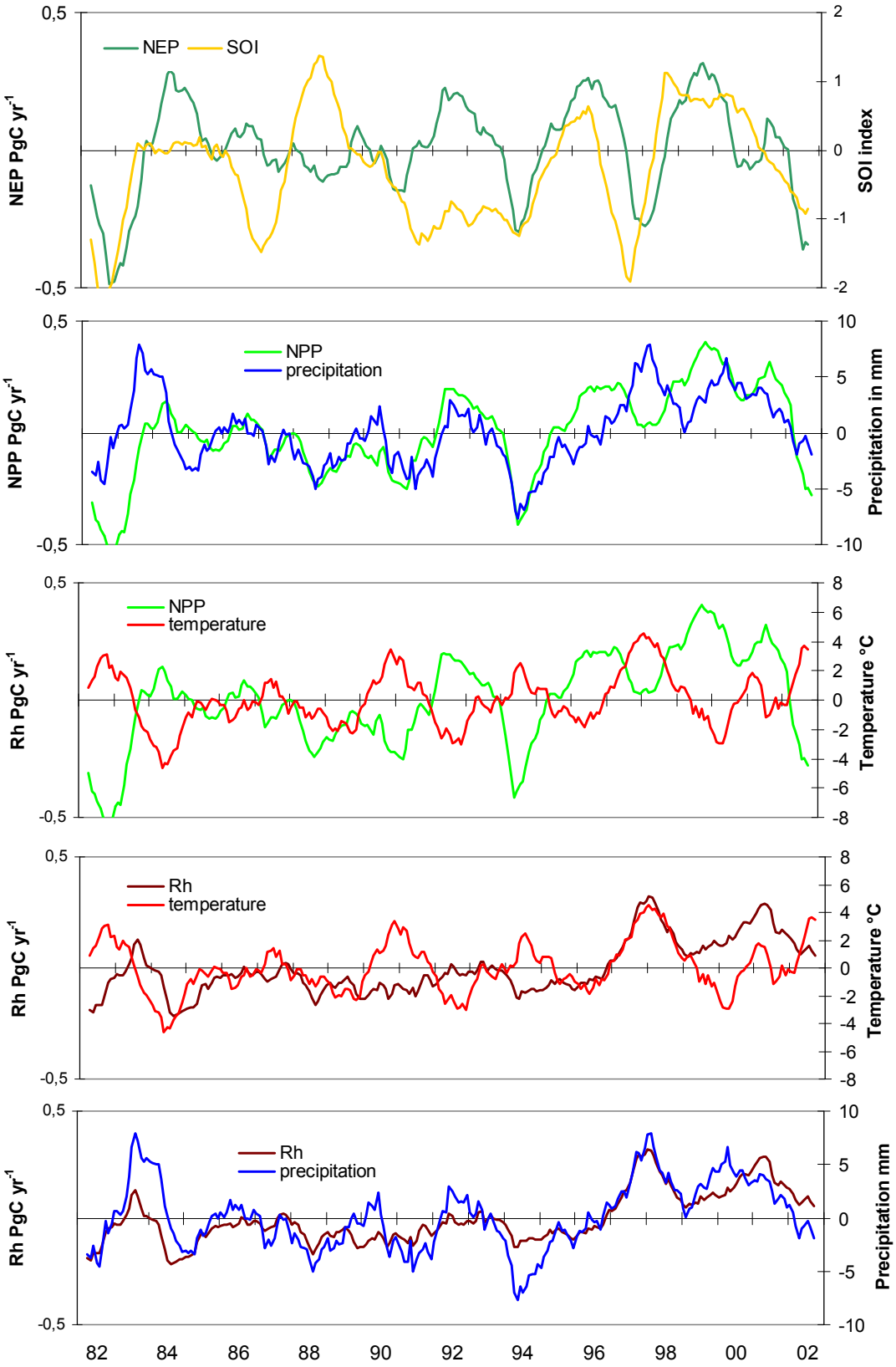

Fig. 5.19. Interannual variability of modelled southern temperate carbon flux compared to climatic parameter anomalies.

The tropical zone encounters a positive trend for the anomalies of all climatic parameters and carbon fluxes including net carbon uptake (+5% per year) over the period 1982 to 2002. The enhanced sink is a consequence of increased precipitation together with rising atmospheric CO_2 content which balances the warmer temperatures as well as the increased soil respiration. However, the enhanced terrestrial uptake is more than offset by the high emissions caused by deforestation and land-use change (see chapter 4.8).

Southern temperate regions: Similar as observed for the northern temperate region, NEP variability is dominated by NPP fluctuations while soil respiration does not show significant variations over time (fig. 5.19). However, it appears that when Rh considerably varies for specific time periods, those variations are also reflected in NEP levels, leading to the conclusion that soil respiration determines the magnitude and timing of the NEP fluctuations. NPP and in particular Rh correlate well to precipitation variability (NPP: $r^2 = 0.43$; Rh: $r^2 = 0.79$). A comparison of time series for NPP and temperature clearly shows less relation (Fig. 5.19). Increasing temperatures can cause a reduction in soil water availability and enhance evapotranspiration. Along with reduced rainfall, NPP and soil respiration activity will further decline in this region. This might imply that the effect of lower soil moisture on NEP variability due to increasing temperature is more pronounced than the reduction of precipitation.

In summary, the visual comparison of carbon fluxes and time series for temperature and precipitation (Figs. 14 to 19) demonstrate a trend for NPP of the northern regions to be more temperature limited while plant production of tropical and southern temperate regions depends more on sufficient humidity, similar to the results of Churkina & Running (1998) and Cao et al. (2002). Soil respiration is affected by both, temperature and precipitation and influences the magnitude and timing of NEP variability. Globally, increasing temperature together with rising atmospheric CO_2 content determine the trend of increasing NPP, which is still balanced by the stimulated soil respiration during the investigated time period.

5.2.3 Response of regional carbon fluxes on large scale anomalous climatic events (NAO and ENSO)

As already shortly noticed above, global climatic anomalous events such as ENSO and NAO have a distinct influence on global carbon flux variability with strong regional influences, as they occur more pronounced in specific regions.

The monthly North Atlantic Oscillation (NAO) index is based on the difference of normalized sea level pressures between Ponta Delgada, Azores (38°N, 26°W) and Stykkisholmur/ Reykjavik, Iceland (66°N, 18°W). Data are available since 1865 (Hurrell 1995, Jones et al. 1997, Rogers 1997, Rogers 2005). The NAO index is a descriptor of the strength of the North

Atlantic westerlies, which influence winter temperatures in Western Europe (Stephenson 1999). A high NAO index is associated with stronger westerlies over the North Atlantic indicating mild and wet maritime winters over Europe. Strong, cold European winters are mainly the effect of weak westerlies and have a low NAO index (Hurrel & Van Loon 1997, Visbeck et al. 2001, Stenseth et al. 2002). The interaction between ENSO and NAO is relatively weak (Alexander & Scott 2002). A correlation analysis applied for NAO index and carbon fluxes for different latitudinal zones shows no correlation, indicating no influence of NAO on carbon fluxes on latitudinal scales (table 5.4). As the NAO predominantly influences the climate of regions between eastern North America and Europe and central Siberia (Visbeck et al. 2001), which is only a part of the boreal and northern temperate zone, the influence might be stronger if regarding smaller regions. Hence, climatic effects of regions that are affected by the NAO and regions that are not affected might statistically cancel out each other on a latitudinal scale. For example, mild winters in Europe and Asia might be observed at the same time when severe winters are reported for eastern Canada and the northwest Atlantic (Hurrell 1995). Furthermore, the NAO is typically occurring during the winter months (December to March). Anyhow, monthly correlations for the northern hemisphere winter period (Dec. to Apr.) indicate no correlation between NAO index and carbon fluxes of the northern temperate and boreal zones.

Latitudinal zone	**Carbon fluxes (and climate)**	**MEI**	**NAO**	**NAO (Dec to Apr)**
Boreal	NEP	-0.11	0.04	-0.02
	NPP	-0.02	-0.05	0.04
	Rh	0.11	-0.10	0.03
Northern temperate	NEP	-0.17	-0.003	0.08
	NPP	-0.14	-0.01	0.11
	Rh	0.03	-0.02	0.08
Tropics	NEP	0.39	0.04	-
	NPP	0.50	0.02	-
	Rh	0.35	-0.03	-
Southern temperate	NEP	0.20	0.002	-
	NPP	0.26	0.02	-
	Rh	0.12	0.03	-

Table. 5.4. Correlations between time series of carbon fluxes and large scale anomalous climatic events for four latitudinal zones

The Multivariate ENSO Index (MEI) is calculated as the monthly anomaly of the mean sea level pressure difference between Tahiti and Darwin (Trenberth 1984, Ropelewski & Jones

1987, Bureau of Meteorology of the Australian Government 2005). Negative values of the MEI often indicate El Niño events with a sustained warming of the central and eastern Pacific, a decrease in the pacific trade winds, followed by strengthened rainfall in the coastal southwest American desert and droughts in eastern and northern Australia, the south-east Asian tropics as well as in the Amazon region and southwest Africa. Positive MEI values are associated with La Niña events, characterized by strong Pacific trades, cooler sea surface temperatures in the eastern and central Pacific, followed by wetter conditions in north-western Australia, south-eastern tropics, and the Amazon (Bradley et al. 1987, Ropelewski & Halpert 1987, Kiladis & Diaz 1989, Diaz & Markgraf 1992, Halpert & Ropelewski 1992, Hoerling et al. 1997, Morin & Ward 1998, Diaz et al. 2001, Sun 2003). Consequently, El Niño events can be associated with lower NPP levels for these regions of the tropics, accompanied by droughts and fire events, leading to a net carbon flux from the biosphere to the atmosphere. During La Niña events increased levels of NPP and a net terrestrial carbon sink can be observed in the tropics due to increased precipitation amounts in the Amazon region and the south-east Asian tropics (Rayner et al. 1999, Asner et al. 2000, Behrenfeld et al. 2001, Potter et al. 2001, Botta et al. 2002, Foley et al. 2002). The correlation analysis shows a distinct latitudinal response of carbon fluxes on MEI for the tropics. With values of $r \geq 0.3994$ (for $p = 0.05$) being statistical significant, NPP shows a relatively strong positive correlation to MEI in the tropics, indicating an enhanced vegetation growth during La Niña events (positive MEI) and reduced growth during the El Niño phase.

Nemani et al. (2003) found that NPP responded with regional differentiation to climatic effects such as ENSO with corresponding increases in the global CO_2 growth rate. For selected latitudinal zones NPP levels were investigated in response to ENSO events and the Mt. Pinatubo eruption in 1991 (Fig. 5.20.A). Overall, it appears that NPP increased over the last twenty years with highest increase of 7.4 % observed for the tropics (22.5°S – 22.5°N). Tropical NPP seems to be dominated by El Niño events.

A comparison to the present results (fig. 5.20.B) shows that LPJ-simulated NPP results are similar in shape and magnitude, producing somewhat larger magnitudes in the boreal, temperate and southern temperate zones. While LPJ-simulated NPP trends for the boreal, northern and southern temperate zones compare closely to the results of Nemani et al. (2003), trend estimates for the tropics are significantly different. Tropical NPP simulated by LPJ shows the highest increase, contributing 63.5% to the global NPP increase between 1982 and 2000. Nemani et al. (2003) estimated only an NPP increase of 42%. They suggest a decline in cloud cover causing increased incoming solar radiation and modified precipitation patterns to be the main reason for this increase. The reason for this difference might be that Nemani et al. (2003) did not account for rising CO_2 contents enhancing plant productivity.

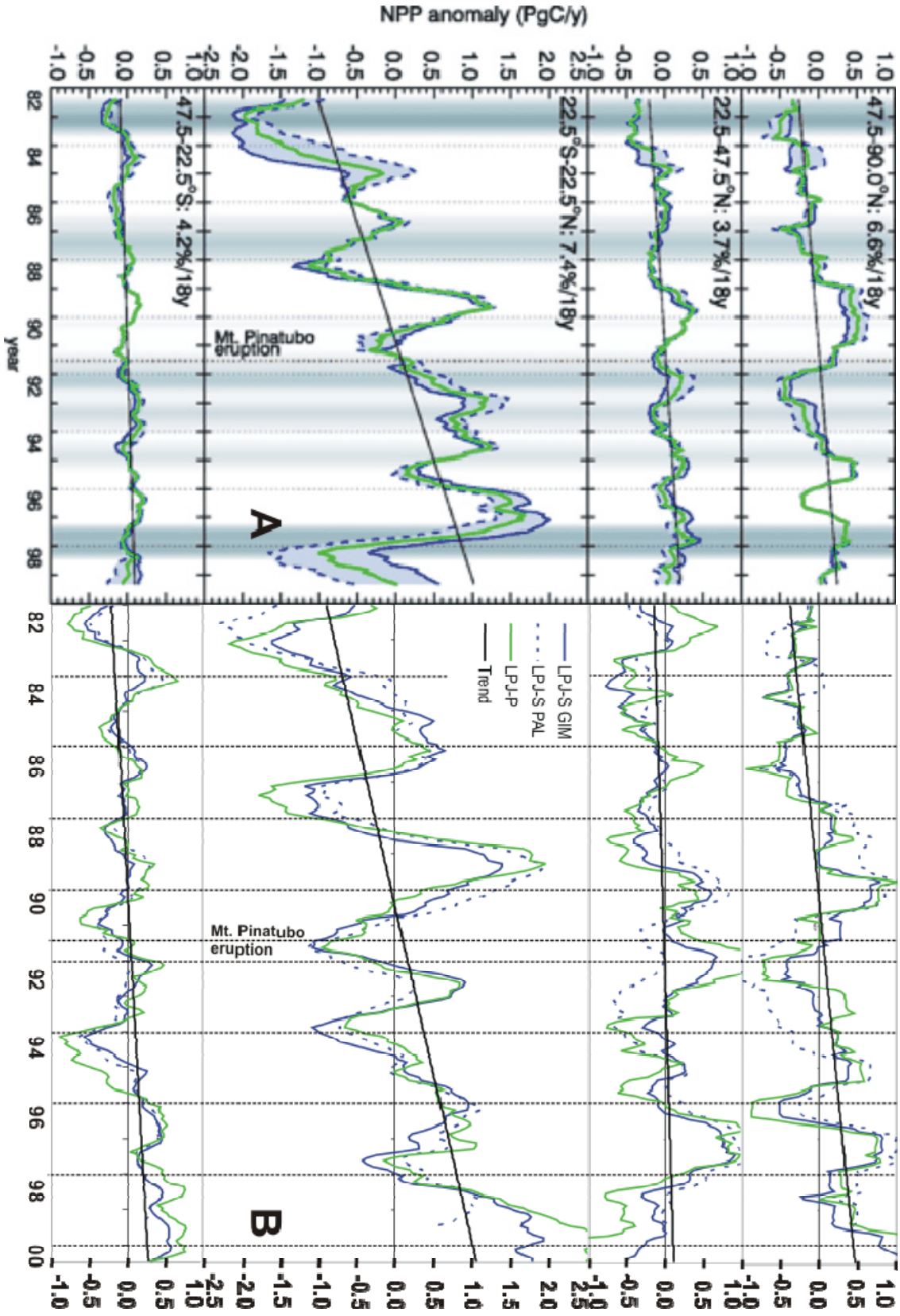

Fig. 5.20. A) Interannual variability in NPP distributed by latitudinal zones from Nemani et al. (2003). Zonal NPP anomalies in each zone are shown for GIMMS (solid blue line), PAL (dashed blue line), and their average (green line). B) Interannual zonal NPP anomalies modelled by LPJ.

Moreover, in their model evapotranspiration and water supply for plants is only controlled by water vapour pressure deficit instead of additionally modelling soil moisture explicitly. This may cause an underestimation of the long-term control of soil moisture leading to modelled drier conditions and an underestimation of NPP.

The tropics display the largest interannual variability of terrestrial CO_2 fluxes (Kindermann et al. 1996, Rayner et al. 2005), and especially the variability of the Amazon region is mainly determined by ENSO (Potter et al. 1999, Rayner et al. 1999, Asner et al. 2000, Prince & Xue 2001, Botta et al. 2002, Cao et al. 2002, Foley et al. 2002, Rödenbeck et al. 2003). MEI anomalies are significantly linked with temperature, wind speed and precipitation anomalies followed by CO_2 flux anomalies (Thompson et al. 1986, Elliot et al. 1991). Following reduced amounts of rainfall due to a shift in convection cells over the Pacific ocean and warmer temperatures, usually a decline in photosynthesis rates and in NPP can be observed during El Niño events. Consequently, respiration rates will be enhanced, contributing to an increase in biomass burning. A close relation between increase in carbon uptake, higher precipitation rates and the MEI index during La Niña periods has been already reported in Fig. 5.18. A time lag between changes in carbon uptake following fluctuations of the MEI and of precipitation of about seven and five months, respectively, can be observed. However, when temperature increases, net terrestrial carbon fluxes declines nearly simultaneously to a source. Estimates of Potter et al. (1999) and Prince & Xue (2001) confirm these findings. Both studies reported a large net source flux from terrestrial vegetation with a time lag of about six months to 1 year following the El Niño events of 1983 and 1987, predominantly caused by a strong decline in NPP during these periods. Foley et al. (2002) confirmed with the observed time lags. They reported a maximum correlation between MEI and simulated NEP with a time lag of 3 months (followed by time lags in precipitation and temperature of the same magnitude). Several modelling studies concerning the Amazon basin (Kindermann et al. 1996, Tian et al. 1998, Prentice & Lloyd 1998, Asner et al. 2000, Potter et al. 2001, Foley et al. 2002) agree on the observation, that the changes in carbon fluxes are determined by changes in precipitation during ENSO events. Botta et al. (2002) reported a time-lag of about 2 years between changes in NPP and soil respiration, due to the longer residence time of carbon in vegetation and soil. This is not reproduced by LPJ, only the relationship between Rh and wetter and warmer conditions is observable.

Time series of anomalies of all carbon fluxes (NEP, NPP, Rh and carbon released by fire) show distinctive patterns for each of the selected latitudinal zones (Fig. 5.21). Positive values of NEP indicate that ecosystem productivity act as a net sink. This may happen due to several mechanisms which may influence NEP alone or in combination with other factors: (1) NPP is significantly high due to favourable conditions for plant productivity which can be either optimal temperatures and/or precipitation depending on the latitudinal zone, (2) Soil respiration

is reduced due to low temperatures or precipitation amounts, and/or (3) a reduction in fire occurrence and/or severity. On the other hand negative NEP anomalies indicate less ecosystem productivity as a result of (1) reduced NPP, (2) enhanced soil respiration, and/or (3) enhanced fire activity. Additionally, a change in temperature and/or incoming solar radiation due to major volcanic eruptions and a change in atmospheric aerosol concentrations may also affect plant productivity (Lucht et al. 2002, Gu et al. 2003).

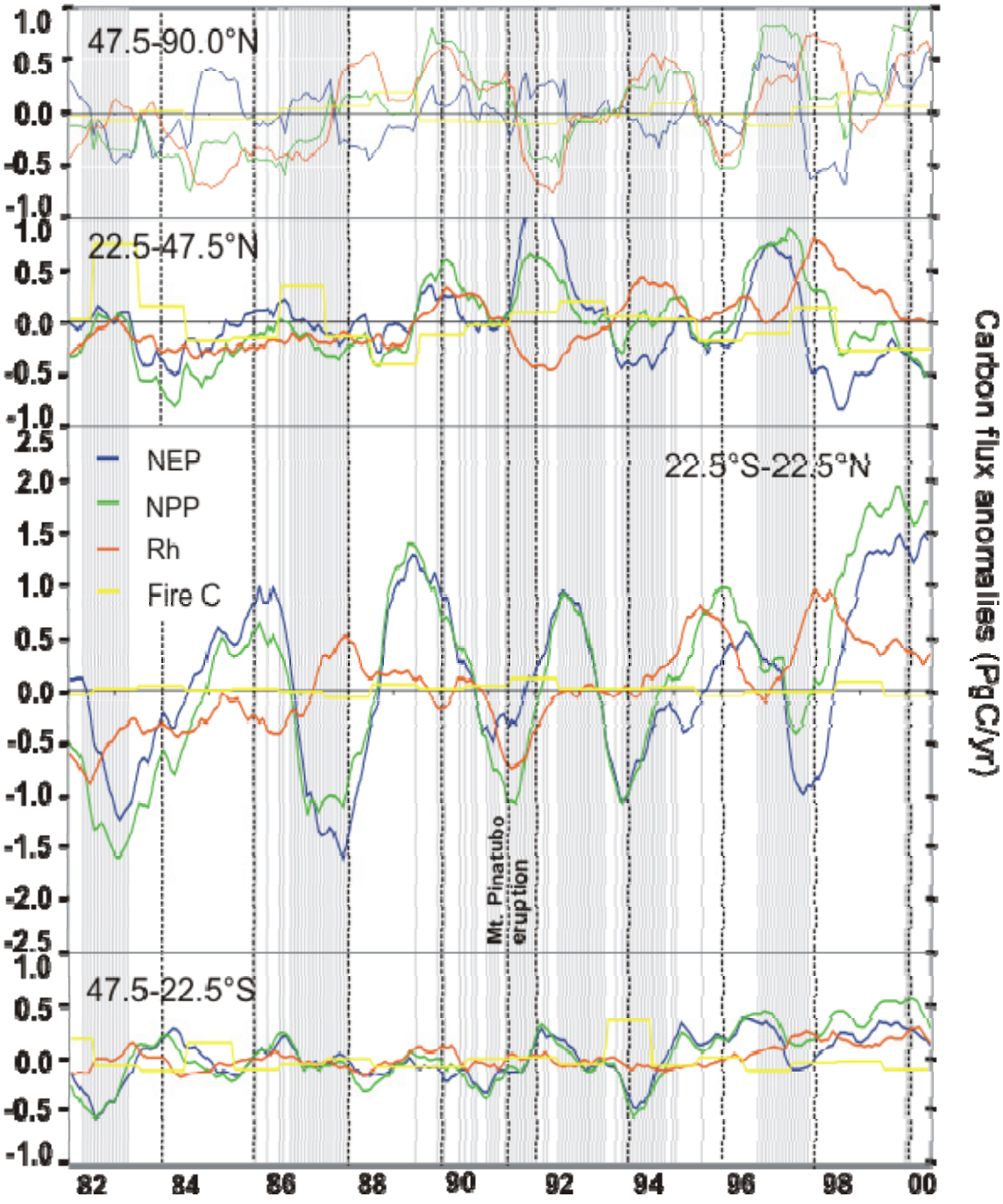

Fig. 5.21. Interannual variability of carbon fluxes (NEP, NPP, Rh, fire carbon) distributed by latitudinal zones as derived from LPJ-S_{GIM}. Negative MEI indicating El Niño events is shown in grey. Positive NEP denotes terrestrial sinks.

For the time period of 1982 to 2000, NEP anomalies of the boreal zone, and to a lesser extent of the northern temperate zone, are considerably determined by peaks in soil respiration (Fig. 5.21). In the tropics and southern latitudes, the influence of soil respiration on NEP variability is relatively low, mainly due to its low interannual variability. Tropical Rh is moderately related to changes of the MEI and precipitation. For the southern temperate region, NEP shows a small to moderately positive correlation to MEI, indicating a net carbon flux to the atmosphere during El Niño years (carbon source: negative NEP anomalies and negative MEI values) and net carbon sink during La Niña periods (positive NEP anomalies and positive MEI values). A comparison of the MEI and carbon fluxes for the regions north of 22.5°N shows almost no influence of ENSO, suggesting that ENSO particularly affects the tropics and southern hemisphere, whereas tele-connections to the northern hemisphere are not prominent within the carbon cycle. Shortly after the El Niño events of 1982/83, 1986/87, and 1997/98 a significant decrease in tropical NPP and NEP can be observed, accompanied by an increase in Rh producing a net source flux of CO_2 to the atmosphere. Especially these events are associated with a strong temperature rise and precipitation decline in the tropics enhancing evapotranspiration (Fig. 5.18). The negative carbon flux anomaly of the 1987-88 El Niño event is visible in the tropics but not in the extratropics, whereas in 1997/98 also a response of the carbon fluxes of the northern mid- and high-latitudes can be seen. This response is related to a positive anomaly in precipitation. Consequently, soil respiration increased exceeding NPP levels in the extratropics, leading to a negative NEP flux anomaly. For the tropics, NPP is even stronger reduced. Generally, tropical NEP shows a reduction of about 0.6 PgC yr^{-1} during El Niño events.

The extraordinary long, but weak El Niño event lasting from 1991 to 1994 shows a somewhat different pattern. While during this event global NEP and NPP were increasing, Rh strongly decreased at the same time. Since at that time the Mt. Pinatubo eruption occurred, it probably had overlaying or strengthening effects due to a general cooling of the troposphere. Following the atmospheric cooling, soil respiration decreased while global NPP was enhanced likely due to an increase in diffuse radiation income. (Hansen et al. 1996, Roderick et al. 2001, Cao et al. 2002, Gu et al. 2003). However, the effects of the Mt. Pinatubo eruption on the radiative regime, on temperature and on carbon fluxes are still part of the scientific debate. Several authors state a general increase of NPP for the boreal zone during the nineties (Myneni et al. 1997, Myneni et al. 2001, Zhou et al. 2001), although NPP declined during 1991 and 1992 after the Pinatubo eruption. Lucht et al. (2002) attribute this decline of NPP to cooler temperatures and a shortage of the growing season. Fig. 5.21 clearly shows that NEP did not decrease as strongly as NPP did. This can be attributed to a lower than usual soil respiration due to the atmospheric cooling, leading to a weak net carbon sink in the boreal zone (see also chapter 6.2).

The northern temperate zone shows two opposite effects after the Pinatubo eruption: While Rh decreased to a minimum, NPP peaks at the same time, producing a considerable net carbon sink for this region. An explanation for increased NPP is proposed by Roderick et al. (2001) who suggested that enhanced photosynthesis rates are responsible due to an increase in diffuse radiation by dispersion of aerosol material from the Pinatubo eruption. Gu et al. (2003) found enhanced noontime rates of photosynthesis by 23% in 1992 and 8% in 1993 a deciduous forest due to an increase in diffuse radiation. Angert et al. (2005) demonstrated in a modelling experiment, that warmer temperatures together with precipitation changes also reproduced the enhanced carbon uptake. Furthermore, although a strengthened diffuse radiation cannot be modelled by LPJ, it nonetheless simulates an enhanced NPP. Therefore, the increase in NPP must have other causes. The enhanced plant productivity might be a result of a slightly reduced air temperature while amounts of precipitation do not change. These conditions lead to a reduction in evapotranspiration while enhancing plant production efficiency at the same time. Nemani et al. (2003) observed this process for tropical regions following the Mt. Pinatubo eruption.

Overall, climate variability and interannual variations of carbon fluxes are low during the 1980s, whereas during the 1990s the interannual variability of both climate and carbon fluxes is strengthened, simultaneously to the occurrence of the Mt. Pinatubo eruption which influences global temperature and radiation regimes.

Globally, the interannual variability of net carbon fluxes is mainly determined by the tropical land ecosystems in the 1980s, whereas during the 1990s the northern temperate and boreal regions additionally contributed to the global fluctuations. This is predominantly attributed to the enhanced uptake of the northern hemisphere due to the climatic and radiative changes after the Mt. Pinatubo eruption (Peylin et al. 2005, Bousquet et al. 2000). Analyses of this study suggest that the main contributor to interannual changes in carbon fluxes is climate fluctuations, i.e. precipitation, for which an increased variability has been observed during the 1990s.

Concluding, the current results could be mostly confirmed by independent studies. A key advance here is that the current LPJ-S version is able to model biogeochemical processes under consideration of satellite observations providing estimates of all important carbon fluxes including ecosystem disturbances in high spatial and temporal resolution. Moreover, also the rising atmospheric CO_2 content and therefore its fertilization effect is considered.

As the tropics showed strongest growth stimulation, they could be identified as main contributor for potential uptake of atmospheric CO_2 as well as they determine the fluctuations of the global CO_2 growth rate, underlining the importance of maintaining the vulnerable tropical ecosystems. In contrast to the results of Nemani et al. (2003), who reported NPP to be the main driver of terrestrial sink dynamics, the current results identify soil respiration as a key

parameter determining interannual fluctuations of carbon uptake and release. Also the dynamics of temporal lags between changes in environmental conditions and carbon fluxes could not be modelled by the approach of Nemani et al. (2003). These results show that the accounting of all carbon cycle components in high temporary and spatial resolution is crucial to understand the biogeochemical carbon dynamics including the limiting factors. This is needed to upgrade our ability to predict future developments of the carbon cycle under changing climatic conditions.

6. SINGULAR EVENTS AND THEIR IMPACT ON THE TERRESTRIAL CARBON CYCLE

6.1 Climatic Events

6.1.1 The El Niño event in 1997/1998

The following chapter investigates some singular events to gain a better understanding on global tele-connections between climatic events such as ENSO or volcanic eruptions and the global carbon cycle. Since observations of NEP, NPP and Rh are sparse in space and time, it is essential to use a predictive model for any further analysis on the regional distribution of carbon fluxes and feedbacks between the biosphere and the atmosphere. Different regions vary distinctively in their response to climate variations. Therefore, the following section investigates one of the strongest El Niño/La Niña events of the 20th century that was observed between 1997 and 1999 (Parker et al. 1998, Davey & Anderson 1999). For the analysis global maps of temperature and precipitation anomalies were compared to resulting global anomalies of NEP to localize the distribution of net carbon sources and sinks. The anomalies for the El Niño year of 1998 cover the time period between 06/1997 and 05/1998, based on the average of the entirely simulated period of 1982 to 2000. Fig. 6.1.A shows warmer temperatures throughout the tropics with maximum temperatures observed for tropical South America. Also the higher latitudes seem to be affected by the El Niño event showing higher than normal values for North America (up to 2°C), but significantly reduced temperatures for Siberia. Precipitation (Fig. 6.1.B) is significantly reduced in the tropical zone, particularly in the Amazon basin and tropical South-east Asia due to a shift of tropical convection cells over the warmer Pacific Ocean (Philander 1990). The North-American West-coast, the South-eastern regions of Brazil and Argentina, as well as the African East-coast and China receive higher amounts of precipitation according to the observed patterns of earlier El Niño events (Wang & Li 1990, Eltahir & Wang 1999, Lau & Weng, 2001, Foley et al. 2002). For South-East Africa, North-Eastern Brazil and Australia precipitation decreased. Carbon flux anomalies are dominated by a significant terrestrial net flux to the atmosphere from tropical regions, particularly from the Amazon region and South-East Asia. These regions are characterized by intensive fire activities during this period following a severe drought (Nakagawa et al. 2000, Siegert et al. 2001, Page et al. 2002).

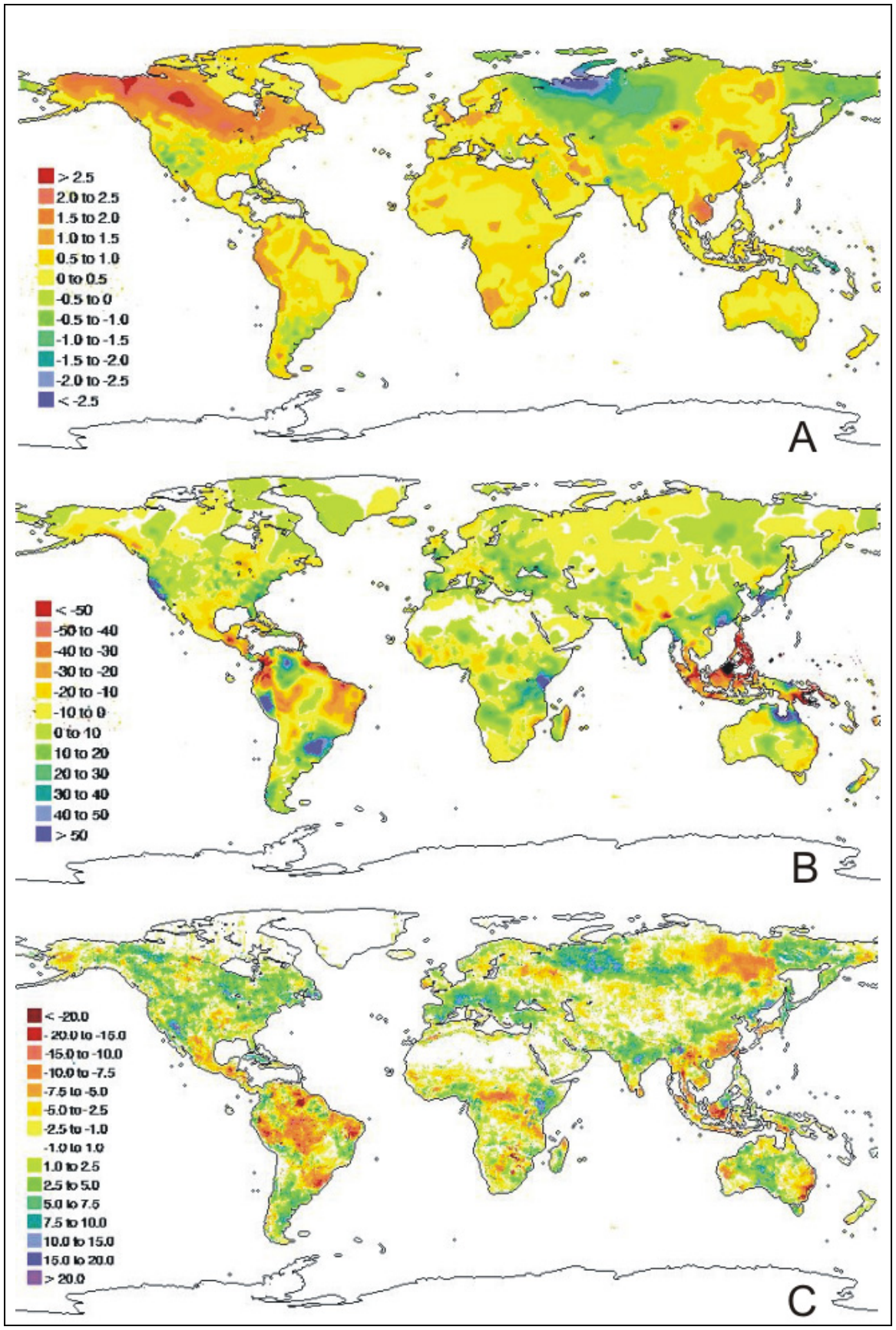

Fig. 6.1. Carbon flux and climate anomalies for the El Niño year of 1998. (A) temperature in °C, (B) precipitation in mm, (C) NEP in gC m-²

Fig. 6.2 shows that the intensive fires during the El Niño event of 1997 in South-East Asia are not simulated by LPJ. Peylin et al. (2005) attributed the inability of LPJ to capture these fire emissions to its lack of considering peat fires as well as easily occurring fires in forests which are disturbed by logging practices (Siegert et al. 2001, Page et al. 2002).

In general, El Niño events also affect precipitation patterns over India by suppressing the annual monsoon regime (Dai & Wigley 2000). However, for the El Niño event of 1997 this pattern is not significant. For this period, LPJ-estimated NPP and NEP in India are not as much reduced as expected for such a strong El Niño event (according to the findings of Cao et al. 2004). During this El Niño, though it was the strongest in the 20th century, some regions experienced wetter conditions than normal. Consequently, the NPP there was not as strongly reduced as during other El Niño events, particularly in North America, East Africa, Europe and India.

The tropics and the southern temperate zone show a moderate decrease of net carbon fluxes (-0.55 and -0.07 PgC yr^{-1}, respectively). While for the tropical region NPP slightly decreases (-0.33 PgC yr^{-1}), soil respiration increases at the same time (+ 0.22 PgC yr^{-1}), but also with little changes. The NEP reduction in the southern temperate regions is mainly caused by a clearly enhanced soil respiration (+ 0.2 PgC yr^{-1}), as a response to increased rainfall.

	Carbon fluxes and Climate parameters	**Tropical zone**	**Southern temperate zone**	**Northern temperate zone**	**Boreal zone**
Annual averages	NEP	0.23	0.05	0.22	0.20
(in PgC yr^{-1})	NPP	29.47	5.36	13.69	13.66
	Rh	26.69	4.79	11.02	11.23
	fireC	1.03	0.18	2.18	0.48
(in °C)	Temperature	25.83	16.97	12.77	-3.26
(in mm yr^{-1})	Precipitation	108.72	74.28	67.91	40.70
Anomalies	NEP	- 0.55	- 0.07	+ 0.66	+ 0.41
(in PgC yr^{-1})	NPP	- 0.33	+ 0.13	+ 0.93	+ 0.67
	Rh	+ 0.22	+ 0.20	+ 0.28	+ 0.26
	fireC	- 0.02	- 0.12	- 0.11	- 0.11
(in °C)	Temperature	+ 0.45	+ 4.83	+ 0.20	- 0.12
(in mm yr^{-1})	Precipitation	- 6.01	+ 7.32	+ 3.96	- 0.67
Anomalies	NEP	- 16.42	- 11.03	+ 32.59	+ 20.34
(in %)	NPP	- 1.11	+ 2.45	+ 7.31	+ 5.17
	Rh	+ 0.81	+ 4.34	+ 2.56	+ 2.38
	fireC	- 1.61	- 38.14	- 4.67	- 18.93
	Temperature	+ 1.79	+ 39.76	+ 1.66	- 3.63
	Precipitation	- 5.24	+ 10.93	+ 5.89	- 1.61

Table 6.1. Carbon fluxes, precipitation and temperature for the El Niño period of 06/97 to 05/98 (with an average MEI of -17.1), anomalies are calculated based on the period 1982 to 2000.

Comparing the climate variables for all ENSO periods with their 20-year average (which is not shown here), suggests little changes for tropical temperature patterns, while rainfall is reduced by 3.6 %, leading to a small decrease in NPP by 2.2% and for Rh by 0.2 %. But due to the small variation ranges of NEP, it shows a reduction of 20 % for all ENSO periods. In most of the temperate North-American regions cooler than normal conditions together with higher precipitation amounts lead to enhanced terrestrial carbon uptake (Fig. 6.1.C). For North America two different types of changes in NEP can be observed: The western and north-eastern region show considerably increased NPP that even exceeds the slightly enhanced soil respiration (not illustrated here) due to wetter and cooler conditions. Some smaller parts of the south-eastern and central region of North America show a strong increase in soil respiration while at the same time only a small to negligible positive NPP anomaly occurs due to wetter conditions without a drop in temperature. In contrast, temperatures warmer than normal together with increased amounts of precipitation are observed for Central Europe. For this region, the increase of NPP still exceeds the simultaneously occurring increase of soil respiration, leading to enhanced carbon uptake. These results are supported by findings of Roedenbeck et al. (2003a) based on atmospheric inversion modelling. An analysis of satellite observations by Buermann et al. (2003) also suggests warmer and greener conditions in North America, China and central Europe during the warm ENSO phase. The greening of these regions might be partly a result of a NAO related pattern, leading to higher precipitation over the Europe-Mediterranean-Central Asian region (Mariotti et al. 2002).

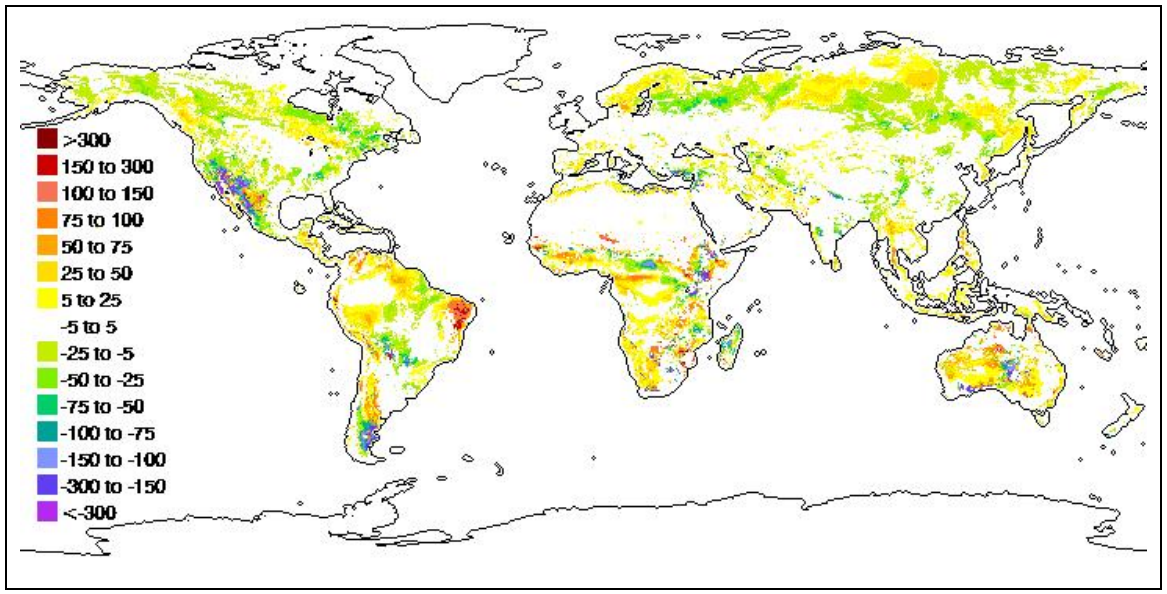

Fig. 6.2. LPJ-simulated carbon released by fires during the El Niño event of 1997/98 (in gC m^{-2})

Not yet fully explained is the strong negative temperature anomaly observed for Siberia that is associated with a positive NEP anomaly. The likely reason is a strongly reduced soil respiration due to lower temperatures. Table 6.1 suggests that for the entire boreal zone NEP significantly

increased, mainly due to an increase in NPP which exceeds an only weak increase in soil respiration rates while at the same time a considerable reduction in fire carbon can be observed (Fig. 6.2). The NPP increase might be explained by the enhanced plant growth due to warmer conditions and the CO_2 fertilization effect. In summary, for the tropical and southern temperate regions the terrestrial carbon release is significantly enhanced, whereas the northern hemisphere shows additional carbon uptake by the biosphere. Tropical NEP responds to a combination of factors, such as a reduction in rainfall and an increase in temperature. For the northern hemisphere the biospheric carbon uptake is due to significantly enhanced NPP as a response to temperatures warmer than average during the warm ENSO period.

6.1.2 The La Niña period in 1998/1999

NEP anomalies are compared to temperature and precipitation anomalies for the time period of the La Niña event of 10/1998 to 09/1999 (Fig. 6.3). Similar patterns to the El Niño event of 1997/98 are observed for temperature of the temperate and boreal region with temperatures warmer than average for North America and a cooling in Siberia. These results correspond to findings by Los et al. (2001), who reported that the land climate on the northern hemisphere can be positively influenced by ENSO events. However, often the ENSO effect is weakened or even cancelled out by climatic patterns associated with the NAO.

Temperature for the tropical zone decreased compared to the previous year, while precipitation rates significantly increased at the same time. In particular, the Amazon region and South-east Asia received more rainfall than other years. Tian et al. (1998) reported that the Amazon basin changes from a net CO_2 source during El Niño years to a net CO_2 sink during the La Niña period. A similar pattern can also be found throughout the whole tropical zone (Cao et al. 2002). An analysis of inverse modelling data results in similar findings for this La Niña period (Roedenbeck et al. 2003a). During this La Niña period, tropical NEP increased by 24 %, mainly determined by an increase in NPP that exceeds the slightly increased rates of soil respiration. Additionally, a reduction of carbon released by fires contributes to the enhanced tropical uptake. Throughout the tropics a surplus of 0.67 $PgCyr^{-1}$ is stored in vegetation (Tab. 6.2). The increase of NEP and NPP in the tropics is much more pronounced during La Niña than is the decrease during El Niño, which may be due to the fact that precipitation increased stronger during La Niña than it decreases during El Niño.

Temperatures warmer than the 20-year average along with slightly increased rates of rainfall favour the enhanced uptake in the southern temperate regions. A net carbon uptake can also be observed for Siberia, due to significantly reduced rates of soil respiration, particularly in the regions where temperature is decreasing.

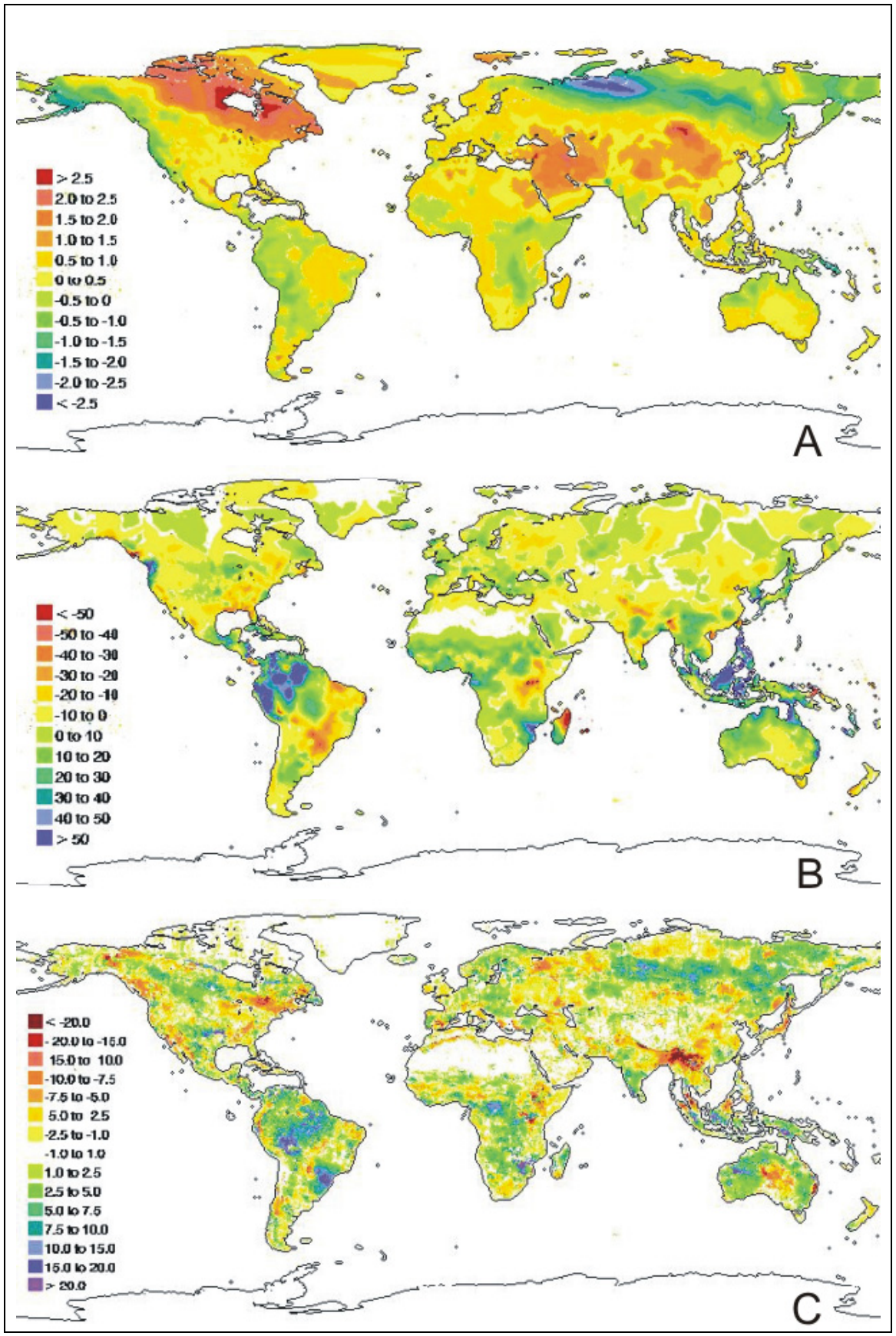

Fig. 6.3. Carbon flux and climate anomalies for the La Niña year of 1999. (A) temperature in °C, (B) precipitation in mm, (C) NEP in gC m-²

	Carbon fluxes	Tropics	Southern temperate	Northern temperate	Boreal
Annual averages	NEP	0.33	0.07	0.12	0.18
(in PgC yr^{-1})	NPP	30.99	5.59	12.62	13.00
	Rh	26.99	4.73	11.19	10.85
	fireC	1.12	0.27	2.02	0.79
(in °C)	Temperature	25.52	16.80	12.77	- 3.58
(in mm)	Precipitation	124.18	68.86	67.91	41.26
Total anomalies	NEP	+ 0.67	+ 0.23	- 0.59	+ 0.13
(in PgC yr^{-1})	NPP	+ 1.19	+ 0.36	- 0.14	+ 0.02
	Rh	+ 0.51	+ 0.13	+ 0.45	- 0.12
	fireC	- 0.23	- 0.02	- 0.27	+ 0.20
(in °C)	Temperature	+ 0.14	+ 4.66	- 0.61	- 0.19
(in mm)	Precipitation	+ 9.46	+ 1.90	+ 0.75	- 0.11
Anomalies	NEP	+ 24.11	+ 35.83	- 29.28	+ 6.63
(in %)	NPP	+ 4.90	+ 6.91	- 1.10	+ 0.14
	Rh	+ 2.73	+ 2.93	+ 4.19	- 1.07
	fireC	- 10.53	- 5.62	- 11.75	+ 32.87
	Temperature	+ 0.56	+ 38.42	- 5.05	- 5.74
	Precipitation	+ 8.24	+ 2.84	+ 1.11	- 0.26

Table 6.2. Carbon fluxes, precipitation and temperature for the La Niña period of 10/98 to 09/99, (with an average MEI of +8.1), anomalies are calculated based on the period 1982 to 2000

In detail, temperature has slightly decreased in the boreal zone, while rainfall is also reduced to some minor extent. The slight increase in NEP for the boreal forest (+ 0.13 PgC yr^{-1}) is the effect of an average NPP while soil respiration rates decline (-0.12 PgC yr^{-1}), even though fire occurred more frequently during this time period. Despite cooler temperatures NPP is constant likely due to the CO_2 fertilization effect. For the northern temperate regions terrestrial uptake decreased, caused by a strengthened soil respiration (+ 0.45 PgC yr^{-1}) and a slight reduction in NPP (- 0.14 PgC yr^{-1}). NPP is mainly reduced due to a slight cooling.

Globally, NEP has increased by about 0.4 PgC yr^{-1} during the La Niña period, which is mainly determined by influence of the tropical regions contributing 0.7 PgC yr^{-1} to the global fluxes and counterbalances the small net carbon source of the northern extratropics. Global NPP increased by 1.4 PgC yr^{-1} during the same time period, exceeding the smaller increase in soil respiration rates (0.9 PgC yr^{-1}).

6.1.3 The warmest years during the investigated period: 2000-2002

The temperature changes during the 20th century with a subsequent warming since the 1970s have been discussed by numerous studies (Hansen et al. 1996, Stott et al. 2000, IPCC 2001, Zeng et al. 2005). The years 2000 to 2005 are the warmest period on record in more than a century of climate measurements (Hansen et al 2001, NASA 2006). Global surface air warming is about 0.75°C in the past century (Hansen et al. 2001) as a consequence of the release of greenhouse gases by humans (IPCC 2001). Globally the warmest year of the 20th century occurred in 1998 (NASA 2004), provoked by a strong El Niño which raised global temperature by about 0.2°C above the long-term average. However, the years 2000 to 2003 need deeper investigation, since during that time period an ENSO-La Niña phase has been observed. During such an event, usually the surface temperature of the Pacific Ocean is cooler than normal, associated with globally lower surface temperatures (NASA 2001). Regionally, Hansen et al. (2001) describe greatest positive temperature anomalies for the boreal zone of North-America, for a band that stretches from Northern Africa over to Central Asia, as well as for the Antarctic peninsula (Palmer Land).

Figs. 6.4.A to D display the anomalies for temperature, precipitation, NPP, and NEP for the time period January 2000 to December 2002, with an average baseline of 1982 to 2002. Obviously, the NEP anomalies for this period are less pronounced than for the ENSO events mentioned before, due to the longer calculation basis of two years which likely smoothes out some peaks. As can be seen in fig. 6.4.A, Temperatures warmer than the long-term average occur predominantly for most of the northern hemisphere. In particular, the north-eastern Siberian region shows a strong temperature increase. In Siberia and temperate central Asia warmer temperatures are combined with wetter conditions, leading to an enhanced vegetation growth which is partially offset by an enhanced soil respiration. Additionally, the Indian and Western pacific oceans, as well as the North Atlantic Ocean were unusually warm during this period providing higher air-humidity and increased rainfall (Reynolds et al. 2002). For North America, warmer temperatures together with a decrease in precipitation are reflected in a decrease in NPP and NEP. For Australia, South-East Asia, Southern Africa and to a lesser extent South America observed lower temperatures can be regionally associated with an increase in precipitation (Fig. 6.3.B). In these regions NPP and net terrestrial uptake are enhanced, confirming the findings, that tropical and southern temperate NEP variability is predominantly determined by NPP and precipitation variations.

Evidently, temperature is significantly increased during the time period of 2000 to 2002, most pronounced in the higher latitudes and in the southern temperate regions. For the tropics, precipitation amounts moderately increased while southern mid-latitudes showed the largest increase.

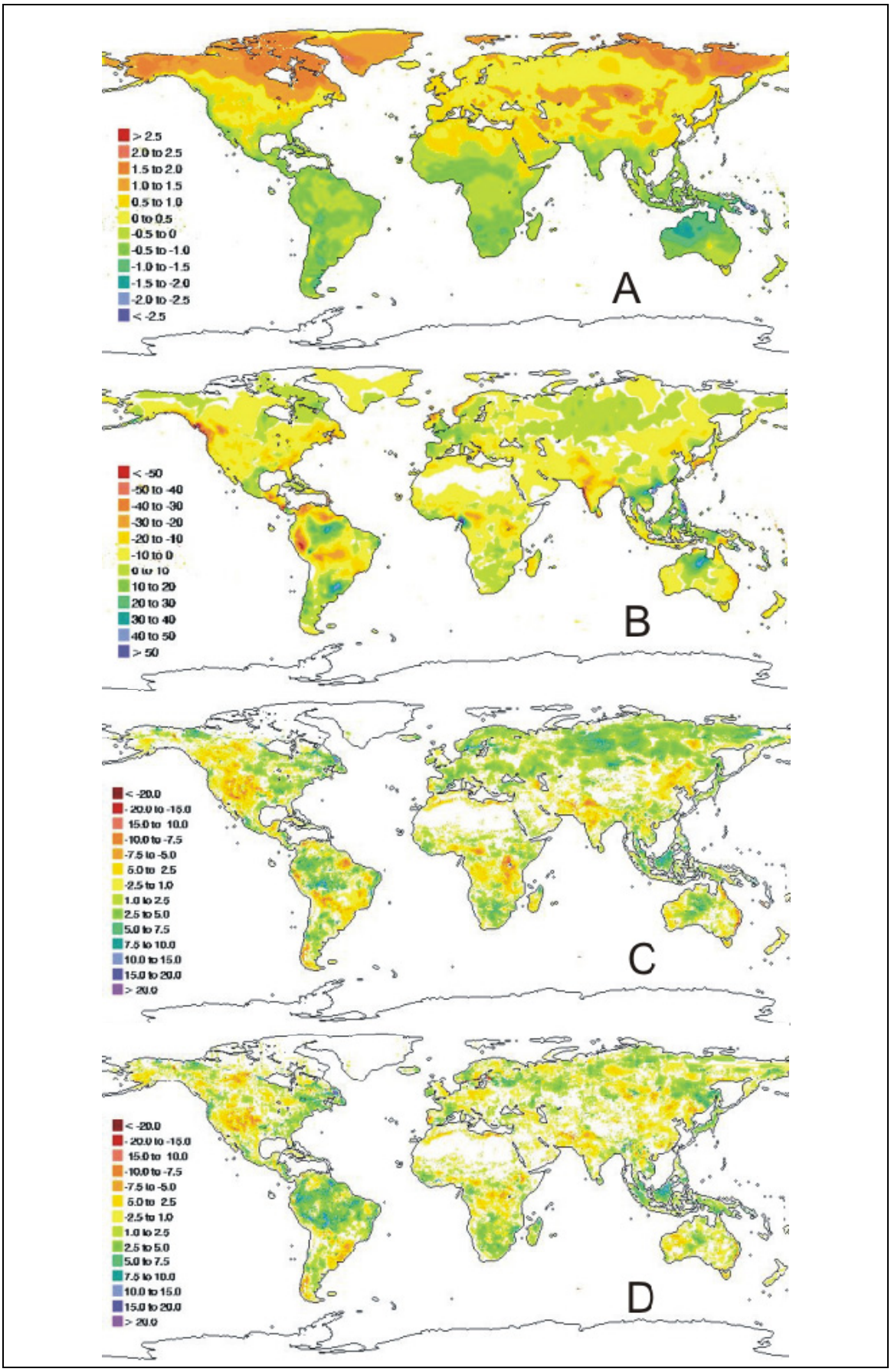

Fig. 6.4. Carbon flux and climate anomalies for the period 2000 to 2002. (A) temperature in °C, (B) precipitation in mm, (C) NPP in gCm^{-2}, (D) NEP in gCm^{-2}

	Carbon fluxes	Boreal	Northern temperate	Tropics	Southern temperate
Annual averages	NEP	0.17	0.07	0.32	0.06
(in PgC yr^{-1})	NPP	13.59	15.62	30.55	4.15
	Rh	11.53	14.79	26.67	3.38
	fireC	1.07	0.44	2.34	0.32
(in °C)	Temperature	- 2.96	12.68	25.50	16.67
(in mm)	Precipitation	41.26	65.79	117.15	70.96
Total anomalies	NEP	+ 0.03	- 1.19	+ 0.60	+ 0.17
(in PgC yr^{-1})	NPP	+ 0.54	+ 2.96	+ 1.10	- 0.99
	Rh	+ 0.51	+ 4.15	+ 0.50	- 1.16
	fireC	- 0.05	- 0.01	+ 0.13	+ 0.04
(in °C)	Temperature	+ 0.46	+ 0.55	+ 0.10	+ 4.53
(in mm)	Precipitation	- 0.12	- 1.55	+ 2.49	+ 4.01
Anomalies	NEP	+ 1.64	- 58.75	+ 18.32	+ 28.62
(in %)	NPP	+ 4.14	+ 23.36	+ 3.73	- 19.36
	Rh	+ 4.60	+ 38.99	+ 1.90	- 25.59
	fireC	- 4.05	- 2.23	+ 5.89	+ 12.11
	Temperature	+13.36	+ 4.55	+ 0.40	+ 27.19
	Precipitation	- 0.29	- 2.31	+ 2.17	+ 5.89

Table 6.3. Carbon fluxes, precipitation and temperature for the warmest period since climate recording (01/2000 – 12/2002), anomalies are calculated based on the period 1982 to 2002

Interestingly, the accentuated warming observed for the boreal zone did not lead to a higher NEP (Tab. 6.3). Although vegetation growth has substantially increased due to warmer temperatures and the enhanced CO_2 fertilization effect (+ 0.54 PgC yr^{-1}), the enhanced plant production is offset by an increase in soil decomposition (+ 0.51 PgC yr^{-1}). These findings expand upon several studies reporting a "boreal greening" (Myneni et al. 1997, Zhou et al. 2001, Bogaert et al. 2002, Nemani et al. 2003) by showing that the observed increase of NPP does not lead to a generally enhanced terrestrial uptake.

Moreover, for the northern mid-latitudes the estimates suggest a significant reduction of the terrestrial uptake during this period, most accentuated in the North American regions, produced by a strongly enhanced soil respiration (+ 4.1 PgC yr^{-1} above the long-term average) which even exceeds the NPP increase (+ 3 PgC yr^{-1}). Likely, a concert of processes lead to this net carbon source flux: Warmer temperatures intensified soil respiration whereas at the same time moderate reduction of rainfall has no limiting effects on the decomposition rates but on the vegetation growth rates. Though, the reduced precipitation limited the enhanced vegetation growth. In contrast, Europe exhibits more rainfall leading to increased NPP which exceeds an enhanced soil respiration. These results suggest that the largest decline in soil carbon storage is found for the northern mid-latitudes, particularly for North America, even exceeding the changes in boreal regions which sustain strongest warming. Furthermore, these results imply that the mid-latitude ecosystems seem to be particular vulnerable to climate change as only

small changes in temperature and precipitation patterns considerably affect terrestrial carbon uptake and release. However, this conclusion must be regarded with caution as variability might be large on smaller regional scales but small regarding latitudinal zones.

For the tropics and southern mid-latitudes a slight increase in precipitation can be attributed to the overlying effects of the extraordinary long La Niña period during 1999/2000. More rainfall leads to a moderate increase of NPP and NEP in the tropics. But tropical carbon uptake is offset by emissions of land-use. The additional carbon uptake of 0.6 PgC yr^{-1} cannot counterbalance the emissions of land-use and land-use change which are estimated to be 2.2 +- 0.8 PgC yr^{-1} in the 1990s (Houghton 2003c). The southern temperate regions experience a strong warming, which is followed by a strong drying causing a reduction in plant productivity and an increase in fire occurrence. But as the drought events lead to a reduction of soil decomposition processes, the net biospheric carbon uptake is still larger than average (Tab. 6.3).

Globally, NEP increased by about 0.4 PgC yr^{-1} during the time period of 2000 to 2002, composed by an increase in NPP and a less pronounced increase in Rh by 1.8 PgC yr^{-1} and 1.4 PgC yr^{-1}, respectively. The tropics and southern temperate region contributed most to the enhanced carbon uptake although it was offset by large amounts of emissions due to land-use change.

Several climate models predict strong warming under rising atmospheric CO_2 for the 21^{st} century leading to an increase in NPP until the 2050s (Cox et al. 2000, Dufresne et al. 2002, Schaphoff et al. 2006). Furthermore, this study suggests that increased biospheric carbon uptake will only occur in tropical and southern temperate regions, where carbon gains are not offset by enhanced soil decomposition. However, as the tropical biospheric carbon uptake is exceeded by the land-use emissions, the terrestrial biosphere is likely to turn to a global carbon source in the future.

6.2 The Mt. Pinatubo Eruption

The CO_2 growth rate significantly declined in 1992 and 1993, being the lowest for the time period of 1983 to 2003 (NOAA 2004; http://www.cmdl.noaa.gov/milestones/2005/). Measurements of atmospheric $\Delta^{13}C$ attribute the reduced atmospheric CO_2 accumulation to an enhanced terrestrial carbon sink of about 2 PgC yr^{-1} (Battle et al. 2000, Francey et al. 2001). Studies based on inverse modelling identified the northern mid- and high latitudes to be the main contributor for the enhanced terrestrial uptake (Fan et al. 1998, Rayner et al. 1999, Bousquet et al. 2000). This extraordinary carbon sink has been traced back to the climatic changes following the Mt. Pinatubo eruption which injected about 20 Mt of SO_2 aerosols into the stratosphere affecting radiation budget and global atmospheric circulation (Hansen et al. 1992, Stenchikov et al. 2002).

Figs. 6.5.A to C compare the anomalies of temperature, precipitation, and NEP for the Post-Pinatubo period. Anomalies are calculated for the months 06/1991 – 05/1993, using a baseline averaged over the time period of 1982 to 2000.

Large volcanic eruptions produce a global cooling for the following two to three years (Hansen et al. 1996, Robock 2000). The aerosol cloud increases the backscattering, and reduces the amount of incoming radiation reaching the Earth's surface, thus leading to a net cooling of the troposphere. Robock & Mao (1992) reported a net cooling most pronounced for the tropics, the Mediterranean region and the Middle East, which is reflected in Fig. 6.5.A. In contrast to the net global cooling, several authors observed a winter warming in the mid-latitudes and the boreal zone of the northern hemisphere following the eruption (Robock and Mao, 1992, Graf et al. 1993, Mao & Robock 1998, Kirchner et al. 1999). The anomalously warm winter temperatures were a result of the aerosol layer heating the tropical stratosphere by absorbing terrestrial and solar IR-radiation. The anomalously warm tropical stratosphere enhances the pole-to-equator temperature gradient and the polar vortex, which in turn triggers the AO and the NAO to a positive phase (Groisman, 1992, Perlwitz & Graf 1995, Robock & Mao 1995, Stenchikov et al. 2002). A positive NAO phase is characterized by a zonally asymmetric warming over North America and Eurasia in high and mid-latitudes, and cooling over Greenland and the Near East. This pattern is partly reproduced in the anomaly calculations in fig. 6.5.A: Eurasia was anomalously warm over the whole period, not only in wintertime. In contrast, in Eastern North America cooler summers cancelled out any wintertime warming. The moderate El Niño event of 1991/1992 additionally contributed to the warming over North America in the winter of 1991/1992 (Stenchikov et al. 2002).

Since the carbon cycle is sensitive to changes in temperature, especially in the temperature-limited northern ecosystems, the eruption should have had an impact on NEP. The anomalously warm winter temperatures imply an earlier onset of spring bud-burst and an enhanced NPP.

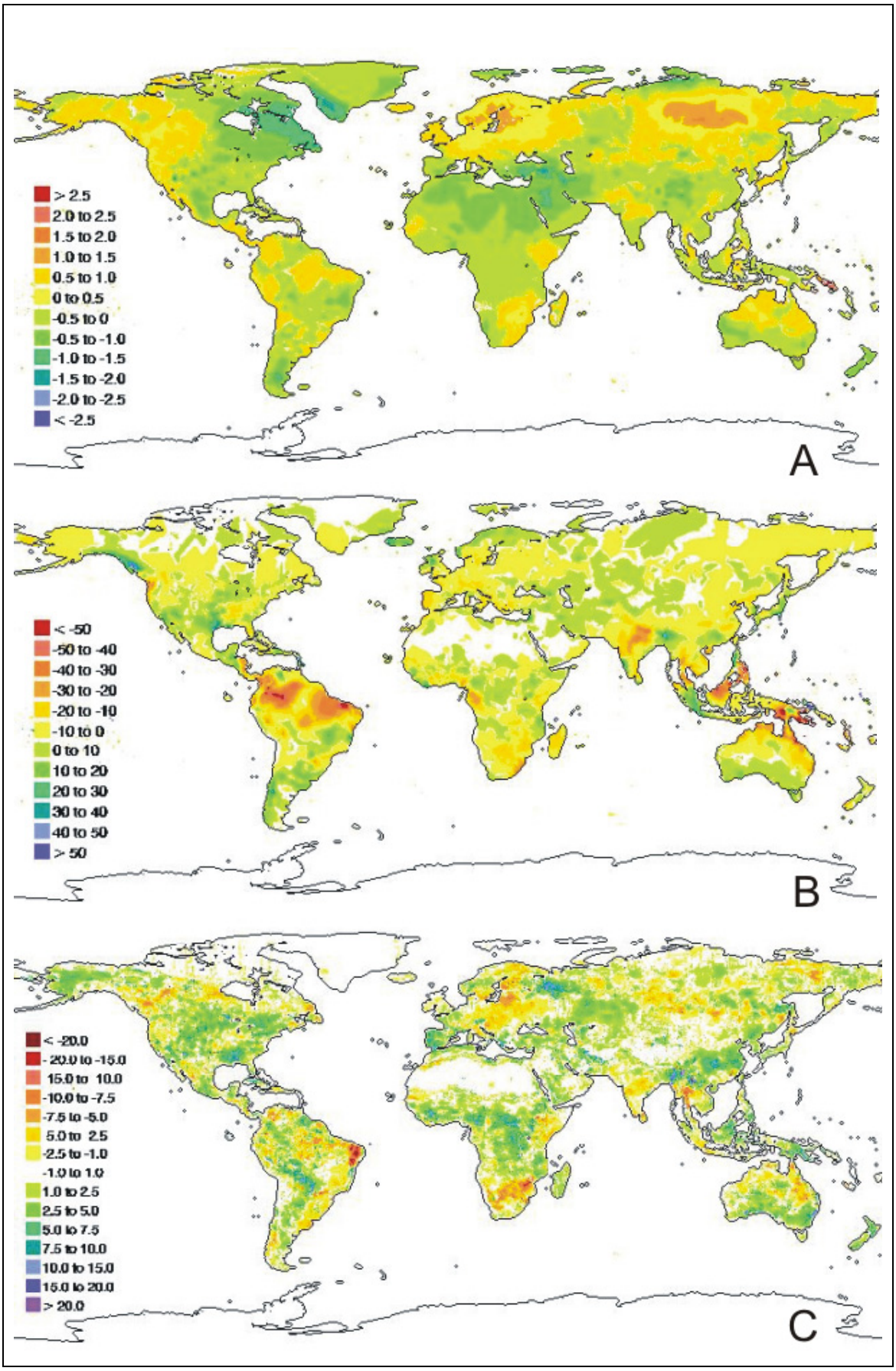

Fig. 6.5. Carbon flux and climate anomalies for the period following the Mt. Pinatubo eruption. (A) temperature in °C, (B) precipitation in mm, (C) NEP in gCm^{-2}.

However, satellite derived NPP modelling suggested a decrease in NPP due to cooler summer temperatures for the northern hemisphere (Zhou et al. 2001), and a reduction in growing season length (Lucht et al. 2002) for the boreal zone. Krakauer & Randerson (2003) reported significantly narrowed tree rings north of 45°N that were even more pronounced in regions north of 60°N. These observations imply a reduced NPP in the years following the Mt. Pinatubo eruption. This NPP reduction was mostly attributed to permafrost encroachment on tree roots causing nutrient and water stress due to the summer cooling.

The current LPJ simulation expands upon these NPP estimations by encountering also soil respiratory processes. LPJ results for Siberia and the entire boreal zone show neither a reduction nor an increase in carbon uptake (+ 0.01 PgC yr^{-1}) according to the results of Jones & Cox (2001). Soil respiration was reduced to an even greater extent than NPP (-0.23 and -0.21 PgC yr^{-1}, respectively) and is responsible for the constant NEP. However, LPJ simulates a moderate increase of NPP for the northern mid-latitudes (+0.29 PgC yr^{-1}) together with a reduction in soil respiration (- 0.25 PgC yr^{-1}) which consequently leads to a strongly enhanced terrestrial uptake of 0.54 PgC yr^{-1}, (equivalent to approximately 25 % of the total NEP during this period). The enhanced NPP can be attributed to an earlier onset of spring bud-burst due to the extraordinary mild winter seasons, as well as to reduced water stress during the cooler summers. Soil respiration reduction is mainly provoked by the summer cooling.

	Carbon fluxes	**Boreal**	**Northern temperate**	**Tropics**	**Southern temperate**
Annual averages	NEP	0.17	0.21	0.29	0.06
(in PgC yr^{-1})	NPP	12.77	13.05	29.53	5.24
	Rh	10.74	10.49	26.07	4.58
	fireC	0.52	2.44	1.11	0.27
(in °C)	Temperature	- 3.32	11.92	25.30	16.61
(in mm)	Precipitation	40.59	66.82	107.32	67.30
Total anomalies	NEP	+ 0.01	+ 0.54	+ 0.14	+ 0.03
(in PgC yr^{-1})	NPP	- 0.21	+ 0.29	- 0.27	+ 0.01
	Rh	- 0.23	- 0.25	- 0.40	- 0.02
	fireC	- 0.11	+ 0.16	+ 0.06	- 0.01
(in °C)	Temperature	- 0.18	- 0.24	- 0.08	+ 4.47
(in mm)	Precipitation	- 0.77	-0.26	- 7.41	+ 0.34
Anomalies	NEP	+ 0.66	+ 26.65	+ 4.14	+ 4.09
(in %)	NPP	- 1.65	+ 2.24	- 0.89	+ 0.20
	Rh	- 2.07	- 2.36	- 1.53	- 0.36
	fireC	- 12.54	+ 6.85	+ 7.16	- 2.97
	Temperature	- 5.23	- 1.94	- 0.32	+ 36.84
	Precipitation	- 1.87	- 0.51	- 0.32	+ 0.51

Table 6.4. Carbon fluxes for the period following the Mt. Pinatubo eruption (06/91 – 05/93). Positive values indicate a carbon sink or enhanced uptake, negative values show reduced uptake. Anomalies are calculated based on the period 1982 to 2000.

Some authors attribute the increased NPP in the northern temperate zone to an enhanced photosynthesis stimulated by diffuse radiation (Roderick et al. 2001, Gu et al. 2003). Angert et al. (2005) tested the hypothesis of enhanced NPP triggered by increased diffuse light income with the CASA model. They pointed out that additional diffuse light income results in an enhanced NPP, but with the effect of lowering the model's ability to exactly simulate the global atmospheric CO_2 growth rate. They conclude that the influence of diffuse radiation is negligible and balanced by the effect of reduced net radiation income. Therefore, NPP should not be affected by the eruption-induced diffuse radiation effects. Angert et al. (2005) demonstrated that the effect of temperature together with changes in precipitation could reproduce the enhanced carbon sink, although being much smaller (0.5 PgC yr^{-1} for each hemisphere) than the observations suggest. The enhanced sink that was observed in 1992-93 is explained to be caused by enhanced oceanic uptake, and reduced biomass burning. Goulden et al. (1996) observed enhanced carbon sequestration in a deciduous forest in New England for the Post-Pinatubo period. Their field experiments suggest enhanced rates of photosynthesis due to an earlier onset of leaf expansion and delayed senescence in autumn. They concluded that the forest carbon exchange responds stronger to single extreme weather events which occur in sensitive phases of the forest, than to a general temperature rise.

As LPJ does not simulate the effects of a greater diffuse light fraction, the enhanced NPP must be an effect of cooler summers and mild winters as well as regionally increased rainfall which is not reflected in the latitudinal mean (Tab. 6.4). These results are supported by other studies (Bousquet et al. 2000, Roedenbeck et al. 2003, Peylin et al. 2005). An analysis of data from inversion modelling (Peylin et al. 2005) suggest enhanced terrestrial carbon uptake located over North America. LPJ results also suggest uptake in South-Western Europe and western Russia/Ukraina driven by increased rainfall together with cooler temperatures. In fact, vegetation of the temperate zone is not temperature-limited, and cooler temperatures i.e. in dry regions result in growth enhancement due to less water stress.

Some observations reported tropical carbon uptake during the 1990s: CO_2 flux measurements in the Amazon region by Grace et al. (1995) indicate a large regional carbon sink of 0.56 PgC yr^{-1} for the period 1992-1993. Ciais et al. (1995) found similar carbon uptake amounts for the northern tropics in 1993 using inverse modelling. However, modelling and observation studies indicate an enhanced tropical uptake during this period, but LPJ only simulates a small positive uptake anomaly for the tropics (+ 0.14 PgC yr^{-1}) for the Post-Pinatubo period (06/191 to 05/1993). The lower latitudes are dominated by radiative cooling effects, as radiation income is higher, thus more sunlight can be blocked by the additional aerosol load coming from the eruption. During the Post-Pinatubo period, the tropics receive a reduced radiation income of 4 W m^{-2} (Self et al. 1996) and the average temperature decreased globally by about 0.5 K (Hansen et al. 1996). The cooling observed after the Mt. Pinatubo eruption is reflected in

reduced evapotranspiration rates leading to a reduction in precipitation for 1-2 years (Hansen et al. 1988, Robock & Liu 1994). This pattern can be clearly observed in the Amazon and south-eastern Tropics (Fig. 6.4.B). Results from a modelling study of Jones & Cox (2001) suggest a large terrestrial sink particularly for the Amazon region due to volcanic forcing being composed of enhanced GPP and reduced plant respiration. In contrast, LPJ simulates a reduction in NEP due to the decreased ampounts of rainfall, probably caused by the simultaneously occurring El Niño. Highest uptake rates can be found throughout the African tropics. The LPJ results suggest that the slightly enhanced tropical carbon utake rates are caused by the strongly reduced soil respiration which even exceed the reduced NPP.

Finally, it has to be noted, that the volcanic signal is superimposed by the simultaneously occurring El Niño event. There is no clear evidence that volcanic eruptions trigger El Niño events, although El Niño events occurred directly after the El Chichón and Mt. Pinatubo eruptions (Self et al. 1997, Robock 2000). However, it is difficult to separate the influence of various environmental impacts, such as volcanic and climatic events, on the carbon cycle variability. E.g. El Niño events have an additional effect on the oceanic carbon uptake, for which an increase also has been observed for the the period 1991 to 1994 ,that has been attributed to the subsequent El Niño event (Le Quéré et al. 2000).

Globally, LPJ-simulated NPP and soil respiration show a decrease by about 0.2 PgC yr^{-1} and 0.9 PgC yr^{-1}, respectively, for the Post-Pinatubo period. These results are in agreement with findings by Jones & Cox (2001), who estimated a reduction of 0.35 PgC yr^{-1} for NPP and 0.9 PgC yr^{-1} for soil respiration. LPJ simulates a global increase of NEP by 0.7 PgC yr^{-1} for the Post-Pinatubo period. The northern temperate region can be identified as the main contributor to the anomalously strong global carbon sink in the years following the Pinatubo eruption as a response to increased rainfall and cooler summer temperatures. The enhanced uptake is due to a reduction in soil respiration which decreased to an even greater extent than NPP did.

7. CONCLUSIONS AND DISCUSSION

A key advance in this study is that a coupling between a process-based dynamic global vegetation model and satellite fPAR observations is feasible and produces reasonable and more realistic results than the stand-alone potential vegetation model. As it is based on climate and on remote sensing data instead of on climate data alone, it allows generating global and regional estimates of ecosystem carbon uptake and release including anthropogenic influence and natural disturbances like fire. This is an important result, as it provides the spatio-temporal patterns of the world's carbon sources and sinks for the last 21 years (1982 to 2002) as well as the main drivers of its interannual variability.

This approach is unique, as to date no direct coupling between a process-based dynamic vegetation model and satellite data has been realized for such a long time period. Most of the remote-sensing based models such as GLO-PEM, TURC or SiB2 are based on the LUE approach and if they account for soil processes they are represented in a simplified way (Ruimy et al. 1996, Sellers et al. 1996, Goetz et al. 2000). The latest published vegetation models VEGAS (Zeng et al. 2004) and TRIFFID (Jones & Cox 2001), even though including fire (VEGAS) or a disturbance rate (TRIFFID), do not account for human influences. Only the CASA model approach (Potter et al. 1993, Field et al. 1995, Thompson et al. 1996, Potter et al. 1999, 2001) can reproduce estimations for a similar time period including remote sensing data and therefore human influence. It is based on a LUE method combined with a sophisticated soil model (Parton et al. 1993, Randerson et al. 1997), but it does not include dynamic vegetation establishment and disturbances such as natural fires. The approach of Knorr & Heimann (2001a & b) combines the process-based vegetation model BETHY with satellite data and a dynamic establishment scheme, but it is only applied to the year 1986. Shortly, Rayner et al. (2005) published first results calculated by the process-based BETHY model for the time period 1979 to 2000. It contains optimized parameters which are derived by using one year of satellite data (1989-1990) to obtain the best match to records of atmospheric CO_2 concentration. However, the approach of Rayner et al. (2005) does not consider rising CO_2 concentrations and the CO_2 fertilization effect, as well as the satellite data input for parameter optimization only consists of one year. Therefore their results are not directly comparable to the current approach which is based on the time series of combined satellite and climate data for 21 years.

Most of the achieved results by the current study could be confirmed by independent studies based on satellite data and LUE models (Cao et al. 2002, Nemani et al. 2003, Potter et al. 2003), on inversion modelling (Rayner et al. 1999, Bousquet et al. 2000, Roedenbeck et al. 2003, Gurney et al. 2004, Peylin et al. 2005), on forest inventories (Goodale et al. 2002), on ocean or climate models coupled with atmospheric inversion modelling (Bopp et al. 2002,

Plattner et al. 2002), and on empirical carbon flux comparisons (Houghton 2003a, House et al. 2003).

However, as several international conventions (Kyoto protocol (UN 1997), IPCC 2001) call for improvement of the understanding of the spatio-temporal behaviour of the terrestrial biosphere, its ability to uptake and release carbon and to partly offset the anthropogenic CO_2 emissions, there is an urgent need for investigations as the present study.

The present approach with a satellite data constraint in a DGVM (LPJ-S) produces generally smaller carbon fluxes (NPP, Rh, fire carbon) than the purely climate-based stand-alone simulation of potential natural vegetation (LPJ-P). The implementation of agricultural areas into the original model enhances NPP and Rh in these areas, whereas biomass is reduced to a more realistic size (WBGU 1988, Mooney et al. 2001). Net carbon uptake (NEP) is reduced by 0.6 PgC yr^{-1} due to the assimilation of the satellite data.

The estimated NPP of 60.0 PgC yr^{-1} now converges significantly with the IPCC results (IPCC 2001). Global soil respiration is found to be 52.3 PgC yr^{-1}, which is comparable to the results of other models (Cramer et al. 2001). Unfortunately, global data on Rh based on measurements are not available for comparison.

The lower carbon fluxes of LPJ-S compared to LPJ-P originate in a combination of several effects. Although in agricultural areas the photosynthesis rate is enhanced, total NPP of croplands is reduced by 5 PgC yr^{-1} due to a reduction in total vegetation cover and potentially by a more realistic seasonality encompassing the winter season with less or without plant productivity. The reduction of NPP in natural areas can be traced back to a more open landscape as observed by the satellite representing the anthropogenic influence. The opening of the landscape is an effect of areas classified as natural areas although containing a small fraction of croplands, as well as forest areas with a less dense vegetation cover. Another cause for the NPP reduction are changes in PFT distribution. The boreal tree line has shifted further south which is closer to reality according to Sitch et al. (2003), who stated that the simulation of a forest-tundra border is located too far north by LPJ-P. Vegetation of very specialized or adapted ecosystems of arid and semi-arid regions such as savannas, which are not included in the original model, are now captured due to the observed seasonality and more open vegetation density. Additionally, the observed greening trend of the Sahel region during the 1990s could be simulated. Concluding, as potential vegetation models prevalently tend to overestimate carbon fluxes, i.e. net primary production (Cramer et al. 1999), the implementation of the satellite data has successfully improved the results.

Fire carbon is significantly reduced to 4.3 PgC yr^{-1}, predominantly due to the fire suppression for agricultural areas, showing much better agreement with an estimate given by Andreae & Merlet (2001). The reduction in natural areas results from combined effects of a more open

vegetation providing less biomass for fire fuel, and from grass domination in residual crop pixels with a higher flammability than forest cover.

Biomass is found to be 638 PgC in the satellite-driven version, comparing well with other estimates, e.g. given by IPCC (2001), WBGU (1988), and Mooney et al. (2001) (Tab. 4.8). 239 PgC are lost due to deforestation and land-use change patterns as seen by the satellite as compared to a world without human influence. This figure takes into account an overestimation of biomass within natural regions by LPJ-P of about 5 to 10 %. The reduction of biomass compares well with the estimated historical carbon emissions since ancient times up to the year 2000 of about 180 to 220 PgC given by DeFries et al. (1999), Houghton (2003c), and House et al. (2002). However, compared to measurements based on forest inventories and satellite observations (Dong et al. 2003), total biomass of the boreal zone still seems to be overestimated, i.e. in the northern tundra regions. Zaehle (2005) considered age-related decline of forest growth to reduce biomass significantly, which can only indirectly be fetched by the satellite data when vegetation greenness and therefore NPP is reduced in older forest stands. Beer (2005) showed that the implementation of correct permafrost simulation into LPJ reduces biomass throughout the boreal zone by about 60 % due to enhanced water stress. The accounting of biomass for the boreal forest could be improved by the satellite data input, as LPJ-S indirectly accounts for water surfaces and less dense vegetation cover influenced by unfavourable environmental conditions such as insufficient soil fertility. Regionally, the satellite data assimilation might lead to shifts in PFT distribution followed by changes in biomass. In some regions within the temperate and boreal forest biomass is reduced due to changes from evergreen needle-leaved forest to broad-leaved summergreen forest or grasses. However, Zaehle (2005) reported a model-inherent overestimation of biomass for conifers, explaining the strong reduction when vegetation cover changes from needle-leaved to broadleaved forest. LPJ-S estimates a higher biomass in tropical regions as it simulates a higher fraction of tropical evergreen broadleaved forest. Moist savanna ecosystems show a decrease in biomass due to the enhanced occurrence of grasses, suggesting that different savanna types and shrub ecosystems are poorly captured in LPJ-P. However, strongest reduction of biomass within the natural areas can be traced back to the occurrence of residual crop pixels that are classified as natural forest in LPJ-S.

Annual harvested carbon is estimated to be 2.7 PgC yr^{-1}, which is of the same order of magnitude as the figures provided by the FAO (2001) (1.99 PgC yr^{-1}) and the IPCC (2000) (3.1 to 4.1 PgC yr^{-1}).

Soil carbon is generally reduced due to deforestation and conversion of forest to agricultural land, as well as due to more open vegetation and a shift of the boreal tree-line further to the south. An according lower input of biomass and litter into the soils is reflected in a reduction of soil carbon of 299 PgC between LPJ-P and LPJ-S, resulting in a global total of 1371 PgC. As

the capacity of soils to sequester carbon is one proposed method to reduce atmospheric carbon dioxide, a correct modelling of soil carbon storage and fluxes is essential. The result achieved with LPJ-S is compares better with inventoried data by Schlesinger (1977) and Post et al. (1982), which seem to be the most reliable estimates as they are based on the most extensive data bases. However, as inventoried data is still fragmentary and highly uncertain, our model results complementary contribute to the wide range of estimates.

These carbon flux estimations demonstrate that it is crucial to fully account for agricultural areas and to make use of satellite data in carbon cycle modelling. Otherwise no realistic view on the world's carbon pools and fluxes is feasible. Hitherto, only the CASA model gives comparable estimations for a similar time period including satellite data (Hicke et al. 2002, Potter et al. 2003, Murayama et al. 2004). In these studies, agricultural modelling is not included, but indirectly represented by the satellite data which captures vegetation cover and seasonality and therefore the sowing and harvesting dates. The approach of Cao et al. (2002), which gives comparable outputs, does not take into account fire occurrence and agricultural areas but it is based on vegetation mapping and satellite data. The approach of Rayner et al. (2005), even though combining process-based modelling with satellite data, only derives parameters based on one year of satellite data input, as well as it does not account for rising atmospheric CO_2 concentrations and the CO_2 fertilization effect.

Under the Kyoto protocol (UN 1997), the use of terrestrial "carbon sinks" to counteract anthropogenic CO_2 emissions was stated to be an essential aim for future development and sustainable actions. Hence, the most important and interesting term in carbon cycle modelling is net ecosystem production (NEP), representing the terrestrial ability to uptake and release carbon. With the approach used here, NEP incorporates not only NPP and Rh, but also carbon released by fire and harvesting, which makes the NEP calculations more realistic.

The implementation of satellite data and agricultural areas have significantly changed and reasonably improved the results of LPJ. Carbon uptake by the terrestrial biosphere has increased between the 1980s and 1990s. LPJ-S estimates a carbon uptake of -0.4 PgC yr^{-1} for the 1980s (1982 to 1989) and -0.9 PgC yr^{-1} for the 1990s, giving an increase of 0.5 PgC yr^{-1} between the two decades. These figures are in the same order of magnitude as the estimations given by the IPCC (2001), Bopp et al. (2002), Plattner et al. (2002), Houghton (2003a), and House et al. (2003). Although our estimations are somewhat higher for the 1980s and lower for the 1990s, these results are much improved compared to LPJ-P (1.1 and 1.4 PgC yr^{-1}, for the 1980s and 1990s, respectively). The difference between LPJ-P and LPJ-S should give the land-atmosphere flux due to land-use change, but it only amounts 0.6 (0.4) PgC yr^{-1} (for the 80s and 90s, respectively), which is too low compared to the estimate of 2.0 PgC yr^{-1} given by Houghton (2003c). Therefore, the assimilation of the satellite data does not accurately reflect changes due to land-use change. Though, Houghton (2003c) does not account for carbon

sources and sinks such as climate change or the CO_2 fertilisation effect, which are included in the LPJ-S model.

The underestimation by LPJ-S for carbon released by land-use change might be the consequence of the modelling spin-up using fPAR data input in cycles in order to adjust to the satellite-observed vegetation composition. In addition, vegetation composition modelling reverts to the fraction of vegetation cover of the previous year. Therefore, the model is not able to reflect short-term changes in land use accurately, influencing the annual carbon fluxes and net terrestrial uptake.

However, absolute figures of the net land-atmosphere flux for the decades compare well with the revised carbon budget of Plattner et al. (2002), presenting a net terrestrial uptake of -0.4 and -0.7 PgC yr^{-1} or with the results of Bopp et al. (2002) who reported a terrestrial uptake of -0.3 and -1.2 PgC yr^{-1} for the 1980s and 1990s, respectively. These results are close to the estimates of the current approach with -0.4 and -0.9 PgC yr^{-1}. The results of LPJ-S identify the tropical and southern temperate regions to contribute most to this increase.

Given a yearly carbon release by land-use change of 2.0 PgC yr^{-1} for the 1980s and 2.2 PgC yr^{-1} for the 1990s (Houghton 2003c) as well as a partial accounting for land-use change by LPJ-S, LPJ-S estimates a total terrestrial carbon sink of -1.8 and -2.7 PgC yr^{-1} for the eighties and nineties, respectively. Given the uncertainties and know deficiencies in other derivations, these new results can be taken to be equally likely. They add to the small pool of available estimates (Tab. 4.13).

This leads to one of the central questions in carbon cycle modelling: the regional distribution of the ‘missing sink’ and the long-term trends in its variability (Fung 2000), which is detectable by the present approach for 1982 to 2002.

Several studies identify a strong terrestrial sink in the northern hemispheric biosphere, especially in the boreal forest zone (Myneni et al. 1997, Schulze et al. 1999, Goetz et al. 2000, Myneni et al. 2001, Zhou et al. 2001, Dargaville et al. 2002, Hicke et al. 2002, Dong et al. 2003). In contrast, the intercomparison of the results of 16 atmospheric inversion models (Gurney et al. 2004) reported a weak net sink (-0.16 PgC yr^{-1}) averaged over 1992 to 1996 for the boreal zone. LPJ-S approximates to this result simulating a small sink for this period (-0.24 PgC yr^{-1}). A small positive trend for NPP of 0.4 PgC yr^{-1} between the two decades can be found. However, some regions of Canada and Siberia exhibit a reduction in NPP, which can be explained by a reduced uptake in summer due to warmer and drier conditions (Angert et al. 2005). Main reason for the weak uptake is the increase in soil respiration as a consequence of warmer temperatures. Estimates for net carbon fluxes from inversion modelling, forest inventories and carbon cycle modelling vary significantly for the northern temperate zone. Results range from a strong sink of -1.96 up to only weak uptake of -0.2 PgC yr^{-1} (Gurney et al. 2004: -1.96 PgC yr^{-1} Houghton 2003a: -0.7 PgC yr^{-1}, Potter et al. 2003: -0.3 PgC yr^{-1}, LPJ-S_{GIM}:

-0.2 PgC yr^{-1}) for the period 1992 to 1996. The strong discrepancies might be a result of choosing a short average time period as year-to-year variations may be very large. The Sahel region has recovered from the severe droughts during the 1980s, changing from a source (0.4 PgC yr^{-1}) during the 1980s to a sink in the 1990s (-0.2 PgC yr^{-1}). Reasons for the Sahel greening are increased precipitation along with the rising atmospheric CO_2 content providing better conditions for plant growth and establishment. Moreover, LPJ-S simulates enhanced uptake rates for the whole tropics between the 1980s and 1990s, increasing by 0.7 PgC yr^{-1} from -0.2 PgC yr^{-1} to -0.9 PgC yr^{-1}. Although the uptake of undisturbed tropical forest can be confirmed by several studies (Grace et al. 1995, Phillips et al. 1998, Tian et al. 1998, Malhi & Grace 2000, Schimel et al. 2001), this is more than offset by emissions from land-use change and deforestation (Heimann 2001, Achard et al. 2002, Gurney et al. 2002, Houghton 2003a, House et al. 2003). Including the emissions of land-use change into the LPJ-derived values, the tropical source of 1.2 PgC yr^{-1} during the 1980s has weakened in the 1990s to 0.5 PgC yr^{-1}, which is close to published estimates. The increase of net fluxes between the decades is mainly due to an enhanced NPP, even exceeding the weaker increase of soil respiration. Cao et al. (2002) suggest that the CO_2 fertilization effect compensates the stress on plant growth occurring due to warmer temperatures.

The presented estimates indicate that the highest potential for enhancement of global carbon uptake lies within the semiarid and dry zones, and the tropical forests. Therefore, further deforestation especially of tropical forests is extremely harmful in terms of carbon sequestration. Additionally tropical reforestation should be intensified, and semiarid areas should be protected to avoid overgrazing to enlarge its sink potential.

The annual CO_2 growth rate is predominantly determined by variations in terrestrial biosphere sources and sinks, as emissions of fossil fuel burning and from land-use change, as well as the ocean uptake do not show a specific interannual variability. This is in good agreement with several studies (Conway et al. 1994, Kaduk & Heimann, 1996, Houghton et al. 1998, Lloyd 1999, Tans & Wallace 1999, Battle et al. 2000, Bousquet et al. 2000, Houghton 2000b, Prince et al. 2000, Schaefer et al. 2002, Le Quéré et al. 2003, Murayama et al. 2004, Rödenbeck et al. 2003a). Changes in atmospheric CO_2 concentration and climate are suggested to be the main drivers for the decadal and interannual variation in terrestrial carbon fluxes (Houghton 2000b, Schaefer et al. 2002, Cao et al. 2002, Nemani et al. 2003). NPP, Rh, fire carbon and therefore the resulting NEP are sensitive to climatic variations. Especially global climatic events such as the ENSO cycle or volcanic eruptions can clearly be seen in the carbon cycle response.

The global standard deviation of NEP, used as a measure of interannual variability (IV), is found to be 0.87 PgCyr^{-1} by LPJ-S for the time period from 1982 to 1994. This figure compares well with other approaches of Conway et al. (1994) (1.1 PgC yr^{-1}), Houghton (2000b) (1.0 PgC yr^{-1}), and Schaefer et al. (2002) (1.3 PgC yr^{-1}), although their results are slightly higher. The

peak-to peak amplitude of the land-atmosphere flux ranges between -0.79 to 2.09 PgC month^{-1}, comparing well to other model estimates and studies based on atmospheric inversion (Kindermann et al. 1996, Bousquet et al. 2000, Cao et al. 2002, Potter et al. 2003, Peylin et al. 2005).

As biospheric activity is linked non-linearly to climate in a complex system of biogeochemical feedbacks, neither temperature nor precipitation variability show the particular patterns found in NEP variability. Secondly, small global variations in carbon fluxes also result from the fact that terrestrial ecosystems act independently, and their individual fluxes largely offset each other. As climatic variability is "enormous on small scales" (Hurrell & Trenberth 1997), it is crucial to survey regional carbon flux and climate variability.

NPP is the main contributor to IV on a global scale, whereas fire carbon shows the highest magnitude in variation, but only in few regions. On a regional scale, the temperate and boreal zone show small to moderate fluctuations of NPP, while highest IV of NPP can be found in tropical and southern hemispheric regions that are directly influenced by the temperature and precipitation patterns of ENSO. The northern hemispheric regions are not tele-connected with the ENSO cycle in terms of carbon cycle response. In the northern temperate zone NEP shows a moderate negative correlation to precipitation, which means that droughts are followed by net carbon fluxes to the atmosphere, but not as strongly as in the tropics. Variations in the boreal zone, which are generally smaller in magnitude, are mainly controlled by NPP variations alone, which are sensitive to temperature variability. In some boreal regions also soil respiration contributes to the interannual variability of NEP, mainly driven by temperature, but additionally dependant on precipitation. Additionally, a correlation of carbon fluxes with the NAO in the northern hemispheric ecosystems cannot be found explicitly, but this is probably an effect of the latitudinal choice of zones for the analysis, as NAO only influences certain parts of Europe and North America. Soil respiration activity responds to rainfall fluctuations in the tropics and small temperature changes in the higher latitudes leading to moderate fluctuations in NEP there. Highest magnitude of NEP interannual variability can be observed in the tropical semi-arid grasslands of Southern America, Africa and Australia, where NEP is predominantly controlled by NPP and fire fluctuations, comparing well with the results of Schaefer et al. (2002). The tropical forests account strongly for the global interannual variations, mainly caused by NPP and Rh variations. There, NPP is predominantly controlled by variations in precipitation, whereas soil respiration is responding to both precipitation and temperature variability. These results agree with the findings of Zeng et al. (2005) and Peylin et al. (2005).

However, a general influence of climate alone causing the distinct variability patterns of NEP cannot be observed explicitly. Probably feedbacks between the climate variables and the various carbon fluxes, and particularly non-linear process interactions within the ecosystems, which are all not independent of each other, are influencing the NEP variability.

The annual CO_2 growth rate is predominantly determined by terrestrial net land uptake and release (NEP), because emissions of fossil fuel burning, from land-use change, as well as the ocean uptake do not show a specific interannual variability. After Nemani et al (2003) interannual changes in NPP are negatively correlated with the global atmospheric CO_2 growth rate, but terrestrial NPP contributes only for a part of the biosphere-atmosphere exchange. We substantially expand upon that study by also including the other components of the terrestrial carbon cycle, soil respiration, carbon released by fire, and a simple crop module for an overall evaluation of terrestrial NEP, rather than just of NPP. In addition, this approach enables us an insight into the processes forming interannual variations of NEP, and therefore the CO_2 growth rate anomalies, i.e. it allows a determination which carbon fluxes contribute most for the fluctuations. A time-lag of two to four months between the extremes of the CO_2 growth rate and the NEP curve, which agrees with the studies of Potter et al. (1999), Botta et al. 2002 (Amazon basin), and Zeng et al. (2005), is caused by the delayed onset of Rh. NPP corresponds directly to changes in atmospheric CO_2 and climate fluctuations, while soil respiration responds gradually to environmental changes, as plant production only successively adds organic material to soil pools. Therefore, the temporal shape of the CO_2 growth rate is mainly determined by NPP, but its magnitudes and timings are determined by Rh, according to Hicke et al. (2002). Fire carbon also follows NPP, balancing the offset produced by the influence of soil respiration. The global range of variation of NEP is between -2.5 and 2.7 $PgCyr^{-1}$.

Globally, for most regions NEP is negatively correlated to temperature as a response to changes in soil respiration. A distinct latitudinal response of NPP to temperature can be observed, with an increase of NPP in the northern extra-tropics when warmer temperatures enhance plant productivity and growing season is prolonged. In addition, elevated atmospheric CO_2 enhances photosynthesis as the plant water use efficiency is advanced, with greater responses at higher temperature. Therefore, in northern cool regions, plant metabolism is stimulated directly by warmer conditions as well as indirectly by the CO_2 fertilization effect (Kirschbaum 1994).

As in the boreal zone, i.e. in permafrost regions, species are more close to their ecological limits, concerning temperature and soil moisture status, NPP is more influenced by climate variations than in the northern temperate regions. NEP variability of the boreal zone shows no direct relation either to NPP or to soil respiration. In contrast, for the northern and southern temperate regions soil respiration is closely related to both temperature and precipitation. It shows higher sensitivity to temperature changes than the photosynthesis rates, leading to the conclusion, that northern hemispheric net carbon fluxes are mainly determined by Rh variability. During the 1980s, when soil respiration of the temperate zone shows low variability, NEP fluctuations are determined by NPP.

Global land-atmosphere flux is dominated by the fluctuations of tropical net fluxes, which are determined by NPP variability. NPP is closely related to temperature (negatively) and

precipitation (positively), which determine soil moisture status and evapotranspiration, influencing the photosynthesis rates. As soil moisture responds with a delay of several months to changes in rainfall, this time-lag can also be found in the correlation between NPP and precipitation. Soil respiration is controlled by both temperature and precipitation. Both can adversely affect soil respiration through changes in litter fall and soil moisture status. As the patterns of temperature and precipitation are closely related to ENSO events, tropical net fluxes show also a distinctive correlation to ENSO with a strong drop during the El Niño phase and an increase during the La Niña episodes.

The tropical zone encounters a positive trend for the anomalies of all climatic parameters and carbon fluxes. NPP increased strongest contributing 63.5 % to the global NPP increase between 1982 and 2000. In contrast, Nemani et al. (2003) estimated only an increase of 43 %, suggesting a decline in cloud cover with increasing solar income and changed precipitation patterns to be the main reasons for this increase. However, they do not account for rising atmospheric CO_2 contents causing enhanced plant growth as well as for an explicitly modelled soil moisture content, which might lead to an underestimation of plant productivity. Cao et al. (2002) suggested the CO_2 fertilization effect to cancel out NPP losses caused by enhanced temperature stress. NEP shows a slightly positive trend as a consequence of increasing NPP which still exceeds the increase in soil respiration. However, the enhanced terrestrial uptake is more than offset by the high emissions caused by deforestation and land-use change.

For the northern latitudes, the increasing trend of NPP is also observable, due to rising temperatures which lead to a elongated growing season and an enhanced CO_2 fertilization effect. But as soil respiration is also stimulated by higher temperatures and an additional litter input into the soils is caused by the enhanced vegetation productivity, the net land-atmosphere flux remains more or less stable. However, an analysis of the future development of carbon pools of Schaphoff et al. (2006) suggests, that further warming will change this sensitive balance to a net carbon source.

El Niño events are characterized by warmer temperatures throughout the tropics along with reduced amounts of precipitation leading to a net carbon flux to the atmosphere. Shortly after the El Niño event of 1997/98, as well as after the events of 1982/83 and 1986/87, a significant decline in tropical NPP together with an increase in Rh and fire occurrence leads to a net source flux of CO_2 to the atmosphere. Generally, tropical net carbon fluxes are reduced by about 0.6 PgC yr^{-1} during El Niño events. During La Niña events opposite climatic patterns are observed in the tropics with decreasing temperatures while at the same time precipitation rates significantly increase. Consequently, net carbon uptake rates are enhanced, due to an increase in NPP that exceeds the slightly increased rates of soil respiration. In particular, for the La Niña period of 1998/1999 a surplus of 0.67 PgC yr^{-1} is stored in tropical vegetation while globally NEP has increased by only 0.4 PgC yr^{-1} as the northern extratropics show a small net carbon

source. It could be pointed out that ENSO events particularly affect the carbon fluxes of the tropical and southern temperate regions, whereas carbon cycle responses connected to ENSO for the northern hemisphere are not prominent. Usually, northern hemispheric net flux response is overlaid by climatic patterns associated with the NAO.

In contrast to the above-mentioned El Niño patterns, a somewhat different pattern occurred during the extraordinary long, but weak El Niño event lasting from 1991 to 1994. During that period, global NPP increased while soil respiration strongly decreased at the same time, leading to an increase in net terrestrial uptake. The simultaneously occurring Mt. Pinatubo eruption is supposed to have caused overlaying effects due to an atmospheric cooling caused by the additional aerosol load in the atmosphere. Global NEP has increased by 0.7 PgC yr^{-1} for the Post-Pinatubo period between June 1991 and May 1993. Main contributor to this increase is the northern temperate zone with an additional terrestrial carbon uptake of 0.54 PgC yr^{-1} being composed of an NPP increase of 0.29 PgC yr^{-1}while at the same time soil respiration decreases by 0.25 PgC yr^{-1}. In contrast to the findings of several authors suggesting additional diffuse radiation income to stimulate photosynthesis and enhance NPP (Roderick et al. 2001, Gu et al. 2003), it could be demonstrated that the carbon cycle mainly responds to climatic changes, as LPJ does not simulate effects of a greater diffuse light fraction. The general cooling during this period is mainly reflected in cooler summers, while the winter seasons were extremely mild (Robock and Mao, 1992, Graf et al. 1993, Mao & Robock 1998, Kirchner et al. 1999, Stenchikov et al. 2002). As a consequence, NPP increased due to an earlier onset of spring-budburst and less water stress during summer (Goulden et al. 1996). The cooler summer temperatures also provoked the reduction in soil respiration. The boreal zone encounters almost no NEP changes (+0.01 PgC yr^{-1}), as a reduction in NPP (-0.21 PgC yr^{-1}) is counterbalanced by a reduction in soil respiration (-0.23 PgC yr^{-1}). A cooling in the tropics leads to reduced evapotranspiration followed by a reduction in NPP (-0.89 PgC yr^{-1}) which is even exceeded by the reduction in Rh (-1.53 PgC yr^{-1}) leading to a small net carbon uptake anomaly (+0.14 PgC yr^{-1}).

An analysis of the warmest period during the investigated time series (2000 to 2002) showed that vegetation growth has substantially increased throughout all latitudes due to warmer conditions and the enhanced CO_2 fertilization effect, which is in agreement with several other studies (Myneni et al. 1997, Nemani et al. 2003, Zhou et al. 2001). However, as these studies only consider NPP growth, the current results extend these findings by showing that this increase in NPP (+ 0.54 PgC yr^{-1}) is offset by an increase in soil respiration (0.51 PgC yr^{-1}) for the boreal zone leading to a more or less neutral net flux. For the temperate zone, in particular in North American regions, soil respiration is even more enhanced (+ 4 PgC yr^{-1}) above the long-term average) followed by a reduction in NEP (-1.2 PgC yr^{-1}). This reduction is counterbalanced by enhanced uptake in the tropics, as they exhibit a strong La Niña event,

leading to a global NEP increase of 0.4 PgC yr^{-1} for this period. The results for the temperate regions suggest that these ecosystems are particularly vulnerable to climatic change as only small changes in temperature and precipitation conditions considerably affect terrestrial carbon fluxes. Furthermore, the results imply that the tropical and southern temperate ecosystems provide greatest potential for future carbon uptake, but only if deforestation rates will be reduced significantly.

In addition to having highlighted and discussed a lot of major results, I should address a few points: One limitation of this work is the scarcity and the extreme variability of global data and measurements from key ecosystems concerning carbon fluxes for comparison and validation. Most available data is restricted to short temporal or small spatial analyses which additionally often vary widely in their results. Anyhow, this underlines the importance of contributing to the small pool of available global data by studies such as the current analysis.

Secondly, as already mentioned above, the results for carbon released by land-use changes are still too low. This is caused by the inherent structure of data assimilation accessing to the previous year to model the present vegetation composition which leads to an underestimation of short-term land-use changes. Another reason is the simplified crop module which does not consider different crop types and year-to year changes. Nevertheless, the current results for carbon released by land-use change are still in the range of uncertainty of comparable analyses. It could also be shown that model improvements such as permafrost simulation and age-related decline of forest growth will further influence carbon storage in vegetation and soils. Further improvements should address these issues.

With the combined approach carbon fluxes are now merging significantly better to independent estimates. The considerable difference between the potential vegetation model and the constrained version concerning land cover, carbon fluxes and storage underlines the importance of including the effects of disturbance and human activities into vegetation models that usually are based on climate data input alone. In fact, carbon flux estimations based on potential vegetation alone are no longer sufficient for any political or scientific statement.

In summary, the current approach provides a more valuable tool for accounting carbon fluxes at large scales than the potential vegetation model, adding some more figures to the still uncertain and sparse pool of available global carbon cycle estimations. It is able to provide carbon cycle accounting on higher spatio-temporal resolution than obtained by inversion modelling. It expands upon the satellite-based modelling by considering biogeochemical processes. The findings concerning the dependence of the annual CO_2 growth rate on changes in soil respiration could demonstrate the importance of explicitly modelling soil carbon processes and its spatio-temporal dynamics. The presented analysis contributes to the understanding of the carbon cycle behaviour under climatic change as well as for anomalous climatic and natural events such as ENSO events or volcanic eruptions. Last, but not least, the results offer a

comprehensive data basis for analysis of global and regional carbon fluxes, which could only be touched for particular cases by the examples presented in this thesis. Finally, the current results might serve as a more realistic baseline to build upon for future projections which consequently are based on climate data input alone.

8. REFERENCES

Abrol, Y.P.I. & Ingram, K.T. (1996), “Effects of higher day and night temperatures on growth and yields of some crop plants.” In: Bazzaz, F.E. (ed.), *Global Climate Change and Agricultural Production*: 123-140.

Achard, F., Eva, H.D., Stibig, H.J. et al. (2002), “Determination of deforestation rates of the world’s humid tropical forests.” *Science* **297**: 999-1002.

Ajtay G.L., Ketner, P. & Duvugneaud P. (1979), “Terrestrial primary production and phytomass.” In: Bolin B., Degens, E.T., Kempe, S. & Ketner, P (eds.), *The Global Carbon Cycle* – SCOPE Report No. 13, Wiley, New York: 129-181.

Albertz, J. (1991), „Grundlagen der Interpretation von Luft- und Satellitenbildern: Eine Einführung in die Fernerkundung.“ Wissenschaftliche Buchgesellschaft, Darmstadt.

Alexander, M.A. & Scott, J.D. (2002), “The influence of ENSO on air-sea interaction in the Atlantic.” *Geophys. Res. Lett.* **29** (14), doi: 10.1029/2001GL014347, 4 pp.

Amthor J.S., and members of the Ecosystem Working Group (1998), “Terrestrial Responses to Global Change.” ORNL Report, Oak Ridge National Laboratory, TN, USA.

Andreae, M.O. & Merlet, P. (2001), “Emission of trace gases and aerosols from biomass burning.” *Glob. Biogeochem. Cycl.* **15** (4): 955-966.

Angert, A., Biraud, S., Bonfils, C., Henning, C.C., Buermann, W., Pinzon J., Tucker, C.J. & Fung, I. (2005), “Drier summers cancel out the CO_2 uptake enhancement induced by warmer springs.” *PNAS* **102** (31): 10823–10827

Angert, A., Biraud, S., Bonfils, C., Biermann, W. & Fung, I. (2004), “CO_2 seasonality indicates origins of post-Pinatubo sink.” *Geophys. Res. Lett.* **31** (L11103): doi: 10.1029/ 2004GL019760.

Anyamba, A., Tucker, C. & Eastman, J.R. (2001), “NDVI patterns over Africa during the 1997/98 ENSO warm event.” *Int. J. Remote Sensing* **22** (10): 1847-1859.

Asner, G.P., Townsend, A.R. & Braswell, B.H. (2000), “Satellite observation of El Niño effects on Amazon forest phenology and productivity.” *Geophys. Res. Lett.* **27** (7): 981– 984.

Asrar, G., Fuchs, M. ,Kanemasu, E.T. & Hatfield, J.H. (1984), "Estimating absorbed photosynthetic radiation and leaf area index from spectral reflectance in wheat." *Agron. J.* **76**: 300-306.

Asrar, G., Kanemasu, E.T. & Yoshida, M. (1985), “Estimates of leaf area index from spectral reflectance of wheat under different cultural practices and solar angle.” *Remote Sens. Environ.* **17**: 1-11.

Asrar, G., Myneni, R.B. & Choudhury, B.J. (1992), “Spatial heterogeneity in vegetation canopies and remote sensing of absorbed photosynthetically active radiation: a modeling study.” *Rem. Sens. Environ.* **41**: 85-103.

Aumont, O., Orr, J.C., Monfray, P. Et al. (2001), “Riverine-driven interhemispheric transport of carbon.” *Glob. Biogeochem. Cycl.* **15**: 393-405.

Bacastow, R.B. (1976), “Modulation of atmospheric carbon dioxide by the Southern Oscillation.“ *Nature* **261**: 116-118

Bach, H. (1998), “Yield estimation of corn based on miltitemporal LANDSAT-TM data as input for an agrometeorological model.” *Pure Appl. Opt.* **7:** 809-825

Baes C.F., Goeller, H,E,, Olson, J,S. & Rotty, R.M. (1976), “The Global Carbon Dioxide Problem.” ORNL Report, Oak Ridge National Laboratory, TN, USA.

Baes, C.F., Goeller, H.E., Olson, J.S. & Rotty, R.M. (1977), “Carbon dioxide and climate – The uncontrolled experiment.” *Am. Scient.* **65**: 310−320.

Ball, J.T., Woodrow, I.E. & Berry, J.A. (1986), “A model predicting stomatal conductance and its contribution to the control of photosynthesis under different environmental conditions.” In: Biggins, J (ed.), *Progress in Photosynthesis Research* **4**: 221-224.

Baret, F. & Guyot, G. (1991), “Potentials and limits of vegetation indices for LAI and APAR assessment.” *Remote Sens. Envir.* **35**: 161-173.

Barford, C. C., Wofsy, S.C., Goulden, M.I., Munger, J.W., Hammond Pyle, E., Urbanski, S.P., Hutyra, L., saleska, S.R., Fitzjarrald, D. & Moore, K. (2001), “Factors controlling long- and short term sequestration of atmospheric CO_2 in a mid-latitude forest.” *Science* **294**: 1688-1691.

Barret, E. C. & Curtis, L.F. (1992), "*Introduction to Environmental Remote Sensing. 3rd Edition.“* Chapman & Hall, London/New York.

Bartalev, S.A., Belward, A.S., Erchov, D.V. & Isaev, A.S. (2003), “A new SPOT4-VEGETATION derived land cover map of Northern Eurasia.” *Int. J. Rem. Sens.* **24** (9): 1977-1982.

Battle, M., Bender, M.L., Tans, P.P., white, J.W.C., Ellis, J.T., Conway, T. & Francey, R.J. (2000), “Global carbon sinks and their variability inferred from atmospheric 0_2 and $delta_{13}C$.” *Science* **287** (31 mar): 2467-2470.

Bazilevich, N. L. (1974), “Geochemical work of the living substance of earth and soil formation.” In: Cave, A.J. (ed.), *Proc. 1st Int. Congress of Ecology,* The Hague: 47−51.

Bazilevich, N.I. & Rodin, R. (1971), “Geographical aspects of biological productivity.” *Soviet. Geography* **12**: 293-317.

Bergner, B., Johnstone, J. & Treseder, K.K. (2004), “Experimental warming and burn severity alter soil CO2 flux and soil functional groups in a recently burned boreal forest.” *Global Change Biology* **10** (12): 1996, doi: 10.1111/j.1365-2486.2004.00868.x

Black, R. & Bliss L. (1980),” Reproductive ecology of Picea mariana (Mill.) at the tree line near Inuvik, Northwest Territories, Canada.” *Ecological Monographs* **50** (3): 331–354.

Bogaert, J., Zhou, L., Tucker, C.J., Myneni, R.B. & Ceulemans, R. (2002), “Evidence for a persistent and extensive greening trend in Eurasia inferred from satellite vegetation index data.” *J. Geophys. Res.* - 107: D11: 10.1029/2001JD001075.

Bohn, H.L. (1976), “Estimate of organic carbon in world soils.“ *J. Am. Soil Sci. Soc.* **40**: 468−470

Bolin, B. (1970), “The carbon cycle.” *Scientific American* **223** (3): 136-146.

Bolin, B., Degens, E.T., Duvigneaud, P. & Kemp, S. (1979), “The global biogeochemical carbon cycle.” In: Bolin, B., Degens, E.T., Kempe, S. & Ketner, P. (eds.), *The Global Carbon Cycle*, SCOPE Report No. 13, Chichester, Wiley: 1-53.

Bonan, G. & Shugart, H. (1989), “Environmental factors and ecological processes in boreal forests.” *Annual Review of Ecology and Systematics* **20**: 1–28.

Bonan, G.B. (1995), “Land-atmosphere interactions for climate system models: coupling biophysical, biogeochemical, and ecosystem dynamical processes.” *Remote Sens. Environ.* **35**: 161-173.

Bopp, L., Le Quéré, C., Heimann, M. & Manning, A.C. (2002), “Climate induced oceanic oxygen fluxes: implications for the contemporary carbon budget.” *Glob. Biogeochemical Cycles* **16** (2): 10.1029/2001gb001445.

Botta, A., Ramankutty, N. & Foley, J. (2002), “Long-term variations of climate and carbon fluxes over the Amazon basin.” *Geophys. Res. Lett.* **29** (9): 10.1029/2002GL013607.

Botta, A., Viovy, N., Ciais, P., Friedlingstein, P. & Monfray, P. (2000), “A global prognostic scheme of leaf onset using satellite data.” *Global Change Biology* **6**: 709-725.

Bousquet, P., Ciais, P., Peylin, P., Ramonet, M. & Monfray, P. (1999), “Inverse modeling of annual atmospheric CO_2 sources and sinks. 1. Method and control inversion.” J. *Geophys. Res. - Atmospheres* **104** (D21): 26,161 - 26,178.

Bousquet, P., Peylin, P., Ciais, P., Le Quéré, C., Friedlingstein, P., Tans, P.P. (2000), "Regional changes in carbon dioxide fluxes of land and oceans since 1980." *Science* **290**: 1342-1346.

Bowen, H.J.M. (1966), "Trace elements in biochemistry." New York. Academic.

Box, E.O., Holben, B.N. & Kalb, V. (1989), "Accuracy of the AVHRR vegetation index as a predictor of biomass, primary productivity, and net CO_2 flux." *Vegetatio* **80**: 71-89

BP (2004), "Statistical Review of World Energy 2004." Online data: http://www.bp.com/sectiongenericarticle.do?categoryId=2012411&contentId=2018340

Bradley, R.S., Diaz, H.F., Kiladis, G.N. & Eischeid, J.K. (1987), "ENSO signal in continental temperature and precipitation records." *Nature* **327**: 497-501.

Braswell, B. H., Schimel, D.S., Linder, E. & Moore, B. (1997), "The response of global terrestrial ecosystems to interannual temperature variability." *Science* **278** (31.Oct.): 870-872.

Broecker, W. S. et al. (1979), "Fate of fossil fuel carbon dioxide and the global carbon budget." *Science* **206**: 409-418

Brown, O. W., Brown, J.W. & Evans, R.H. (1985), "Calibration of Advanced Very High Resolution Radiometer observations." *J. Geophys. Res. - Atmospheres* **90**: 11,667 - 11,677.

Brown, S. & Lugo, A.E. (1982), "The storage and production of organic matter in tropical forests and their role in the global carbon cycle." *Biotropica* **14**: 161-187.

Brown, S. (1997), "Estimating Biomass and Biomass Change of Tropical Forests: a Primer." *FAO Forestry Paper* – 134, Rome.

Buchmann, N., Schulze, E.-D. (1999), "Net CO_2 and H_2O fluxes of terrestrial ecosystems." *Global Biogeochem. Cycles* **13** (3): 751-760.

Buermann, W., Anderson, B., Tucker, C.J., Dickinson, R.E., Lucht, W., Potter, C.S. & Myneni, R.B. (2003), "Interannual covariability in Northern Hemisphere air temperatures and greenness associated with El Niño-Southern Oscillation and the Arctic Oscillation." *J. Geophys. Res. - Atmospheres* **108** (D13): Art. No. 4396.

Buitenhuis, E.T.C., Le Quéré, C., Aumont, O., Bunker, A., Hirst, A., Ikeda, T., O'Brien, T. & S. Piontkowski (*in prep.*), "Biogeochemical fluxes mediated by mesozoic plankton." to be submitted to *Glob. Biogeochem. Cycl.,* online data access: http://www.bgc-jena.mpg.de/~corinne.lequere/interannual/PISCEST_globalflx.ann

Bureau of Meteorology of the Australian Government (2005), "Southern Oscillation Index – monthly values." data access: ftp.bom.gov.au

Bussieres, N., de Seve, D. & Walker, A.E. (2002), "Evaluation of MODIS snow cover products over Canadian regions." IEEE *Geoscience and Remote Sensing Symposium IGARSS* 2002, Vol. 4: 2302-2304

Cao, M. K. & Woodward, F.I. (1998b), "Net primary and ecosystem productions and carbon stocks of terrestrial ecosystems and their response to climate change." *Global Change Biology* **4**: 185-198.

Cao, M., Prince, S.D. & Shugart, H.H. (2002), "Increasing terrestrial carbon uptake from the 1980s to the 1990s with changes in climate and atmospheric CO_2." *Glob. Biogechem. Cycl.* **16** (4): doi: 10.1029/2001GB001553.

Cao, M., Prince, S.D., Small, J. & Goetz, S.J. (2004), "Remotely sensed interannual variations and trends in terrestrial net primary productivity 1981-2000." *Ecosystems* **7**: 233-242.

Cao, M.K. & Woodward, F.I. (1998a), "Dynamic responses of terrestrial ecosystem carbon cycling to global climate change." *Nature* **393**:249-252.

Cardille, J. A., Foley, J. A. & Costa, M.H. (2002), "Characterizing patterns of agricultural land use in Amazonia by merging satellite classifications and census data." *Glob. Biogeochem. Cycl.* **16** (3): 10.1029/2000GB001386.

Carlson, T.N. & Ripley, D.A. (1997), "On the relation between NDVI, fractional vegetation cover, and leaf area index." *Rem. Sens. Environ.* **62** (3): 241-252.

Carvalho, J.A. Jr., Higuchi, N., Araujo, T.M. & Santos, J.C. (1998), "Combustion completeness in a rainforest clearing experiment in Manaus, Brazil." *J. Geophys. Res. – Atmospheres* **103**: 13195-13199.

Chang, J.T. & Wetzel, P.J. (1991), "Effects of spatial variation of soil moisture and vegetation on the evolution of a prestorm environment: A numerical case study." *Monthly Weather Review* **119**: 1368-1390.

Chen, J.M. & Cihlar, J. (1996), "Retrieving leaf area index of boreal conifer forests using landsat TM images." *Remote Sens. Environ.* **55**: 153-162.

Churkina, G. & Running, S.W. (1998), "Contrasting controls on the Estimated Productivity of Global Terrestrial Biomes." *Ecosystems* **1** (2): 206-215.

Ciais, P., Denning, A.S., Tans, P.P., Berry, J.A., Randall, D.A., Collatz, G.J., Sellers, P.J., White, J.W.C., Trolier, M., Meijer, H.A.J., Francey, R.J., Monfray, P. & Heimann, M. (1997), "A three-dimensional synthesis study of d18O in atmospheric CO_2. - 1. Surface fluxes." *J Geophys Res - Atmospheres* **102** (D5): 5857-5872.

Ciais, P., Tans, P.P., Trolier, M., White, J.W.C. & Francey, R.J. (1995), "A large northern hemisphere terrestrial CO_2 sink indicated by the 13C/12C ratio of atmospheric CO_2." *Science* **269** (25. Aug.): 1098-1102.

Cihlar, J., Chen, J. & Li, Z. (1997), "Seasonal AVHRR mulitchannel data sets and products for studies of surface-atmosphere interactions." *J. of Geophysical Research* **102** (D24): 29.625-29.640.

Cihlar, J., St Laurent, L. & Dyer, J.A. (1991), "Relation between the normalized vegetation index and ecological variables." *Remote Sens. Envir.* **35**: 279 - 298.

Cogley, J.G. (1998), "GGHYDRO—Global Hydrographic Data, Release 2.2." Trent Climate Note 98-1, Department of Geography, Trent University, Peterborough, Ont., Canada

Cohen, W.B. & Justice, C.O. (1999), "Validating MODIS terrestrial ecology products: Linking in situ and satellite measurements." *Rem. Sens. Environ.* **70** (1): 1-3.

Collatz, G. J., Ball, J.T., Grivet, C. et al. (1991), "Physiological and environmental regulation of stomatal conductance, photosynthesis and transpiration: a model that includes a laminar boundary layer." *Agricultural and Forest Meteorology* **54**: 107-136.

Collatz, G., J., Ribas-Carbo, M. & Berry, J.A. (1992), "Coupled photosynthesis-stomatal conductance model for leaves of C4 plants." *Australian Journal of Plant Physiology* **19**: 519-538.

Conway, T. J., Tans, P.P., Waterman, L.S., Thoning, K.W., Kitzis, D.R., Masarie, K.A. & Zhang, N. (1994), "Evidence for interannual variability of the carbon cycle from the National Oceanic and Atmospheric Administration/Climate Monitoring and Diagnostics Laboratory Global Air Sampling Network." *J. Geophys. Res.* **99** (D11): 22,831-22,855.

Cox P.M., Betts R.A., Jones C.D., Spall S.A. & Totterdell I.J. (2000), "Acceleration of global warning due to carbon-cycle feedbacks in a coupled climate model." *Nature* **48**: 184-187.

Cox, P. (2001), „Description on the TRIFFID Dynamic Global Vegetation Model." *Technical Report* **24**, Hadley Centre, Met Office.

Cox, P.M., Betts, R.A., Bunton, C.B., Essery, R.L.H., Rowntree, P.R. & Smith, J. (1999), "The impact of new land surface physics on the GCM simulation of climate and climate sensitivity." *Clim. Dyn.* **15**: 183-203.

Cox, P.M., Betts, R.A., Jones, C.D., Spall, S.A. & Totterdell, I.J. (2000), "Acceleration of global warming due to carbon-cycle feedbacks in a coupled climate model", *Nature* **408**: 184-187.

Cox, P.M., Huntingford, C. & Harding, R.J. (1998), "A canopy conductance and photosynthesis model for use in a GCM land surface scheme." *J. Hydrol.* **212-213**: 79-94.

Cramer, W., Bondeau, A., Schaphoff, S., Lucht, W., Smith, B. & Sitch, S. (2004), "Tropical forests and the global carbon cycle: Impacts of atmospheric CO_2, climate change and rate of deforestation." *Phil Trans Roy Soc B* **359 (35)**:331-343, doi: 10.1098/rstb. 2003.1428

Cramer, W., Bondeau, A., Woodward, F.I., Prentice, I.C., Betts, R.A., Brovkin, V., Cox, P.M, Fisher, V., Foley, J.A., Friend, A.D., Kucharik, C., Lomas, M.R., Ramankutty, N., Sitch, S., Smith, B., White, A. & Young-Molling, C. (2001), "Global response of terrestial ecosystem structure and function to CO_2 and climate change: results from six dynamic global vegetation models." *Global Change Biology* **7**: 357-373.

Cramer, W., Kicklighter, D.W., Bondeau, A., Moore, B., Churkina, G., Nemry, B., Ruimy, A., Schloss, A.L. and the participants of the Potsdam NPP model intercomparison (1999), "Comparing global models of terrestrial net primary productivity (NPP): overview and key results." *Global Change Biology* **5** (Supp.1): 1-15.

Curtis, P.S. & Wang, X. (1998), " A meta-analysis of elevated CO_2 effects on woody plant mass, form, and physiology." *Oecologia* **133**: 299-313

Dadhwal, V. K., Shah, A.K. & Vora, A.B. (1996), "Changes in carbon flow through Indian agroecosystem between 1950-51 and 1985-86." *J. of Environmental Biology* **17** (4): 311-316.

Dai, A. & Wigley, T.M.L. (2000), "Global patterns of ENSO-induced precipitation. *Geophys. Res. Lett.* **27**: 1283-1286.

Dargaville, R., McGuire, A.D. & Rayner, P. (2002), "Estimates of large-scale fluxes in high latitudes from terrestrial biosphere models and an inversion of atmospheric CO_2 measurements." *Climatic Change* **55**(1-1): 273-285. Suchen und nachschauen!

Davey, M.K. & Anderson, D.L.T. (1999), "A comparison of the 1997/98 El Niño with other such events." *Weather* **54**: 295-302.

DeFries, R.S., Hansen, M.C., Townshend, J.R.G., Janetos, A.C. & Loveland, T.R. (2002), "A new global 1-km dataset of percentage tree cover derived from remote sensing." *Global Change Biology* **6** (2): 247-254, doi:10.1046/j.1365-2486.2000.00296.x

DeFries, R.S., R.A. Houghton, M.C. Hansen, C.B. Field, D. Skole, et al, (2002b): Carbon emissions from tropical deforestation and regrowth based on satellite observations for the 1980s and 1990s. Proc. Natl. Acad. Sci. U.S.A., 99(22), 14256-14261.

Dewar, R.C. (1996), "The correlation between plant growth and intercepted radiation: an interpretation in terms of optimal plant nitrogen content." *Annals of Botany* **78** (1): 125-126.

Diaz, H.F. & Markgraf, V. (1992), "El Niño: Historical and Paleoclimatic Aspects of the Southern Oscillation." Cambridge University Press, 476 pp.

Diaz, H.F., Hoerling, M.P. & Eischeid, J.K. (2001), "ENSO variability, teleconnections, and climate change." *Int. J. Climatol.* **21**: 1845-1862.

Dickinson, R. E. (2000), "How coupling of the atmosphere to ocean and land helps determine the timescales of interannual variability of climate." *J. Geophys. Res.* **105**(D15): 20,115 - 20,119.

Dixon, R.K., Brown, S., Houghton, R.A., Solomon, A.M., Trexler, M.C. & Wisniewski, J. (1994), " Carbon pools and flux of global forest ecosystems." *Science* **263**:185-190.

Döll, P. & Siebert, S. (2002), "Global modeling of irrigation water requirements." *Water Resources Research* **38** (4): 8-1, doi: 10.1029/2001WR000355

Dong, J., Kaufmann, R.K., Myneni, R.B., Tucker, CJ., Kauppi, P.E., Liski, J., Buermann, W., Alexeyev, V. & Hughes, M.K. (2003), "Remote Sensing estimates of boreal and temperate forest woody biomass: carbon pools, sources and sinks." *Remote Sens. Envir.* **84**: 393-410.

Dufresne, J.L., Friedlingstein, P., Berthelot, M., Bopp, L., Ciais, P., Fairhead, L., Treut, Le H. & Monfray, P. (2002), "On the magnitude of positive feedback between future climate

change and the carbon cycle", *Geophys. Res. Lett.* **29** (10): 1405, doi: 10.1029/2001GL013777.

Eklundh L. & Olsson L. (2003), "Vegetation index trends for the African Sahel 1982-1999", *Geophys. Res. Lett.* **30**: 131-134.

Eklundh, L. & Sjöström, M. (2005), "Analysing vegetation changes in the Sahel using sensor data from Landsat and NOAA." Talk held at the 31st International Symposium on Remote Sensing of Environment, June, 20-24, St. Petersburg.

Elliot, W.P., Angell, J.K. & Thoning, K.W. (1991), "Relation of atmospheric CO_2 to tropical sea and air temperatures and precipitation." *Tellus* **43B**: 144-155, 1991.

Eltahir, E. A. B. & Wang, G. (1999), "Nilometers, El Niño and climate variability." *Geophys. Res. Lett.* **26** (4): 489-492.

Enting, I. G. (2002), "Inverse Problems in Atmospheric Constituent Transport." Cambridge University Press.

Esser, G. (1987), "Sensitivity of global carbon pools and fluxes to human and potential climatic impacts." *Tellus* **39B**: 245-260.

Esser, G. (1994), „Eingriffe der Landwirtschaft in den Kohlenstoffkreislauf." Landwirtschaft, Bd. 1. Enquete-Kommission 'Schutz der Erdatmosphäre' des Dt. Bundestags.

Esser, G., Hoffstadt, J., Mack, F. & Wittenberg, U. (1994), "High Resolution Biosphere Model, Documentation, Model Version 3.0." *Mitt. Inst. Pflanzenökol. der JLU Gießen* **2**: 68.

Fan, S., Gloor, M., Mahlman, J., Pacala, S., Sarmiento, J., Takahashi, T. & Tans, P. (1998), "A large terrestrial carbon sink in North America implied by atmospheric and oceanic carbon dioxide data and models." *Science* **282**: 442-446.

FAO (1991), "The digitized soil map of the world (Release 1.0)," **Vol. 67/1**: Food and Agriculture Organization of the United Nations.

FAO (1992), "The Forest Resources of the Tropical Zone by Main Ecological Regions." by Forest Resources Assessment 1990 Project, United Nations Conference on Environment and Development, Rio de Janeiro.

FAO (1997), "State of the world's forests." Rome, Italy.

Farquhar, G. D. (1997), "Carbon dioxide and vegetation." *Science* **278**: 1411.

Farquhar, G. D., Lloyd, J., Taylor, J.A., Flanagan, L.B., Syvertsen, J.P., Hubick, K.T., Wong, S.C. & Ehleringer, J.R. (1993), "Vegetation effects on the isotope composition of oxygen in atmospheric CO_2." *Nature* **363** (3 June): 439-442.

Farquhar, G.D., von Caemmerer, S. & Berry, J.A. (1980), "A biochemical model of photosynthetic CO_2 assimilation in leaves of C3 plants." *Planta* **149**: 78-90.

Feely, R. A., Sabine, C.L., Lee, K., Berelson, W., Kleypas, J., Fabry, V.J. & Millero, F.J. (2004), "Impact of anthropogenic CO_2 on the $CaCO_3$ system in the oceans." *Science* **305**: 362-366.

Field, C. B., Jackson, R.B. & Mooney, H.A. (1995), "Stomatal responses to increased CO_2: implications from the plant to the global scale." *Plant Cell and Environment* **18**: 1214-1225.

Field, C. B., Randerson, J.T. & Malmström, C. (1995), "Global Net Primary Production: Combining Ecology and Remote Sensing." *Remote Sens. Envir.* **51**: 74-88.

Field, C.B., Behrenfeld, M.J., Randerson, J.T, Falkowski, P. (1998), "Primary production of the biosphere: Integrating terrestrial and oceanic components." *Science* **81**:237-240.

Flato, G.M. & Boer, G.J. (2001), "Warming asymmetry in climate change simulations", *Geophysical Research Letters* **28**: 195-198.

Foley, J. A., Botta, A., Coe, M.T. & Costa, M.H. (2002), "El Niño - Southern Oscillation and the climate, ecosystems, and rivers of Amazonia." *Glob. Biogeochemical Cycles* **16** (4), doi:

10.1029/2002GB001872.

Foley, J. A., Prentice, I.C., Ramankutty, N., Levis, S., Pollard, D., Sitch, S. & Haxeltine, A. (1996), "An integrated biosphere model of land surface processes, terrestrial carbon balance, and vegetation dynamics." *Glob. Biogeochem. Cycl.* **10** (4): 603-628.

Foley, J.A. (1994), "Net primary productivity in the terrestrial biosphere: The application of a global model." *J. Geophys. Res.* **99**: 20773-20783.

Folland, C. K., Karl, T.R., Christy, J.R., Clarke, R.A., Gruza, G.V., Jouzel, J., Mann, M.E., Oerlemans, J., Salinger, M.J. & Wang, S.W. (2001), "Observed climate variability and change. *Climate Change 2001: The Scientific Basis* (IPCC)." T. Houghton (ed.), New York, Cambridge University Press: 183-237.

Food and Agriculture Organization (FAO) (2001), "FAO Statistical Databases (FAOSTAT)." CD-ROM, Rome.

Francey, R.J., Allison, C.E., Trudinger, C.M., Rayner, P.J., Enting, I.G. & Steele, L.P. (2001), "The interannual variation in global atmospheric delta13C and its link to net terrestrial exchange." Paper pres. 6th International Carbon Dioxide Conference, Sendai, Japan, 2001.

Friedl, M.A., Melver, D.K., Hodges, J.C.F., Zhang, X.Y., Muchoney, D., Strahler, A.H., Woodcock, C.E., Gopal, S., Schneider, A. & Cooper, A. (2002), "Global land cover mapping from MODIS algorithms and early results." *Rem. Sens. Environ.* **83** (1-2): 287-302.

Friedl, M.A., Muchoney, D., McIver, D., Gao, F., Hodges, J.C.F. & Strahler, A.H. (2000), "Characterization of North American land cover from NOAA-AVHRR data using the EOS MODIS land cover classification algorithm." *Geophys. Res. Lett.* **27**: 977-989.

Friedlingstein, P., Dufresne, J.-L., Cox, P.M. & Rayner, P. (2003), "How positive is the feedback between climate change and the carbon cycle?" *Tellus* **55B** (2): 692-700.

Friedlingstein, P., Fung, I.Y., Holland, E.A., John, J.G., Brasseur, G.P., Erickson, D.J. & Schimel, D.S. (1995), "On the contribution of the biospheric CO_2 fertilization to the missing sink." *Glob. Biogeochem. Cycl.* **9**: 541-556

Friend, A. D., Stevens, A.K., Knox, R.G. & Cannell, M.G.R. (1997), "A process-based, terrestrial biosphere model of ecosystem dynamics (Hybrid v3.0)." *Ecological Modelling* **95**: 249-287.

Friend, A.D. & White, A. (2000), "Evaluation and analysis of a dynamic terrestrial ecosystem model under preindustrial conditions at the global scale." *Global Biogeochem. Cycles* **14**: 1173-1190.

Frolking, S., McDonald, K., Kimball, J., Way, J., Zimmermann, R. & Running, S. (1999), "Using the space-borne NASA scatterometer (NSCAT) to determine the frozen and thawed seasons." *J. Geophys. Res.* **104** (D22): 27895– 27907.

Fung, I. (2000), "Variable Carbon Sinks." *Science* **290** (5495): 1313.

Gao, F., C. B. Schaaf, A. H. Strahler, A. Roesch, W. Lucht, and R. Dickinson (2005), "MODIS bidirectional reflectance distribution function and albedo Climate Modeling Grid products and the variability of albedo for major global vegetation types." *J. Geophys. Res.* **110** D01104, doi:10.1029/2004JD005190.

Gerten, D., Bondeau, A., Hoff, H., Lucht, W., Schaphoff, S. & Smith, P. (2004b), "Assessment of ‚green' water fluxes with a Dynamic Global Vegetation model." in: Webb, B., Arnell, N., Onof, C., MacIntyre, N., Gurney, R. & Kirby, C. (eds.), *Hydrological Science and Practice for the 21st century*. **Vol 1**, British Hydrological Society: 29-35.

Gerten, D., Hoff, H., Bondeau, A., Lucht, W., Smith, P., Zaehle, S. (2005), "Contemporary "green" water flows: simulations with a dynamic global vegetation and water balance model." *Physics and Chemistry of the Earth* **30**: 334–338.

Gerten, D., Schaphoff, S. & Lucht, W. (*2006*), "Potential future changes in water limitation of the terrestrial biosphere." *Climatic Change*, *in press.*

Gerten, D., Schaphoff, S., Haberlandt, U., Lucht, W. & Sitch, S. (2004a), “Terrestrial vegetation and water balance – hydrological evaluation of a dynamic global vegetation model.“ *J. Hydrology* **286**: 249-270.

Giglio, L., Descloitres. J., Justice, C.O. & Kaufman, Y. J. (2003), “An Enhanced Contextual Fire Detection Algorithm for MODIS.” *Remote Sensing of Environment* **87**: 273–282

Gobron, N., Aussedat, A., Pinty, B., Taberner, M. & Verstraete, M. (2004), “Medium Resolution Imaging Spectrometer (MERIS) – Level 2 Land Surface Products Algorihtm Theoretical Basis Document.” *JRC Publications* No. **EUR 21387** EN, Ispra, Italy

Goetz, S. J., Prince, S.D., Small, J. & Gleason, A.C.R. (2000), “Interannual variability of global terrestrial primary production: Results of a model driven with satellite observations.” *J. Geophys. Res.* **105** (D15): 20.077-20.091.

Goldewijk, K.K., Van Minnen, J.G., Kreileman, G.J.J., Vloebeld, M. & Reemans, R. (1994), “Simulating the carbon flux between the terrestrial environment and the atmosphere.” *Water, Air and Soil Pollution* **76**: 199-230.

Goodale, C.L., Apps, M.J., Birdsey, R.A., Field, C.B., Heath, L.S., Houghton, R.A., Jenkins, J.C., Kohlmaier, G.H., Kurz, W., Liu, S.R., Nabuurs, G.J., Nilsson, S. & Shvidenko, A.Z. (2002), “Forest carbon sinks in the Northern Hemisphere.” *Ecological Applications* **12** (3): 891-899.

Gordon, C., Cooper, C., Senior, C.A., Banks, H.T., Gregory, J.M., Johns, T.C., Mitchell, J.F.B. & Wood, R.A. (2000), “The simulation of SST, sea ice extents and ocean heat transports in a version of the Hadley Centre coupled model without flux adjustments”, *Climate Dynamics* **16**: 147-168.

Gordon, H.R., Brown, J.W. & Evans, R.H. (1988), "Exact Rayleigh scattering calculations for use with the Nimbus-7 coastal zone color scanner." *Applied Optics* **27**: 2111-2122.

Goudriaan, J & Ketner, P. (1984), “Are land biota a source or a sink for CO2?” Paper presented at the C.E.C. Symposium "Interaction between climate and biosphere. Osnabruck 1983. In: *Progress In Biometeorology* **3**: 247-252.

Goulden, M. L., Munger, J. W., Fan, S. M., Daube, B. C. & Wofsy, S. C. (1996), “Exchange of carbon dioxide by a deciduous forest: Response to interannual climate variability.” *Science* **271**: 1576–1578.

Goulden, M.L., Wofsy, S.C., Harden, J.W., Trumbore, E., Crill, P.M., Gower, S.T., Fries, T., Daube, B.C., Fan, S.-M., Sutton, D.J., Bazzaz, A. & Munger, J.W. (1998), “Sensitivity of boreal forest carbon balance to soil thaw.” *Science* **279**: 214-217.

Gower, S.T., Kucharik, C.J. & Norman, J.M. (1999), “Direct and indirect estimation of leaf area index, fAPAR, and net primary production of terrestrial ecosystems.” *Rem. Sens. Environ.* **70**: 29-51

Grace, J., Lloyd, J., McIntyre, J., Miranda, A.C., Meir, P., Miranda, H., Nobre, C., Moncrieff, J.B., Massheder, J., Malhi, Y., Wright, I.R. & Gash, J. (1995), “ Carbon dioxide uptake by an undisturbed tropical rainforest in South West Amazonia 1992-1993.” *Science* **270**: 778-780

Graf, H.-F., Kirchner, I., Robock, A. & Schult, I. (1993), ”Pinatubo eruption winter climate effects: Model versus observations.” *Clim. Dyn.* **9**: 81–93.

Groisman, P.Y. (1992), “Possible regional climate consequences of the Pinatubo eruption: An empirical approach.” *Geophys. Res. Lett.* **19**: 1603–1606.

Gu, L., Baldocchi, D.D., Wofsy, S.C., Mnger, J.W., Michalsky, J.J., Urbanski, S.P. & Boden, T.A. (2003), “Response of a deciduous forest to the Mount Pinatubo eruption: enhanced photosynthesis.” *Science* **299**:2035-2038.

Gurney, K. R., Law, R.M., Denning, A.S., Rayner, P.J., Baker, D, Bousquet, P., Bruhwilerk L., Chen, Y.-H., Ciais, P., Fan, S., FungI, I.Y., Gloor, M., Heimann, M., Higuchi, K., JohnI, J., Maki, T., Maksyutov, S., Masariek, K., Peylin, P., Prather, M., Pak B.C., Randerson, J., Sarmiento, J., Taguchi, S., Takahashi, T. and C.-W. & Yuen (2002), “Towards robust

regional estimates of CO_2 sources and sinks using atmospheric transport models." *Nature* **415** (7.Feb.): 626-630.

Gurney, K. R., Law, R.M., Denning, A.S., Rayner, P.J., Pak, B.C., Baker, D., Bousquet, P., Bruhwiler, L., Chen, Y.-H., Ciais, Fung, I.Y., Heimann, M., John, J., Maki, T., Maksyutov, S., Peylin, P., Prather, M. & Taguchi, S. (2004), "Transcom 3 inversion intercomparison: Model mean results from the estimation of seasonal carbon sources and sinks." *Glob. Biogechemical Cycles* **18**(GB1010): doi: 10.1029/2003GB002111.

Gutman, G. & Ignatov, A. (1998), "The derivation of the green vegetation fraction from NOAA/AVHRR data for use in numerical weather prediction models." *Int. J. Rem. Sens.* **19** (8): 1533-1543.

Gutman, G. (1999), "On the use of long-term data of land reflectances and vegetation indices derived from the advanced very high resolution radiometer." *J. Geophys. Res.* **104**: 6241-6255.

Haberl, H., Erb, K.H., Krausmann, F., Loibl, W., Schulz, N. & Weisz, H. (2001), "Changes in ecosystem processes induced by land use: Human appropriation of aboveground NPP and its influence on standing crop in Austria." *Glob. Biogeochem. Cycl.* **15** (4): 929-942.

Hall, D.O. & Scurlock, J.M.O. (1993), "Biomass production and data." In: Hall, D.O. et al. (eds.), *Photosynthesis and Production in a Changing Environment*: a Field and Laboratory Manual. Chapman and Hall, London: 425-444.

Hall, F. G., Huemmrich, K.F., Goetz, S.J., Sellers, P.J. & Nickeson, J.E. (1992), "Satellite remote sensing of surface energy balance: success, failures, and unresolved issues in FIFE." *J.Geophys. Res.* **97**: 19,061-10,089.

Halpert, M.S. & Ropelewski, C.F. (1992), "Surface temperature patterns associated with the El Niño-Southern Oscillation." *J. Clim.* **5**: 577-593.

Hansen, J., Fung, I., Lacis, A., Rind, D., Lebedeff, S., Ruedy, R., Russell, G. & Stone, P. (1988), "Global climate changes as forecast by the Goddard Institute for Space Studies three-dimensional model." *J. Geophys. Res.* **93**: 9341–9364.

Hansen, J., Lacis, A., Ruedy, R. & Sato, M. (1992), "Potential Climatic Impact of Mount-Pinatubo Eruption." *Geophys. Res. Lett.* **19** (2): 215-218

Hansen, J., Ruedy, R., Sato, M. & Lo, K. (2002), "Global warming continues." *Science* **295**: 275.

Hansen, J., Ruedy, R., Sato, M., Imhoff, M., Lawrence, W., Easterling, D., Peterson, T. & Karl, T. (2001), "A closer look at United States and global surface temperature change." *J. Geophys. Res.* **106**: 23947.

Hansen, J., Sato, M., Ruedy, R., Lacis, A., Asamoah, K., Borenstein, S., Brown, E., Cairns, B., Caliri, G., Campbell, M., Curran, B., de Castro, S., Druyan, L., Fox, M., Johnson, C., Lerner, J., McCormick, M.P., Miller, R.L., Minnis, P., Morrison, A., Pandolfo, L., Ramberran, I., Zaucker, F., Robinson, M., Russell, P., Shah, M., Stone, P., Tegen, I., Thomason, L., Wilder, J. & Wilson, H. (1996), "A Pinatubo climate modeling investigation." In Fiocco, G., Fua, D. & Visconti, G. (eds.), *The Mount Pinatubo Eruption: Effects on the Atmosphere and Climate*. NATO ASI Series Vol. I 42, pp. 233-272. Springer-Verlag. Heidelberg, Germany.

Hansen, M.C., DeFries R.S., Townshend J.R.G., Sohlberg R., Dimiceli C. & Carroll M. (2002), "Towards an operational MODIS continuous field of percent tree cover algorithm: examples using AVHRR and MODIS data." *Remote Sensing of Environment* **83** (1): 303-319.

Hansen, M.C., DeFries, R.S., Townshend, J.R.G. & Sohlberg, R. (2000), "Global land cover classification at 1km spatial resolution using a classification tree approach." *Int. J. Remote Sens.* **21**: 1331-1364.

Haxeltine, A. & Prentice, I.C. (1996), "BIOME3: an equilibrium terrestrial biosphere model based on ecophysiological constraints, resource availability, and competition among plant functional types." *Glob. Biogeochem. Cycl.* **10**: 693-709.

Haxeltine, A., Prentice, I.C. & Cresswell, I.D. (1996), "A coupled carbon and water flux model to predict vegetation structure." *Journal of Vegetation Science* **7** (5651-666).

Heimann, M. & Keeling, C.D. (1989), A three-dimensional model of atmospheric CO_2 transport base don observed winds, 2, Model description and simulated tracer experiments. *Aspects of climate variability in the Pacific and Western Americas*. Washington, American Geophys. Union. **55:** 237-275.

Heimann, M. (2001), "Atmospheric inversion calculations performed for the IPCC Third Assessment Report." Chapter 3 (The carbon cycle and atmospheric CO_2), Jena.

Heimann, M., Esser, G., Haxeltine, A. et al. (1998), "Evaluation of terrestrial carbon cycle models through simulations of the seasonal cycle of atmospheric CO_2: First results of a model intercomparison study." *Glob. Biogeochem. Cycl.* **12** (1): 1-24.

Hicke, J. A., Asner, G.P., Randerson, J.T., Tucker, C., Los, S., Birdsey, R., Jenkins, J., Field, C. & Holland, E. (2002), "Satellite-derived increases in net primary productivity across North America, 1982-1998." *Geophys. Res. Lett.* **29** (10): 10.1029/2001GL013578.

Hickler, T., Eklundh, L., Seaquist, J.W., Smith, B., Ardö, J., Olsson, L., Sykes, M.T. & Sjöström, M. (2005), "Precipitation controls Sahel greening trend." *Geophys. Res. Lett.,* **32**, L21415, doi:10.1029/2005GL024370.

Hirst, A.C., Gordon, H.B. & O'Farrell, S.P. (1996), "Global warming in a coupled climate model including oceanic eddy-induced advection", *Geophys. Res. Lett.* **23**: 3361-3364.

Hoerling, M. P., A. Kumar & Zhong, M. (1997), "El Niño, La Niña, and the nonlinearity of their teleconnections." *J. Climate* **10**: 1769-1786.

Holben, B. & Justice, C. (1981), "An examination of spectral band ratioing to reduce the topographic effect on remotely sensed data." *Int. J. Rem. Sensing* **2**: 115-133.

Holland, E. A., et al. (1997), "Variations in the predicted spatial distribution of atmospheric nitrogen deposition and their impact on carbon uptake by terrestrial ecosystems." *J. Geophys. Res.* **102**: 15,849– 15,866.

Hollinger, D., Goltz, S., Davidson, E., Lee, J., Tu, K. & Valentine, H. (1999), "Seasonal patterns and environmental control of carbon dioxide and water vapour exchange in an ecotonal boreal forest." *Global Change Biology* **5**(8): 891–902.

Holmen, K. (1992), "The Global Carbon Cycle." In: Butcher, S., Charlson, R., Orians, G. & Wolfe, G. (eds.), *Global Biogeochemical Cycles*, London, Academic Press: 237-262.

Houghton, R A. (2000a), "A new estimate of global sources and sinks of carbon from land-use change." *EOS* **81** (suppl): 281.

Houghton, R.A (2003a), "Why are estimates of the terrestrial carbon balance so different?" *Global Change Biology* **9**: 500-509.

Houghton, R.A. (1999), "The annual net flux of carbon to the atmosphere from changes in land use 1850-1990." *Tellus* **51B**: 298-313.

Houghton, R.A. (2000b), "Interannual variability in the global carbon cycle." *J. Geophys. Res.* **105** (D15): 20,121-20,130.

Houghton, R.A. (2003b), "The Contemporary Carbon Cycle, in Treatise of Geochemistry." In: Schlesinger, W. & Duke, J (eds.), *Biogeochemistry* **8**, Elsevier.

Houghton, R.A. (2003c), "Revised estimates of the annual net flux of carbon to the atmosphere from changes in land use and land management 1850-2000." *Tellus* **55B**: 378-390.

Houghton, R.A., Davidson, E.A. & Woodwell, G.M. (1998), "Missing sinks, feedbacks, and understanding the role of terrestrial ecosystems in the global carbon balance." *Glob. Biogeochem. Cycl.* **12** (1): 25-34.

House, J. I., Prentice, I.C. & LeQuéré, C. (2002), "Maximum impacts of future reforestation and deforestation on atmospheric CO_2." *Global Change Biology* **8**: 1047-1052.

House, J. I., Prentice, I.C., Ramankutty, N., Houghton, R.A. & Heimann, M. (2003), "Reconciling apparent inconsistencies in estimates of terrestrial CO_2 sources and sinks." *Tellus* **55B**: 345-363.

House, J.I. & Hall, D.O. (1999), "Estimates of biomass and productivity." Http://www .savannas.net/savprod.htm

Huete A.; Didan K.; Miura T.; Rodriguez E.P.; Gao X.; Ferreira L.G. (2002), "Overview of the radiometric and biophysical performance of the MODIS vegetation indices." *Remote Sensing of Environment* **83** (1): 195-213.

Huete, A. R. (1988), "A Soil-adjusted vegetation index (SAVI)." *Remote Sens. Envir.* **25**: 295-309.

Hughes, J.K., Valdes, P.J. & Betts, R.A. (2004), "Dynamical properties of the TRIFFID Dynamic Global Vegetation Model." *Hadley Centre Technical Note* No. **56**, Met Office.

Huntingford, C., Cox, P. & Lenton, T. (2000), "Contrasting responses of a simple terrestrial ecosystem model to global change." *Ecol. Modell.* **134**: 41-58.

Hurrell, J.W. & Trenberth, K.E (1997), "Spurious trends in satellite MSU temperatures from merging different satellite records." *Nature* 386: 164-167, doi: 10.1038/386164a0

Hurrell, J.W. & Van Loon, H. (1997), "Decadal variations in climate associated with the North Atlantic Oscillation." *Clim. Change* **36** (3-4): 301-326.

Hurrell, J.W. (1995), "Decadal trends in the North Atlantic Oscillation and relationships to regional temperature and precipitation. *Science* **269**, 676-679.

IMAGE Team (2001), "The IMAGE 2.2 Implementation of the SRES Scenarios: A Comprehensive Analysis of Emissions, Climate Change and Impacts in the 21st Century." RIVM CD-ROM Publication 481508018. Bilthoven: National Institute for Public Health and the Environment.

IPCC (1994), "Climate Change 1994, Radiative Forcing of Climate Change and an Evaluation of the IPCC IS92 Emission Scenarios." J. T. Houghton, L. G. Meria Filho, J. Bruce, Hoesung Lee, B. A. Callander, E. Haites, N. Harris and K. Maskell (eds.) for the Intergovernmental Panel on Climate Change, Cambridge University Press, Cambridge, Great Britain

IPCC (2000), "Land Use, Land-Use Change, and Forestry. A special report of the IPCC." Cambridge, Cambridge University Press.

IPCC (2001), "Emmissions Scenarios - Summary for Policymakers." http://www.grida.no/climate/ipcc/spmpdf/sres-e.pdf, 27 pp.

Jackson, R.B., Canadell, J., Ehleringer, J.R., Mooney, H.A., Sala, O.E. & Schulze, E.D. (1996), "A global analysis of root distributions for terrestrial biomes." *Oecologia* 108 (3): 389-411

Jackson, R.B., Mooney, H.A. & Schulze, E.D. (1997), "A global budget for fine root biomass, surface area, and nutrient contents." *Proc. Natl. Acad. Sci. USA* 94: 7362-7366.

Jacob, F., Olioso, A., Weiss, M., Baret, F. &Hautecoeur, O. (2002), "Mapping short-wave albedo of agricultural surfaces using airborne PolDER data." *Rem. Sens. Environ.* **80** (1): 36-46.

James, M.E. & Kalluri, S.N.V. (1994), "The Pathfinder AVHRR land data set: An improved coarse resolution data set for terrestrial monitoring." *Int. J. Rem. Sensing* **15**: 3347-3363.

Janssens, I. A., Freibaier, A., Ciais, P., Smith, P., Nabuurs, G.J., Folberth, G., Schlamadinger, B., Hutjes, R.W.A., Ceulemans, R., Schulze, E.D., Valentini, R. & Dolman, A.J. (2003), "Europe's Terrestrial Biosphere Absorbs 7 to 12 % of European Anthropogenic CO_2 Emissions." *Science* **300**: 1538-1542.

Jarvis, P. & Jarvis, M. (1964), "Growth rates of woody plants." *Physiologia Plantarum* **17**(3): 654–666.

Jobbaggy E.G., Jackson R.B. (2000), "The vertical distribution of soil organic carbon and its relation to climate and vegetation." *Ecol. Appl.* **10**: 423 – 436.

Johnson, E.A. & Gutsell, S.L. (1994), “Fire frequency models, methods and interpretations.” *Advances in Ecological Research* **25**: 239–287.

Jones, C.D. & Cox, M.C. (2001), “Modeling the volcanic signal in the atmospheric CO_2 record.” *Glob. Biogeochem. Cycl.* **15** (2): 453-465.

Jones, C.D., Cox, P.M., Essery, R.L.H., Roberts, D.L. & Woodage, M.J. (2003), “Strong carbon cycle feedbacks in a climate model with interactive CO_2 and sulphate aerosols”, *Geophys. Res. Lett.* **30** (9): 1479, doi:10.1029/2003GL0 16867.

Jones, P. & Kelly, P. (1996), “The effect of tropical explosive volcanic eruptions on surface air temperature.” In: Fiocco, G., Fua, D. & Visconti, G. (eds.), *The Mount Pinatubo eruption*, NATO ASI Ser., Ser. **I** (42): 95-111.

Jones, P.D., Jónsson, T. & Wheeler, D. (1997), “Extension to the North Atlantic Oscillation using early instrumental pressure observations from Gibraltar and South-West Iceland.” *Int. J. Climatol.* **17**: 1433-1450.

Joos, F., Prentice, I.C., Sitch, S., Meyer, R., Hooss, G., Plattner, G-K., Gerber, S. & Hasselmann, K. (2001), “Global warming feedbacks on terrestrial carbon uptake under the Intergovernmental Panel on Climate Change (IPCC) emission scenarios”, *Glob. Biogeochem. Cycl.* **15**: 891-907.

Justice C.O., Giglio L., Korontzi S., Owens J., Morisette J.T., Roy D., Descloitres J., Alleaume S., Petitcolin F. & Kaufman Y. (2002), “The MODIS fire products.” *Remote Sensing of Environment* **83** (1): 244-262

Justice, C.O., Townshend, J.R.G., Holben, B.N. & Tucker, C.J. (1985), "Analysis of the phenology of global vegetation using meteorological satellite data." *Int. J. Rem. Sensing* **6**: 1271-1318.

Justice, C.O., Vermote, E., Townshend, J.R.G., Defries, R., Roy, D.P., Hall, D.K., Salomonson, V.V., Privette, J.L., Riggs, G., Strahler, A., Lucht, W., Myneni, R.B., Knyazikhin, Y., Running, S.W., Nemani, R.R., Zhengming, W., Huete, A.R., van Leeuwen, W., Wolfe, R.E., Giglio, L., Muller, J., Lewis, P. & Barnsley, M.J. (1998), “The Moderate Resolution Imaging Spectroradiometer (MODIS): land remote sensing for global change research.” *IEEE Trans. Geosc. Remote Sensing* **36** (4): 1228-1249

Kaduk, J., Heimann, M. (1996), “Assessing the climate sensitivity of the global terrestrial carbon cycle model SILVAN.” *Phys. Chem. Earth* **21**(5-6): 529-535.

Kaplan, J. O. (2001), “Geophysical Applications of Vegetation Modelling.” *PhD Thesis*: University of Lund, 128 pp.

Kaplan, J. O., Bigelow, N.H., Prentice, I.C., Harrison, S.P., Bartlein, P.J., Christensen, T.R., Cramer, W., Matveyeva, N.V., McGuire, A.D., Murray, D.F., Razzhivin, V.Y., Smith, B., Walker, D.A., Anderson , P.M., Andreev, A.A., Brubaker, L.B., Edwards, M.E. & Lozhkin, A.V. (2003), “Climate change and Arctic ecosystems: 2. Modeling, paleodata-model comparisons, and future projections.” *J. Geophys. Res.* **108** (D19): 8171, doi:10.1029/2002JD002559.

Kasischke, E., French, N., Harrell, P., Christensen, N., Ustin, S.L. & Barry D. (1993), “Monitoring of wildfires in boreal forests using large area AVHRR NDVI composite image data.” *Rem. Sens. Environ.* **45** (1): 61-71

Kaufman, Y.J. & Tanré, D. (1992), “Atmospherically resistant vegetation index (ARVI) for EOS_MODIS.” *IEEE Trans. Geosci. Remote Sens.* **30**: 261-270.

Kaufmann, R.K., Zhou, L., Knyazikhin, Y., Shabanov, N.V., Myneni, R.B. & Tucker, C.J. (2000), “Effect of Orbital Drift and Sensor Changes on the Time Series of AVHRR Vegetation Index Data.” *IEEE Trans. Geosc. Remote Sensing* **38** (6): 2584-2597.

Keeling, C. D., Bacastow, R.B., Carter, A.L., Piper, S.C, Whorf, T.P., Heimann, M., Mook, W.G. & Roeloffzen, H. (1989), “A three dimensional model of atmospheric CO_2 transport based on observed winds: 1. Analysis of observational data.” In: Peterson, D.H.E (ed.), *Aspects of Climate Variability in the Pacific and the Western Americas.* Washington, American Geophysical Union: 165-236.

Keeling, C. D., Whorf, T.P., Wahlen, M. & van der Plicht, J. (1995), "Interannual extremes in the rate of rise of atmospheric carbon dioxide since 1980." *Nature* **375** (6533): 666-670.

Keeling, C.D. & Whorf, T.P. (2004), "Atmospheric carbon dioxide concentrations, Mauna Loa Observatory, Hawaii, 1958-2003." Carbon Dioxide Research Group, Scripps Institution of Oceanography, University of California, URL: http:// cdiac.esd.ornl.gov/ftp/trends/co2/ maunaloa.co2

Keeling, C.D. and T.P. Whorf. (2004), "Atmospheric CO_2 records from sites in the SIO air sampling network." In: Trends: A Compendium of Data on Global Change. Carbon Dioxide Information Analysis Center, Oak Ridge National Laboratory, U.S. Department of Energy, Oak Ridge, Tenn., U.S.A, 13.02.2004, ftp://cdiac.esd.ornl.gov/pub/maunaloa-co2/maunaloa.co2

Keeling, C.D. and T.P. Whorf. (2005), "Atmospheric CO_2 records from sites in the SIO air sampling network." In: Trends: A Compendium of Data on Global Change. Carbon Dioxide Information Analysis Center, Oak Ridge National Laboratory, U.S. Department of Energy, Oak Ridge, Tenn., U.S.A.

Keeling, R.F., Piper, S.C. & Heimann, M. (1996), "Global and hemispheric CO_2 sinks deduced from changes in atmospheric CO_2 concentration." *Nature* **381**: 218-221.

Kicklighter, D. W., Bondeau, A., Schloss, A.L. et al. (1999), "Comparing global models of terrestrial net primary productivity (NPP): global pattern and differentiation by major biomes." *Global Change Biology* **5** (Supp.1): 16-24.

Kidwell, K. et al. (1991), "NOAA polar orbiter data (TIROS-N, NOAA-6, NOAA-7, NOAA-8, NOAA-9, NOAA-10, NOAA-11, and NOAA-12) users guide." Washington, D.C., NOAA/NESDIS.

Kiladis, G. N. & Diaz, H.F. (1989), "Global climatic anomalies associated with extremes in the Southern Oscillation." *J. Climate* **2**: 1069-1090.

Kindermann, J., G. Wurth, G. H. Kohlmaier, and F. W. Badeck (1996), "Interannual variation of carbon exchange fluxes in terrestrial ecosystems." *Glob. Biogeochem. Cycl.* **10** (4), 737–755.

King, A. W., Post, W.M. & Wullschleger, S.D. (1997), "The potential response of terrestrial carbon storage to changes in climate and atmospheric CO_2." *Climate Change* **35**: 199-227.

King, M.D., Menzel, W.P., Kaufman, V.J., Tanre, D. & Gao, S. (2003), "Cloud and aerosol properties, precipitable water, and profiles of temperature and water vapor from MODIS." *IEEE Trans. Geosci. Remote Sensing* **41** (2): 1442

Kirchgeßner, M. (1987), „Tierernährung" DLG-Verlag, Frankfurt (Main).

Kirchner, I., Stenchikov, G.L., Graf, H.-F., Robock, A. & Antuna, J. C. (1999), "Climate model simulation of winter warming and summer cooling following the 1991 Mount Pinatubo volcanic eruption." *J. Geophys. Res.* **104**: 19,039 –19,055.

Kirschbaum, M.U.F (1994), "The sensitivity of C3 photosynthesis to increasing CO2 concentration: A theoretical analysis of its dependence on temperature and background CO2 concentration." *Plant Cell Environ.* 17: 747-754.

Kirschbaum, M.U.F. (2000), "Will changes in soil organic carbon act as a positive or negative feedback on global warming?" *Biogeochemistry* **48** (1): 21-51.

Klein A.G. & Barnett A.C. (2003), "Validation of daily MODIS snow cover maps of the Upper Rio Grande River Basin for the 2000-2001 snow year." *Rem. Sens. Environ.* **86** (2): 162-176.

Knorr, W. & Heimann, M. (1995), "Impact of drought stress and other factors on seasonal land biosphere CO_2 exchange studied through an atmospheric tracer transport model." *Tellus* **47B** (4): 471-489.

Knorr, W. (1997), "Satellite Remote Sensing and Modelling of the Global CO_2 Exchange of Land Vegetation: A Synthesis Study." MPI für Meteorologie, Examensarbeit Nr. 49. Hamburg, Germany,.

Knorr, W. (2000), "Annual and interannual CO_2 exchanges of the terrestrial biosphere: process-based simulations and uncertainties." *Global Ecol Biogeogr.* **9**: 225-252.

Knorr, W., Heimann, M. (2001a), "Uncertainties in global terrestrial biosphere modeling - 1. A comprehensive sensitivity analysis with a new photosynthesis and energy balance scheme." *Glob. Biogeochem. Cycl.* **15**(1): 207-225.

Knorr, W., Heimann, M. (2001b), "Uncertainties in global terrestrial biosphere modeling - Global Constraints for a process-based vegetation model." *Glob. Biogeochem. Cycl.* **15**(1): 227-246.

Körner, C. (2000), "Biosphere responses to CO_2-enrichment." *Ecological Applications* **10**: 1590-1619.

Kovda, V. A. (1971), "The problem of biological and economic productivity of the earth's land areas." *Soviet Geography* **12**: 6-23.

Krakauer, N.Y. & Randerson, J.R. (2003), "Do volcanic eruptions enhance or diminish net primary production? Evidence from tree rings." *Glob. Biogeochem. Cycl.* **17** (4), 1118, doi: 10.1029/2003GB002076

Krinner, G., Viovy, N., de Noblet-Ducoudré, N., Ogée, J., Polcher, J., Friedlingstein, P., Ciais, P., Sitch, S. & Prentice, I.C. (2005), "A dynamic global vegetation model for studies of the coupled atmosphere-biosphere system." *Glob. Biogeochem. Cycl.* **19**, GB1015, doi:10.1029/2003GB002199.

Kucharik, C. J., Foley, J.A., Delire, C., Fisher, V.A., Coe, M.T., Gower, S.T., Lenters, J., Molling, C., Norman, J.M. & Ramankutty, N. (2000), "Testing the performance of a dynamic global ecosystem model: water balance, carbon balance and vegetation structure." *Glob. Biogeochem. Cycl.* **14** (3): 795-826, doi: 10.1029/ 1999GB001138.

Kucharik, C.J. (2003), "Evaluation of a Process-Based Agro-Ecosystem Model (Agro-IBIS) across the U.S. Corn Belt: Simulations of the Interannual Variability in Maize Yield." *Earth Interactions* **7**: 1-33.

Kumar, M. and Monteith, J.L. (1982), "Remote sensing of crop growth." In: Smith, H. (ed.), *Plants and the daylight spectrum*. Academic Press, New-York, 133-144.

Kurz, W.A. & Apps, M.J. (1999), "A 70-year retrospective analysis of carbon fluxes in the Canadian forest sector." *Ecol. Appl.* **9**: 526-547.

Lacaze, R. Roujean, J.L. & Gouterbe, J.P. (1999), „Spatial distribution of Sahelian land surface properties from airborne POLDER multiangular observations." *J. Geophys. Res.* **104**: 12131-12146.

Lau, K.M. & Weng, H. (2001), „Coherent Modes of Global SST and Summer Rainfall over China: An Assessment of the Regional Impacts of the 1997-98 El Niño." *J. Clim.* **14** (6): 1294-1308

Law, R. M. (1999), "CO_2 sources from a mass-balance inversion: Sensitivity to the surface constraint." *Tellus* **51B**: 254–265.

Le Quéré, C., Aumont, O., Bopp, L., Bousquet, P., Ciais, P., Francey, R., Heimann, M., Keeling, C.D., Keeling, R.F., Keshghi, H., Peylin, P., Piper, S.C., Prentice, I.C. & Rayner, P.J. (2003), "Two decades of ocean CO_2 sink variability." *Tellus* **55B**: 649-656.

Le Quéré, C., Orr, J.C., Monfray, P., Aumont, O. & Madec, G. (2000), "Interannual variability of the ocean sink of CO_2 from 1979 through 1997." *Glob. Biogeochem. Cycl.* **14** (4): 1247 - 1265.

Leemans, R. (1991), "Sensitivity analysis of a forest succession model." *Ecological Modeling* **53**: 247-262.

Levy, P.E., Cannell, M.G.R. & Friend, A.D. (2004), "Modelling the impact of future changes in climate, CO 2 concentration and land use on natural ecosystems and the terrestrial carbon sink." *Global Environmental Change* **14**: 21–30.

Lieth, H. (1975), "Primary Production of the Major Vegetation Units of the World." In: Lieth, H.W. & Whittaker, R.H. (eds.), Primary Productivity of the Biosphere, *Ecological Studies* **14**. New York, Springer.

Lifermann, A., Counil, J.-L., Martinuzzi, J.-M. & Perbos, J. (1995), "General outlines of the POLDER experiment." *Proc. SPIE* **2583**: 245-252.

Lillesand, T.M. & Kiefer, R.W. (1994), "Remote Sensing and Image Interpretation." Third Edition, Wiley and Sons.

Lindroth, A., Grelle, A. & Moren, A.S. (1998), "Long-term measurements of boreal forest carbon balance reveal large temperature sensitivity." *Global Change Biology* **4**: 443-450.

Liu, Q. & Huete, A. (1995), "A feedback based modification of the NDVI to minimize canopy background and atmospheric noise." *IEEE Trans. Geosci. Remote Sens.* **33**: 457-465.

Lloyd, J. & Taylor, J.A. (1994), "On the temperature dependence of soil respiration." *Functional Ecology* **8**: 315-323.

Lloyd, J. (1999), "Current perspectives on the terrestrial carbon cycle." *Tellus* **51B**: 336-342.

Lloyd, L. & Farquhar, G.D. (1996), "The CO_2 dependence of photosynthesis, plant growth responses to elevated atmospheric CO_2 concentrations, and their interaction with soil nutrient status. I. General principles and forest ecosystems." *Functional Ecology* **10**: 4-32.

Long, S.P. (1991), "Modification of the response of photosynthetic productivity to rising temperature by atmospheric CO_2 concentrations: has its importance been underestimated?" *Plant, Cell and Environment* **14**: 729-739.

Los, S.O. (1998), "Estimation of the ratio of sensor degradation between NOAA AVHRR channel 1 and 2 from monthly NDVI composites." *IEEE Trans. Geosci. Remote Sens.* **36**: 202-213.

Los, S.O., Collatz, G.J., Bounoua, L., Sellers, P.J. & Tucker, C.J. (2001), "Global Interannual Variations in Sea Surface Temperature and Land Surface Vegetation, Air Temperature, and Precipitation." *J. Climate* **14** (7): 1535-1549.

Loveland, T.R., Reed, B.C., Brown, J.F., Ohlen, D.O., Zhu, Z., Yang, L. & Merchant, J.W. (2000), "Development of a global land cover characteristics database and IGBP DISCover from 1 km AVHRR data." *Int. J. Rem. Sens.* **21** (6-7): 1303-1330

Lucas, R.M., Xiao, X., Hagen, S. & Frolking, S. (2002), "Evaluating TERRA-1 MODIS data for discrimination of tropical secondary forest regeneration stages in the Brazilian Legal Amazon." *Geophys. Res. Lett.* **29** (8), doi: 10.1029/ 2001GLO13375.

Lucht, W., Prentice, I.A., Myneni, R., Sitch, S., Friedlingstein, P., Cramer, W., Bousquet, P., Buermann, W., Smith, B. (2002), "Climatic control of the high-latitude vegetation greening trend and Pinatubo effect." *Science* **296** (31 May): 1687-1689.

Lucht, W., Schaphoff, S., Cramer, W. & Prentice, C. (*in prep.*), "Earth's biosphere depressed as atmospheric CO_2 soars." (to be submitted to *Science*), 2005.

Luedeke, M. K. B., F.-W. Badeck, R. D. Otto, Ch. Haeger, S. Doenges,J. Kindermann, G. Wuerth, T. Lang, U. Jaekel, A. Klaudius, P. Ramge, St. Habermehl, G. H. Kohlmaier (1994), "The Frankfurt biosphere model: a global process-oriented model for the seasonal and longterm CO_2 exchange between terrestrial ecosystems and the atmosphere. Part I: model description." *Climate Research* **4**: 143-166.

Magnani, F., Mencuccini, M. & Grace, J. (2000), "Age-related decline in stand productivity: The role of structural acclimation under hydraulic constraints." *Plant, Cell and Environment* **23**: 251-263.

Malhi, Y. & Grace, J. (2000), "Tropical forests and atmospheric carbon dioxide." *Trends Ecol. Evol.* **15**: 332-337

Malhi, Y., Baldocchi, D.D. & Jarvis, P.G. (1999), "The carbon balance of tropical, temperate and boreal forests." *Plant, Cell and Environment* **22** (6): 715-740.

Mann, M. E., Bradley, R.S., & Hughes, M.K. (1998), "Global-scale temperature patterns and climate forcing over the past six centuries." *Nature* **392**: 779-787.

Mao, J. & Robock, A. (1998), "Surface air temperature simulations by AMIP general circulation models: Volcanic and ENSO signals and systematic errors*." J. Clim.* **11**: 1538–1552.

Mariotti, A., Struglia, M.V., Zeng, N. & Lau, K.M. (2002), "The hydrological cycle in the Mediterranean region and implications for the water budget of the Mediterranean Sea." *J. Clim.* 15: 1674-1690

Marland, G. and R. M. Rotty. (1983), "Carbon Dioxide Emissions from Fossil Fuels: A Procedure for Estimation and Results for 1950-1981." DOE/NBB-0036, TR003, U. S. Department of Energy, Washington, D.C.

Matear, R. J., Hirst, A.C. (1999), "Climate change feedback on the future oceanic CO_2 uptake." *Tellus* Series B, **51**: 722-733.

Matsushita, B., Namura, M. (2002), "Integrating remotely sensed data with an ecosystem model to estimate net primary productivity in East Asia." *Rem. Sens. Environ.* **8**: 58-66.

Matthews E. (1984), "Global inventory of the pre-agricultural and present biomass." In: Lieth, H. et al. (eds.), *Interactions between Climate and Biosphere*, Swets and Zeitlinger, Lisse, Switzerland: 237-246.

McCloy, K. R., Los, S., Hojsgaard, S. Tucker, C.J. & Smith, P. (2005), "Trends in green vegetative development 1981-2000 as detected by the AVHRR Satellite sensor." (*in prep.*)

McCormick, M., Thomason, L.. & Trepte, C. (1995), "Atmospheric effects of the Mount Pinatubo eruption." *Nature* **373**: 399-404.

McGuire, A. D., Melillo, J.M., Kicklighter, D.W. & Joyce, L.A. (1995), "Equilibrium responses of soil carbon to climate change: empirical and process-based estimates." *J. of Biogeography* **22**: 785-796.

McGuire, A. D., Melillo, J.M., Kicklighter, D.W., Pan, Y., Xiao, X., Helfrich, J., Moore, B., Vorosmarty, C.J. & Schloss, A. (1997), "Equilibrium response of global net primary production and carbon storage to doubled atmospheric carbon dioxide: Sensitivity to changes in vegetation nitrogen concentration." *Glob. Biogeochem. Cycl.* **11** (2): 173-189.

McGuire, A., Melillo, J., Joyce, L., Kicklighter, D., Grace, A., Moore, B. & Vorosmarty, C. (1992), "Interactions between carbon and nitrogen dynamics in estimating net primary productivity for potential vegetation in North America." *Glob. Biogeochem. Cycl.* **6**: 101-124.

McGuire, A. D., Prentice, I. C., Ramankutty, N., Reichenau, T., Schloss, A., Tian, H., Williams, L. J. & Wittenberg, U. (2001), "Carbon balance of the terrestrial biosphere in the twentieth century: Analyses of CO_2, climate and land use effects with four process-based ecosystem models." *Glob. Biogeochem. Cycl.* **15** (1): 183-206.

McPhaden, M.J. (1999), "Genesis and Evolution of the 1997-98 El Niño." *Science* 283: 950-954.

Melillo, J.M., Kicklighter, D.W., McGuire, A.D., Peterjohn, W.T. & Newkirk, K.M. (1995), "Global change and its effects on soil organic carbon stocks." In: Zepp, R.G. & Sonntag, C.H. (eds.), *Role of nonliving organic matter in the Earth's carbon cycle*. New York: 175-189.

Menzel, A., Fabian, P. (1999), "Growing season extended in Europe." *Nature* **397**: 659.

Monsi, M. & Saeki, T. (1953), "Über den Lichtfaktor in den Pflanzengesellschaften und seine Bedeutung für die Stoffproduktion." *Jpn. J. Bot.* **14**: 22-52.

Monteith J.L. & Unsworth M.H. (1990), "Principles of environmental physics." Edward Arnold, London, 291 pp.

Monteith, J.L. (1965), "Light distribution and photosynthesis in field crops." *Ann. Bot.* **29**: 17-37.

Monteith, J.L. (1972), "Solar radiation and productivity in tropical ecosystems." *J. Appl. Ecol.* **9**: 747-766.

Monteith, J.L. (1977), "Climate and efficiency of crop production in Britain." *Philos. Trans. R. Soc. London* Ser. B **281**: 271-294.

Moron, V. & Ward, M.N. (1998), "ENSO teleconnections with climate variability in the European and African sectors." *Weather* **53**: 287-295.

Moulin, S., Bondeau, A. & Delécolle, R. (1998), "Combining agricultural crop models and satellite observations from field to regional scales." *Int. J. Remote Sensing* **19** (6): 1021-1036.

Mukai, S. & Sano, I. (1999), "Retrieval algorithm for atmospheric aerosols based on multi-angle viewing of ADEOS/POLDER." *Earth Planets Space* **51**: 1247–1254.

Mukai, S., Sano, I., Hirata, T. & Holben, B.N (2002), "Global map of water vapor content from ADEOS/POLDER and NASA/AERONET." *IEEE Internat. Geoscience and Remote Sensing Symposium*, IGARSS '02, Vol. **6**: 3218-3220

Murayama, S., Taguchi, S. & Higuchi, K. (2004), "Interannual variation in the atmospheric CO_2 growth rate: role of atmospheric transport in the Northern Hemisphere." *J Geophys Res - Atmopheres* **109** (D02305): doi: 10.1029/ 2003JD003729.

Myneni, R. B., Dong, J., Tucker, C.J. et al. (2001), "A large carbon sink in the woody biomass of northern forests." *Proc. of the National Academy of Sciences of the USA* **98** (26): 14784-14789.

Myneni, R. B., Hall, F.G., Sellers, P.J. & Marshak, A.L. (1995a), "The interpretation of Spectral Vegetation Indices." *IEEE Transactions of Geoscience and Remote Sensing* **33**(2): 481-486.

Myneni, R. B., Keeling, C.D., Tucker, C.J., Asrar, G. & Nemani, R.R. (1997a), "Increased plant growth in the northern high latitudes from 1981 to 1991." *Nature* **386** (17/04): 698-702.

Myneni, R. B., Maggion, S., Iaquinta, J., Privette, J.L., Gobron, N., Pinty, B., Kimes, D.S., Verstraete, M.M. & Williams, D.L. (1995b), "Optical remote Sensing of Vegetation: Modeling, Caveats and Algorithms." *Remote Sens. Envir.* **51**: 169-188.

Myneni, R. B., Nemani, R.R. & Running, S.W. (1997b), "Estimation of global leaf area index and absorbed PAR using radiative transfer models." *IEEE Transactions on Geoscience and Remote Sensing* **35** (6): 1380-1393.

Myneni, R.B., Hoffman, S., Knyazikhin, Y., Privette, J.L., Glassy, J., Tian, Y., Wang, Y., Song, X., Zhang, Y., Smith, G.R., Lotsch, A., Friedl, M., Morisette, J.T., Votava, P., Nemani, R.R. & Running, S.W. (2002), "Global products of vegetation leaf area and fraction absorbed PAR from year one of MODIS data." *Remote Sensing of Environment* **83**: 214–231

Nakagawa, M., Tanaka, K., Nakashizuka, T., Ohkubo, T., Kato, T., Maeda, T., Sato, K., Miguchi, H., Nagamasu, H., Ogino, K., Teo, S., Hamid, A.A. & Seng, L.H. (2000), "Impact of severe drought associated with the 1997–1998 El Niño in a tropical forest in Sarawak." *Journal of Tropical Ecology* **16**:355-367.

NASA GISS (2004), "Global Temperature Trends: 2004 Summation." http://www.giss.nasa.gov/data/update/gistemp/2004/

NASA GISS (2006), "Global Temperature Trends: 2005 Summation." http://data.giss.nasa.gov/gistemp/2005/

NASA GISS-Goddard Institute for Space Studies (2001), "Global Temperature Trends: 2001 Summation." http://www.giss.nasa.gov/research/observe/surftemp/ 2001.html

Nemani, R. R., Keeling, C.D., Hashimoto, H., Jolly, W.M., Piper, S.C., Tucker, C.J., Myneni, R.B. & Running, S.W. (2003), "Climate-Driven Increases in Global Terrestrial Net Primary Production from 1982 to 1999." *Science* **300**: 1560-1563.

New, M., Hulme, M. & Jones, P.D. (1999a), "Representing twentieth century space-time climate variability. Part 1: development of a 1961-90 mean monthly terrestrial climatology." *J Climate* **12**: 829-856.

New, M., Hulme, M. & Jones, P.D. (1999b), "Representing twentieth century space-time climate variability. Part 2: development of 1901-1996 monthly grids of terrestrial surface climate." *unpublished*.

Nilsson, S., Shvidenko, A., Stolbovoi, V., Gluck, M., Jonas, M. & Obersteiner, M. (2000), „ Full carbon account for Russia." International Institute for Applied Analysis, Laxenburg, Austria, available at: http://www.iiasa.ac.at/Admin/ PUB/Documents/IR-00-021.pdf.

NOAA (1981), "National holdings of environmental satellite data of the National Oceanic and Atmospheric Administration." Washington, D.C., NOAA/NESDIS

NOAA (1985), "Hydrologic and land sciences applications of the National Oceanic and Atmospheric Administration polar-orbiting satellite data." Washington, D.C., NOAA/ NESDIS

NOAA (1994), "National Oceanic and Atmospheric Administration Retrospective satellite data price list, satellite products list and ordering procedures." Washington, D.C., NOAA/ NESDIS

NOAA (2003): 11/2003 Citation: http://www.mlo.noaa.gov/LiveData/FDataccg.htm.

NOAA (2004), "Climate of 2003 – Annual Review." National climatic Data Center, http://www.ncdc.noaa.gov/oa/climate/research/2003/ann/global.html

Oechel, W. C., Hastings, S.J., Vourlitis, G., Jenkins, M., Riechers, G. & Grulke, N. (1993), "Recent change of arctic tundra ecosystems from a net carbon-dioxide sink to source." *Nature* **361**: 520-523.

Oechel, W. C., Vourlitis, G.L., Hastings, S.J., Zulueta, R.C., Hinzmann, L. & Kane, D. (2000), "Acclimation of ecosystem CO_2 exchange in the Alsakan Arctic in response to decadal climate warming." *Nature* **406**: 978-981.

Olson, J.S., Watts, J.A., Allison, L.J. (1983), "Carbon in Live Vegetation of Major World Ecosystems." TR004, U.S. Department of Energy, Washington D.C.

ORNL (1990), "C-content: Glossary: Carbon Dioxide and Climates." ORNL/CDIAC-39, Carbon Dioxide Information Analysis Center, Oak Ridge National Laboratory, Oak Ridge, Tennessee.

Orr, J. C., Maier-Reimer, E., Mikolajewicz, U., Monfray, P., Sarmiento, J.-L. and co-authors (2001), "Estimates of anthropogenic carbon uptake from four three-dimensional global ocean models." *Glob. Biogeochem. Cycl.* **15**: 43-60.

Page, S.E., Siegert, F., Rieley, J.O., v. Boehm, H.-D., Jaya, A. & Limin, S. (2002), „The amount of carbon released from peat and forest fires in Indonesia during 1997." *Nature* **420**: 61-65.

Parker, D.E., Horton, E.B. & Gordon, M. (1998), "Global and regional climate in 1997." *Weather* **54**: 173-188.

Parton, W. J., Scurlock, J.M.O., Ojima, D.S., Gilmanov, T.G., Scholes, R.J. et al. (1993), "Observations and modeling of biomass and soil organic matter dynamics for the grassland biome worldwide." *Glob. Biogeochem. Cycl.* **7**(4): 785-809.

Perlwitz, J. & Graf, H.-F. (1995), "The statistical connection between tropospheric and stratospheric circulation of the Northern Hemisphere in winter." *J. Clim.* **8**: 2281–2295.

Peylin, P., Bousquet, P., LeQuéré, C., Sitch, S., Friedlingstein, P., McKinley, G., Gruber, N., Rayner, P. & Ciais, P. (2005), "Multiple constraints on regional CO_2 flux variations over land and oceans." *Glob. Biogeochem. Cycl.* **19** GB1011, doi: 10.1029/2003GB002214

Peylin, P., P. Bousquet, P. Ciais, and P. Monfray, (1999), “Differences of CO2 flux estimates based on a “time-dependent” versus a “time-independent” inversion method.” In: Kasibhatla, P., Heimann, M., Rayner, P., Mahowald, N., Prinn, R.G. & Hartley, D.E. (eds.), Inverse Methods in Global Biogeochemical Cycles, *Geophysical Monograph Series* **114**: 295-309.

Philander, S. G. (1990), “El Nin˜o, La Nin˜a, and the Southern Oscillation.” Academic Press, San Diego, Calif., 1990.

Phillips, O.L., Malhim Y., Higuchi, N., Laurance, W.F., Nunez, P.V., Vasquez.R.M., Laurance, S.G., Ferreira, L.V., Stern, M., Brown, S. & Grace, J. (1998), “Changes in the carbon balance of tropical forests: evidence from long-term plots.” *Science* **282**: 439-442.

Pierce, L. & Running, S. (1995), “The effects of aggregating sub-grid land surface variation on large-scale estimates of net primary production.” *Landscape Ecology* **10** (4): 239–253.

Pinty, B. & Verstraete, M.M. (1992), “GEMI: a non-linear index to monitor global vegetation from satellites.” *Vegetatio* **101**: 15-20.

Pinzon, J. E., Pierce, J.F., Tucker, C.J. et al. (2001), “Evaluating coherence of natural images by smoothness membership in Besov spaces.” *IEEE Trans. Geosci. Remote Sens.* **39** (9): 1879-1889.

Plattner, G.-K., Joos, F. & Stocker, T.F. (2002), “Revision of the global carbon budget due to changing air-sea oxygen fluxes.” *Glob. Biogeochem. Cycl.* **16** (4): doi: 10.1029/2001GB001746.

Post, W. M., King, A.W. & Wullschleger, S.D. (1996), “Soil organic matter models and global estimates of soil organic carbon.” In: Powlson, D., Smith, P. & Smith, J.U. (eds.), *Evaluation of soil organic matter models using existing long-term datasets*. Berlin, Springer: 201-222.

Post, W., King, A.W., Wullschleger, S.D. (1997), “Historical variations in terrestrial biospheric carbon storage.” *Glob. Biogeochem. Cycl.* **11**: 99-109.

Post, W.M., Emanuel, W.R., Zinke, P.J. & Stangenberger, A.G. (1982), “ Soil carbon pools and world life zones.” *Nature* **298**: 156-159

Post, W.M., King, A.W. & Wullschleger, S.D. (1996), “Soil Organic Matter Models and Global Estimates of Soil Organic Carbon.” In: Powlson, D.S. et al. (eds.), Evaluation of Soil Organic Matter Models, *NATO ASI Series* I **38**, Berlin, Heidelberg: 201-222

Potter C.S. (1999), “Terrestrial biomass and the effects of deforestation on the global carbon cycle.” *BioScience* **49**: 769-778.

Potter, C. S., Klooster, S. & Brooks, V. (1999), “Interannual variability in terrestrial net primary production: exploration of trends and controls on regional to global scales.” *Ecosystems* **2**: 36-48.

Potter, C. S., Klooster, S., Myneni, R., Genovese, V., Tan, P.-N. & Kumar, V. (2003), “Continental scale comparisons of terrestrial carbon sinks estimated from satellite data and ecosystem modeling 1982-1998.” *Global and Planetary Change* **39**: 201-213.

Potter, C. S., Randerson, J.T., Field, C.B., Matson, P.A., Vitousek, P.M., Mooney, H.A. & Klooster, S.A. (1993), “Terrestrial ecosystem production: a process model based on global satellite and surface data.” *Glob. Biogeochem. Cycles* **7**(4): 811-841.

Potter, C., S. Klooster, C. Reis de Carvalho, V. B. Genovese, A. Torregrosa, J. Dungan, M. Bobo, and J. Coughlan (2001), “Modeling seasonal and interannual variability in ecosystem carbon cycling for the Brazilian Amazon region.” *J. Geophys. Res.,* **106** (D10), 10,423– 10,446, 2001.

Prentice, I. C. & Lloyd, J. (1998), “C-quest in the Amazon Basin.” Nature **396**: 619–620.

Prentice, I. C., Cramer, W., Harrison, S.P. et al. (1992), “A global biome model based on plant physiology and dominance, soil properties and climate.” *J. Biogeography* **19**: 117-134.

Prentice, I. C., Farquhar, G.D., Fasham, M.J.R., Goulden, M.L., Heimann, M., Jaramillo, V.J., Kheshgi, H.S., Le Quéré,C., Scholes, R.J. & Wallace, D.W.R. (2001), "The Carbon Cycle and Atmospheric Carbon Dioxide." in: Houghton et al. (eds.), *Climate Change 2001: The Scientific Basis.* Contribution of the Working Group I to the Third Assessment Report of the Intergovernmental Panel on Climate Change, Cambridge, New York: 183-238.

Prince, S. D. & Xue, C.Y. (2001), "Inter-Annual Land Surface Variation." *Annual Report on NASA Grant*, **NAGS 9329**. http://lcluc.gsfc.nasa.gov/products/pdfs/Report-Prince2001.pdf, 26.09.02.

Prince, S. D., Haskett, J., Steininger, M., Strand, H. & Wright, R. (2001), "Net primary production of U.S. midwest croplands from agricultural harvest yield data." *Ecological Applications* **11** (4): 1194-1205.

Prince, S. D., Haskett, J., Steininger, M., Strand, H. & Wright, R. (2001), "Net primary production of U.S. midwest croplands from agricultural harvest yield data." *Ecol. Appl.* **11** (4): 1194-1205.

Prince, S.D. & Goward, S.N. (1995), "Global primary production: a remote sensing approach." *J. of Biogeography* **22**: 815-835.

Prince, S.D., Goward, S.N., Goetz, S. & Czajkowski, K. (2000), "Interannual Atmosphere-Biosphere Variation: Implications for observation and modeling." *J Geophys. Res.* **105** (D15): 20,055-20,063.

Rahman, H. & Dedieu, G. (1994): "SMAC: a simplified method for the atmospheric correction of satellite measurements in the solar spectrum." *Int. J. Remote Sensing* **15** (1): 123-143.

Raich, J.W. & Schlesinger, W.H. (1992),"The global carbon dioxide flux in soil respiration and its relationship to vegetation and climate." *Tellus* **44B**: 81-99.

Ramankutty, N. & Foley, J. (1998), "Characterizing patterns of global land use: An analysis of global croplands data." *Global Biogeochem. Cycles* **12** (4): 667–685.

Ramankutty, N., Foley, J.A., Norman, J. & McSweeney, K. (2002),"The global distribution of cultivable lands: current patterns and sensitivity to possible climate change." *Global Ecology & Biogeography* **11**: 377-392.

Randerson, J.T., Thompson, M.V., Conway, T.J., Fung, I.Y. & Field, C.B. (1997), "The contribution of terrestrial sources and sinks to trends in the seasonal cycle of atmospheric carbon dioxide." *Glob. Biogeochemical Cycles* **11** (4): 535-560.

Rao, C.R.N. & Chen, J. (1995), "Inter-satellite calibration linkages for visible and near-infrared channels of the Advanced Very High Resolution radiometer on the NOAA-7, -9, and -11 spacecraft." *Int. J. Rem. Sens.* **16**: 1931-1942.

Rao, C.R.N. (1993), "Nonlinearity corrections for the thermal infrared channels of the Advanced Very High Resolution Radiometer: assessment and recommendations for corrections." *NOAA Technical Report NESDIS* **69**. NOAA/NESDIS. Washington, DC.

Rao, C.R.N. and Chen, J. (1996), "Post-launch calibration of the visible and nearinfrared channels of the Advanced Very High Resolution Radiometer on the NOAA-14 spacecraft." *Int. J. Remote Sens.* **17**: 2743-2747.

Rast M. & Bezy J.L. (1999), "The ESA Medium Resolution Imaging Spectrometer MERIS a review of the instrument and its mission." *Int. J. Rem. Sens.* **20** (9): 1681-1702

Rayment, M.B. & Jarvis, P.G. (2000), "Temporal and spatial variation of soil CO_2 efflux in a Canadian boreal forest." *Soil Biology and Biochemistry* **32**: 35-45.

Rayner, P.J. & Law, R.M. (1999), "The interannual variability of the global carbon cycle - keynote perspective." *Tellus* **51B** (2): 210-212.

Rayner, P.J., Enting, I.G., Francey, R.J. & Langenfelds, R. (1999), "Reconstructing the recent carbon cycle from atmospheric CO_2, delta13C and O_2/N_2 observations." *Tellus* **51B**: 213-232.

Rayner, P.J., Scholze, M., Knorr, W., Kaminski, T., Giering, R. & Widmann, H. (2005), “Two decades of terrestrial Carbon fluxes from a Carbon Cycle Data Assimilation System (CCDAS).” *Global Biogeochemical Cycles* **19**: doi:10.1029/2004GB002254.

Reeves, M.C., Winslow, J.C. & Running, S.W. (2001), “Mapping Weekly Rangeland Vegetation Productivity Using MODIS Algorithms.” *J. Range Manage.* **54**: A90-A105

Reichenau, T.G. & Esser, G. (2003), “Is interannual fluctuation of atmospheric CO_2 dominated by combined effects of ENSO and volcanic aerosols?“ *Glob. Biogeochem. Cycl.* **17** (4), 1094, doi: 10.1029/2002GB002025.

Reid, W.V. et al. (2005), “Millennium Ecosystem Assessment Synthesis Report - Pre-publication Final Draft Approved by MA Board on March 23, 2005”, http://www.millenniumassessment.org//en/Products.Synthesis.aspx

Reynolds, R.W., Rayner, N.A., Smith, T.M., Stokes, D.C. & Wang, W. (2002), “An improved in situ and satellite SST analysis.” *J. Climate* **15**: 1609–1625.

Robock, A. & Mao, J.P. (1992), “Winter warming from large volcanic eruptions.” *Geophys. Res. Lett.* **19** (24): 2405-2408

Robock, A. & Mao, J.P. (1995), “The volcanic signal in surface temperature observations.” *J. Clim.* **8** (5): 1086– 1103.

Robock, A. & Y. Liu, Y. (1994), “The volcanic signal in Goddard Institute for Space Studies three-dimensional model simulations.” *J. Clim.* **7**: 44–55.

Robock, A. (2000), “Volcanic eruptions and climat.” *Rev. Geophys.* **38** (2): 191– 219.

Rödenbeck, C., Houweling, S., Gloor, M. & Heimann M (2003b), “Time-dependent atmospheric CO2 inversions based on interannually varying tracer transport.” *Tellus* **55B**: 488-497.

Rödenbeck, C., Houweling, S., Gloor, M. & Heimann, M. (2003a), “CO_2 flux history 1982-2001 inferred from atmospheric data using a global inversion of atmospheric transport.” *Atm. Chem. Phys.* **3** (6): 1919-1964.

Roderick, M. L., Farquhar, G. D., Berry, S. L., and Noble, I. R. (2001), “On the direct effect of clouds and atmospheric particles on the productivity and structure of vegetation.” *Oecologia* **129**: 21–30.

Roeckner, E., Oberhuber, J.M., Bacher, A., Christoph, M. & Kirchner, I. (1996), “ENSO variability and atmospheric response in a global coupled atmosphere-ocean GCM”, *Climate Dynamics* **12**: 737-754.

Rogers, J.C. (1997), “North Atlantic storm track variability and its association to the North Atlantic Oscillation and climate variability of Northern Europe.” *Journal of Climate* **10** (7), 1635-1647.

Rogers, J.C. (2005), “Monthly NAO Index based on raw anomalies.” provided by the World Monthly Station Climatology WMSSC, data access: http://polarmet.mps.ohio-state.edu/NAO/Rogers_NAO_monthly_raw_anomalies.txt).

Ropelewski, C.F. & Halpert, M.S. (1987), “Global and regional scale precipitation patterns associated with the El Niño-Southern Oscillation.” *Monthly Weather Rev.* **115**: 1606-1626.

Ropelewski, C.F. & Jones, P.D. (1987), "An Extension of the Tahiti-Darwin Southern Oscillation Index", *Monthly Weather Review* **115**: 2161-2165

Roujean, J. L., Leroy, M. & Deschamps, P.-Y. (1992), “A Bidirectional Reflectance Model of the Earth's Surface for the Correction of Remote Sensing Data.” *J. Geophys. Res.* **97** (D18): 20455-20468.

Rouse, J. W., Jr., Haas, R., H., Deering, D. W., Schell, J. A. & Harlan, J. C. (1974), Monitoring the vernal advancement and retrogradation (green wave effect) of natural vegetation; *NASA/GSFC Type III Final Report*, Greenbelt, MD., p. 371.

Ruimy, A., Dedieu, G. & Saugier, B. (1996), "TURC: A diagnostic modle of continental gross primary productivity and net primary productivity." *Glob. Biogeochem. Cycles* **10**(2): 269-285.

Ruimy, A., Kergoat, L., Bondeau, A. (1999), "Comparing models of terrestrial net primary productivity (NPP): analysis of differences in light absorption and light-use efficiency." *Global Change Biology* **5** (Supp.1): 56-64.

Ruimy, A., Saugier, B. & Dedieu, G. (1994), "Methodology for the estimation of terrestrial net primary productivity from remotely sensed data." *J. Geophys. Res.* **99**(D3): 5263-5283.

Running, S. W. & Hunt, E.R. (1993), "Generalization of a forest ecosystem process model for other biomes, Biome-BGC, and an application for global-scale models." In: Ehleringer, J.R. & Field, C.B. (eds.), *Scaling Physiological Processes: Leaf to Globe*. Academic Press, San Diego: 141-158.

Running, S.W., Nemani, R., Glassy, J.M. & Thornton, P.E. (1999), "MODIS daily photosynthesis (PSN) and annual net primary procution (NPP) product (MOD17)."Algorithm Theoretical Basis Document, Version 3.0. http://www.ntsg.umt.edu/modis/ATBD/ATBD_MOD17_v21.pdf

Sabine, C. L., Feely, R.A., Gruber, N., Key, R.M., Lee, K., Bullister, J.L., Wanninkhof, R., Wong, C.S., Wallace, D.W.R., Tilbrook, B., Millero, F.J., Peng, T.-H., Kozyr, A., Ono, T. & Rios, A.F. (2004), "The oceanic sink for anthropogenic CO_2." *Science* **305**: 367-371.

Sader, S., Waide, R.B., Lawrence, W.T. & Armondt, J. (1989), "Tropical forest biomass and successional age class relationships to a vegetation index derived from Landsat TM data." *Rem. Sens. Environ.* **28**: 143-156.

Saint, G. (2000), "Vegetation: an earth observation system to monitor the biosphere." In: Verstraete, M.M., Menenti, M. & Peltoniemi, J.(eds.), Observing land from space: science, customers and technology, *Advances in Global Change Research* **4**, Dordrecht, Boston, London: 291-301.

Salomonson, V.V. (1988), " The moderate resolution imaging spectrometer (MODIS)." *IEEE Geosci. Remote Sens. Newslett.* **12**: 11-15.

Sarmiento, J. L., Hughes, T.M.C., Stouffer, R.J. & Manabe, S. (1998), "Simulated response of the ocean carbon cycle to anthropogenic climate warming." *Nature* **393**: 245-249.

Saugier, B., Roy, J. & Mooney, H.A. (2001), "Estimations of global terrestrial productivity: Converging to a single number?" In: Roy, J., Saugier, B. & Mooney, H.A. (eds.), *Terrestrial Global Productivity*. San Diego, London, Academic Press**:** 542-558.

Savage, K., Moore, T.R. & Crill, P.M. (1997), "Methane and carbon dioxide exchanges between the atmosphere and northern boreal forest soils." *J. Geophys. Res. – Atmospheres* **102**: 29279-29288.

Schaaf C.B., Gao F., Strahler A.H., Lucht W., Li X., Tsang T., Strugnell N.C., Zhang X., Jin Y., Muller J.-P., Lewis P., Barnsley M., Hobson P., Disney M., Roberts G., Dunderdale M., Doll C., d'Entremont R.P., Hu B., Liang S., Privette J.L. & Roy D. (2002), " First operational BRDF, albedo nadir reflectance products from MODIS." *Remote Sensing of Environment* **83** (1): 135-148.

Schaefer, K., Denning, A.S., Suits, N., Kaduk, J., Baker, I., Los, S. & Prihodko, L. (2002), "Effect of climate on interannual variability of terrestrial CO_2 fluxes." *Glob. Biogeochem. Cycles* **16** (4): 1102, doi:10.1029/2002GB001928.

Schaphoff, S., Lucht, W., Gerten, D., Sitch, S., Cramer, W. & Prentice, I.C. (2006), „Terrestrial biosphere carbon storage under alternative climate projections." *Climatic Change* 74, doi: 10.1007/s10584-005-9002-5 .

Schimel, D. D., House, J.I., Hibbard, K.A., Bousquet, P., Ciais, P., Peylin, P., Braswell, B.H., Apps, M.J., Baker, D., Bondeau, A., Canadell, J., Churkina, G., Cramer, W., Denning, A.S., Field, C.B., Friedlingstein, P., Goodale, C., Heimann, M., Houghton, R.A., Melillo, J.M., Moore III, B., Murdiyarso, D., Noble, I., Pacala, S.W., Prentice, I.C., Raupach, M.R., Rayner, P.J., Scholes, R.J., Steffen, W.L. & Wirth, C. (2001), "Recent patterns and

mechanisms of carbon exchange by terrestrial ecosystems." *Nature* **414** (08.Nov.): 169-172.

Schimel, D. S., D. Alves, I. Enting, M. Heimann, F. Joos, D. Raynaud, and T. Wigley, (1996), " CO_2 and the carbon cycle", in: Houghton et al. (eds.), *Climate Change*, 76–86, Cambridge Univ. Press, New York.

Schimel, D. S., Enting, I.G., Heimann, M., Wigley, T.M.L., Raynaud, D., Alves, D. & Siegenthaler, U. (1995), CO_2 and the carbon cycle. In: J. T. Houghton, Meira Filho, L.G., Bruce, J., Lee, H., Callander B.A., Haites, E., Harris, E. & Maskell, K. (eds.), *Climate Change 1994: Radiative Forcing of Climate Change and an Evaluation of the IPCC IS92 Emission Scenarios*. Cambridge, Cambridge University Press**:** 35-71.

Schlesinger, W. H. (1990), "Evidence from chronosequence studies for a low carbon-storage potential of soils." *Nature* **348**: 233-234.

Schlesinger, W.H. (1977), "Carbon Balance in Terrestrial Detritus." *Annual Review of Ecology and Systematics* **8** (Nov.): 51-81 (doi: 10.1146/annurev.es. 08.110177.000411)

Schulze, E. D., Lloyd, J., Kelliher, F.M., Wirth, C., Rebmann, C., et al. (1999), "Productivity of forests in the Eurosiberian boreal region and their potential to act as a carbon sink - a synthesis." *Global Change Biology* **5**: 703-722.

Scurlock, J.M.O., Asner, G.P., Gower, S.T. (2001), "Worldwide Historical Estimates and Bibliography of Leaf Area Index, 1932-2000." ORNL Technical Memorandum TM-2001/268, Oak Ridge National Laboratory, Oak Ridge, Tennessee, U.S.A.

Seemann, S.W., Li, J., Menzel, W.P., Gumley, L.E. (2002), "Operational Retrieval of Atmospheric Temperature, Moisture, and Ozone from MODIS Infrared Radiances." *Journal of Applied Meteorology* **42** (8): 1072-1091.

Self, S., Rampino, M.R., Zhao, J. & Katz, M.G. (1997), "Volcanic aerosol perturbations and strong El Nin˜o events: No general correlation." *Geophys. Res. Lett.* **24**: 1247–1250.

Self, S., Zhao, J.-X., Holasek, R.E., Torres, R.C. & King, A.J. (1996), "The atmospheric impact of the Mount Pinatubo eruption." In: Newhall, C.G. & Punongbayan, R.S. (eds.), *Fire and Mud: Eruptions and lahars of Mount Pinatubo*, Philippines, Philippine Institute of Volcanology and Seismology, Quezon City, and University of Washington Press, Seattle: 1089-1115.

Self, S., Zhao, J.X., Holasek, R.E., Torres, R.C. & King, A.J. (2006), "The Atmospheric Impact of the 1991 Mount Pinatubo Eruption." http://pubs.usgs.gov/pinatubo/self/index.html;latest demand: Feb., 13th 2006

Sellers, J. P., Los, S.O., Tucker, C.J., Justice, C.O., Dazlich, D.A., Collatz, G.J. & Randell, D.A. (1996b) "A revised land surface parameterization (SiB2) for atmospheric GCMs. Part II: The generation of global fields of terrestrial biophysical parameters from satellite data." *J Climate* **9**: 706-737.

Sellers, J. P., Randell, D.A., Collatz, G.J., Berry, J.A., Field, C.B., Dazlich, D.A., Zhang, C., Collelo, G.D. & Bounua, L. (1996), "A revised land surface parameterization (SiB2) for atmospheric GCMs. Part I: model formulation." *J. Climate* **9**: 676-705.

Sellers, P.J., Berry, J.A., Collatz, G.J., Field, C.B. & Hall, F.G. (1992), "Canopy Reflectance, Photosynthesis, and Transpiration. III. A Reanalysis Using Improved Leaf Models and a New Canopy Integration Scheme." *Int. J. Remote Sensing* **42**: 187-216.

Sellers, P.J., Mintz, Y., Sud, Y.C. & Dalcher, A. (1986), "A simple biosphere model (SiB) for use within general circulation models." *J. Atmos. Sci.* **43**: 505-531.

Sellers, P.J., Tucker, C.J., Collatz, G.J., Los, S.O., Justice, C.O., Dazlich, D.A. & Randall, D.A. (1994), "A global 1 x 1 NDVI data set for climate studies. Part 2: The generation of global fields of terrestrial biophysical parameters from NDVI." *Int. J. Remote Sens.* **15**: 3519-3545.

Shvidenko, A. & Nilsson, S. (2000), " Fire and the carbon budget of Russian forests. In: Kasischke, E. & Stockes, B.J. (eds.), *Fire, climate change and carbon cycling in the boreal forest.* Springer, New York: 289-331

Shvidenko, A. & Nilsson, S. (2002), "Dynamics of russian forests during 1961 – 1998 and the carbon budget: implication of long-period forest inventory data." *Clim. Change* **55**:5-37.

Siegenthaler, U. & Sarmiento, J.L. (1993), "Atmospheric carbon dioxide and the ocean." *Nature* **365**: 119-125.

Siegert, F., Ruecker, G., Hinrichs, A. & Hofmann, A.A. (2001), „ Increased damage from fires in logged forests during droughts caused by El Niño." *Nature* **414**: 437-440

Sitch, S. (2000), "The role of vegetation dynamics in the control of atmospheric CO_2 content." PhD thesis, University of Lund, Sweden, 213 pp.

Sitch, S., Smith, B., Prentice, I.C., Arneth, A., Bondeau, A., Cramer, W., Kaplan, J.O., Levis, S., Lucht, W., Sykes, M.T., Thonicke, K. & Venevsky, S. (2003), "Evaluation of ecosystem dynamics, plant geography and terrestrial carbon cycling in the LPJ Dynamic Global Vegetation Model." *Global Change Biology* **9**: 161-185.

Six, K.D. & Maier-Reimer, E. (1996), "Effects of plankton dynamics on seasonal carbon fluxes in an ocean and general circulation model." *Glob. Biogeochem. Cycles* **10** (4): 559-583.

Slater, P.N., Biggar, S.F., Holm, R.G., Jackson, R.D., Mao, Y., Moran, M.S., Palmer, J.M. & yuan, B. (1987), "Reflectance- and radiance-based methods for the inflight absolute calibration of multispectral sensors." *Rem. Sens. Environ.* **22**: 11-37.

Smil, V. (ed.) (2003), "The Earth's Biosphere: Evolution, dynamics, and change." MIT Press.

Smith, T.M., Weishampel, J.F., Shugart, H.H. & Bonan, G.B. (1992), "Response of terrestrial C storage to climate change: modeling C dynamics at varying temporal and spatial scales." *Water, Air & Soil Pollution* **64** (1-2): 307-326.

Spanner, M., Pierce, L.L., Running, S.W. & Peterson, D.L. (1990), "The seasonality of AVHRR data of temperate coniferous forests - Relationship with leaf area index" *Rem. Sens. Environ.* **33**: 97-112

Stenchikov, G., Robock, A., Ramaswamy, V., Schwarzkopf, M.D., Hamilton, K. & Ramachandran, S. (2002), "Arctic Oscillation response to the 1991 Mount Pinatubo eruption: Effects of volcanic aerosols and ozone depletion." *J. Geophys. Res.* **107** (D24): 4803, doi: 10.10029/2002JD002090.

Stenseth, N.C., Mysterud, A., Ottersen,G., Hurrell, J.W., Chan, K.-S. & Lima, M. (2002), "Ecological effects of climate fluctuations." *Science* **297**: 1292-1296.

Stephenson, D.B. (1999), "The North Atlantic Oscillation – thematic website." URL=http://www.met.rdg.ac.uk/cag/NAO.

Steyaert, L. T., Hall, F.G. & Loveland, T.R. (1997), "Land cover mapping, fire regeneration, and scaling studies in the Canadian boreal forest with 1 km AVHRR and Landsat TM data." *J. Geophys. Res.* **102** (D24): 29581-29598

Stibig, H.-J., Beuchle, R. & Achard, F. (2003), "Mapping of the tropical forest cover of insular Southeast Asia from SPOT4-Vegetation images." *Int. J. Rem. Sens.* **24** (18): 3651-3662.

Stolbovoi V., Fischer, G., Ovechkin, V.S. & Rozhkova, S. (eds.) (1998), "The IIASA-LUC Project Georeferenced Database of the Former U.S.S.R., Vol. 4: Vegetation." Interim Report IR-98, International Institute for Applied Systems Analysis, Laxenburg, Austria.

Stott, P.A. Tett, S.F.B. , Jones, G.S., Allen, M.R., Mitchell, J.F.B., Jenkins, G.J. (2000), "External control of 20th century temperature by natural and anthropogenic forcings." *Science* **290**: 2133-2137.

Strahler, A., Muchoney, D., Borak, J., Friedl, M., Gopal, S., Lambin, E. & Moody, A. (1999), "MODIS Land Cover Product." Algorithm Theoretical Basis Document (ATBD), Version 5.0, MODIS Land Cover and Land-Cover Change. Boston University

Strahov V. (1998), "Forest State Account, 1998. Land Resources of Russia" CD-ROM, International Institute for Applied Systems Analysis, Laxenburg, Austria.

Sun, D.-Z. (2003), "A possible effect of an increase in the warm-pool SST on the magnitude of El Niño warming." *J. Climate* **16**: 185-205.

Takemata, K. Izumiya, T. Kawata, Y. (2000), “Estimation of the BRDF of land surfaces from ADEOS/POLDER imagedata.” *IEEE Internat. Geoscience and Remote Sensing Symposium*, IGARSS 2000, Vol. 5: 1945-1947

Tans, P. P., Fung, I.Y. & Takahashi, T. (1990), “Observational constraints on the global atmospheric CO_2 budget.” *Science* **247**: 1431-1438.

Tans, P. P., Wallace, D.W.R. (1999), “Carbon cycle research after Kyoto - keynote perspective.” *Tellus* **51B**: 562-571.

Tansey, K., Grégoire, J.-M., Binaghi, E., Boschetti, L., Brivio, P.A., Ershov, D., Flasse, S., Fraser, R., Graetz, D., Maggi, M., Peduzzi, P., Pereira, J., Silva, J., Sousa, A. & Stroppiana, D. (2004), “A Global Inventory of Burned Areas at 1 Km Resolution for the Year 2000 Derived from Spot Vegetation Data.” *Climatic Change* **67** (2-3): 345-377.

Teillet, P. M. (1992), “An algorithm for the radiometric and atmospheric correction of AVHRR data in the solar reflective channels.” *Rem. Sens. Environ.* **41** (2-3): 185-195.

Thompson, M. L., I. G. Enting, G. I. Pearman and P. Hyson (1986), “Interannual variation of atmospheric CO_2 concentration.” *J. Atmos. Chem.* **4:** 125-155, 1986.

Thompson, M. V., Randerson, J.T., Malmström, C.M. & Field, C.B. (1996), “Change in net primary production and heterotrophic respiration: How much is necessary to sustain the terrestrial carbon sink?” *Global Biogeochemical Cycles* **10**(4): 711-726.

Thonicke, K., Venevsky, S., Sitch, S. & Cramer, W. (2001), “The role of fire disturbance for global vegetation dynamics: coupling a fire into a Dynamic Global Vegetation Model.” *Global Ecology & Biogeography* **10**: 661-677.

Tian, H., Mellilo, J.M., Kicklighter, D.W., McGuire, A.D. & Helfrich III, J.V.K. (1999), “The sensitivity of terrestrial carbon storage to historical climate variability and atmospheric CO_2 in the United States.” *Tellus* **51B**: 414-452.

Tian, H., Mellilo, J.M., Kicklighter, D.W., McGuire, A.D., Helfrich III, J.V.K., Moore III, B. & Vörösmarty, C.J. (1998), “Effect of interannual climate variability on carbon storage in amazonian ecosystems.” *Nature* **396** (17.Dec): 664-667.

Townsend, A. R., Braswell, B.H., Holland, E.A. & Penner, J.E. (1996), “Spatial and temporal patterns in terrestrial carbon storage due to deposition of fossil fuel nitrogen.” *Ecol. Appl.* **6**: 806– 814.

Townshend, J.R.G. & Justice, C.O. (2002), “Towards operational monitoring of terrestrial systems by moderate-resolution remote sensing.” *Rem. Sens. Environ.* **83** (1-2): 351-359.

Trenberth, K.E. & Hoar, T.J. (1996), "The 1990-1995 El Niño-Southern Oscillation Event Longest on Record." *Geophys. Res. Lett.* **23**:57-60

Trenberth, K.E. (1984), "Signal versus Noise in the Southern Oscillation" *Monthly Weather Review* **112**: 326-332

Trenberth, K.E. (1997), “The definition of El Niño.” *Bulletin of the American Meteorological Society* **78** (12): 2771-2777.

Trotter, C.M., Dymond, J.R.& Goulding, C.J. (1997), “Estimation of timber volume in a coniferous plantation forest using Landsat TM”, *Int. J. Rem. Sens.* 18 (10): 2209-2223.

Tucker, C. J., Slayback, D.A., Pinzon, J.E., Los, S.O., Myneni, R.B. & Taylor, M.G. (2001), “Higher Northern Latitude NDVI and Growing Season Trends from 1982 to 1999.” *Int. J. Biometeorology* **45** (4): 1184-1190.

Tucker, C.J. (1979), “Red and photographic infrared linear combinations for monitoring vegetation.” *Remote Sens. Environ.* **8**: 127-150.

Tucker, C.J., Gatlin, J.A. & Schneider, s.R. (1984), “Monitoring vegetation in the Nile delta with NOAA-6 and NOAA-7 AVHRR imagery.“ *Photogrammetric Engineering and Remote Sensing* 65: 679-688

Turner, D. P., Gower, S.T., Cohen, W.B., Gregory, M. & Maiersperger, T.K. (2002), "Effects of spatial variability in light use efficiency on satellite-based NPP monitoring." *Remote Sens. Envir.* **80** (3): 397-405.

Unsworth, M.H.H. & Hogsett, W.E. (1996), "Combined effects of changing CO2, temperature, UV-B radiation and O3 on crop growth." In: Bazzaz, F.E. (ed.), *Global Climate Change and Agricultural Production*. Chichester: 171-197.

USDA (1997), "Soil organic carbon of the world." United States Department of Agriculture, National Resources Conservation Services, http://soils.usda.gov/use/worldsoils/mapindex/soc.html

Valentini, R., Matteucci, G., Dolman, A.J., Schulze, E.D., Remann, C., Moors, E.J., Granier, A. & Gross, P. (2000), "Respiration as the main determinant of carbon balance in european forests." *Nature* **404**: 861-864.

Vermote, E. & Kaufman, Y.J. (1995), "Absolute calibration of AVHRR visible and near-infrared channels using ocean and cloud views." *Int. J. Rem. Sens.* **16** (13): 2317-2340.

Vermote, E., Santer, R., Deschamps, P.Y. et al. (1992), "In-flight calibration of large field of view sensors at short wavelengths using Rayleigh-scattering." *Int. J. Rem. Sens.* **13** (18): 3409-3429.

Vermote, E.E. & El Saleous, N. (1994), „Stratospherical aerosol perturbing effect on remote sensing of vegetation: operational method fort he correction of AVHRR composite NDVI." *SPIE Atmospheric Sensing and Modeling* **2311**: 19-29.

Veroustraete, F., Sabbe, H. & Eerens, H. (2002), "Estimation of carbon mass fluxes over Europe using the C-Fix model and Euroflux data." *Remote Sensing of Environment* **83**: 376-399.

Visbeck, M.H., Hurrell, J.W., Polvani, L. & Cullen, H.M. (2001), "The North Atlantic Oscillation: Past, present, and future." *Proc. Natl. Acad. Sci. USA* **98** (23): 12876-12877, doi: 10.1073/pnas.231391598

Wagner, W., Scipal, K., Pathe, C., Gerten, D., Lucht, W. & Rudolf, B. (2003), "Evaluation of the agreement between the first global remotely sensed soil moisture data with model and precipitation data." *J Geophys Res* **108** (D19): 4611-4620

Wallace, D.W.R. (2001), "Storage and transport of excess CO_2 in the oceans: The JGOFS/WOCE Global CO_2 Survey." In: Siedler, G., Church, J. & Gould, W.J. (eds.), *Ocean Circulation and Climate* **77**: Observing and Modelling the Global Ocean. Academic Press, San Diego: 489-521.

Wang, W.-C. & Li, K. (1990), "Precipitation Fluctuation over Semiarid Region in Northern China and the Relationship with El Niño/Southern Oscillation." *J. Clim.* 3 (7): 769-783

Waring, R. H., Landsberg, J.J. & Williams, M. (1998), "Net primary production of forests: a constant fraction of gross primary production?" *Tree Physiology* **18**: 129-134.

Warnant, P., Francois, L., Strivay, D. & Gérard, J.-C. (1994), "CARAIB - a global model of terrestrial biological productivity." *Glob. Biogeochemical Cycles* **8**: 255-270.

Watson, A. J., Nightingale, P.D. & Cooper, D.J. (1995), "Modeling atmosphere ocean CO_2 transfer." *Philosophical Transactions of the Royal Society of London - Series B: Biological Sciences* **348**: 125-132.

WBGU (1988), "Die Anrechnung biotischer Quellen und Senken im Kyoto-Protokoll: Fortschritt oder Rückschlag für den globalen Umweltschutz?" *Sondergutachten Wissenschaftlicher Beirat der Bundesregierung Globale Umweltveränderungen*, Bremerhaven, 76 pp.

Weinreb, M. P., Hamilton, G., Brown, S. & Koczor, R.J. (1990), "Nonlinearity corrections in calibration of Advanced Very High Resolution Radiometer infrared channels." *J. Geophys. Res.* **95**: 7,381-7,388.

White DM, G. D., Ping CL, Michaelson G (2004), "Characterizing soil organic matter quality in arctic soil by cover type and depth." *Cold regions science and technology* **38** (1): 63-73.

White, A., Cannell, M.R. & Friend, A.D. (2000): "CO_2 stabilization, climate change and the terrestrial carbon sink", *Global Change Biology* **6**: 817-833.

Whittaker, R.H. & Liekens, G.E. (1973), "The biosphere and man." In: Lieth, H. & Whittaker, R.H. (eds.), *Primary Productivity of the Biosphere*, Springer, New York: 305-328.

WMO (1999), "1999 closes the warmest decade and warmest century of the last millennium according to WMO annual statement on the global climate – preliminary report,.", http://www.wmo.ch/web/Press/Press644.html

Woodward, F. I., Smith, T.M. & Emanuel W.R. (1995), "A global land primary productivity and phytogeography model." *Glob.l Biogeochem. Cycl.* **9** (4): 471-490.

Woodward, F.I. (1987), "Climate and Plant Distribution." Cambridge University Press, New York.

Woodward, F.I. (1995), "Ecophysiological controls of conifer distributions." In: Smith, W.K. & Hinckley, I.M. (eds.), *Ecophysiology of coniferous forests*, Academic Press, San Diego: 79–94.

Woodwell, G. M., Mackenzie, F. T. Houghton, R. A., Apps, M., Gorham, E. & Davidson, E. (1998), "Biotic feedbacks in the warming of the earth." *Clim. Change* **40**: 495–518.

Wu, A. Li, Z. & Cihlar, J. (1995), "Effects of land cover type and greenness on advanced very high resolution radiometer bidirectional reflectances: Analysis and removal." *J. Geophys. Res.* **100**: 9179-9192.

Xiao, X., Kicklighter, D.W., Melillo, J.M., McGuire, A.D., Stone, P.H. & Sokolov, A.P. (1997), "Linking a global terrestrial biogeochemical model and a 2-dimensional climate model: implications for the carbon budget." *Tellus* **49B**: 18-37

Yamamoto, H., Hashimoto, T., Seki, M., Yuda, N., Mitomi, Y., Yoshioka, H., Honda, Y. & Igarashi, T. (2005), "The initial evaluation of ADEOS-II/GLI land products for vegetation monitoring." *Proceedings of SPIE*, Vol. **5655**: 241-252.

Zeng, N. (2003), "Glacial-interglacial atmospheric CO_2 changes – the glacial burial hypothesis." *Adv. Atmos. Sci.* **20**: 677-693

Zeng, N., Mariotti, A. & Wetzel, P. (2005), "Terrestrial mechanisms of interannual CO_2 variability." *Glob. Biogeochem. Cycl.* **19**, GB1016, doi:10.1029/2004GB002273

Zeng, N., Qian, H., Munoz, E. & Iacono, R. (2004), "How strong is carbon-climate feedback under global warming ? " *Geophys. Res. Lett.* **31** L20203, doi: 10.1029/2004GL020904

Zeng, N., Shuttleworth, J.W. & Gash, J.H.C. (2000), "Influence of temporal variability of rainfall on interception loss: I. Point analysis." *J. Hydrol.* **228**: 228-241.

Zhang, Y. (2001), "LAI and FPAR estimation and land cover identification with multi-angle multi-spectral satellite data." Dissertation, Boston University.

Zheng, D., Prince, S. & Wright, R. (2003), "Terrestrial net primary production estimates for 0.5° grid cells from field observations - a contribution to global biogeochemical modeling." *Global Change Biology* **9**: 46-64.

Zhou, L., Kaufmann, R.K., Tian, Y., Myneni, R.B. & Tucker, C.J. (2003), "Relation between interannual variations in satellite measures of northern forest greenness and climate between 1982 and 1999." *J. Geophys. Res.* **108** (D1,4004): doi: 10.1029/ 2002JD002510,2003.

Zhou, L., Tucker, C.J., Kaufmann, R.K., Slayback, D., Shabanov, N.V. & Myneni, R.B. (2001), "Variations in northern vegetation activity inferred from satellite data of vegetation index during 1981 to 1999." *J. Geophys. Res.* **106** (D17): 20.069-20.083.

Zobler, L. (1986), "A world soil file for global climate modelling." *NASA Technical Memorandum* **87802**: 32pp.

ANNEX

USDA global soil organic carbon map (USDA, 1997)

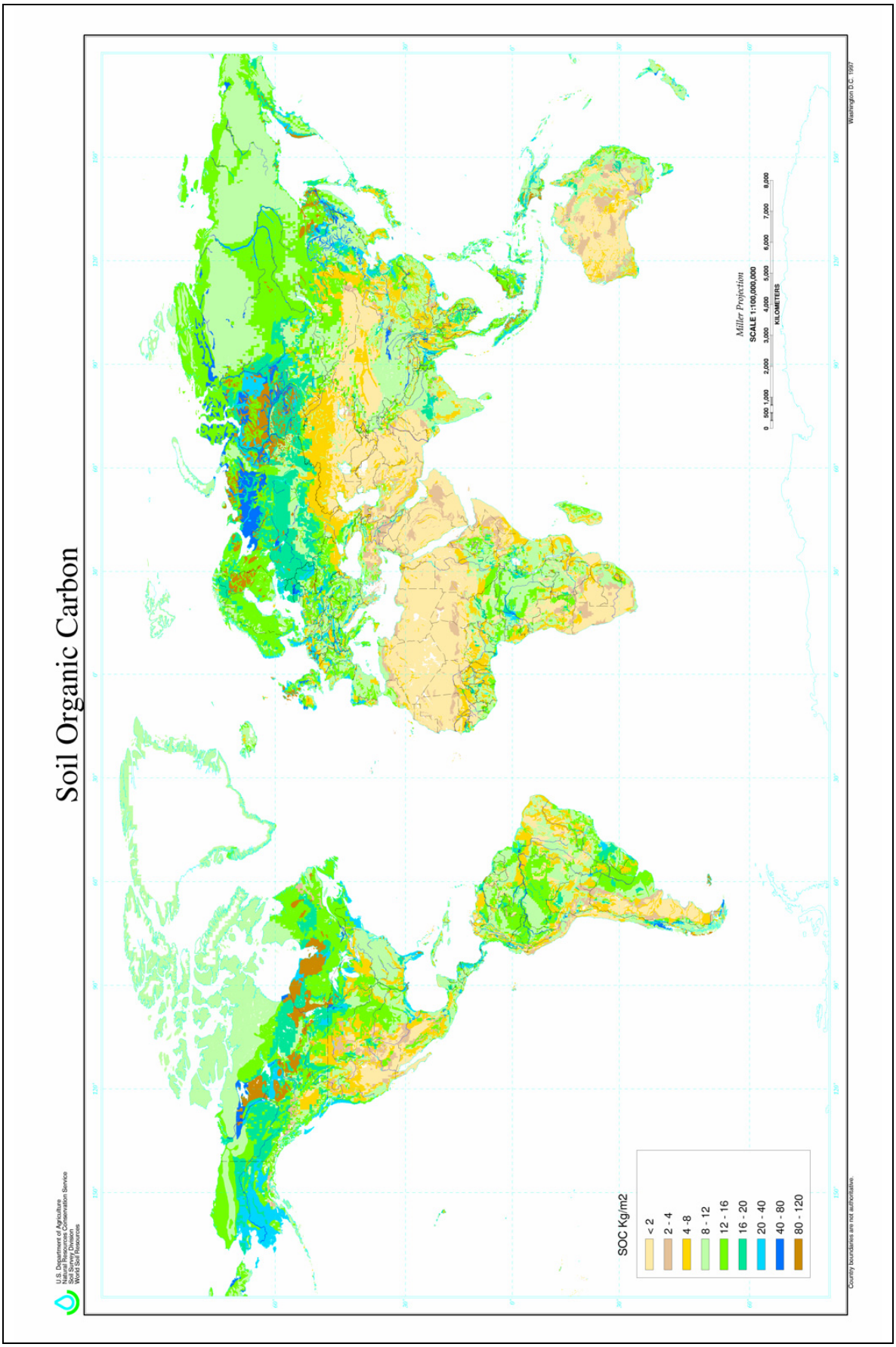

Global figues for all carbon fluxes derived by LPJ for the last two decades of the 20th century

1980s (average 1982 – 1989)

Parameter	**Unit**	**LPJ-P**	**LPJ-C**	**LPJ-S_{GIM}**	**LPJ-S_{PAL}**	**Difference LPJ-P–LPJ-S_{GIM}**
NPP	PgC yr^{-1}	69.6	71.9	58.9	58.6	11.0
Rh	PgC yr^{-1}	60.1	62.8	51.5	51.0	8.6
Fire C	PgC yr^{-1}	8.4	4.9	4.4	4.2	4.0
Harvested C	PgC yr^{-1}	0	3.2	2.6	2.6	- 2.6
NEE	PgC yr^{-1}	1.1	1.1	0.4	0.8	0.7
Biomass	PgC	905	664	634	610	271
Soil C	PgC	1669	1595	1370	1341	299
Runoff	km^3 yr^{-1}	35.9	40.8	43.8	45.3	- 7.9

1990s (average 1990 – 1999)

Parameter	**Unit**	**LPJ-P**	**LPJ-C**	**LPJ-S_{GIM}**	**LPJ-S_{PAL}**	**Difference LPJ-P–LPJ-S_{GIM}**
NPP	PgC yr^{-1}	71.4	73.9	60.8	59.7	10.6
Rh	PgC yr^{-1}	61.5	64.4	52.9	52.2	8.6
Fire C	PgC yr^{-1}	8.5	4.9	4.3	4.0	4.2
Harvested C	PgC yr^{-1}	0	3.3	2.8	2.8	- 2.8
NEE	PgC yr^{-1}	1.4	1.4	0.9	0.8	0.5
Biomass	PgC	913	670	641	618	272
Soil C	PgC	1672	1599	1371	1342	301
Runoff	km^3 yr^{-1}	35.6	40.5	44.2	45.5	- 9.9

Increase (negative: decrease) between the 1980s and 1990s

Parameter	**Unit**	**LPJ-P**	**LPJ-C**	**LPJ-S_{GIM}**	**LPJ-S_{PAL}**
NPP	PgC yr^{-1}	1.8	2.0	1.9	1.1
Rh	PgC yr^{-1}	1.4	1.6	1.4	1.2
Fire C	PgC yr^{-1}	0.1	0	- 0.1	- 0.2
Harvested C	PgC yr^{-1}	0	0.1	0.2	0.2
NEE	PgC yr^{-1}	0.3	0.3	0.5	0
Biomass	PgC	8	6	7	8
Soil C	PgC	3	4	1	1
Runoff	km^3 yr^{-1}	-0.3	-0.3	0.4	0.2

Carbon fluxes derived by LPJ-S_{GIM} split for latitudinal zones for the 1980s and 1990s

1980s (average 1982 – 1989)

Parameter	Unit	boreal	Northern temperate	tropics	Southern temperate
NPP	PgC yr^{-1}	12.1	11.5	29.1	5.3
Rh	PgC yr^{-1}	10.5	9.7	25.9	4.8
Fire C	PgC yr^{-1}	1.1	0.5	2.3	0.3
Harvested C	PgC yr^{-1}	0.4	1.3	0.7	0.2
NEE	PgC yr^{-1}	0.1	0.1	0.2	0
Biomass	PgC	177	61	359	32
Soil C	PgC	773	219	197	81
Runoff	km^3 yr^{-1}	8.6	6.4	25.9	2.3

1990s (average 1990 – 1999)

Parameter	Unit	boreal	Northern temperate	tropics	Southern temperate
NPP	PgC yr^{-1}	12.5	11.5	30.9	5.6
Rh	PgC yr^{-1}	10.7	9.8	26.9	5.0
Fire C	PgC yr^{-1}	1.2	0.5	2.2	0.3
Harvested C	PgC yr^{-1}	0.4	1.4	0.8	0.2
NEE	PgC yr^{-1}	0.2	-0.2	0.9	0.1
Biomass	PgC	180	62	365	31
Soil C	PgC	773	219	197	81
Runoff	km^3 yr^{-1}	8.1	5.6	28.7	2.4

Increase (negative: decrease) between the 1980s and 1990s

Parameter	Unit	boreal	Northern temperate	tropics	Southern temperate
NPP	PgC yr^{-1}	0.4	0.0	1.8	0.3
Rh	PgC yr^{-1}	0.2	0.1	1.0	0.2
Fire C	PgC yr^{-1}	0.1	0.0	-0.1	0.0
Harvested C	PgC yr^{-1}	0.0	0.1	0.1	0.0
NEE	PgC yr^{-1}	0.1	-0.3	0.7	0.1
Biomass	PgC	3	1	6	-1
Soil C	PgC	0	0	0	0
Runoff	km^3 yr^{-1}	-0.5	1.2	2.8	0.1